INFORMATION TO USERS

This manuscript has been reproduced from the microfilm master. UMI films the text directly from the original or copy submitted. Thus, some thesis and dissertation copies are in typewriter face, while others may be from any type of computer printer.

The quality of this reproduction is dependent upon the quality of the copy submitted. Broken or indistinct print, colored or poor quality illustrations and photographs, print bleedthrough, substandard margins, and improper alignment can adversely affect reproduction.

In the unlikely event that the author did not send UMI a complete manuscript and there are missing pages, these will be noted. Also, if unauthorized copyright material had to be removed, a note will indicate the deletion.

Oversize materials (e.g., maps, drawings, charts) are reproduced by sectioning the original, beginning at the upper left-hand corner and continuing from left to right in equal sections with small overlaps.

Photographs included in the original manuscript have been reproduced xerographically in this copy. Higher quality 6" x 9" black and white photographic prints are available for any photographs or illustrations appearing in this copy for an additional charge. Contact UMI directly to order.

ProQuest Information and Learning
300 North Zeeb Road, Ann Arbor, MI 48106-1346 USA
800-521-0600

UMI®

Experimental Investigation and Modeling of

Anisotropic Etching of Silicon in Tetra-Methyl Ammonium Hydroxide

Anand Pandy

A Thesis

in

The Department

of

Electrical and Computer Engineering

Presented in Partial Fulfilment of the Requirements

for the Degree of Master of Applied Science at

Concordia University

Montreal, Quebec, Canada

April 2002

© Anand Pandy, 2002

National Library of Canada

Bibliothèque nationale du Canada

Acquisitions and Bibliographic Services

Acquisitions et services bibliographiques

395 Wellington Street
Ottawa ON K1A 0N4
Canada

395, rue Wellington
Ottawa ON K1A 0N4
Canada

Your file Votre référence

Our file Notre référence

The author has granted a non-exclusive licence allowing the National Library of Canada to reproduce, loan, distribute or sell copies of this thesis in microform, paper or electronic formats.

L'auteur a accordé une licence non exclusive permettant à la Bibliothèque nationale du Canada de reproduire, prêter, distribuer ou vendre des copies de cette thèse sous la forme de microfiche/film, de reproduction sur papier ou sur format électronique.

The author retains ownership of the copyright in this thesis. Neither the thesis nor substantial extracts from it may be printed or otherwise reproduced without the author's permission.

L'auteur conserve la propriété du droit d'auteur qui protège cette thèse. Ni la thèse ni des extraits substantiels de celle-ci ne doivent être imprimés ou autrement reproduits sans son autorisation.

0-612-68445-8

Canada

ABSTRACT

Experimental Investigation and Modeling of

Anisotropic Etching of Silicon in Tetra-Methyl Ammonium Hydroxide

Anand Pandy

Anisotropic etching of silicon is a fundamental process in micro-systems technology (MST) and in the fabrication of micro-electromechanical systems (MEMS). This work addresses the fundamental atomic mechanisms of anisotropic etching of single-crystal silicon, by wagon-wheel-based under-etch experiments of {110} and {100} silicon in TMAH at 25wt%, 19wt%, 17wt%, 15wt%, 12wt% and 9wt% at 80°C. The under-etched surfaces often consist of two to three facets. The inclination angles of these facets are categorized in two modes, as being defined either by periodic bond chains, or by rows of atoms each having two dangling bonds. Using the facet information, a simple atomic model is applied to the under-etch rates, based on removal frequencies of the chains or rows (f_p and f_k), and based on steps on flat {111} planes. Variations of under-etched surfaces near enough to {111} planes are well-matched by the model. Planes near {110} and {100} cannot be matched by this simple formulation. Effective f_k and f_p are calculated for all the experimental cases. The etching of the same crystallographic features can vary substantially at different geometrical attitudes, in identical etchant conditions.

ACKNOWLEDGEMENTS

I wish to express my deep sense of gratitude to my thesis supervisor Dr. Leslie M. Landsberger for his valuable guidance, encouragement, precious time spent in giving me valuable ideas and an insight into this field of research. I am also extremely grateful to Dr. Mojtaba Kahrizi who supported me in carrying out the research in the laboratory and for his guidance.

It is my privilege to thank my beloved parents Mr. A. Pandy and Mrs. Pa. Suriyakumari in providing me with moral, emotional and monetary support to do this research. My special thanks to my wife who has supported me during the completion of the thesis. I also wish to express my sincere thanks to all my other family members and friends in this regard.

I am extremely grateful to all the faculty members and staff of the Department Of Electrical and Computer Engineering and the Concordia University for giving me an opportunity to do this thesis and to be a part in contributing to the technical world.

It is my blessed privilege to salute all the personalities who were both directly and indirectly supporting me in carrying out the project successfully.

Last but not the least, I wish to thank the Almighty God who helped me in the successful completion of this project.

TABLE OF CONTENTS

CHAPTER 1

Introduction 1

1.1 Micromachining, Anisotropic Etching 1

1.2 Reasons for Interest in TMAH 2

1.3 Why use Si{110} in MEMS? 3

1.4 Why use Si{110} to Study Anisotropic Etch Mechanisms? 4

1.5 Experimental and Modeling Strategy 5

1.6 Summary of Chapters 7

CHAPTER 2 8

Background on Anisotropic Etching of Silicon 8

2.1 Silicon Micromachining 8

2.2 General Background 8

2.2.1 Miller Index Notation Used in this Work: 9

2.3 Background on Anisotropic Etching of Si{100} 10

2.4 Background on Anisotropic Etching of Si{110} 12

2.5 The Anisotropic Etchants 15

2.5.1 KOH and Metallic Hydroxides 16

2.5.2 EDA, EDP, TMAH, NH_4OH, N_2H_4 and Gallates 17

2.6 Etchant Conditions 18

2.7 Additives to Etchants 18

2.8 Selectivity of etchant 18

2.9 Etch Mechanisms 19

2.9.1 Oxidation Dissolution Model 20

2.9.2 Hydration Model 20

2.9.3 Electrochemical Model 21

2.9.4 Crystallographic Model 22

CHAPTER 3 23

Atomic Modeling 23

3.1 Types of Atomic Structure 23

3.2 Steps on a Flat Plane 25

3.3 Silicon: Steps on a {111} Plane 25

3.3.1 Step height: 26

3.3.2 Step width 27

3.4 Types of steps 28

3.5 Calculation of Etch-Rate 29

3.5.1 Assumptions 29

3.6 Pairs of {111} Planes in {100} and {110} Silicon Wafers 32

3.6.1 {111} Planes and <110> Lines 32

3.6.2 Pairs of {111} Planes with <110> Intersection Lines 33

3.6.3 Pairs of {111} Planes and Under-Etched Planes 39

3.6.4 Mask-Edge Angles, Rotation Angles and Inclination Angles 45

3.6.4.1 Deviation Angle δ vs. θ in the (100) System 46

3.6.4.1.1 PBC-defined Planes: 46

3.6.4.1.2 Kink-defined Planes: 46

3.6.4.2 Inclination angle α vs. δ in the (100) system 46

3.6.4.2.1 PBC-defined Planes 46

3.6.4.2.2 Kink-defined Planes 46

3.6.5 Derivation of the Deviation angle δ vs. θ and Inclination angle α vs. δ in the (110) System 47

3.6.5.1 PBC-Defined Planes 47

3.6.5.1.1 PBC-defined Planes, Angle Range: (P-35-60) 48

3.6.5.1.2 PBC-defined Planes, Angle Range (P-60-90): 48

3.6.5.2 Kink-defined Planes 48

3.6.5.2.1 Kink-defined planes, Angle range (K-35-45): 48

3.6.5.2.2 Kink-defined planes, Angle Range (K-45-90): 48

CHAPTER 4 50

Experimental and Measurement Techniques and Procedures 50

4.1 Overview 50

4.2 Experimental and Observation Procedures 50

4.2.1 Experimental Design 50

4.2.2 The Etch Station 51

4.2.3 Sample Preparation 52

4.2.4 The Mask 55

4.2.5 Etch Experimental Procedure 55

4.3 Measured Quantities 57

4.4 Measurement Procedures, and Techniques 59

4.4.1 Mask Under-cut 59

4.4.1.1 Under-Etch Rate Calculation 60
4.4.2 Etch Depth 60
4.4.3 Under-Etched Surface Horizontal Projection (UESHP) 61
4.5 Oxide Removal, Re-measure 61
4.5.1 Inclination Angle Calculation 62
4.6 SEM Procedures 62
CHAPTER 5 64
Experimental Results, and Match to Model 64
5.1 Experimental Results: Organized by TMAH Concentration 64
5.1.1 Etching in 25wt% TMAH 66
5.1.1.1 Si{110} etched at 80°C 66
5.1.1.2 Si{100} etched at 80°C 72
5.1.2 Etching in 19wt% TMAH 76
5.1.2.1 Si{110} etched at 80°C 76
5.1.2.2 Si{100} etched at 80°C 83
5.1.3 Etching in 17wt% TMAH 87
5.1.3.1 Si{110} etched at 80°C 87
5.1.3.2 Si{100} etched at 80°C 94
5.1.4 Etching in 15wt% TMAH 98
5.1.4.1 Si{110} etched at 80°C 98
5.1.4.2 Si{100} etched at 80°C 105
5.1.5 Etching in 12wt% TMAH 109
5.1.5.1 Si{110} etched at 80°C 109
5.1.5.2 Si{100} etched at 80°C 116

5.1.6 Etching in 9wt% TMAH ... 121

5.1.6.1 Si{110} etched at 80° C ... 121

5.1.6.2 Si{100} etched at 80°C ... 127

CHAPTER 6 ... 131

Removal Rates Fitting and Discussion ... 131

6.1 Etch Depth, Etch Rates and Removal Frequencies ... 131

6.1.1 Removal Frequencies ... 132

6.1.1.1 Crystal basics ... 132

6.1.1.2 Kink removal frequency {100} ... 133

6.1.1.3 PBC removal frequency {110} ... 134

6.2 Under Etch, Etch Rates and Removal Frequencies ... 136

6.3 Under-Etched Planes: PBC's and Kink-Rows ... 139

6.4 Under-Etch Rate Model Fit to Calculate Removal Frequencies ... 140

6.4.1 (100) Silicon Etching ... 143

6.4.1.1 TMAH 25wt% Case ... 143

6.4.1.2 TMAH 15wt% Case ... 144

6.4.1.3 TMAH 12wt% Case ... 145

6.4.2 (110) Silicon Etching ... 145

6.4.2.1 TMAH 25wt% Case ... 145

6.4.2.2 Other Concentrations ... 147

6.4.3 Removal rate vs. TMAH Concentration ... 148

6.4.3.1 Removal Frequencies in Si(100) ... 148

6.4.3.2 Removal Frequencies in Si(110) ... 149

6.5 Comparison to {110} and {100} Etch Rates Studied by Other Researchers 151
6.5.1 (100) Silicon 151
6.5.2 (110) Silicon 153
6.6 Etched Surface Roughness 154
6.6.1 Roughness on (100) Surface 154
6.6.2 Roughness on (110) Surface 156
CHAPTER 7 158
Conclusions, Contributions and Suggestions for Future Work 158
7.1 Conclusions: 158
7.2 Contributions: 160
7.3 Suggestions for Future Work 162
References 164
Appendix A 172
Appendix B 191

LIST OF FIGURES

Figure 2.1 Etching a concave mask pattern, the final etch cavity is bounded by the slowest-under-etching planes. 10

Figure 2.2 Etching a convex mask pattern exposes fast-etching planes. 11

Figure 2.3 Anisotropically etched cavity formed in a Si{110}. 12

Figure 2.4 Figure to show the cross-sections of anisotropically etched Si{110}. 12

Figure 2.5 Etch progression of a cavity in {110} silicon: 3D view and top view 13

Figure 2.6 Orientation of (111) planes which form the side walls of etch cavity on (110) silicon.. 13

Figure 2.7 More details on the final cavity in Figure 2.5, showing cross-sections of the cavity at three locations. 14

Figure 2.8 Atomic level representations of the different cross-sections of the etched cavity. 14

Figure 2.9 Etching of rectangular windows (length l >> width w) (a) with length aligned parallel to vertical {111} planes and (b) with width aligned parallel vertical {111} plane. 15

Figure 3.1 Kink structure 23

Figure 3.2 PBC structure 24

Figure 3.3 Simple steps on a flat plane, showing the step width, *s* and step height *h*. 25

Figure 3.4 Steps on a (111) plane, and illustration of crystallographic step-width and step-height.. 26

Figure 3.5 Step-height, visualized in a conventional unit cell of silicon crystal lattice. 26

Figure 3.6 Body diagonal of silicon unit cell, to calculate the step-height. 27

Figure 3.7 Schematics of the silicon unit cell, to calculate the step-width. 28

Figure 3.8 Two types of steps with respect to the flat [111] plane: The PBC-defined plane is [212] and Kink-row defined plane is [121]. 28

Figure 3.9 Special case where the PBC-defined plane is (101) and the kink-row defined plane is (010). 29

Figure 3.10 Illustration of sequential exposure of PBC's to attack by the etchant. First A is attacked, then B. 30

Figure 3.11 Crystallographic illustration to show that the kink removal rate on a PBC is much greater than the formation rate of new kinks on a previously intact PBC. 30

Figure 3.12 Crystallographic illustration to show most of the kinks in a row has to be etched before the next row of kinks can be attacked. 31

Figure 3.13 ER(θ_K), for f_K = 5e+5 and ER(θ_P), for f_P = 6e+5 32

Figure 3.14 {111} planes in the Si cubic conventional unit cell, assuming a (100) top wafer surface. 33

Figure 3.15 {111} planes in Si cubic conventional unit cell, assuming a (110) top wafer surface. 34

Figure 3.16 Illustration on the pair of {111} planes and their <110> line of intersection. 35

Figure 3.17 Pair of {111} planes in (100) silicon. Note that the cubic grid no longer represents a single conventional unit cell, rather, it represents many unit cells, to illustrate the periodic bond chain along the line 36

Figure 3.18 Types of relevant pairs of {111} planes in (110) silicon. 37

Figure 3.19 Theoretical inclination angle of emerging planes vs. deviation angles in Si(100)........ 47

Figure 3.20 Theoretical inclination angle of emerging planes vs. deviation angles in Si(110) 49

Figure 4.1 Schematic of the TMAH etch station. 52

Figure 4.2 Process flow for sample preparation. 54

Figure 4.3 Wagon-wheel mask pattern and individual spoke details. 55

Figure 4.4 Relationship between the wafer flat and deviation angles δ on (100) and (110) silicon. 58

Figure 4.5 Illustration of the measurements made on etched samples, simple single faceted cases. 58

Figure 4.6 Illustration of the measurements made when the under-etched side wall is composed of three facets. 59

Figure 4.7 Illustration of Mask Under Cut on a single spoke. 60

Figure 4.8 Illustration of Depth measurement on a single spoke. 61

Figure 4.9 Scanning Electron Micrographs of a wagon-wheel spoke. At left, the cavity sidewalls and bottom have been carefully aligned to be perpendicular to the micrograph view. 63

Figure 5.1 Si(110) etched in 25wt% TMAH at 80°C; (a) Under-etch rate, Si(110), (b) Inclination angle, and (c) Facet details. 66

Figure 5.2 Scanning electron micrographs taken at various deviation angles for the {110} silicon etched in 25wt% TMAH at 80° C. 67

Figure 5.3 Si{100} etched in 25wt% TMAH at 80°C; (a) Under-etch rate, (b) Inclination angle, and (c) Facet details. 72

Figure 5.4 Scanning electron micrographs taken at various deviation angles for the {100} silicon etched in 25wt% TMAH at 80° C. 73
Figure 5.5 Si(110) etched in 19wt% TMAH at 80°C; (a) Under-etch rate, (b) Inclination angle, and (c) Facet details. 76
Figure 5.6 Scanning electron micrographs taken at various deviation angles for the {110} silicon etched in 19wt% TMAH at 80° C; 77
Figure 5.7 Si{100} etched in 19wt% TMAH at 80°c; (a) Under-etch rate, (b) Inclination angle, (c) Facet details. 83
Figure 5.8 Scanning electron micrographs taken at various deviation angles for the {100} silicon etched in 19wt% TMAH at 80° C............................. 84
Figure 5.9 Si{110} etched in 17wt% TMAH at 80°C; (a) Under-etch rate, (b) Inclination angle, and (c) Facet details. 87
Figure 5.10 Scanning electron micrographs taken at various deviation angles for the {110} silicon etched in 17wt% TMAH at 80° C. 88
Figure 5.11 Si{100} etched in 17wt% TMAH at 80°C; (a) Under-etch rate, (b) Inclination angle, and (c) Facet details. 94
Figure 5.12 Scanning electron micrographs taken at various deviation angles for the {100} silicon etched in 17wt% TMAH at 80° C 95
Figure 5.13 Si{110} etched in 15wt% TMAH at 80°C; (a) Under-etch rate, Si(110), (b) Inclination angle, and (c) Facet details. 98
Figure 5.14 Scanning electron micrographs taken at various deviation angles for the {110} silicon etched in 15wt% TMAH at 80° C. 99

Figure 5.15 Direction of roughness on the spoke at deviation angle $\delta = 90^o$ 104

Figure 5.16 Si{100} etched in 15wt% TMAH at 80°C; (a) Under-etch rate, (b) Inclination angle, and (c) Facet details. 105

Figure 5.17 Scanning electron micrographs taken at various deviation angles for the {100} silicon etched in 15wt% TMAH at 80° C. 106

Figure 5.18 Si{110} etched in 12wt% TMAH at 80° C; (a) Under-etch rate, (b) Inclination angle, and (c) Facet details. 109

Figure 5.19 Scanning electron micrographs taken at various deviation angles for the {110} silicon etched in 12wt% TMAH at 80° C. 110

Figure 5.20 Si{100} etched in 12wt% TMAH at 80°C; (a) Under-etch rate, (b) Inclination angle, (c) Facet details. 116

Figure 5.21 Scanning electron micrographs taken at various deviation angles for the {100} silicon etched in 12wt% TMAH at 80°C 117

Figure 5.22 Si{110} etched in 9wt% TMAH at 80°C; (a) Under-etch rate, (b) Inclination angle and (c) Facet details. 121

Figure 5.23 Scanning electron micrographs taken at various deviation angles for the {110} silicon etched in 9wt% TMAH at 80° C. 122

Figure 5.24 Si{100} etched in 9wt% TMAH at 80°C; (a) Under-etch rate, (b) Inclination angle, (c) Facet details. 127

Figure 5.25 Scanning electron micrographs taken at various deviation angles for the {100} silicon etched in 9wt% TMAH at 80° C. 128

Figure 6.1 Etch rates of {100} and {110} vs. TMAH Concentration 132

Figure 6.2 Silicon unit cube and representation of inter atomic distances. 133

Figure 6.3 Layers of {100} planes to illustrate the step length 134

Figure 6.4 Layers of {110} planes to illustrate the step length 135
Figure 6.5 Removal Rates vs. TMAH Concentration 136
Figure 6.6 Illustration of emerging planes and etch rate calculation 137
Figure 6.7 Etch rates of {100} and {110} planes vs TMAH concentration 139
Figure 6.8 Experimental (100) UER data for 25wt% TMAH and fitted theoretical UER curves with corresponding kink removal frequency (#/hr). .. 143
Figure 6.9 Experimental (100) UER data for 15wt% TMAH and fitted theoretical UER curves with corresponding PBC removal frequency (#/hr). .. 144
Figure 6.10 Experimental (100) UER data for 12wt% TMAH and fitted theoretical UER curves with corresponding PBC removal frequency (#/hr). .. 145
Figure 6.11 Experimental (110) UER data for 25wt% TMAH and fitted theoretical UER curves with corresponding PBC and kink removal frequencies (#/hr). 146
Figure 6.12 Experimental UER data for 19wt%, 17wt% and 15wt% TMAH and fitted theoretical UER curves with corresponding PBC and kink removal frequencies (#/hr). 147
Figure 6.13 Experimental UER data for 12wt% and 9wt% TMAH and fitted theoretical UER curves with corresponding PBC and kink removal frequencies (#/hr). 148
Figure 6.14 Removal rate vs. TMAH concentration. The P-35-60-90 type is seen only at 9wt% TMAH etch. 150
Figure 6.15 Etch rates of (100) Vs. TMAH concentration, from various work. 152
Figure 6.16 Etch rates of (110) Vs. TMAH concentration, from various work. 153
Figure 6.17 Surface roughness of Si(100) etched in various concentrations of TMAH. 155
Figure 6.18 Surface roughness of Si(110) etched in various concentrations of TMAH. 156
Figure 6.19 Hillocks on the ~(100) surface, the 2nd facet of the under-etched surface. 157

LIST OF TABLES

Table 5.1 Si {110} etched in 25wt%TMAH 69

Table 5.2 Si{100} etched in 25wt% TMAH 74

Table 5.3 Si{110} etched in 19wt% TMAH 79

Table 5.4 Si{100} etched in 19wt% TMAH 84

Table 5.5 Si{110} etched in 17wt% TMAH 90

Table 5.6 Si{100} etched in 17wt% TMAH 97

Table 5.7 Si{110} etched in 15wt% TMAH 102

Table 5.8 Si{100} etched in 15wt% TMAH 107

Table 5.9 Si{110} etched in 12wt% TMAH 113

Table 5.10 Si{100} etched in 12wt% TMAH 119

Table 5.11 Si{110} etched in 9wt% TMAH 125

Table 5.12 Si{100} etched in 9wt% TMAH 129

Table 6.1 Etch rates of {100} and {110} vs. TMAH Concentration 131

Table 6.2 Removal Rates vs. TMAH Concentration 135

Table 6.3 Emerging Planes on (110) Silicon 137

Table 6.4 Emerging Planes on (100) Silicon 137

Table 6.5 Etch Rates of {100} and {110} planes vs. TMAH Concentration 138

Table 6.6 Step width of Various Planes on (100) Silicon 142

Table 6.7 Step width of Various Planes on (110) Silicon 142

Table 6.8 First facet of the Under-etched surface on Si(100) etched in 25wt% TMAH 143

Table 6.9 First facet of the Under-etched surface on Si(110) etched in 25wt% TMAH 145

Table 6.10 PBC/Kink Removal Frequency on Si(100) 149

Table 6.11 PBC/Kink Removal Frequency on Si(100) 149

Table 6.12 Etch Rate of Si (100), Comparison 152

CHAPTER 1

Introduction

1.1 Micromachining, Anisotropic Etching

Bulk micromachining of single-crystal silicon has been extensively used to fabricate a wide variety of micro-devices, micro-sensors and micro-actuators, and micro-systems [1 - 5]. In the past decade, this field, often called Micro Electro Mechanical Systems (MEMS) or Microsystems technology (MST), has seen a dramatic increase in research and development activity. There have been many such micro-fabricated sensors made available in the market. One common example is the accelerometer based air-bag controller in cars. In a MEMS device, a mechanical sensor is often coupled with a control/computing integrated circuit. The ability to integrate both the sensor and the electronic circuits on a single silicon chip is one of the factors making this field attractive. There are techniques to integrate MEMS micro-sensors with CMOS circuitry (called CMOS-compatible MEMS [4-7]. Anisotropic etching of silicon to create mechanical structures is one of the most commonly used techniques because of its reliable etch anisotropy, its low cost and relative ease of use. Silicon micromachining is given most prominence, since silicon is the primary substrate material used for fabricating microelectronic integrated circuits. In addition, the good mechanical properties of silicon [8] make it the right candidate to fabricate mechanical structures. Another commonly used material in the semiconductor industry, gallium arsenide, can not be used to fabricate integrated microsystems because its mechanical properties are not as advantageous as those of silicon.

Although anisotropic etching of silicon has been widely employed to fabricate integrated sensors [9], the fundamental atomic mechanisms of anisotropic silicon etching are still not clear. Much experimental research work has been done to study anisotropic etching of both {100} and {110} silicon [10 - 22]. Although simple cavities bounded by slow-

est-etching planes {111} planes are routinely etched, the etching of more complex structures remains difficult because of repeatability concerns. Many researchers have developed models to explain the anisotropic etch mechanisms [15 - 25], but they are inadequate to provide an accurate theoretical modeling. It is likely that more interesting structures will be achievable if the atomic mechanism is better understood. [26]

"The main effort of science is to describe what happens in nature, in as complete and concise a form as possible. In physics this effort involves observing natural phenomena, relating these observations to previously established theory, and finally establishing a physical model for the observations. The primary purpose of the model is to allow the information obtained in present observations to be used to understand new experiments. Therefore the most useful models are expressed mathematically, so that quantitative explanations of new experiments can be made succinctly in terms of established principles.", from B Streetman [27]. In accord with Streetman's thought, this work endeavors to advance the understanding of the fundamental etching mechanism in silicon, by relating the experimental data to a geometric model of the surfaces etched.

In the interests of advancing the understanding of basic atomic mechanisms of anisotropic etching of silicon, this work presents a systematic experimental investigation of anisotropic etching of silicon in Tetra-Methyl Ammonium Hydroxide (TMAH). In particular, mask under-etch experiments on Si{110} and Si{100} are done, and the experimental data are used to model the etch anisotropy in silicon.

1.2 Reasons for Interest in TMAH

Many anisotropic etchants have been used to etch silicon such as KOH, EDP, NaOH, hydrazine. Tetra-methyl ammonium hydroxide (TMAH) has received much attention in recent years due to several attractive properties [10, 16, 28-31]. TMAH is non-toxic when compared to other etchants, such as EDP [6]. TMAH is compatible with standard CMOS

processes [4 - 6]. TMAH has been successfully used with additives to obtain certain etch properties, such as aluminum passivation during wet etch [32, 33]. Additives in the TMAH also alter the etch anisotropy and selectivity [34]. In addition to these reasons, it is being used here for study of atomic mechanisms, because it can be used in a wide range of concentrations from 5% to 25%, and exhibits significantly different etch characteristics as a function of concentration.

1.3 Why use Si{110} in MEMS?

Si{100} is very widely used in standard complementary metal-oxide-semiconductor (CMOS) fabrication, in which the MEMS are also incorporated [4 - 6]. The structures that can be formed using Si{100} are very limited due to its crystallographic properties. On the other hand the Si{110} provides a wide variety of under-etched planes and hence more complex structures can be etched on {110} silicon.

Anisotropic etching of {110} silicon finds application in the fabrication of high-aspect ratio stationary micro-structures and low-voltage electrostatic micro-actuators for optical applications [9, 35]. The {111} side-walls obtained by anisotropically etching {110} silicon are atomically smooth and give high performance optical quality surfaces. The reflectivity of the smooth {111} surfaces is so great that they can be used as optical mirrors. These high quality optical mirrors find application in fiber-optic communication systems. These anisotropically etched mirrors may form the core of silicon optical micro-benches.

High aspect ratio micro-structures with atomically smooth, vertical side-walls can be achieved by anisotropically etching {110} because of the high etching selectivity between {111} and the {110} planes. These deep and narrow vertical grooves etched with high precision offer numerous applications. A few applications include large-area capacitor fabricated by etching closely spaced grooves, and vertical multi-junction solar cells [36].

Trench capacitors fabricated in {110} silicon can be used if {110} silicon wafers are

adapted to the manufacture of CMOS circuits. CMOS circuits on {110} may rise in importance when low temperature ICs become more important in the world of high-temperature superconductors and low-temperature CMOS logic circuits. This is because of the two fold mobility advantage of holes along certain azimuthal directions (relative to {100} wafers) at 77K allows much more balanced CMOS circuits on {110} silicon than on {100} silicon [37]. All these advantages make the {110} silicon very promising for MEMS applications. Characterization of anistropic etching of Si{110} is very important and will provide us with rich data to design MEMS structures on Si{110}. Devices fabricated in {110} silicon wafers include diffraction gratings, narrow slits, miniature fluidic devices such as pumps and valves, grooves for optical fiber alignment and cantilever beams for accelerometers.

1.4 Why use Si{110} to Study Anisotropic Etch Mechanisms?

This research uses an approach based on the relation of experimental observations of geometrical features, to the underlying crystal structure. The aim is to identify ranges of data which obey simple atomic models, and ranges of data which require more complex modeling. Si{110} is studied, due to the rich complexity of under-etched planes exposed during under-etch experiments. Etching Si{110} provides us with the etch data for planes made of Periodic-Bond-Chains (PBC's), whose indices are of the form {hhk} where h > k [12, 38]. The simplest form of the PBC structure is the surface of the {110} plane; other planes of this family have more complicated forms of PBC-based structures. The analysis is supplemented by Si{100} experiments. The other type of structure used in this work is rows of "*kinks*". Kinks are defined as atoms each having two dangling bonds free to interact with the etchant, and two back-bonds [12, 39]. Si{100} planes are fields of such features, with row and bond orientations alternating from one atomic layer to the next. In other words the {100} surface is made of rows of kinks (k-row). Other planes in the k-row family, which are of the form {h k k} where h > k, are made of more complicated kink-

based structures. In general, the bulk of prior experimental data shows that most etched planes can be modeled as one of these two families of planes.

1.5 Experimental and Modeling Strategy

The fundamental aim of this thesis is to advance the understanding and modeling of the atomic mechanisms in wet anisotropic etching of silicon. One test of the validity of any model is its ability to match a wide variety of experimental data by variation of a small number of parameters, in accord with physical intuition.

This work considers the under-etch behavior of {110} and {100} silicon. The variation of under-etch rates and under-etched surface geometries with mask-edge orientation, and other variables such as etchant concentration (as will be discussed in Chapter 2), provides a rich field of phenomena to analyze.

The conceptual development of this thesis consists of:

(a) Conducting experimental etches on {110} and {100} silicon using a wagon-wheel mask to obtain full sets of under-etch data as a function of mask-edge deviation angle at different etchant concentrations.

(b) Detailed observation of the under-etched surfaces by scanning electron microscopy (SEM), to carefully describe the multiple under-etched facets and how they vary with deviation angle.

(c) Formulation of simple atomic models of etch rate vs. deviation angle for a given kink-row or pbc-removal rate. The deviation angle is measured from a given {111} plane, where the etch rate is at a deep minimum. (This deviation is considered in the abstract, independent of physical wafer orientation).

(d) Separating the under-etch data into sections corresponding to variations from par-

ticular {111} planes oriented within the {110}-wafer system.

(e) Applying the model to each of these sections to determine fit vs. non-fit, and finding the equivalent k-row and pbc-removal rates.

(f) Obtaining {100} etch data under identical conditions, and performing a similar fitting exercise in the {100} system to compare extracted etch parameters.

(g) Since some regions do not fit the simple model well, comparing the non-fitting regions between {110} and {100} to determine whether the non-fitting aspects have a common geometrical source.

(h) Doing the above analyses on TMAH etches at a variety of concentrations, from the typical 25%, down to 9%, and looking for systematic variations in extracted parameters and non-fitting regions of the data.

It is hoped that this approach can offer an organized geometrical view of the experimental data, and provide a road map to indicate which aspects of anisotropic etching require more complex theory to explain.

Based on the above plan, the overall goals of this thesis are to:

(1) provide an organized framework for geometrical examination of experimental anisotropic etch data.

(2) examine whether simple atomic models involving constant k-row removal frequencies and pbc-removal frequencies are useful in understanding the complexity of the underetch data.

(3) outline aspects of anisotropic etch data to which simple geometrical models readily apply, and aspects to which such models fail to apply.

1.6 Summary of Chapters

In accord with the above plan, the thesis will be organized as follows:

Chapter 2 will discuss the previous research in this field.

Chapter 3 will outlay the principles and details of the (relatively simple) atomic models considered in this work.

Chapter 4 will detail the experimental and measurement techniques and procedures employed to obtain the experimental data.

Chapter 5 will present the experimental results, along with the predicted behavior from the model. These graphs, tables and lists will cover all of the cases of {110} and {100} silicon, and different etchant concentrations used in this work. Several particularly interesting facet geometries will be considered and explained in detail.

Chapter 6 will fit the experimental data to the model and will discuss the fits of the model to the data, highlighting both the fits and non-fits, and considering the meaning of the fitted parameters. The implications on the mechanisms of anisotropic etching of silicon will be discussed, and further avenues of study suggested.

Finally, *Chapter 7* will summarize the conclusions, contributions, and suggested future directions.

CHAPTER 2

Background on Anisotropic Etching of Silicon

2.1 Silicon Micromachining

There are a number of techniques that can be used to shape the silicon wafer to form micro-structures, called *bulk Micromachining* because the bulk silicon is being etched. There are other techniques to deposit and pattern thin films to produce complex micro-structures on the surface of the silicon wafer, called *surface micromachining.*

Etching can be classified into two categories, isotropic and anisotropic etching. In isotropic etching, the etchants attack the material being etched at the same rate in all directions. Anisotropic etchants etch the material in different rates for different directions, called orientation dependent etching (ODE) [9]. Due to the anisotropic behavior of the etchant, there is more control of the shapes produced. Some etchants attack silicon at different rates depending on the concentration, called concentration dependent etching. The concentration of the impurities in silicon or the concentration of the etchant change the etch characteristics. In addition, the temperature of the etchant and additive added to the etchant also change the etch characteristics [16 - 37]. In general, etch anisotropy can vary substantially depending on etchant, etchant concentration, temperature, additives and impurity concentration of silicon substrate, leading to widely differing etched shapes, in both concave and convex configurations.

2.2 General Background

Etch anisotropy is the variation of etch rate with direction in the crystal. In bulk silicon micromachining, the interaction of the etchant with the different Si lattice surfaces results in anisotropic etch. Mask shapes and etch anisotropy of Si in a particular etchant determine the final shapes of the 3-dimensional structures achieved [9, 28, 40]. For example

convex vs. concave mask shapes yield completely different etched Si features. It is generally known that, because of geometrical considerations, etched concave shapes tend to expose slowest-etching planes, whereas etched convex shapes tend to expose fastest-etching planes [41].

2.2.1 Miller Index Notation Used in this Work:

In order to represent planes and surfaces in the silicon crystal structure, the following Miller Index notation is used in this work:

To represent a specific plane having intercepts to the coordinate axes (1/*h*, 1/*k*, 1/l) : (*hkl*). Note that overbars above an index means the negative direction with respect to the coordinate system. For example, the $(\bar{h}k\bar{l})$ plane has intercepts (-1/*h*, 1/*k*, -1/*l*).

To represent a specific direction vector (*h*,*k*,*l*) with respect to the coordinate axes: [*hkl*].

To represent a family of equivalent planes (such as the entire family of (100), (010), (001), $(\bar{1}00)$, $(0\bar{1}0)$ and $(00\bar{1})$): {100}.

To represent a family of equivalent directions (such as the entire family of [110], [101], [011], $[\bar{1}10]$, $[1\bar{1}0]$, $[\bar{1}\bar{1}0]$, $[\bar{1}01]$, $[10\bar{1}]$, $[\bar{1}0\bar{1}]$, $[0\bar{1}1]$, $[01\bar{1}]$ and $[0\bar{1}\bar{1}]$: <110>.

2.3 Background on Anisotropic Etching of Si{100}

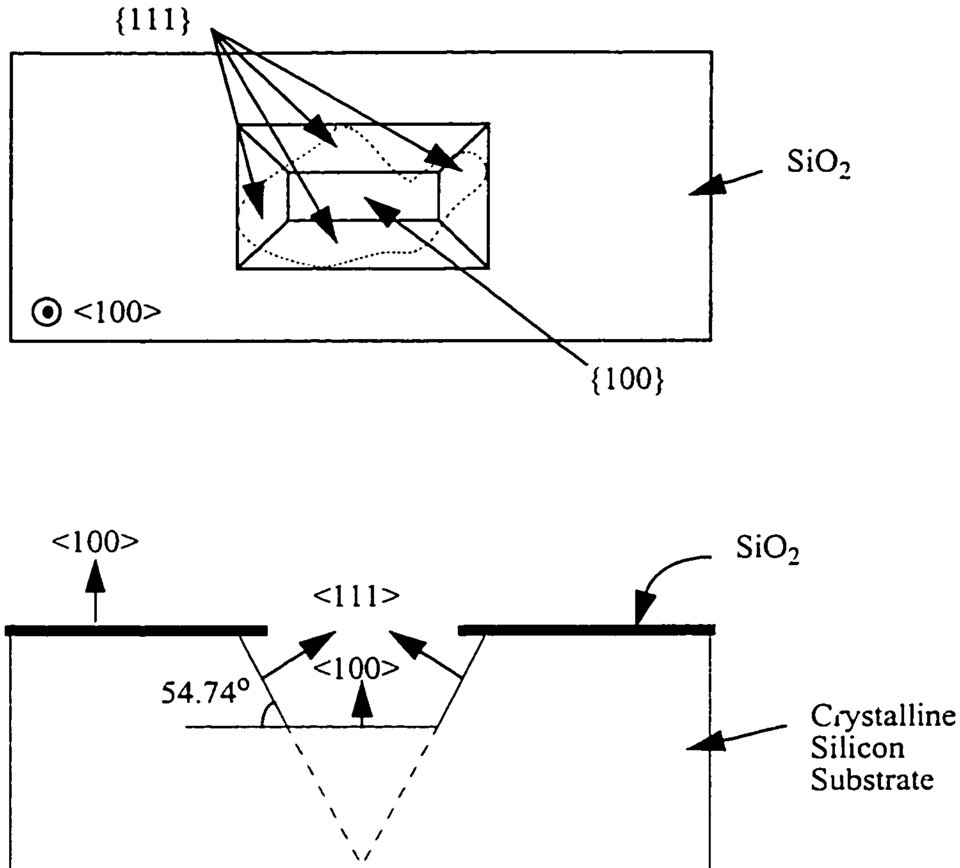

FIGURE 2.1: Etching a concave mask pattern, the final etch cavity is bounded by the slowest-under-etching planes.

The etching of an arbitrarily-shaped concave mask pattern, such as the one shown in Figure 2.1, leads to the selection of slow-under-etching planes. After a long enough etch time, only the slowest-under-etching planes will remain [8, 28, 41]. These are the familiar {111} planes. A convex shape, such as the one shown in Figure 2.2, on the other hand, exposes fast-etching planes, for example {411} or {212} planes [41 - 45]. Note that the etched planes in the two cases differ both in their intersection with the top masked surface and in their angle of inclination to the horizontal. In fact, the Figure 2.2 has both the concave and convex mask patters. The rectangle is the concave mask and the circle is the convex mask, so both the slow and fast etching planes are obtained as a result of etching this mask pattern.

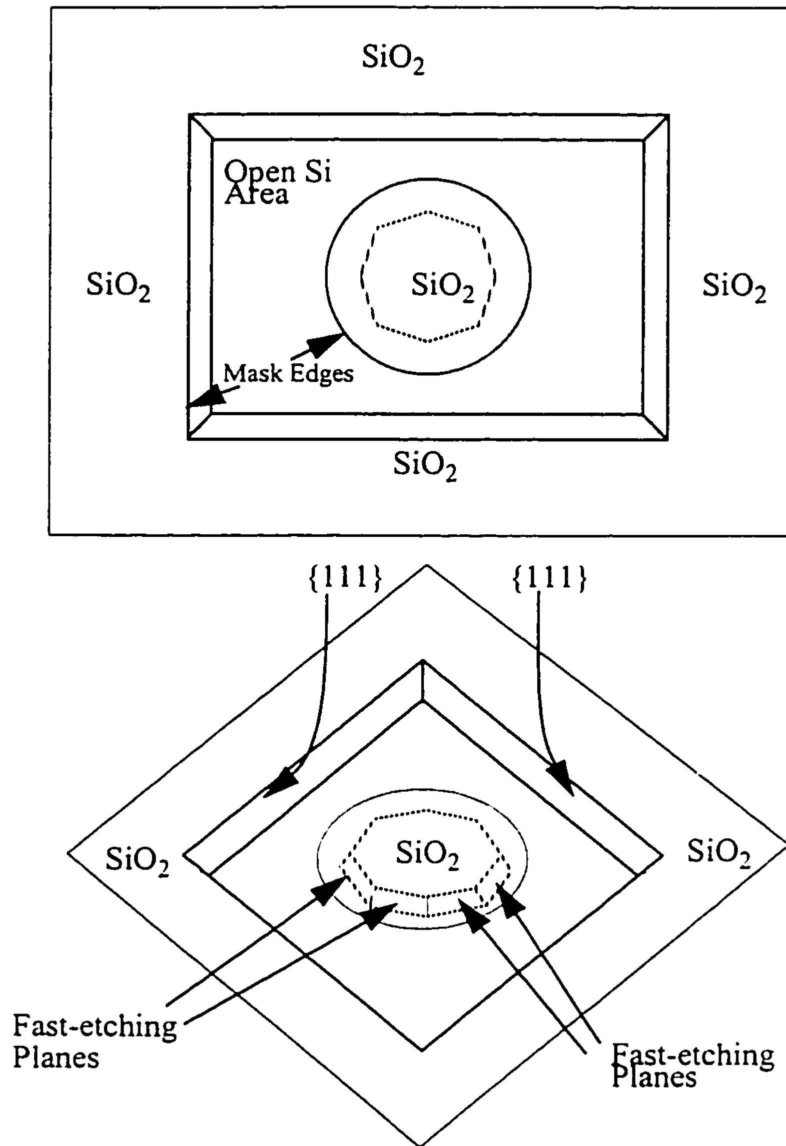

FIGURE 2.2: Etching a convex mask pattern exposes fast-etching planes.

2.4 Background on Anisotropic Etching of Si{110}

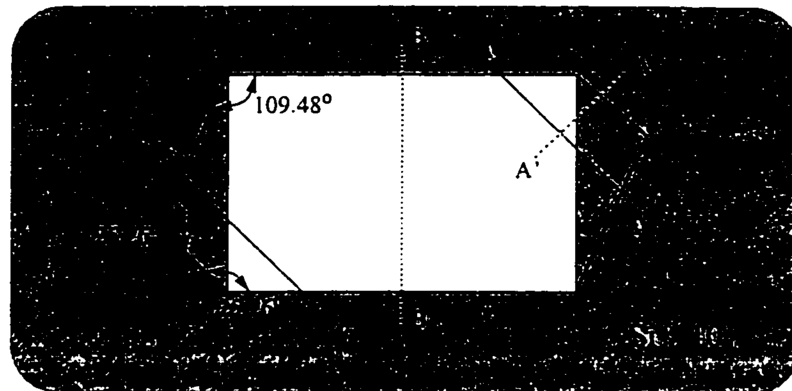

FIGURE 2.3: Anisotropically etched cavity formed in a Si{110}.

The etching on {110} silicon is in contrast to etching of {100} silicon. In {100} silicon the infinite etch cavity will always be a four sided (square or a rectangle, depending on the initial silicon open area), and the etched side-walls are all at 54.74° to the {100} silicon surface [40, 41]. On the other hand, in the {110} silicon, different geometrical structures are obtained after the etch. The final etched cavity in a {110} silicon will be either a rhombus or a hexahedron, depending on the size of opening and the etch time [40, 46 - 49].

When {110} silicon is etched with a rectangular mask pattern as shown in Figure 2.3, after a finite length of time, the final etch cavity will be a hexahedron. Cross-sections at two different regions of the etched cavity are shown in Figure 2.4.

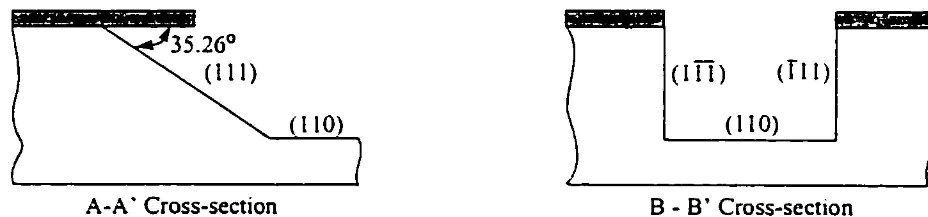

FIGURE 2.4: Figure to show the cross-sections of anisotropically etched Si{110}.

The progression of etching a rectangular mask pattern (as shown in Figure 2.3) is shown in Figure 2.5. From the figure we can clearly see the formation of the (1 1 1) planes which define the etch cavity.

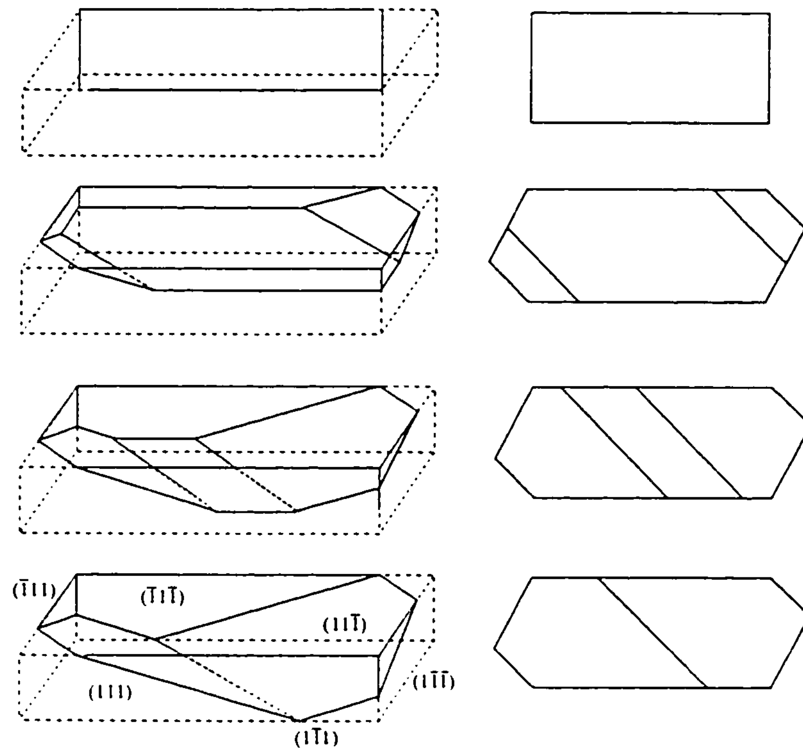

FIGURE 2.5: Etch progression of a cavity in {110} silicon: 3D view (left) and top view (right) [46, 47]: The last diagrams indicate the final cavity, bounded on all sides by {111} planes. Dashed line indicate the {111} planes which are perpendicular to the {110} wafer surface.

The Figure 2.6 below shows the direction of the {1 1 1} planes which form the side walls of the etch cavity.

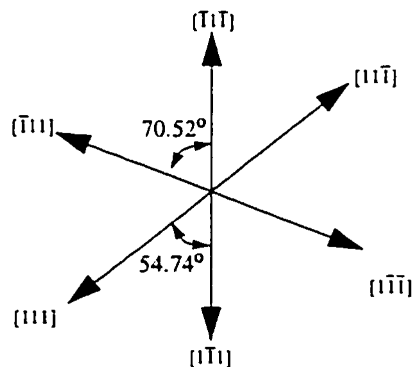

FIGURE 2.6: Orientation of {111} planes which form the side walls of etch cavity on {110} silicon.

In addition to the sample cavity cross-section shown in Figure 2.4, various other cross-sections of the etched cavity is shown below in Figure 2.7. As can be seen from the figure, though the side walls of the cavity are composed of {111} planes, the cross-sections at different locations of the cavity have a different shape. This anisotropic etch properties can be used as an advantage to etch the desired cavity shape.

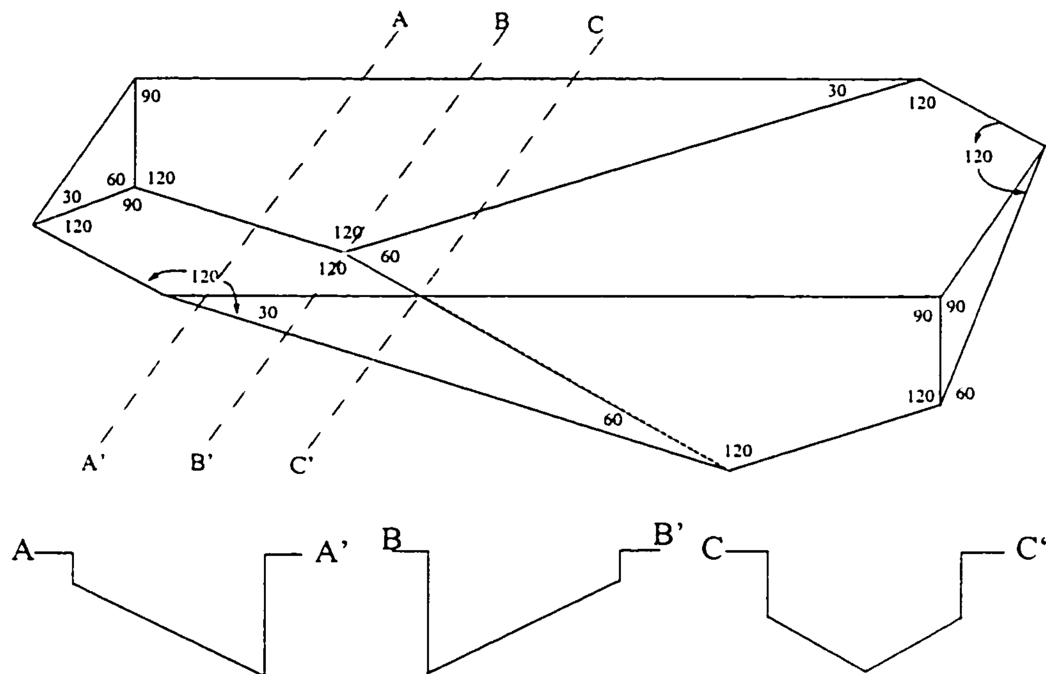

FIGURE 2.7: More details on the final cavity in Figure 2.5, showing cross-sections of the cavity at three locations.

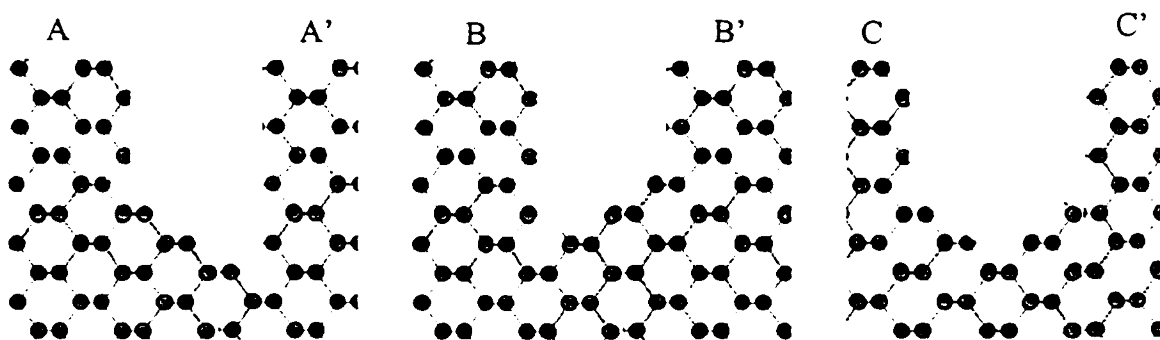

FIGURE 2.8: Atomic level representations of the different cross-sections of the etched cavity.

The mask dimensions and alignment play a vital role in shape of the etch cavity that is formed as a result of anisotropic etching. As a simple example, consider a mask with the length very much greater than the width; aligning the mask at different directions yields a totally different etch cavity [46]. This is shown in Figure 2.9 below.

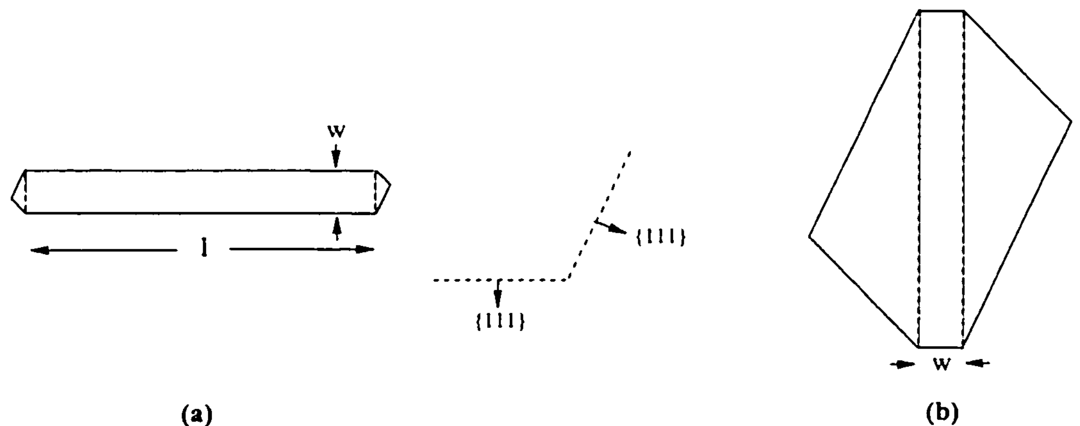

FIGURE 2.9: Etching of rectangular windows (length l >> width w) (a) with length aligned parallel to vertical {111} planes and (b) with width aligned parallel vertical {111} plane.

Cavities with vertical side walls can be etched if the pattern is aligned to the $(1\,\bar{1}\,\bar{1})$ or the $(\bar{1}\,1\,\bar{1})$ plane or the wafer-flat. And similarly cavities of V-grooves with side-walls inclined at 35.26^{o} can be etched if the pattern is aligned to the $(1\,1\,\bar{1})$ or the $(\bar{1}\,\bar{1}\,\bar{1})$ planes.

2.5 The Anisotropic Etchants

The ability to selectively etch bulk crystalline silicon provides a powerful technique in fabricating precise three-dimensional structures. Most anisotropic etching of crystalline silicon is based on liquid-phase chemical reactions[1 - 5, 40 - 49], with a few using vapor phase and plasma etching [7].

There have been a variety of wet chemical etchants used for bulk micromachining [9, 10, 21, 28, 40, 45, 49 - 51]. A large number of alkaline-type etchants exhibit anisotropic behavior, i.e.having different etch rates in various crystallographic planes. The chemicals used as anisotropic silicon etching include ethylene diamine (EDA, $NH_2(CH_2)NH_2$),

pyrocatechol commonly known as EDP (C_6H_4 $(OH)_2$), potassium hydroxide (KOH), ammonium hydroxide (NH_4OH) and more recently Tetra methyl ammonium hydroxide (TMAH) [50]. In this work, TMAH has been used a the anisotropic etchant. TMAH has many advantages over the other etchants: it is CMOS compatible, and less harmful [16].

The primary research in this field was done on systems based on KOH, hydrazine, and also ethylenediamine(EDA) with pyrocatechol as an accelerator [9]. Even though EDA and hydrazine are advantageous over the metallic hydroxides like KOH and NaOH in that they have a slow etch rate of SiO_2, they don't possess very high crystallographic etch ratios and demand extreme care in their usage due to their high toxicity. In the following sections, some of the results are summarized from the literature on all the alkaline-based etchants.

2.5.1 KOH and Metallic Hydroxides

The KOH:water system has become the major etchant used for micromachining applications. The results from the recent reviews are summarized in the subsequent discussion. Other Metallic Hydroxides include NaOH, LiOH, CsOH, and RbOH [50].

KOH has advantages over all other metallic hydroxides for most purposes. However, some special properties of each one appear suitable for particular applications. The relative etch rates of Si in the metallic hydroxides are in the following order, NaOH > KOH > LiOH > RbOH > CsOH [52], at equivalent molar concentrations. NaOH possesses less anisotropy compared to KOH. Rapid diffusion of Na relative to other metals in gate oxides prevents its use in production of CMOS integrated MEMS. Moreover, the difficulty in purifying metallic hydroxides to be devoid of impurities like Fe, Cu and other heavy metals hampers their frequent use [50].

2.5.2 EDA, EDP, TMAH, NH_4OH, N_2H_4 and Gallates

Certain nonmetallic solutions are preferred in Si micromachining for their advantages stated below over metallic solutions:

- greater chemical purity
- greater etching selectivity relative to oxides and heavily p-type Si.

Even though Ethylenediamine and ethylenediamine-pyrocatechol (EDP) (faster etching) have some disadvantages from the environmental viewpoint (toxic), the primary advantage in their widespread use is their much improved selectivity of Si etch rate compared with that of SiO_2, being 100 times more selective than KOH. EDA and EDP also act as excellent p-type etch stops, with the etch rate at a boron concentration $1 \times 10^{19}/cm^3$ being about 140 times larger than at $1 \times 10^{20}/cm^3$. EDP is a superior p+ etch-stopping system. The anisotropic etching between {100} and {111} is in the order of 25:1, which is very low compared to that of KOH etchants [50]. Tetramethyl Ammonium Hydroxide (TMAH) is used more nowadays due to its following advantages:

- Adequate anisotropy [51]
- Lower toxicity than EDP [16]
- High selectivity for Si relative to oxide [51]
- Availability in high purity form [10]
- Common availability due to its use as a positive photoresist developer [10]

TMAH is less favored for use with a p-type etch stop as its p-type stop ratio at $1 \times 10^{19}/cm^3$ and $1 \times 10^{20}/cm^3$ is only 5. It is found that even various additives like H_2O_2 do not improve the p-type selectivity of TMAH. During etching of Si in TMAH, EDP in particular composition ranges and also in KOH water compositions below about 18 wt%, formation of pyramidal hillocks has been observed [12, 50]. Most of the organic hydroxides appear to have this problem significantly. NH_4OH acts also as an anisotropic etchant apart from its primary usage as a cleaning agent for Si, many researchers have used NH_4OH as an anisotropic etchant. It is available in high levels of purity.

Due to the overall advantages of TMAH, it is being widely used as an anisotropic etchant.

2.6 Etchant Conditions

Etch behavior of all of the above mentioned wet chemical anisotropic etchants with or without additives is affected by the physical and chemical conditions of the etchant. Etching with a particular concentration of etchant at different temperatures result in completely different anisotropic etch behavior [28, 48, 49]. And different etchant concentrations result in totally different anisotropic results [22, 48, 49, 53]. Researchers have observed that stirring the liquid etchant during the etch impacts the etch properties [28, 54].

2.7 Additives to Etchants

Different alkaline etchants have different etching characteristics and selectivities, depending on the chemical compositions and temperature. Some times additives are added to the etchant to change both the etch rate and selectivity. Different compositions can produce different desired effects. Few examples of additives used are pyrazine: a small amount of pyrazine is added with EDP. iso-propyl alcohol: IPA is used with TMAH to change the etch rates [16, 55]. Low etching of Al in TMAH occurs when excess Si is added in TMAH, which proves to be beneficial in CMOS compatible etching [32].

2.8 Selectivity of etchant

Selectivity is defined as the ratio of the etch rates of the desired direction to those of the undesired. So, the higher the selectivity, the better defined the geometry. This makes the study of etch-rates of all directions vital. In general the etch-rate is slowest in the <111> directions. Many researchers have provided such selectivity data about the common planes {100}, {110} and {111} [28, 32, 48, 49]

Selectivity of the masking materials is also very important [51]. Most common mask-

ing layers are silicon oxide or silicon nitride [28, 33]. Most anisotropic etchants discussed exhibit very low etch-rates on silicon oxide and silicon nitride, this makes these materials very good masking material during anisotropic etching. Selectivity between various planes and selectivity between masking material and silicon planes are very vital information that are required to design and etch MEMS devices. For example, the thermal oxide (SiO_2) mask etch rate is ten times lower in TMAH than that of KOH (high selectivity). This makes TMAH a better etchant. However, the {100}/{111} etch rate ratio of TMAH is somewhat lower than that of KOH, which is an advantage for KOH over TMAH [51].

2.9 Etch Mechanisms

The anisotropic etching of crystallographic silicon can be *VERY ROUGHLY* explained with the density of dangling bonds on the various planes [21, 47]. Considering the low index planes, the densities of dangling bonds on silicon (and other diamond structures) or the dangling bond densities on the planes can directly be related to the etch differences. The dangling bond densities on different orientations are 1.36×10^{15}, 0.96×10^{15} and 0.78×10^{15} cm^{-2} on the {100}, {110}, and {111} planes respectively [19, 38]. The ratios are 1:0.71:0.58 for {100}:{110}:{111} respectively, this can explain the case when the ER {100} > ER{110} > ER{111}. And in all etch cases, the {111} plane is found to have the slowest etch-rate, this can be directly related to the available bond density of the {111} plane. In the same argument, the {100} plane should etch the fastest and then the {110} plane. This is true in most of the cases [12, 32], but there are cases where the {110} etches faster than the {100} plane [12, 21, 28]. In all cases the {111} plane etches slower than the {100} and {110} planes [21, 28, 32, 35, 36, 49]

There is also simple reasoning based on the oxidation rates of the various planes. The oxidation rates of the three major low index planes fall in the order; {111} > {110}> {100}. During wet chemical etching, SiO_2 is formed on the silicon due to the chemical reaction. Such oxides grow faster on the {111} plane than the {110} or the {100} plane.

From the well known fact that the etchants have a high silicon to oxide selectivity [28, 33], we can come the conclusion that the etch rates will follow {111} < {110} < {100}.This matches with the reasoning based on the bond densities, but still fails to explain the experimental results where ER{100} < ER{110} [12, 21, 28]. The following section presents some of the other etch models proposed by some researchers.

2.9.1 Oxidation Dissolution Model

The "working hypothesis" by Kendall [56] explains the etching of {100} and {110} planes faster than {111} planes in KOH:water solutions. It is stated that rapid oxidation of {111} compared to the other planes block the etching of these planes. This is consistent with the etching data on thermal SiO_2 and on Si{111} at 85° C. It is apparent that the etch rates on the three planes show much larger differences than the available bond densities, so the bond densities alone cannot explain these large differences in the etch rates, hence this simple "working hypothesis" was developed based on the fact that the {111} planes oxidize much faster than the other planes. The oxidation rate difference is more prominent at lower temperatures (room temperatures) than the regular oxidation temperatures of > 900° C. Mostly all etches are done at low temperatures, at room temperature or less that 90° C. So while etching the {111} surface, it is said to be almost instantaneously covered with a SiO_2 film (hydrated silicon oxide) during etching. This passivates the {111} plane and blocks its subsequent dissolution. Hence in this simple model, the etch rate is limited by the dissolution of the silicon oxide film and thus explains the slower etch rate of {111} planes.

2.9.2 Hydration Model

This model, developed by Kendall [19] and Glembocki et al. [57, 58], proposes that the hydration complexes of K^+ and OH^- are the dominant factor and the {111} is blocked from etching by an inactive complex. Anisotropic etching is explained with the water

hydration of the OH^- ion along with a sort of geometrical hindrance of the {111}. Although these works explain the etching on a KOH system, this model should be applicable for all alkaline etchants, including TMAH. The model also proposes that the etch rates of other planes should drop to zero when the etch solution is saturated with KOH. The model quantitatively substantiates from the observation that the etch rate of Si on the {100} and {110} has a distinct maximum at about 22 wt% KOH, and the fact that the etch rate falls to near zero near the solubility limit of KOH in water. This phenomenon can be observed in TMAH etches, where the etch rates are drastically higher at lower concentrations (5wt% TMAH), when compared to high concentration etch (25wt%) [32, 21].

The hydration model is based on the reaction below, and uses literature values of chemical activity of water in KOH to obtain hydration numbers of K^+ and OH^- ions in KOH or the equivalent values for other hydroxides.

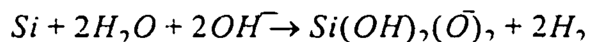

$$Si + 2H_2O + 2OH^- \rightarrow Si(OH)_2(O^-)_2 + 2H_2$$

The etch rate is related to the hydration number; higher hydration numbers result in faster etching. The mean hydration number is 5 at low concentrations of KOH and is 3 at 50% KOH [19]. This explains the slow etch rates at higher concentrations.

2.9.3 Electrochemical Model

This model was suggested by Seidel et al [59]. In this model, the etching process is said to occur in two steps. The first one is an oxidation where four hydroxide ions react with one surface Si atom and results in the injection of four electrons into the conduction band. The second step is reduction, in which the injected electrons react with water molecules to form new hydroxide ions and hydrogen. The anisotropy property is explained as being due to the small differences of the energy levels of the back bond surface states as a function of the crystal orientation. The geometrical explanation of the "energy levels of the back bond surface states" should be precise enough for this model to be applied to

explain the anisotropy of etching. Also, the Seidel model involving the inverse fourth power of water concentration (and OH to the 0.25 power), does not agree with the experimental data at either low or high concentrations [50]. Apart from the atomic details of the surfaces, the anisotropic etching depends also mainly in the chemical activity of the reactants. Nevertheless, it is the atomic details of the surfaces that determine the actual rates of dissolution of the various Si surfaces.

2.9.4 Crystallographic Model

All of the above explained models explain/model the etch rate differences in certain conditions and are not able to fully explain the anisotropic etch behavior. This makes it necessary to look into other means of modeling, the crystallographic modeling. This crystallographic modeling in this work tries to explain the etch anisotropy with the crystallographic structures of the planes being etched. This is the main topic of this work and the later chapters model the etch based on the silicon crystal structure and compares the derived model to the experimental data collected in this work.

CHAPTER 3

Atomic Modeling

In order to study in detail the mechanisms of anistropic etching it is necessary to study the etching of different crystallographic planes. Hence this work uses both Si{100} and Si{110} for the study. Si{110} is the focus because it exposes a wider variety of crystallographic features, as will be explained in this Chapter.

3.1 Types of Atomic Structure

This work explores the etch mechanism in silicon by considering two basic atomic structures, *kinks* and *periodic-bond-chains*. A ***kink*** is defined as an atom which has two dangling bonds free to interact with the etchant, and two bonds to the bulk silicon below the etch front (two back bonds). A ***Periodic-Bond-Chain*** (PBC), is defined as being made up of a sequence of atoms, each having one dangling bond free to interact with the etchant, one back bond and two bonds to other atoms having the same configuration (in other words not back bonds) [12, 19, 23, 38]. The kink and PBC structures are shown in Figures 3.1 and 3.2 respectively.

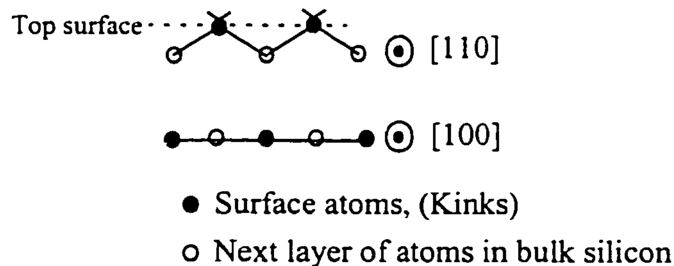

Figure 3.1: Kink structure

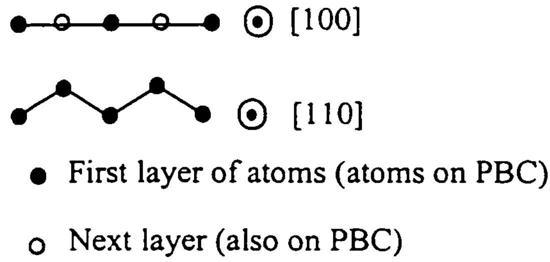

Figure 3.2: PBC structure

The surface made only by kinks is a {100} plane and the surface made only by the PBC's is a {110} plane. When studying anisotropic etching, the etch characteristics are usually represented by the ratio of {100} to {110} etch rate. As reported by many researchers the etch-rate ratio {110}/{100} is greater or less than unity [12, 21, 28, 32, 60]. This depends on many factors such as the etchant, etchant concentration, temperature, etch conditions (stirring), and any additives to the etchant. TMAH is the etchant used in this study due to its advantages stated over the other silicon etchants as described in Chapter 2.

Studying the etch mechanism of simple structures, kinks and PBC's will lead to a model to explain the anisotropic etching. This leads us to select {100} (kinks) and {110} (PBC) silicon substrates for the etch experiments. Etch experiments were done on both {100} and {110} silicon for different concentrations of TMAH (25, 19, 17, 15, 12 and 9wt%) at 80° C, and the etch rates, under-etched-surface angles and roughness were studied. These were then compared to the theoretical analyses that are done in this Chapter, and the kink and PBC removal frequencies are calculated.

3.2 Steps on a Flat Plane

This analysis begins with a simple model of etching based on the movements of steps [21]. Figure 3.3 depicts an etching surface defined by steps on a flat plane. The step-advance-width s is defined as the distance of the minimum identifiable unit that a step advances. The flat plane is represented by the line pq and the other lines parallel to it. The step-height h is defined as the spacing between two flat planes. The angle θ is defined as the angle between the flat plane pq and the etching surface composed of the steps. A similar work has been presented by M. Elwenspoek [61].

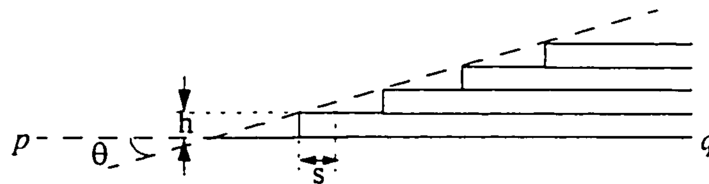

Figure 3.3: Simple steps on a flat plane, showing the step width, s and step height h.

Assuming that in a unit of time ($1/f$) the etch propagates by one step-advance-width on each step (all steps simultaneously), the etch rate ER(θ), could then be calculated by

$$ER(\theta) = s(\sin\theta)f \quad \text{(Eq 3.1)}$$

3.3 Silicon: Steps on a {111} Plane

In silicon, the obvious flat planes are {111} planes due to its high atomic density. The {111} plane is shown in Fig. 3.4. The Fig. 3.4 shows the specific [111] direction as a reference for the coordinate system and planes discussed in the analysis. Given this choice of (111) plane, one must also specify the orientation of the steps with respect to the crystal lattice. Again, there is an obvious choice, <110>-directed lines, since these define the intersections between most pairs of low-index planes:

- pairs of {111} planes.
- any {111} plane and any {110} plane.
- any {111} plane and any {100} plane.

Also, PBC's extend in <110> directions, providing readily identifiable steps, as seen in Figs. 3.4 - 3.12. The step-advance width, s, and inter-plane height, h, are shown. Assuming that there is an average step removal frequency f_s (#/time), the etch-rate as a function of angle is given by $ER(\theta) = (f_s) \times (s) \times \sin\theta$

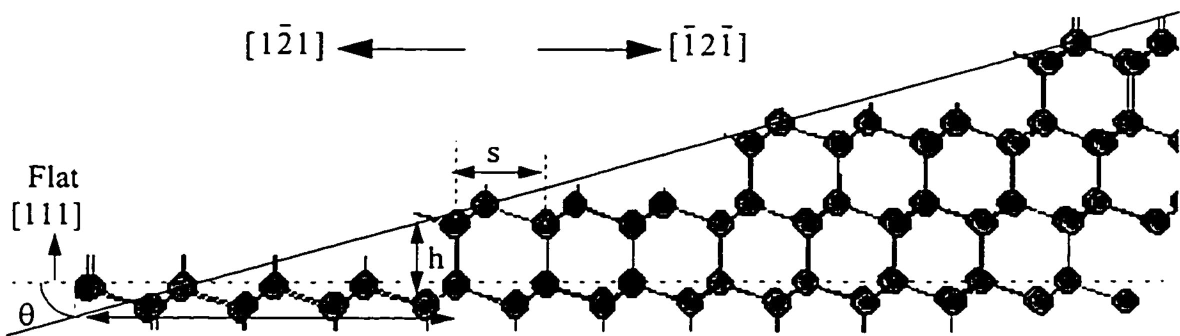

Figure 3.4: Steps on a (111) plane, and illustration of crystallographic step-width and step-height.

3.3.1 Step height:

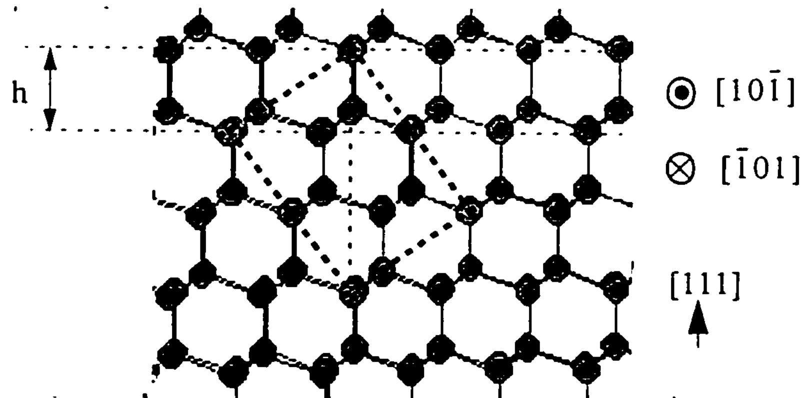

Figure 3.5: Step-height, visualized in a conventional unit cell of silicon crystal lattice.

The step-height, h, can be visualized and calculated by properly orienting a conventional unit cell of the silicon crystal lattice. Since this view is in a <110> direction, specif-

ically the $[\bar{1}01]$ direction in this diagram, the view is from one edge of the conventional unit cell, and the appropriate orientation is shown by the overlaid rectangle in Figure 3.5. Figure 3.6 aids further in showing that h is one third of the body diagonal of the unit cell. Thus

$$h = \frac{\sqrt{3}a}{3} = 0.577a = 3.1133\overset{o}{A} \qquad \text{(Eq 3.2)}$$

where is $a = 5.43\overset{o}{A}$ the silicon lattice constant.

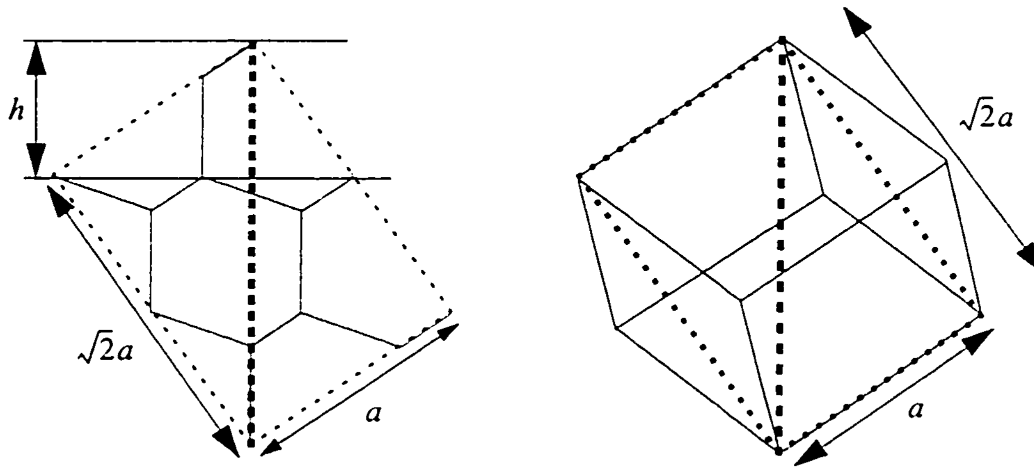

Figure 3.6: Body diagonal of silicon unit cell, to calculate the step-height.

3.3.2 Step width

Similarly, the step advance width, s, can be visualized and calculated to be half the distance PQ in Figure 3.7. The step advances in the $[\bar{1}2\bar{1}]$ direction by removal of groups of atoms (see Figure 3.10). From Figure 3.7, the step-width is half of the distance PQ, hence

$$s = \frac{\sqrt{3/2}}{2}a = 0.61a = 3.3123\overset{o}{A} \qquad \text{(Eq 3.3)}$$

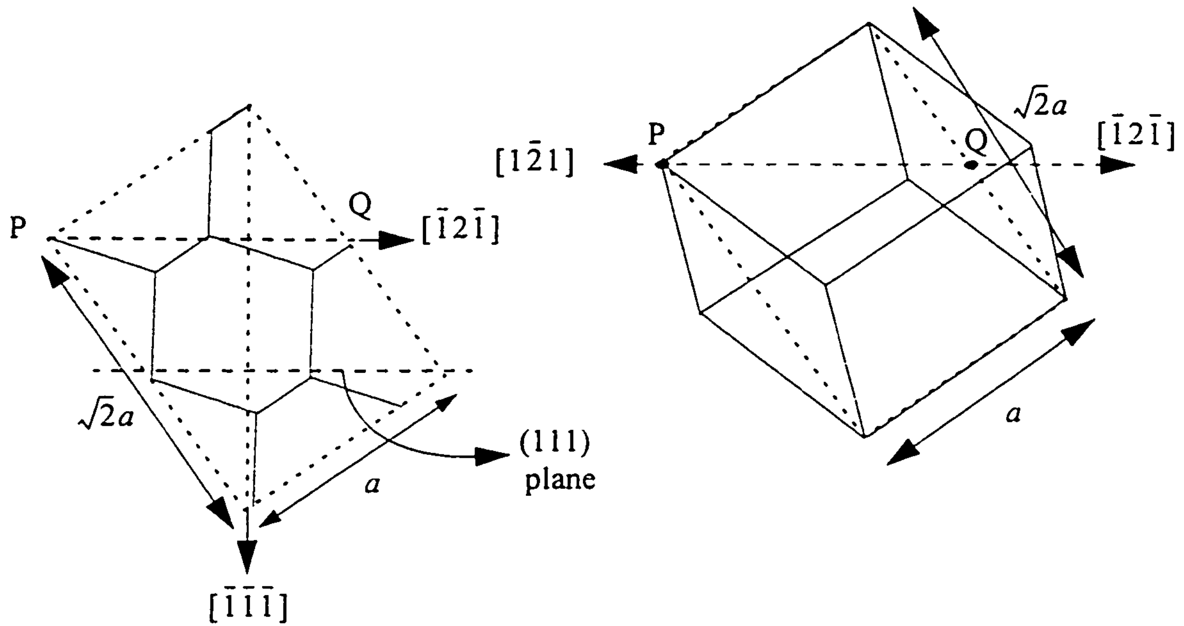

Figure 3.7: Schematics of the silicon unit cell, to calculate the step-width.

3.4 Types of steps

There are two types of steps that can be considered with respect to a flat {111} plane. In this work they are called "PBC-defined" (Periodic-bond-chain-defined) and "Kink-row" defined. Figure 3.8 shows these two types of steps with respect to the (111) plane. Here, the PBC-defined plane is the (212) plane and the kink-row defined plane is the (121) plane. A similar configuration of planes are presented by J. G. E. Gardeniers [38].

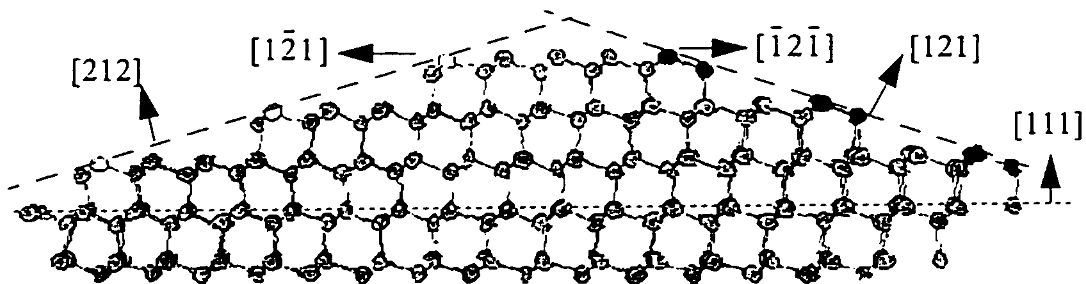

Figure 3.8: Two types of steps with respect to the flat [111] plane: The PBC-defined plane is [212] and Kink-row defined plane is [121].

As a special case, where the PBC-defined plane is the (101) plane, and the Kink-row defined plane is the (010), is shown in Figure 3.9. This figure shows the maximum density of intact PBC's on the (101) plane and the maximum density of intact kinks on the (010) plane.

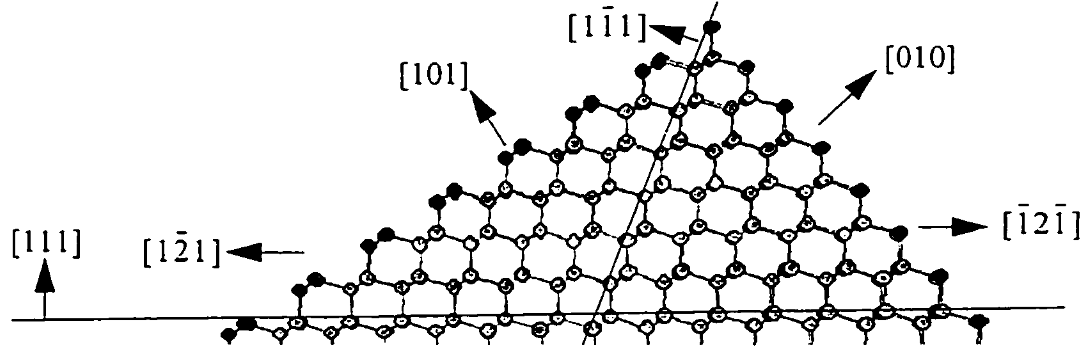

Figure 3.9: Special case where the PBC-defined plane is (101) and the kink-row defined plane is (010).

3.5 Calculation of Etch-Rate

Using the above definitions and calculations, the etch rates of the PBC and Kink-defined planes can be given by:

PBC-defined planes:

$$ER_P = s \times a \times f_P \times \sin\theta_P = 3.3123\mathring{A} \times f_P \times \sin\theta_P \qquad \text{(Eq 3.4)}$$

Kink-defined planes:

$$ER_K = s \times a \times f_K \times \sin\theta_K = 3.3123\mathring{A} \times f_K \times \sin\theta_K \qquad \text{(Eq 3.5)}$$

3.5.1 Assumptions

In order for the above relations to hold, several assumptions must be applicable.

(1) Each PBC on the etch-front plane must be removed mostly as a unit, before the next one is removed. This situation is depicted in Figure 3.10. PBC A must be entirely removed before PBC B is attacked, and PBC B must be removed before PBC C is attacked.

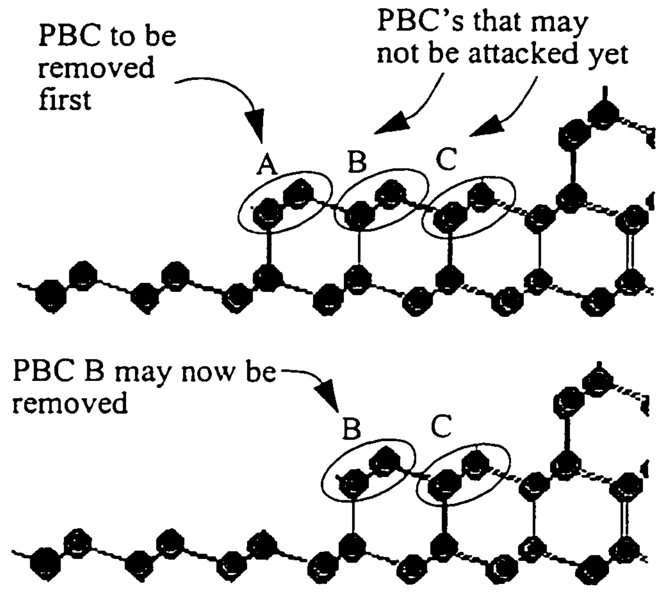

Figure 3.10: Illustration of sequential exposure of PBC's to attack by the etchant. First A is attacked, then B.

(2) Assumption (1) implies that the rate of removal of a kink on a PBC must be much greater than the rate of formation of new kinks on a previously intact PBC. These concepts are illustrated in Figure 3.11.

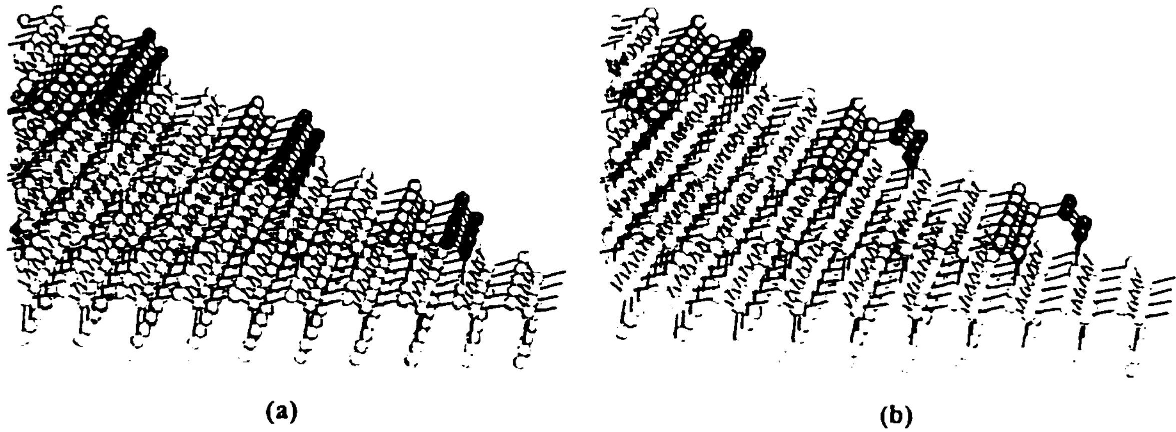

Figure 3.11: Crystallographic illustration to show that the kink-row removal rate on a PBC is much greater than the formation rate of new kinks on a previously intact PBC.

(3) In order for $ER(\theta_K)$ to hold, entire rows of kinks must be mostly removed before the next row of kinks is attacked. This situation is depicted in Figure 3.12.

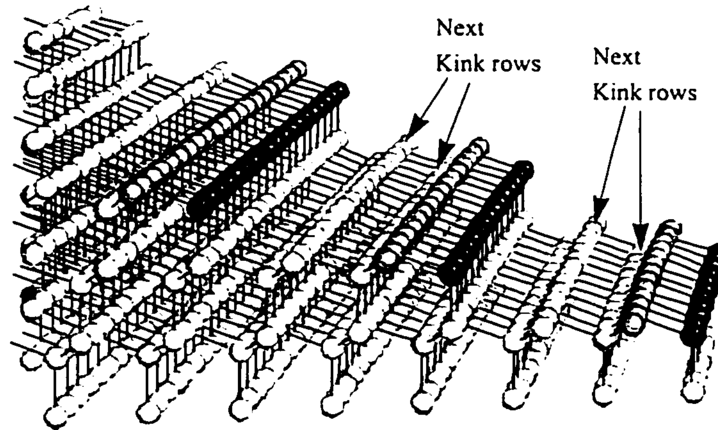

Figure 3.12: Crystallographic illustration to show most of the kinks in a row has to be etched before the next row of kinks can be attacked.

While the assumptions in (1) and (2) above are intuitively plausible, since the kink on the PBC has a greater number of dangling bonds than an atom on an intact PBC (2 dangling bond vs. 1 dangling bond). However, assumption (3) is not intuitively obvious. In this idealized model, each kink in a kink-row can be reasonably assumed to be independent of others. Thus the requirement that they all be removed in a row is not clear. However, the experimental data in Chapter 5 will show empirically that there are enough experimental cases where this assumption must hold, to validate its inclusion in this model.

It should also be noted that the removal of PBC's and kink-rows in a row-by-row manner is highly idealized. In reality the the atoms are removed randomly according to probabilities determined by the chemical interaction with the etchant. Thus, these assumptions correspond to much higher probabilities of atom removal from a given kink-row or pbc, once at least one atom has already been removed.

The plots in Figure 3.13 show what $ER(\theta_K)$ and $ER(\theta_P)$ would be, based on these simplistic assumptions. f_K refers to the rate of removal of kink-row and f_P refers to the rate of removal of entire PBC's (in # of removals per hour).

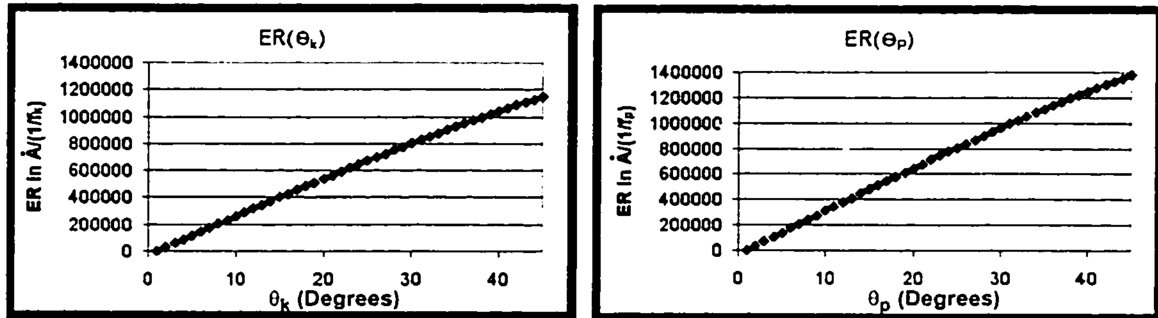

Figure 3.13: $ER(\theta_K)$, for f_k = 5e+5 #/hr and $ER(\theta_P)$, for f_p = 6e+5 #/hr

3.6 Pairs of {111} Planes in {100} and {110} Silicon Wafers

3.6.1 {111} Planes and <110> Lines

In Section 3.5 above, the etch rates are modeled as a function of angles, θ, away from a flat {111} plane, where the planes are defined by intact PBC's or kink-row. These intact PBC's and kink-rows extend in <110> directions (e.g. $[10\bar{1}]-[\bar{1}01]$ in Figures 3.4 - 3.12). The planes made from intact PBC's have Miller Indices of the form {hhk} where h > k. The planes made from kink-rows have Miller indices of the form {hkk} where h > k. These planes correspond to rotations away from a {111} plane around a <110> axis by an angle θ_P or θ_K.

There are several different {111} planes in the silicon crystal structure. Each one can potentially serve as flat plane to which θ can be referenced. The orientation of these {111} planes with respect to the actual wafer surface is of critical importance in understanding the etch behavior.

Figures 3.14 (a), (b), (c) and (d) show the {111} planes in the case where the silicon wafer surface is the (100). The $(111), (1\bar{1}1), (11\bar{1})$ and $(1\bar{1}\bar{1})$ are inclined at 54.7° to the horizontal (100) top wafer surface [9], while the opposite planes, $(\bar{1}\bar{1}\bar{1}), (\bar{1}1\bar{1}), (\bar{1}\bar{1}1)$ and $(\bar{1}11)$, are inclined at 125.3° to the (100). The 54.7° inclined planes are those commonly seen bounding etched cavities on (100) silicon. The inverted 125.3°-inclined planes are also seen experimentally, but seldom.

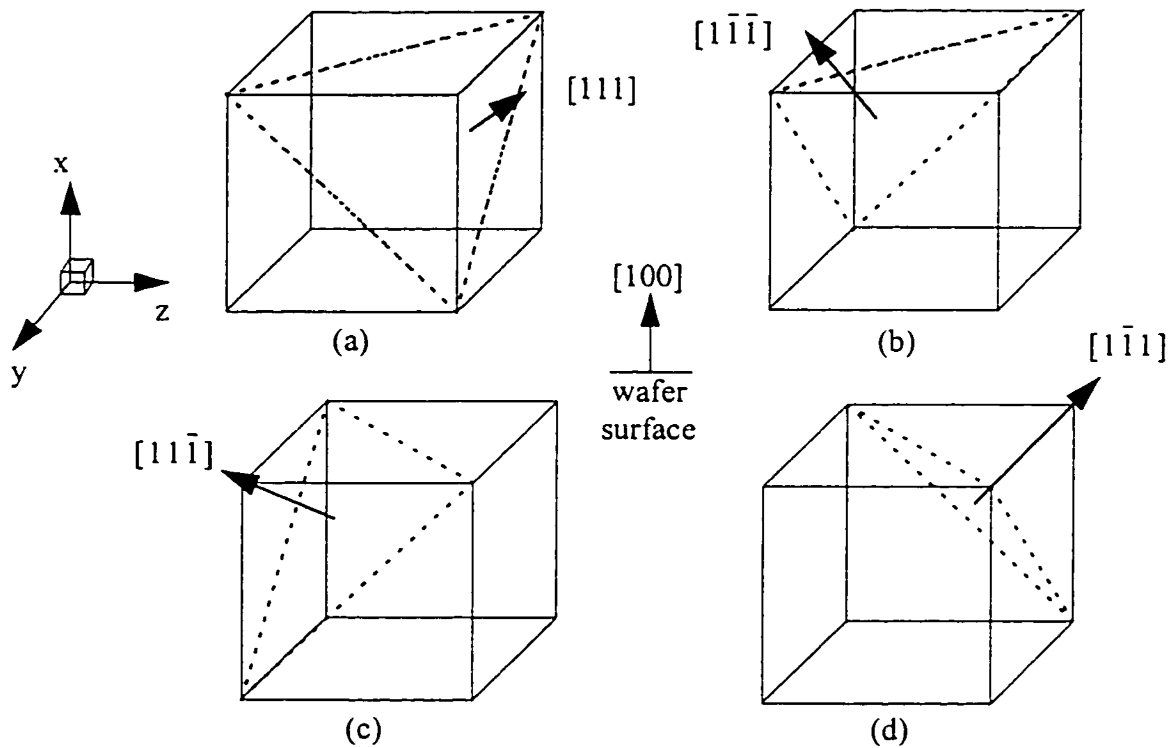

Figure 3.14: {111} planes in the Si cubic conventional unit cell, assuming a (100) top wafer surface.

3.6.2 Pairs of {111} Planes with <110> Intersection Lines

Figures 3.15 (a), (b), (c) and (d) show the {111} planes in the case where the wafer surface is the (110). The four vertical (90°-inclined) planes, $(\bar{1}11), (1\bar{1}1), (\bar{1}1\bar{1}), (1\bar{1}\bar{1})$ represent those commonly found bounding parallelogram-shaped cavities in {110} silicon. The (111) and $(11\bar{1})$ are inclined at 35.3° to the horizontal, and are also commonly found.

The $(\bar{1}\bar{1}\bar{1})$ and $(\bar{1}\bar{1}1)$ in this system are 144.7° inclined (inverted), and are very rarely seen in silicon micromachining.

In this work, it is found to be most convenient and useful to consider pairs of $\{111\}$ planes, along with an intersection line in the <110> direction. These intersection lines are described by a pair of opposite directions, for example $[10\bar{1}]-[\bar{1}01]$ in Figure 3.5. Thus, the particular system described in Figures 3.4-3.12 is the $(111)-[10\bar{1}]-[\bar{1}01]-(1\bar{1}1)$, identifying the pair of $\{111\}$ planes and the intersection line.

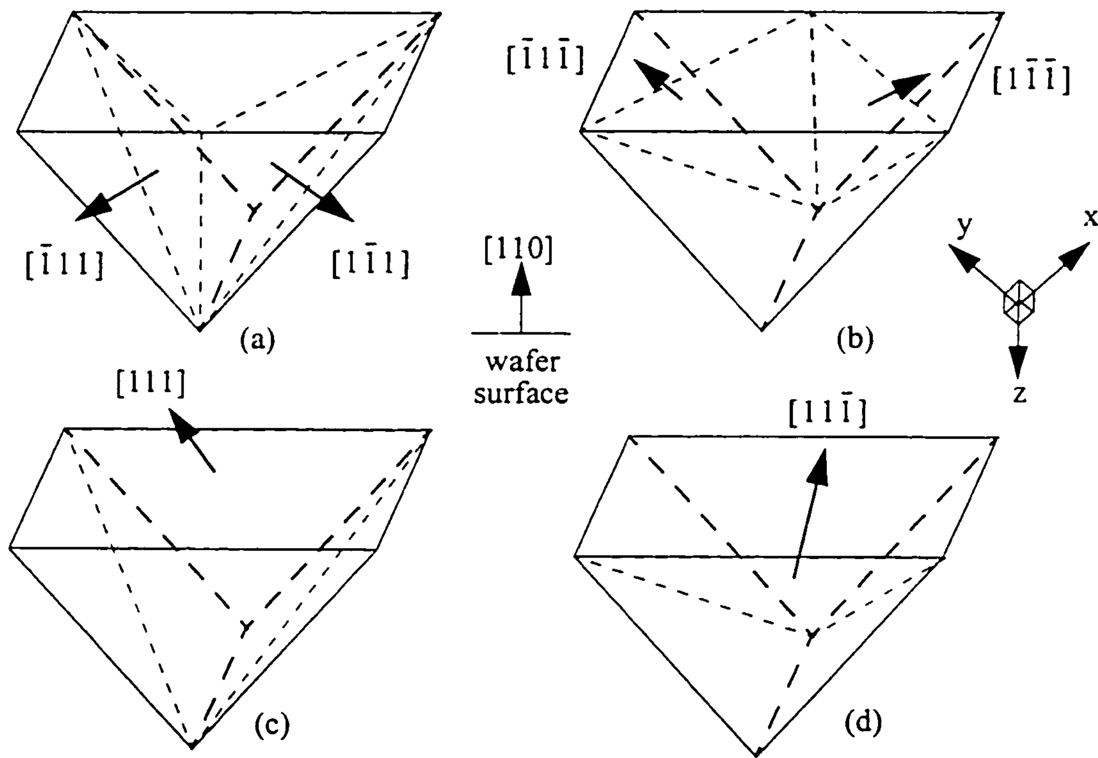

Figure 3.15: {111} planes in Si cubic conventional unit cell, assuming a (110) top wafer surface.

In (100) wafers, one type of relevant pair is shown in Figure 3.17. This is the $(111)-[1\bar{1}0]-[\bar{1}10]-(11\bar{1})$ pair, illustration on Figure 3.16 shows how this pair is obtained from the model cube. The $[1\bar{1}0]-[\bar{1}10]$ line is indicated as a PBC in Fig 3.17.

The other common pairs are:

- $(1\bar{1}1)-[110]-[\bar{1}\bar{1}0]-(1\bar{1}\bar{1})$
- $(1\bar{1}\bar{1})-[101]-[\bar{1}0\bar{1}]-(11\bar{1})$
- $(111)-[10\bar{1}]-[\bar{1}01]-(1\bar{1}1)$

These three pairs are crystallographically equivalent to the pair shown in Figure 3.17 because all of the {111} planes are 54.7° inclined, and all of the <110> lines are inclined at 45° to the horizontal wafer surface.

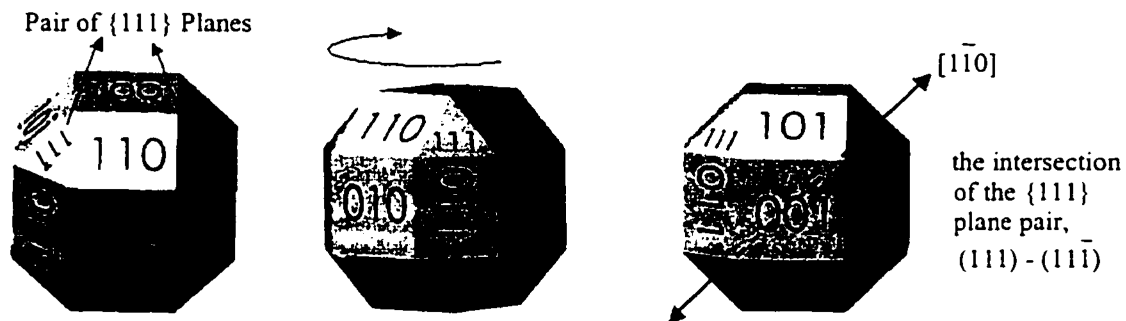

Figure 3.16: Illustration on the pair of {111} planes and their <110> line of intersection.

As outlined in Sections 3.3 and 3.6.1, particular planes between the two {111} planes in a pair can be achieved using rotations of angles θ_P and θ_K around the associated intersection <110> line. For example in the $(111)-[1\bar{1}0]-[\bar{1}10]-(11\bar{1})$ system, these rotated planes will intersect the top (100) surface on a line whose orientation varies between AB and BC. This will be discussed in more detail in Section 3.6.3.

There are four more pairs of {111} planes in the {100} wafer system, they are

- $(11\bar{1})-[011]-[0\bar{1}\bar{1}]-(\bar{1}1\bar{1})$
- $(111)-[0\bar{1}1]-[01\bar{1}]-(\bar{1}11)$
- $(1\bar{1}1)-[0\bar{1}\bar{1}]-[011]-(\bar{1}\bar{1}1)$
- $(1\bar{1}\bar{1})-[0\bar{1}1]-[01\bar{1}]-(\bar{1}\bar{1}\bar{1})$

In each of these pairs the intersection line is a <110> line which is horizontal in the (100) coordinate system. These are not relevant to the present analysis because with these

pairs, full rotation of θ_P, θ_K, from one $\{111\}$ to the other, does not change the orientation of the intersection with the (100) wafer surface.

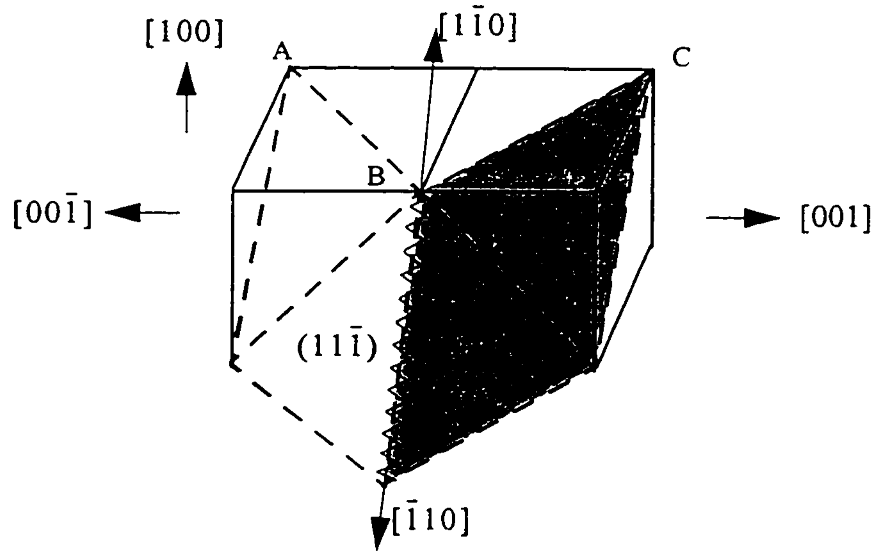

Figure 3.17: A pair of {111} planes in (100) silicon. Note that the cubic grid no longer represents a single conventional unit cell, rather, it represents many unit cells, to illustrate the periodic bond chain along the line $[\bar{1}10]-[1\bar{1}0]$.

In (110) wafers, there are three main types of relevant pairs of $\{111\}$ planes [9]. They are illustrated in Figures 3.18 (a), (b) and (c). The left of Figure 3.18(a) shows that the conventional cubic grid is tilted so that the (110) plane is horizontal, to represent the (110) wafer surface. At the right of Figure 3.18(a), two $\{111\}$ planes are shown to be vertical in this coordinate system. They intersect with an angle of 70.6° at a vertical <110> line. This is the case of $(\bar{1}11)-[110]-[\bar{1}\bar{1}0]-(1\bar{1}1)$. The convex intersection of these two planes as shown is (ideally) a kink-row.

In Figure 3.18(b), two vertical $\{111\}$ planes intersect at an angle of 109.4° at a vertical <110> line. In this case it is the pair $(1\bar{1}1)-[110]-[\bar{1}\bar{1}0]-(1\bar{1}\bar{1})$. The convex intersection of these planes is (ideally) an intact PBC.

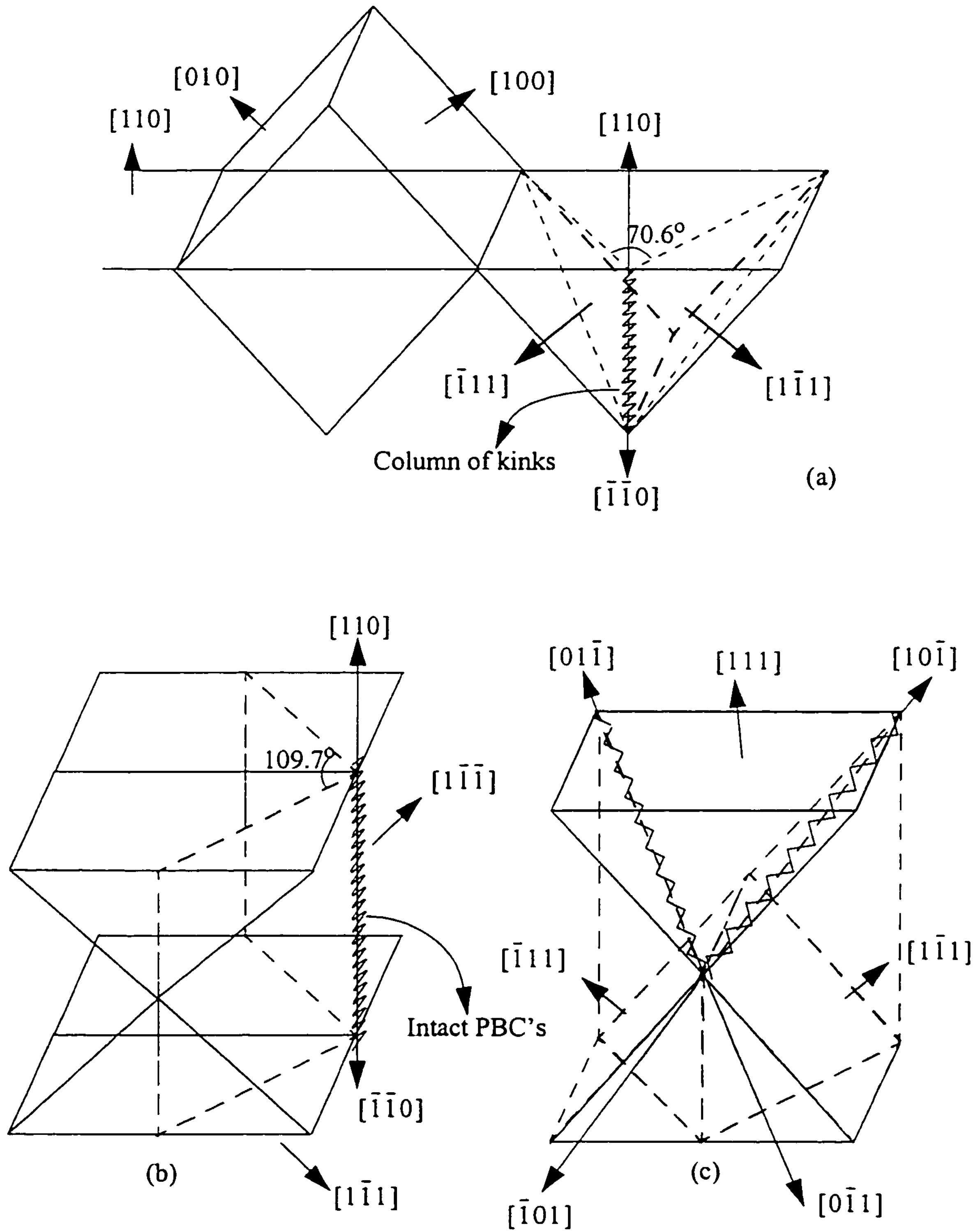

Figure 3.18: Types of relevant pairs of {111} planes in (110) silicon.

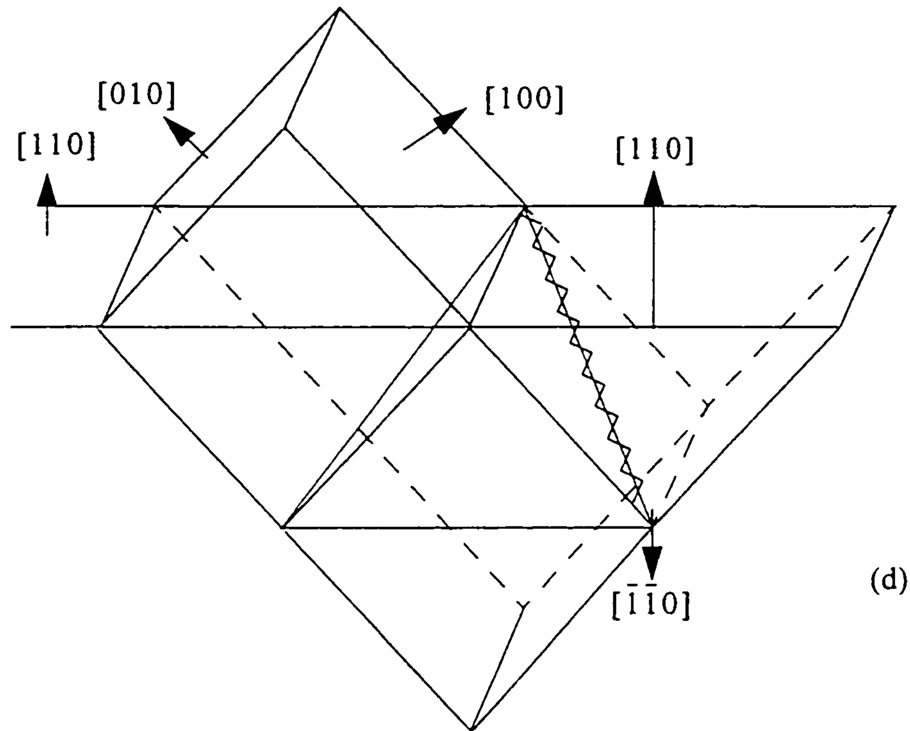

Figure3.18: Types of relevant pairs of {111} planes in (110) silicon.

In Figure 3.18(c), vertical {111} planes intersect a 35.3°-inclined {111} at a <110> line which is inclined at 30° to the wafer surface. The two intersections depicted are composed of intact PBC's. There are four equivalent pairs of this type. In this coordinate system, they are

- $(111)-[01\bar{1}]-[0\bar{1}1]-(\bar{1}11)$
- $(111)-[10\bar{1}]-[\bar{1}01]-(1\bar{1}1)$
- $(11\bar{1})-[011]-[0\bar{1}\bar{1}]-(\bar{1}1\bar{1})$
- $(11\bar{1})-[101]-[\bar{1}0\bar{1}]-(1\bar{1}\bar{1})$

In Figure 3.18(d), the same planes are depicted as in Figure 3.18(c), but they are arranged such that the intersections are kink-rows instead of PBC's. In this case, the pairs of planes will be related to those listed above, but the plane rotations will pass through 45°-inclined {100} planes (kinks) instead of {110} planes (PBC's). In particular, the 45°-inclined {100} planes corresponding to each of the relevant pairs of planes are listed here:

- $(111)-[01\bar{1}]-[0\bar{1}1]-(1\bar{1}\bar{1})$ (100)
- $(111)-[10\bar{1}]-[\bar{1}01]-(\bar{1}1\bar{1})$ (010)
- $(11\bar{1})-[011]-[0\bar{1}\bar{1}]-(1\bar{1}1)$ (100)
- $(11\bar{1})-[101]-[\bar{1}0\bar{1}]-(\bar{1}11)$ (010)

There is another pair of {111} planes, the $(111)-[\bar{1}10]-[1\bar{1}0]-(\bar{1}\bar{1}1)$, in which the intersection line is horizontal. As in the (100)-wafer case, this is not considered relevant to the present analysis because full rotation of θ_P and θ_K does not change orientation of the intersection with the (110) wafer surface.

In Figure 3.18(d), a 35.3°-inclined {111} plane intersects a 45°-inclined {100} at a <110> line. There are four equivalent pairs of this type. In this coordinate system, they are

- $(111)-[01\bar{1}]-[0\bar{1}1]-(100)$
- $(111)-[10\bar{1}]-[\bar{1}01]-(010)$
- $(11\bar{1})-[101]-[\bar{1}0\bar{1}]-(010)$
- $(11\bar{1})-[011]-[0\bar{1}\bar{1}]-(100)$

3.6.3 Pairs of {111} Planes and Under-Etched Planes

As described above in Section 3.6.2, particular planes in between each pair of {111} planes can be achieved using rotations of angles θ_P and θ_K around the associated intersection line. These rotated planes will intersect the top wafer surface on a line. The variation of orientations of these lines will be determined by the geometrical attitude of the pair of {111} planes to the wafer surface.

These intersection lines of planes with the wafer surface will correspond to mask-edge angles in the analysis of under-etch data. The planes defined by particular rotations of θ_P and θ_K in a given system will correspond to the under-etched plane surfaces observed.

For example, it was mentioned in Figure 3.17 for (100) planes, that the rotated planes will intersect the top surface on a line whose orientation varies between lines AB and AC. The deviation angle in the (100) plane will vary analytically with the rotation angle, θ.

In the case of (100) wafers, there is only one relevant type of pairs of planes, those depicted in Figure 3.17. Associated with this type of pair, the inclination angle can vary from 54.7° through 45° and back to 54.7°, if θ_P is used. Or it can vary from 54.7° through 90°, then to 125.3°, if θ_K is used. Alternatively it can vary from 125.3° through 135° and back to 125.3°, if θ_P is used. Finally, it can vary from 125.3° through 90° to 54.7°, if θ_K is used. All of these rotations in Figure 3.17 are done around the line $[1\bar{1}0]-[\bar{1}10]$.

The above defined planes are represented with the following shorthand notation for later use in this thesis:

- **P-54-45-(54)**

  . $(11\bar{1})-[1\bar{1}0]-[\bar{1}10]-(111)$, the convex case most-easily seen in Figure 3.17.

54° Inclined Plane	45° Inclined Plane	54° Inclined Plane
(111)	(101)	$(1\bar{1}1)$
$(1\bar{1}1)$	$(1\bar{1}0)$	$(1\bar{1}\bar{1})$
$(1\bar{1}\bar{1})$	$(10\bar{1})$	$(11\bar{1})$
$(11\bar{1})$	(110)	(111)

- **P-126-135-(126)**

  .$(\bar{1}\bar{1}1)-[1\bar{1}0]-[\bar{1}10]-(\bar{1}\bar{1}\bar{1})$ the concave underside of the two planes shown in Figure 3.17

126° Inclined Plane	135° Inclined Plane	126° Inclined Plane
$(\bar{1}11)$	$(\bar{1}01)$	$(\bar{1}\bar{1}1)$
$(\bar{1}\bar{1}1)$	$(\bar{1}\bar{1}0)$	$(\bar{1}\bar{1}\bar{1})$
$(\bar{1}\bar{1}\bar{1})$	$(\bar{1}0\bar{1})$	$(\bar{1}1\bar{1})$
$(\bar{1}1\bar{1})$	$(\bar{1}10)$	$(\bar{1}11)$

- **K-54-90-(126)**

  . $(11\bar{1})-[1\bar{1}0]-[\bar{1}10]-(\bar{1}\bar{1}\bar{1})$ from the $(11\bar{1})$ to the underside of the (111)

54° Inclined Plane	90° Inclined Plane	54° Inclined Plane
(111)	(001)	$(\bar{1}\bar{1}1)$
$(1\bar{1}1)$	$(0\bar{1}0)$	$(\bar{1}\bar{1}\bar{1})$
$(1\bar{1}\bar{1})$	$(00\bar{1})$	$(\bar{1}1\bar{1})$
$(11\bar{1})$	(010)	$(\bar{1}11)$

- **K-126-90-(54)**

  . $(\bar{1}\bar{1}1)-[1\bar{1}0]-[\bar{1}10]-(111)$ from the underside of the $(11\bar{1})$ to the (111)

126° Inclined Plane	90° Inclined Plane	54° Inclined Plane
$(\bar{1}11)$	(001)	$(1\bar{1}1)$
$(\bar{1}\bar{1}1)$	$(0\bar{1}0)$	$(1\bar{1}\bar{1})$
$(\bar{1}\bar{1}\bar{1})$	$(00\bar{1})$	$(11\bar{1})$
$(\bar{1}1\bar{1})$	(010)	(111)

The above notation has the form t-r-m-s, where: t is the type of microscopic feature defining the plane: P represents PBC's, K represents kinks. r is the inclination angle of the reference plane for the rotation by θ, this is the inclination angle with respect to the horizontal wafer surface. m is the inclination angle of the rotated plane midway between the pair of {111} planes. s is the inclination angle of the second (non-reference) {111} plane.

In the above notation, the angle s is parenthesized to indicate that the original reference of the rotation may be important. Considering again Figures 3.6, 3.9, any plane perpendicular to the page can be thought of as being rotated from the (111) or from the $(1\bar{1}1)$. In most cases, the behavior will be shown to be symmetric, such that the rotation may be considered to be from the nearest {111} plane. However, to account for the possibility that in some cases the behavior may not be symmetric, the rotation reference plane angle, r, is listed first, and the other {111} member, s, of the pair is listed last, in parentheses. The number in the middle, m, is the angle of the plane when the rotation is exactly halfway between the two {111} planes.

In the case of (110) wafers, there are more types of relevant pairs of {111} planes. They are summarized as follows:

- **P-35-60-(90)**
  .In Figure 3.18 (c), this corresponds to the rotation from the 35.3°-inclined (111) plane to either of the two vertical {111} planes shown.

35° Inclined Plane	60° Inclined Plane	90° Inclined Plane
(111)	(101)	$(1\bar{1}1)$
$(11\bar{1})$	$(01\bar{1})$	$(\bar{1}1\bar{1})$

- **P-90-60-(35)**

.In Figure 3.18 (c), this corresponds to the reverse rotation from either of the two vertical {111} planes to the 35.3° inclined (111) plane.

90° Inclined Plane	60° Inclined Plane	35° Inclined Plane
$(1\bar{1}\bar{1})$	$(10\bar{1})$	$(11\bar{1})$
$(\bar{1}11)$	(011)	(111)

- **P-90-90-(90)**

.In Figure 3.18 (b), this corresponds to the rotation (either way) between the pair of vertical {111} planes shown.

- **P-145-120-(90)**

.In Fig 3.18 (c), this corresponds to the rotation from the underside of the (111) plane to the underside of either of the two vertical planes shown.

145° Inclined Plane	120° Inclined Plane	90° Inclined Plane
$(\bar{1}\bar{1}1)$	$(1\bar{1}1)$	$(1\bar{1}1)$
$(\bar{1}\bar{1}\bar{1})$	$(\bar{1}0\bar{1})$	$(\bar{1}1\bar{1})$

- **P-90-120-(145)**

.In Figure 3.18 (c), this corresponds to the rotation from the underside of either of the two vertical {111} planes to the underside of the (111).

90° Inclined Plane	120° Inclined Plane	145° Inclined Plane
$(1\bar{1}\bar{1})$	$(0\bar{1}\bar{1})$	$(\bar{1}\bar{1}\bar{1})$
$(\bar{1}11)$	$(\bar{1}0\bar{1})$	$(\bar{1}\bar{1}1)$

• **K-35-45-(90)**

.In Figure 3.18 (d), this corresponds to the rotation from the 35.3°-inclined (111) plane to a vertical {111} plane through the 45°-inclined {100} plane.

35° Inclined Plane	45° Inclined Plane	90° Inclined Plane
$(11 1)$	(100)	$(1\bar{1}\bar{1})$
$(11\bar{1})$	(010)	$(\bar{1}11)$

• **K-90-45-(35)**

.In Figure 3.18 (d), this corresponds to the reverse rotation from the 35.3°-inclined (111) plane to a vertical {111} plane through the 45°-inclined {100} plane.

90° Inclined Plane	45° Inclined Plane	35° Inclined Plane
$(1\bar{1}1)$	(100)	$(11\bar{1})$
$(\bar{1}1\bar{1})$	(010)	(111)

• **K-90-90-(90)**

.In Figure 3.18(a), this corresponds to rotation either way between the pair of vertical {111} planes shown.

• **K-145-135-(90)**

.In Figure 3.18(d), this corresponds to the rotation from the under-side of the 35.3°-inclined (111) plane to a vertical {111} plane through the 45°-inclined {100} plane.

145° Inclined Plane	135° Inclined Plane	90° Inclined Plane
$(\bar{1}\bar{1}1)$	$(0\bar{1}0)$	$(1\bar{1}\bar{1})$
$(\bar{1}\bar{1}\bar{1})$	$(\bar{1}00)$	$(\bar{1}11)$

• **K-90-135-145**

.In Figure 3.18(d), this corresponds to the rotation from the under-side of the vertical {111} plane to the underside of the (111) plane through the underside of a 45°-inclined (135°-inclined) {100} plane.

90° Inclined Plane	135° Inclined Plane	145° Inclined Plane
$(1\bar{1}1)$	$(0\bar{1}0)$	$(\bar{1}\bar{1}\bar{1})$
$(\bar{1}1\bar{1})$	$(\bar{1}00)$	$(\bar{1}\bar{1}1)$

3.6.4 Mask-Edge Angles, Rotation Angles and Inclination Angles

Having outlined the many possibilities for plane rotations involving the different pairs of planes in each of the (100) and (110) systems, the relationships between the angles θ_P, θ_K, mask-edge angle (δ), and plane inclination angle with respect to the wafer surface (α), must be derived.

In the (100) system, the mask-edge angle (δ) will be measured with respect to the intersection of the horizontal wafer surface with a vertical {100} plane [4, 21, 28, 32, 33], chosen to be the (001)-(100) intersection. In the (110) system, the mask-edge angle (δ) will be measured with respect to the intersection of the intersection of the horizontal wafer surface with one of the 35.3^{o} inclined planes, chosen to be (110)-(111). The derivations for

the relationships between deviation angle δ, rotation angle θ and inclination angle α for the both the (100) and (110) system are derived in Appendix A and the relationships are summarized in the sections below.

3.6.4.1 Deviation Angle δ vs. θ in the (100) System

3.6.4.1.1 PBC-defined Planes:

The relation between deviation angle δ and θ_p for the PBC-defined planes is given as

$$\delta = \text{atan}[\sqrt{2}\tan(35.3^o - \theta_p)] \text{ for } 0 \le \theta_p \le 35.3^o$$

3.6.4.1.2 Kink-row defined Planes:

The relation between deviation angle δ and θ_k for the kink-row defined planes is given as $\delta = \text{atan}[\sqrt{2}\tan(35.3^o + \theta_k)]$ for $0 \le \theta_k \le 54.7^o$

3.6.4.2 Inclination angle α vs. δ in the (100) system

3.6.4.2.1 PBC-defined Planes

The relation between deviation angle δ and inclination angle α_p for the PBC-defined planes is given as

$$\alpha_p = \text{atan}\left(\frac{1}{\cos\delta}\right) \text{ for } 0^o \le \delta \le 45^o.$$

3.6.4.2.2 Kink-row defined Planes

The relation between deviation angle δ and inclination angle α_k for the PBC-defined planes is given as

$$\alpha_k = \text{atan}\left(\frac{1}{\sin\delta}\right) \text{ for} 270^o \le \delta \le 315^o \text{ or } 0^o \le \delta \le 45^o.$$

In addition to these PBC-based and kink-row based planes there are other PBC-based and kink-row based which are the inverse of these planes at the same deviation angles. Figure 3.19 illustrates the inclination angles of these planes vs. deviation angle δ in addition to the standard planes. Due to the symmetric nature of emerging planes over the range of deviation angles, only a 90° range is shown in the figure.

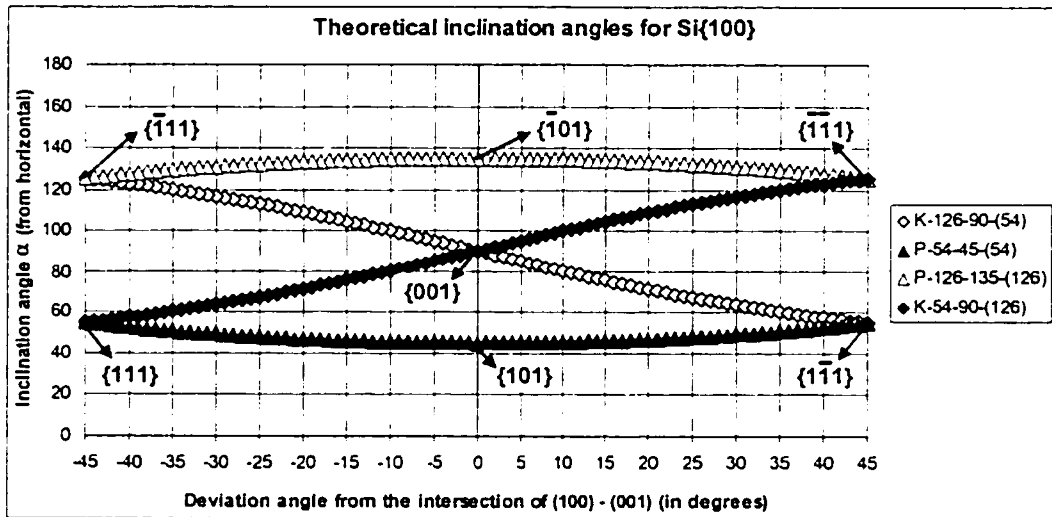

Figure 3.19: Theoretical inclination angle of emerging planes vs. deviation angles in Si(100).

3.6.5 Derivation of the Deviation angle δ vs. θ and Inclination angle α vs. δ in the (110) System

Similar to the derivation in the (100) coordinate system, the relationship between deviation angle δ, rotation angle θ and inclination angle α for the (110) system is derived and the relationships are summarized below.

3.6.5.1 PBC-Defined Planes

Due to the complexity of the plane variations in this (110) geometrical construct, the PBC-defined planes are split into two ranges of rotation angles.

3.6.5.1.1 PBC-defined Planes, Angle Range: $0^o \le \theta_p \le 35.26^o$ ***(P-35-60):***

$$\delta = \operatorname{atan}\frac{FR}{FH} = \operatorname{atan}\left(\frac{1}{\sqrt{2}} - \tan(35.26^o - \theta_P)\right), \text{ for } 0^o \le \theta_p \le 35.26^o.$$

$$\alpha = \operatorname{acos}\left(\frac{\sqrt{2} - \tan\delta}{\sqrt{3 + 2\tan\delta(\tan\delta - \sqrt{2})}}\right), \text{ for } 0^o \le \theta_p \le 35.26^0.$$

3.6.5.1.2 PBC-defined Planes, Angle Range $35.26^o \le \theta_p \le 70.5^o$ ***(P-60-90):***

$$\delta = \operatorname{atan}\left(\frac{1}{\sqrt{2}} + \tan(\theta_P - 35.26^o)\right), \text{ for } 35.26^o \le \theta_p \le 70.5^o$$

$$\alpha = \operatorname{acos}\left(\frac{\sqrt{2} - \tan\delta}{\sqrt{3 + 2\tan\delta(\tan\delta - \sqrt{2})}}\right) \text{ for } 35.26^o \le \theta_p \le 70.5^o.$$

3.6.5.2 Kink-row defined Planes

3.6.5.2.1 Kink-row defined planes, Angle range $0^o \le \theta_p \le 54.7^o$ ***(K-35-45):***

$$\delta = \operatorname{atan}\left(\frac{\sqrt{2} - \tan(54.7 - \theta_K)}{\sqrt{2}\tan(54.7 - \theta_K)}\right), \text{ for } 0^o \le \theta_p \le 54.7^o$$

$$\alpha = \operatorname{acos}\left(\frac{\sqrt{2} + \tan\delta}{\sqrt{3 + 2\tan\delta(\tan\delta + \sqrt{2})}}\right), \text{ for } 0^o \le \theta_k \le 54.7^o\,^o.$$

3.6.5.2.2 Kink-row defined planes, Angle Range $54.7^o \le \theta_p \le 109.5^o$ ***(K-45-90):***

$$\delta = \operatorname{atan}\left(\frac{\tan(\theta_K - 54.7^o)\sqrt{2}}{\sqrt{2} + \tan(\theta_K - 54.7^o)}\right) + 90^o, \text{ for } 54.7^o \le \theta_p \le 109.5^o$$

$$\alpha = \operatorname{acos}\left(\frac{-(\tan\delta + \sqrt{2})}{\sqrt{2 + (1 + \sqrt{2}\tan\delta)^2}}\right), \text{ for } 54.7^o \le \theta_p \le 109.5^o.$$

See Appendix A for the derivations. The deviation angle vs. inclination angle of the emerging plane in the entire range of deviation angle is plotted in the Figure 3.20.

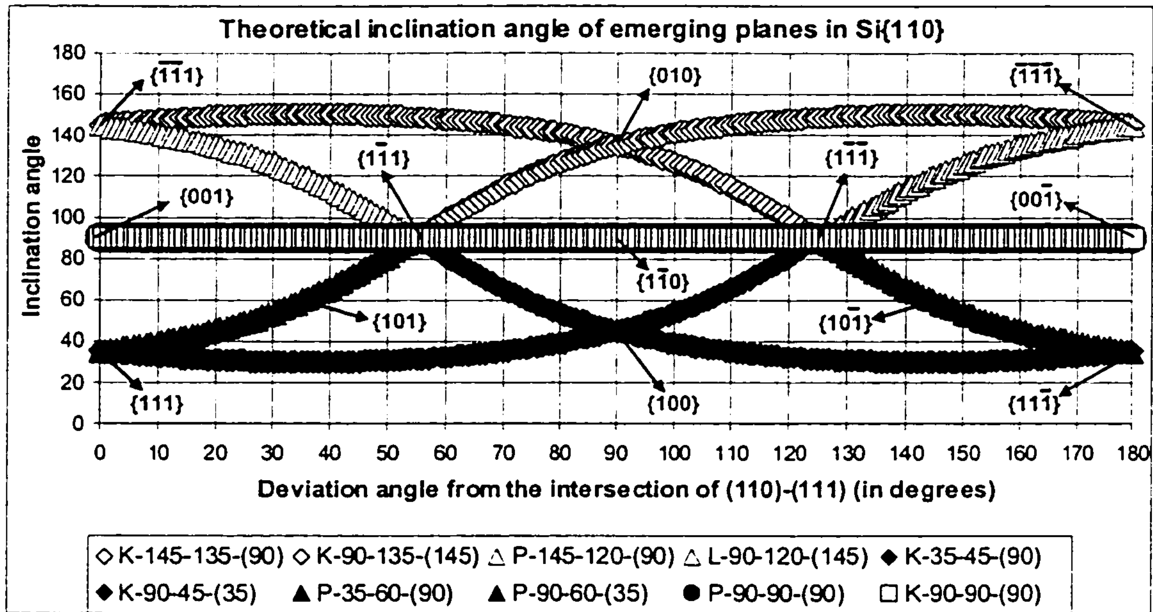

Figure 3.20: Theoretical inclination angle of emerging planes vs. deviation angles in Si(110)

CHAPTER 4

Experimental and Measurement Techniques and Procedures

4.1 Overview

To model the etch anisotropy of silicon, one needs to collect extensive experimental data that can be used in modeling the etch phenomena. While full characterization of etch anisotropy would require etching of a 3-dimensional structure such as a sphere [53], this variation can be partially characterized by under-etch experiments. Many researchers have employed under-etch experiments as a practical method of obtaining information about etch anisotropy under particular conditions [21, 22, 28, 32, 33, 41, 45, 51]. With the under-etch experiments carefully designed one can extract a lot of useful data about various crystallographic silicon planes.

This chapter details the experimental setup, the etch station, experimental procedure and the etch experiments that were done to etch Si{100} and Si{110}. The {100} and {110} silicon wafers were etched with different concentrations of etchant, Tetra-Methyl Ammonium Hydroxide (TMAH). This chapter also describes the observation techniques and different critical observation parameters that are recorded from the experiments for future analysis and modeling.

4.2 Experimental and Observation Procedures

4.2.1 Experimental Design

In the process of modeling anisotropic etching of crystallographic silicon, the etch phenomena are believed to be dependent on the etchant and the etch conditions. With this in mind, the experiments were designed for this work. This work mainly focuses on the etch rate variation for different concentrations of the etchant. For simplicity, the etchant temperature is always maintained at 80°C and the etch is performed without any stirring. And

there was no additives added to the etchant (TMAH). Etchant concentrations of 25%, 19wt%, 17wt%, 12wt%, and 9wt% were used for the experiments. Due to the expected large under-etch rates on {110} silicon, the Si{110} samples were etched for 50 minutes. The {100} silicon samples were etched for 60 minutes.

4.2.2 The Etch Station

All the etches described in this work are done in the etch station schematically shown in Fig. 4.1. Most liquid based wet anisotropic etching is done on a similar setup [28, 49]. As can be seen from the figure, the etch apparatus consists of a beaker, reflux condenser with thermometer hole and water inlet and outlet ports. The beaker containing the etchant is immersed in an oil bath, which can be electrically heated and maintained at the required temperature by a temperature controller.

An oil bath was used to heat the etchant instead of a hot plate, this better maintains the temperature uniformity of the etchant. The immersed mercury thermometer monitors the temperature of the etchant with an accuracy of +/- 0.5°C. The temperature of the etchant cannot be controlled directly, rather the temperature of the oil bath can be. The temperature of the etchant is not same as the maintained temperature of the oil bath, the temperature of the etchant is lower than the temperature of the oil bath. In order to maintain the TMAH at 80°C, the oil bath was maintained at 87°C [28].

The reflux condenser cap is used to condense the evaporated etchant vapor and thus to maintain the concentration of the etchant over the time of etching process. The reflux cap is connected to cold running water through the water in and out ports during all the etch experiments. The cold water in the reflux cap condenses the etchant vapors when they come in contact with the reflux cap and the condensed etchant drips back to the etchant solution in the beaker maintaining the concentration level of the etchant.

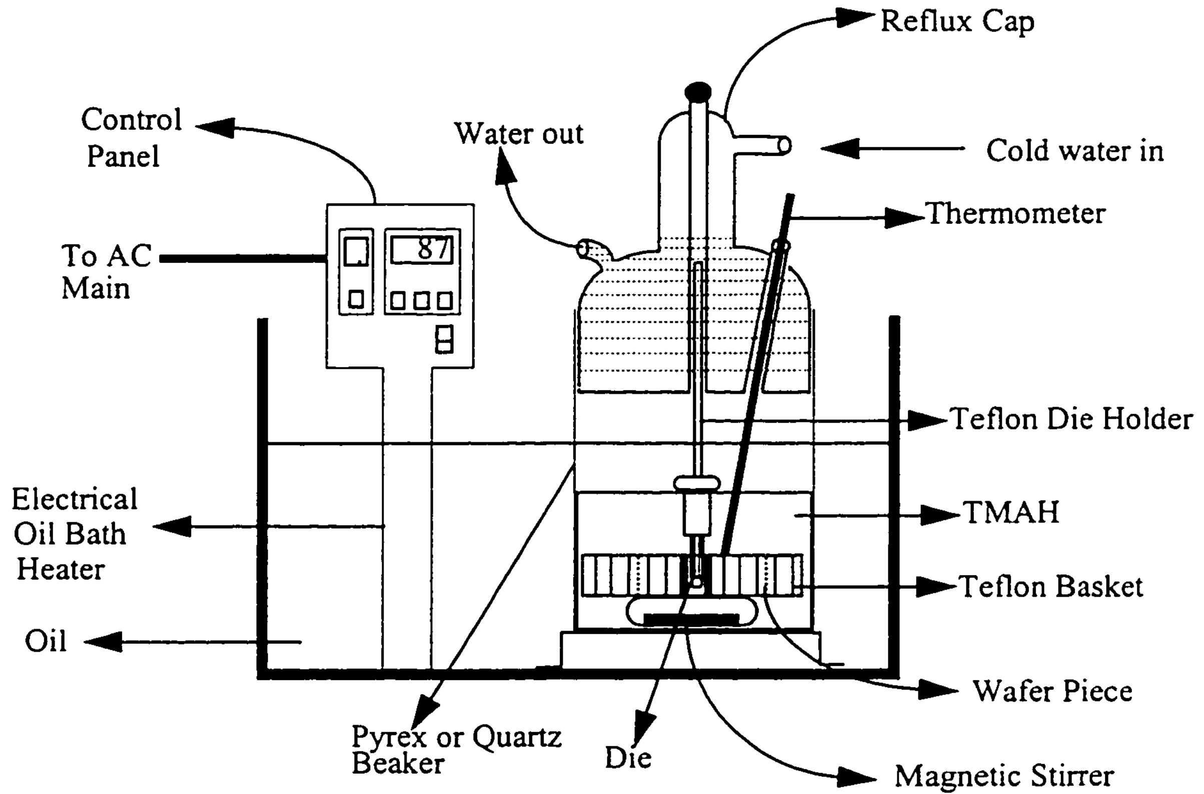

FIGURE 4.1: Schematic of the TMAH etch station.

A specially made teflon basket is used to hold the silicon samples in the etchant. If necessary the etchant can be stirred using the teflon coated magnetic stirrer. The setup also has a special teflon holder that can be used to hold small diced silicon dies.

4.2.3 Sample Preparation

Lightly-doped n-type double side polished Si{110} and single side polished Si{100} wafers are cut into sizes of 2 x 1 inches rhombus and 1 x 1 inch squares respectively. These cut samples are cleaned using the RCA cleaning procedure (Appendix B), then the cleaned samples are thermally wet-oxidized for to grow an oxide thickness of 0.5 μm. As discussed in earlier chapters thermal oxide acts as an excellent mask for TMAH etches. In all the experiments in this work thermally grown oxide is used as the masking material due to its superior masking properties. On all the samples, oxide is grown using wet oxida-

tion process at 1100°C for a sufficient length of time to grow the required the required thickness of oxide that can act as a mask during the etching. Approximately an oxide of 0.5 μm thick is grown, due to the very low etch rate of oxide this 0.5 μm can act as a protective mask during the entire etching process of 60 minutes.

The thermally-oxidized samples are then patterned with the wagon-wheel mask pattern shown in Figure 4.3. Using the common photolithography techniques, the wagon-wheel mask pattern is printed on the polished side of the samples.

During the photolithography process, after exposing UV light through the wagon-wheel mask, the photo-resist on the spokes are removed by the developing process and thus exposes the oxide below it. This exposed oxide on the spokes are then etched using BOE (Buffered oxide etch) process, during this BOE process the photo-resist on the other area protects the oxide below it. After the BOE process, the samples are then rinsed in acetone to remove the remaining photo-resist. At this step the samples are ready for anisotropic etch experiments. Figure 4.2 shows the process flow that is used to prepare the samples for the etch experiments.

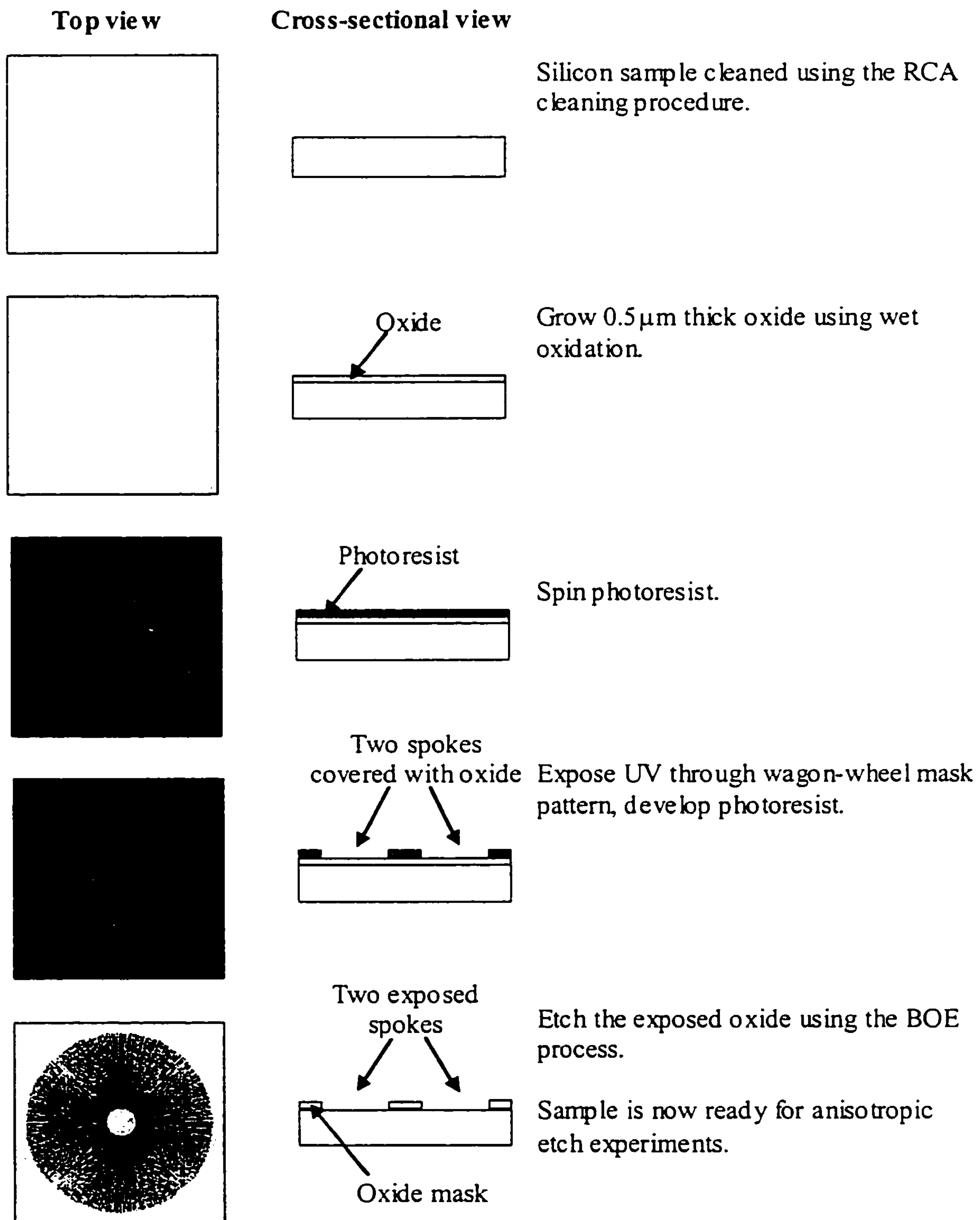

FIGURE 4.2: Process flow for sample preparation.

4.2.4 The Mask

In order to do the under-etch experiments one has to carefully design a mask that will expose an etch pattern at every degree. This will allow the etchant to etch patterns at each and every degree. For this a circular pattern mask with spoke like pattern at every degree for 360° is designed. Due to the wheel like shape of the mask, it is called a wagon wheel mask [21, 22, 32, 33, 51]. The mask is shown in Figure 4.3, the mask has spokes at every 1° having dimensions 1.95cm x 170mm. Each spoke on the mask has a number marked beside it. This helps a lot while making the under etch measurements.

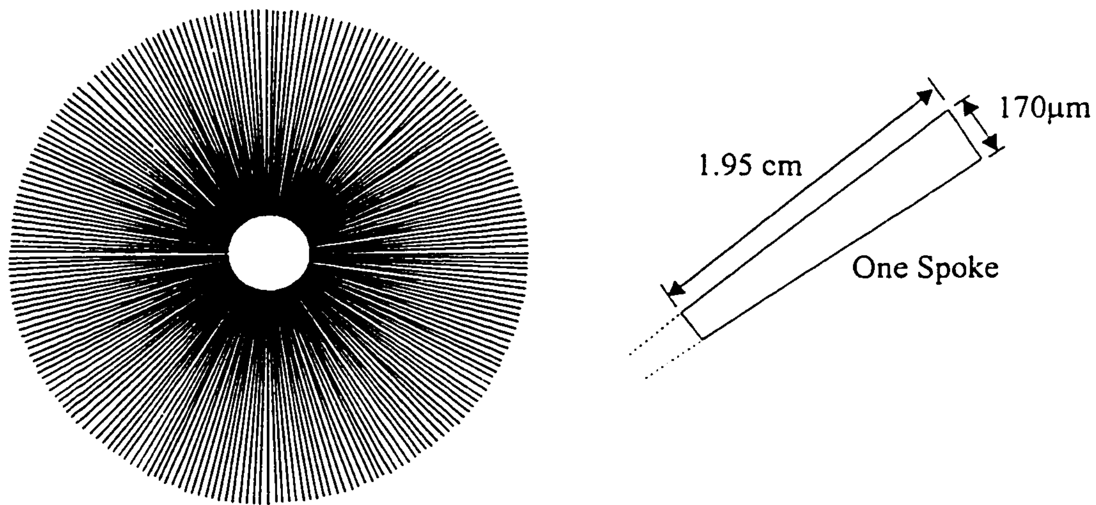

FIGURE 4.3: Wagon-wheel mask pattern and individual spoke details.

4.2.5 Etch Experimental Procedure

The etch station described in section 4.2.2 is used for all the etch experiments in this work. As explained earlier in section 4.2.1, all etches for the Si{110} were done at 80°C, un-stirred, for 50 minutes in various concentrations of TMAH (25 wt% to 9 wt.%). And etches for the Si{100} were done at 80°C, un-stirred, for 60 minutes in various concentrations of TMAH (25 wt% to 9 wt.%). The initial TMAH concentration was 25 wt.% in water, lower concentrations of TMAH for etching were obtained by diluting the 25 wt.% TMAH with appropriate amounts of DI water (deionized water). The 25wt.% TMAH was purchased from a single source, Moses Lake Industries Inc., Manassas, VA.

The required amount of fresh 25wt% TMAH was taken in a clean beaker and the needed quantity of DI water was added to it to get the desired concentration of TMAH. It was made sure that the TMAH water solution was at least 500ml, so that silicon samples can be fully submerged in the etchant during the etching process. The pH of diluted TMAH was measured so as to maintain repeatability of TMAH concentration. The beaker with the TMAH was carefully placed in the oil bath and is then closed with the reflux cap. The required temperature of the oil bath, 87° C is set on the temperature controller's control panel and the heater is turned on. This set temperature of 87°C maintains the TMAH at a temperature of 80°C [28]. The coolant water flow on the reflex cap was turned on. During the experiment the temperature of the TMAH solution was often monitored using the mercury thermometer.

The patterned silicon samples are dipped in dilute HF, to remove any native oxide formed on the exposed silicon on the spokes. These samples are then rinsed in DI water and are stored immersed in a beaker containing DI water. As soon as the temperature of the etchant reaches the required temperature of 80°C, the silicon samples are carefully loaded on the teflon basket. The reflux cap was carefully opened and the teflon basket with the samples is slowly inserted into the beaker until the samples fully submerge in the TMAH. The reflux cap was then carefully placed on the beaker to cover the beaker. And the mercury thermometer is then inserted into TMAH solution. Then the timer is turned on to record the etch time. The samples are left in the etchant for the desired length of time, and the etchant temperature is often monitored on the mercury thermometer.

After etching for the required time, the heater and the coolant water are turned off and the reflux cap is carefully removed from the beaker. The teflon basket is then removed from the etchant. The samples are the removed from the teflon basket and are then very carefully rinsed in DI water without damaging the overhanging oxide resulted from the etch process. The samples are then rinsed in methanol and again in DI water and then are

dried by gently blowing nitrogen using the nitrogen gun. Using methanol during the rinse and drying steps helps to avoid any stiction problems which are common during the drying process which tend to damage the overhanging oxide. At all times these dried samples are handled very gently so that the overhanging oxide is not damaged. The over hanging oxide is measured to calculate the etch rate of the under-etched plane.

4.3 Measured Quantities

In order to study the etch properties, the etch cavity of spoke at each degree is studied in detail; this enables to find the etch rates of various crystallographic planes thus the etch anisotropy. The observations made are the mask under-cut (MUC), under-etched surface horizontal projection (UESHP) and depth (D) of the etched cavity. Figure 4.5 shows the measured quantities. All these measurements were measured using an optical microscope.

Each spoke corresponds to a particular mask-edge deviation angle, δ, measured from the intersection of two reference planes. In the case of Si{110}, δ is measured from the intersection of the horizontal (110) wafer surface with a (111) plane. And in the case of Si{100}, δ is measured from the intersection of the horizontal (100) wafer surface with a (001) plane.

When the sample is put into the etchant, the etchant starts to etch away the open silicon (in the spoke area), the oxide mask protects the other areas. When the silicon is being etched away, the interface between the oxide mask on the spoke corner and the open silicon area begins to expose a particular crystallographic silicon plane to the etchant. Due to the anisotropic etch properties of the etchant, it etches different crystallographic planes at different etch rates, this makes each spoke to be uniquely etched. This can be seen from the experimental results. Due to the symmetric nature of crystallographic planes, only a certain range of deviation angles are needed to be studied. From Chapter 3, in case of Si(100) a range of 45° is required and in the case of Si(110) a range of 90° is required. In

most cases, more measurements were taken, which are useful and enhance the reliability of the experiments.

Figure 4.4 below shows the shape of the Si(100) and Si(110) samples after they are cut from the silicon wafer. The Si(100) samples are always a square, as they cleave at 90°. On the (100) silicon, the {111} planes are found to intersect the surface at 90° to each other. The Si(110) samples are always a rhombus, because of their cleavage angles. On the (110) silicon, the {111} planes no longer intersect at 90° [47]. The figure also shows the relationship between the water-flat (WF) and the deviation angle δ used in this work.

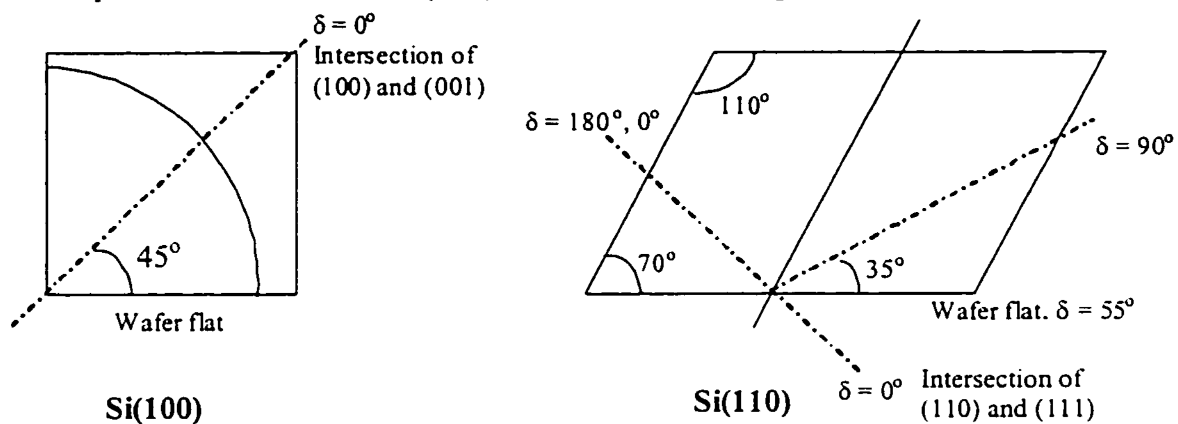

FIGURE 4.4: Relationship between the wafer flat and deviation angles δ on (100) and (110) silicon.

The Figure 4.5 below illustrates the three measurements made on all samples the UER, UESHP and D [22, 28]. The figure shows the simplest case of etching, where the under-etched side wall is single faceted. Etching in different concentrations and at different deviation angles the side wall is composed of 2 or 3 facets. Figure 4.6 shows a case where the under-etched side wall is composed of three facets.

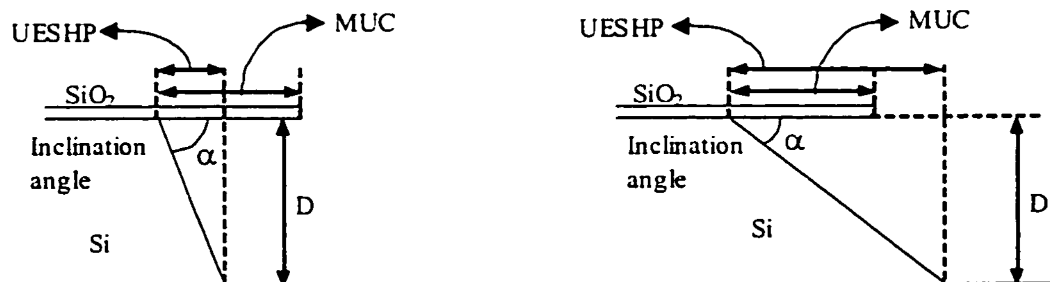

FIGURE 4.5: Illustration of the measurements made on etched samples, simple single faceted cases.

In certain cases when the side is made of two or three facets, 3-faceted side wall is shown in the figure above. In such cases the UESHP and D were measured as shown in the figure and the inclination angle was calculated. This calculated inclination angle gives the composite of all the three facets. SEM were done to find the exact inclination angle of each facet.

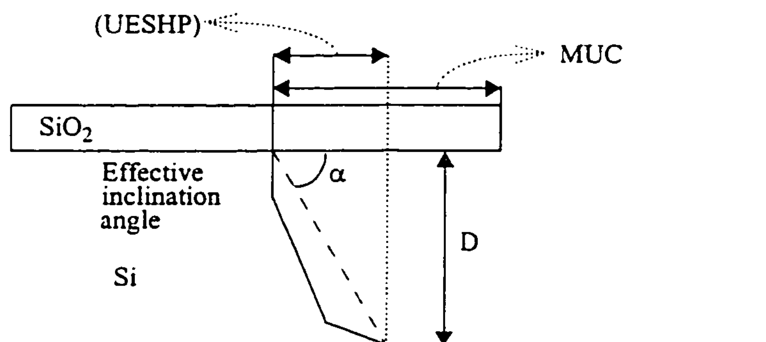

FIGURE 4.6: Illustration of the measurements made when the under-etched side wall is composed of three facets.

In all cases the measurements for UESHP and D were repeated after the oxide was removed, this was done to get more accurate measurements which was a little tough to measure with the oxide on the sample.

4.4 Measurement Procedures, and Techniques

4.4.1 Mask Under-cut

After etching the sample in TMAH, the sample is washed in methanol and DI water. Then it is dried very carefully, by gently blowing nitrogen so as to not damage the over-hanging oxide. An optical microscope was used to measure the UER. Viewing under the microscope, the mask undercut can clearly be seen due to the color of the overhanging oxide. The overhanging oxide being translucent, it can be clearly distinguished from the oxide on the silicon. Using the required magnification on the optical microscope, the hair-line cross in the eyepiece of the microscope is aligned to the mask edge oxide. The distance from the oxide mask edge to the line of intersection of the emerging plane (top facet) with the oxide was measured. This distance gives the mask undercut (MUC) obtained

from the time the sample was etched in TMAH. From the MUC data and the etch time the UER, under-etch per hour can be calculated.

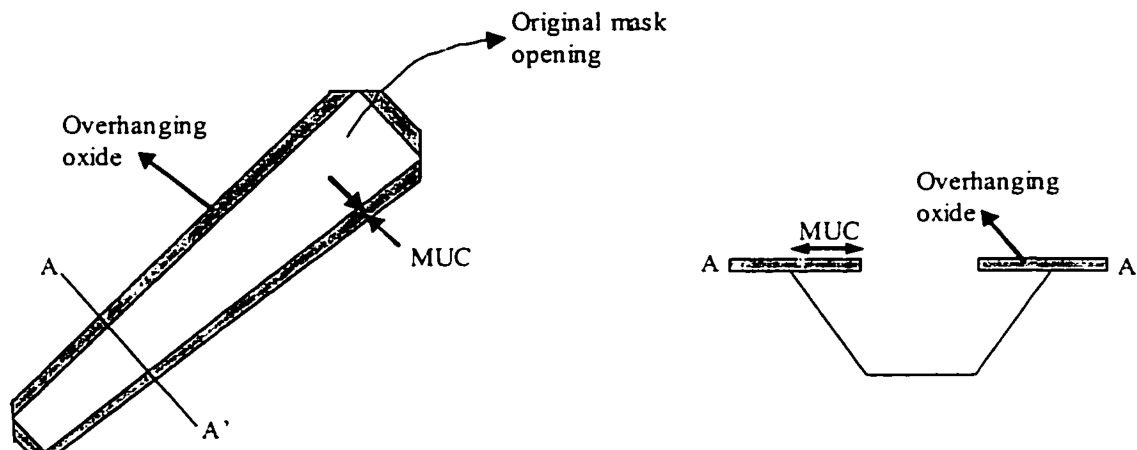

FIGURE 4.7: Illustration of Mask Under Cut on a single spoke.

The same measurements were made for all the spokes. The labels near the end of each spoke were used to identify each spoke for measurement. The maximum magnification was most often used.

4.4.1.1 Under-Etch Rate Calculation

The under-etch rate is defined as the rate at which the etchant etches the top or the first facet of the under-etched emerging surface. From the measured MUC and the known etch time t in hours, the under-etch rate of the emerging under etched surface can be calculated as $UER = \frac{MUC}{t} \mu m/h$

4.4.2 Etch Depth

On each spoke the etch depth of the cavity was measured. These measurements were also made using the optical microscope. First the bottom of the etched cavity was focused and the reading on the circular scale on the microscope focusing knob was noted. Then the top surface of the wafer was focused and the second reading on the circular scale was noted. The difference between the first and the second readings gives the etch depth. Each unit in the circular scale corresponds to 1 μm at all magnifications. Figure 4.8 below shows

how the measurements were recorded.

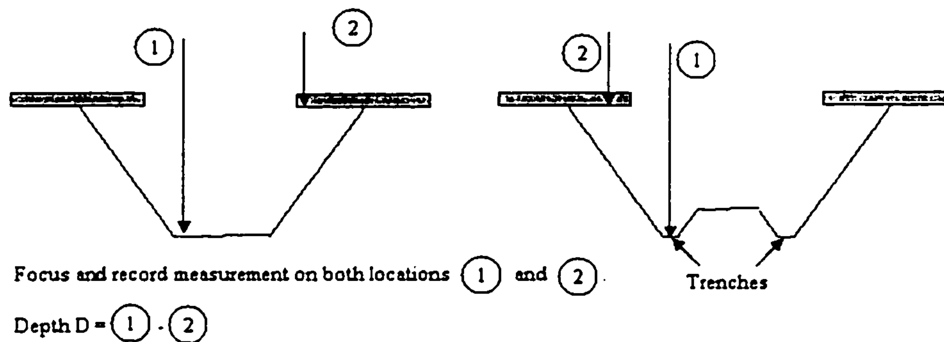

FIGURE 4.8: Illustration of Depth measurement on a single spoke.

In cases when the etched cavity has trenches on the sides, the etch depth was measured on the trenches and not on the center. The depth of the trench was measured so that the inclination angle of the emerging plane can be calculated. The etch depth in the center of the cavity (higher than the trench) was also measured, enabling calculation of the depth of the trench from the center etched surface. All depth measurements were made in the same way, focusing on the bottom surface and then on the top.

4.4.3 Under-Etched Surface Horizontal Projection (UESHP)

The measurement of the UESHP was done by focusing on the bottom of the etched cavity, the zero on hair-line cross in the eyepiece was aligned to the line of intersection of the under-etched surface and the emerging plane. Then the microscope was focused on the top surface of the sample without moving the microscope table. The distance from zero on the hair-line cross to the line of intersection of the emerging plane and the top oxide surface was measured. Care was taken to use the proper multiplying factor for the magnification used.

4.5 Oxide Removal, Re-measure

As verification, the oxide was removed and then the depth and the UESHP were re-measured. The sample was dipped in buffered oxide etchant (BOE) to remove the over-

hanging masking oxide. It was then rinsed in DI water and dried by blowing nitrogen. The depth and the UESHP measurements were repeated using the same measurement procedures as explained in the previous section. These measurements after oxide removal were more reliable, allowing accurate inclination angles to be calculated.

4.5.1 Inclination Angle Calculation

The effective inclination angle (EIA or α) of the emerging plane under-etched plane can be calculated from the measured UESHP and D by

$$\text{Effective inclination angle} = \tan^{-1}\left(\frac{D}{UESHP}\right)$$

By this method of calculation, the inclination angle of each facet of the under-etched surface can not be calculated. A cross-sectional view of the spoke is required to know the inclination angle of each facet. Scanning electron micrographs are taken to study each facet of the under-etched emerging surface in detail.

The acronyms used in the later sections of the thesis are listed below.

MUC - Mask Under Cut
UER - Under-Etch Rate
UESHP - Under-Etched Surface Horizontal Projection
α - Effective inclination angle
α_n - Inclination angle of facet n.
D - Depth of etched cavity

4.6 SEM Procedures

A scanning electron microscope was used to observe the inclination angles of individual facets. Scanning electron micrographs were taken when desired. Using the electron microscope the cross-section of the etched spoke was viewed, this gave a very clear picture of the emerging planes and the number of facets on it. Also the inclination angles of each facet were estimated from the micrograph. The trenches were more clear and easily studied on the SEM.

The sample to be studied on the SEM was carefully cleaved in a way that the cross-sections were available for the spokes to be studied. Then the cleaved sample is then coated with a very fine layer of gold, so that it can be examined in the electron microscope. After coating, the sample was placed inside the vacuum chamber of the SEM, the sample was then carefully studied viewing the cross-sections of the spokes at different angles. The etched surface roughness and the emerging plane roughness and the facets were studied in detail. Scanning electron micrographs were taken whenever necessary. For any SEM that required a cross-sectional view of a spoke, the spoke was carefully aligned such that both its sidewalls and its bottom surface were perpendicular to the image view. In this way, angles measured on the resulting micrograph would be accurate representations of the inclination angles of the underetched facets. Fig. 4.9 shows examples of SEMs taken on Si{100}, where Fig. 4.9(a) shows the carefully-aligned cross-sectional view. Fig. 4.9(b) shows the facet details of the same underetched surfaces, in a plan view.

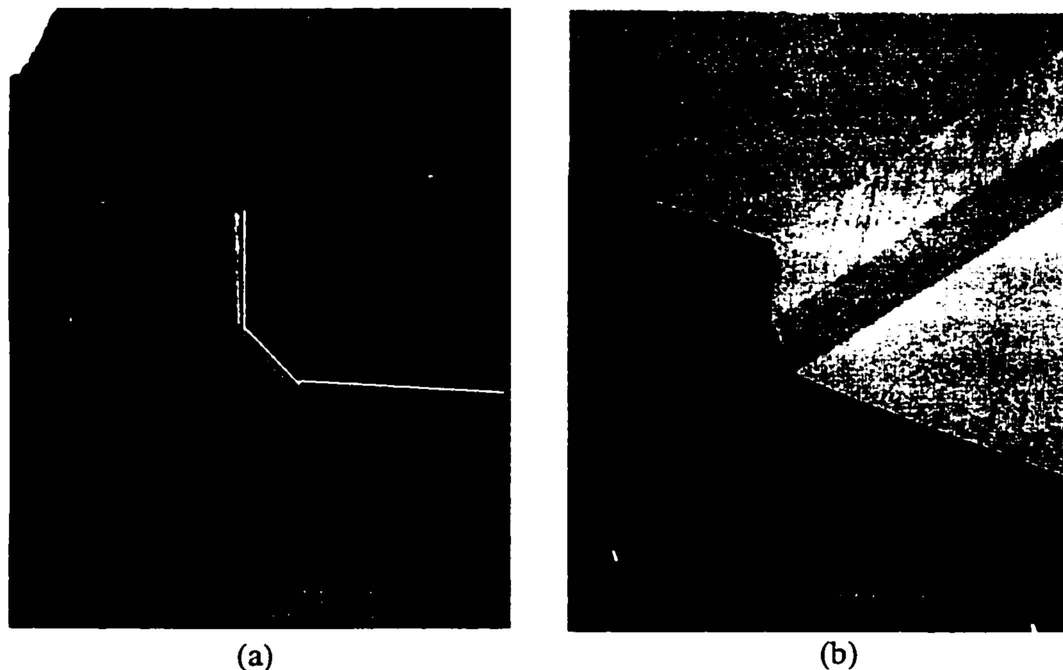

(a) (b)

FIGURE 4.9: Scanning Electron Micrographs of a wagon-wheel spoke. At left, the cavity sidewalls and bottom have been carefully aligned to be perpendicular to the micrograph view.

CHAPTER 5

Experimental Results, and Match to Model

5.1 Experimental Results: Organized by TMAH Concentration

Si{110} and Si{100} samples were etched in TMAH at various concentrations: 25, 19, 17, 15, 12, 9 wt%, all at 80° C. At each concentration, the under-etch distances were measured by an optical microscope, as explained in Chapter 4. Based on the measurements, the under-etch rates (UER) and effective inclination angles were calculated and plotted for each case. Also, cross-sectional scanning electron micrographs (SEMs) were made on many of the spokes for all concentrations, enabling detailed study of the facets of the under-etched emerging surfaces. This Chapter presents the under-etch rates and facet inclination angles in detail.

For each concentration and silicon orientation, Si{110} and Si{100}, the following data is reported:

- *Graph of under-etch rate vs. mask-edge deviation angle:* The under-etch distances (directly measured) are divided by the experimental etch time.
- *Graph of effective inclination angle vs. mask-edge deviation angle:* The under-etched surface is assumed to be a single facet, and an *effective* inclination angle is calculated from the measured etch depth and observed horizontal projection of the under-etched surface.
- *Graph of details of facet inclination angles vs. mask-edge deviation angle:* The inclination angles of up to three facets are identified using the SEMs below and the theoretically-expected inclinations of particular pbc- and k-row defined planes (see section 3.6 and the table below.)

- *Sample SEMs at various representative deviation angles:* Many SEMs were taken at many deviation angles, of which a representative selection is shown here. The facet inclination angles, α_i, can be estimated to within +/-2° for the smooth surfaces, from the micrographs. By matching the estimates to the theoretical expectations, accurate identifications are possible by the graph above.
- *Tabular compilation of the facet descriptions as a function of mask-edge deviation angle ranges:* Systematic variations are identified, and related to the "Model Identifiers" as described in Section 3.6, pbc- or kink-row defined model planes. Also, the smoothness of the etched surfaces were studied. This table and the comments below combine all relevant observed information about the under-etched surfaces and inclination angles.
- *Comments on the facet descriptions and deviation angle ranges.*

5.1.1 Etching in 25wt% TMAH

5.1.1.1 Si{110} etched at 80°C

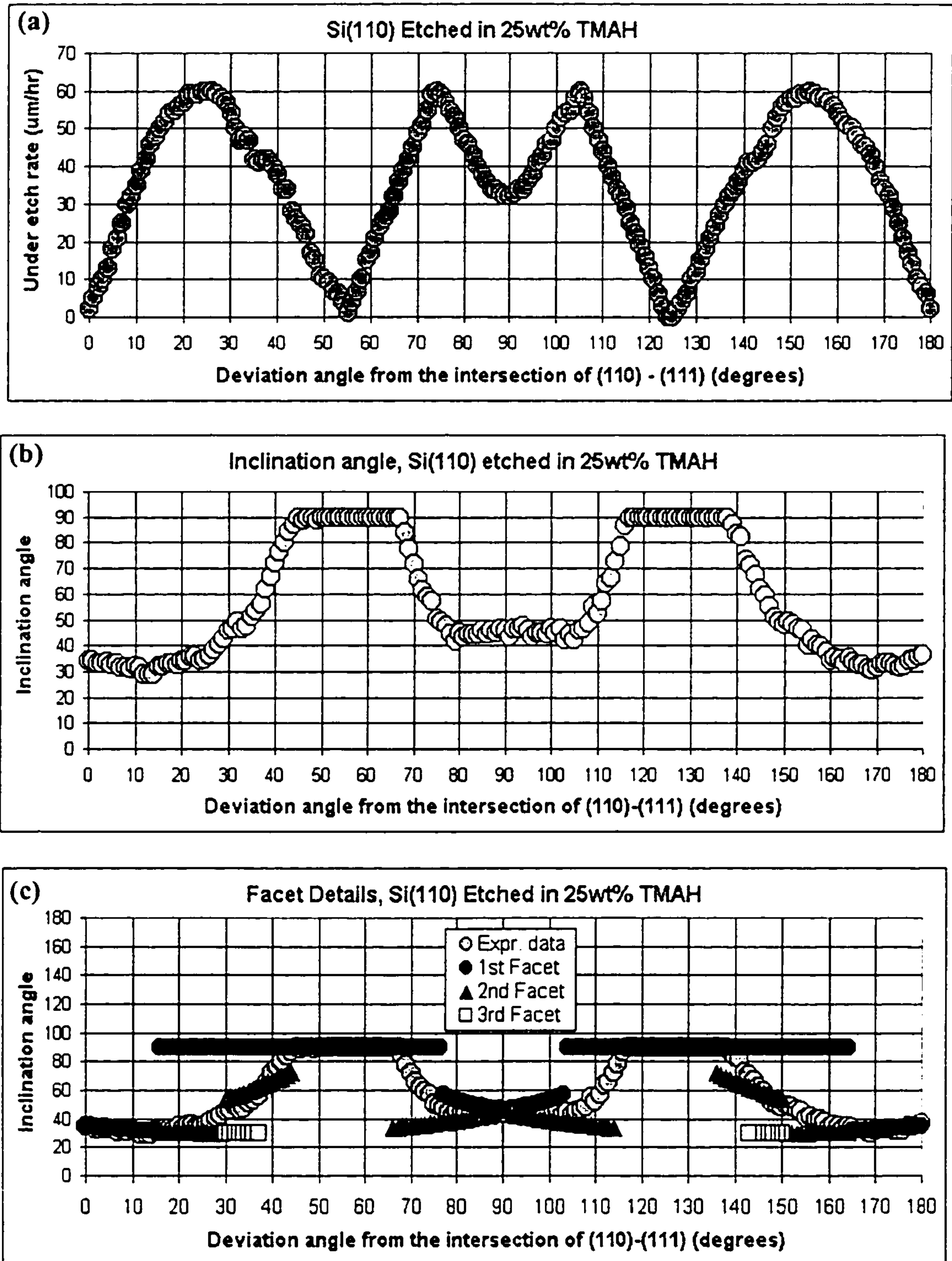

FIGURE 5.1: Si(110) etched in 25wt% TMAH at 80°C; (a) Under-etch rate, Si(110), (b) Inclination angle, and (c) Facet details.

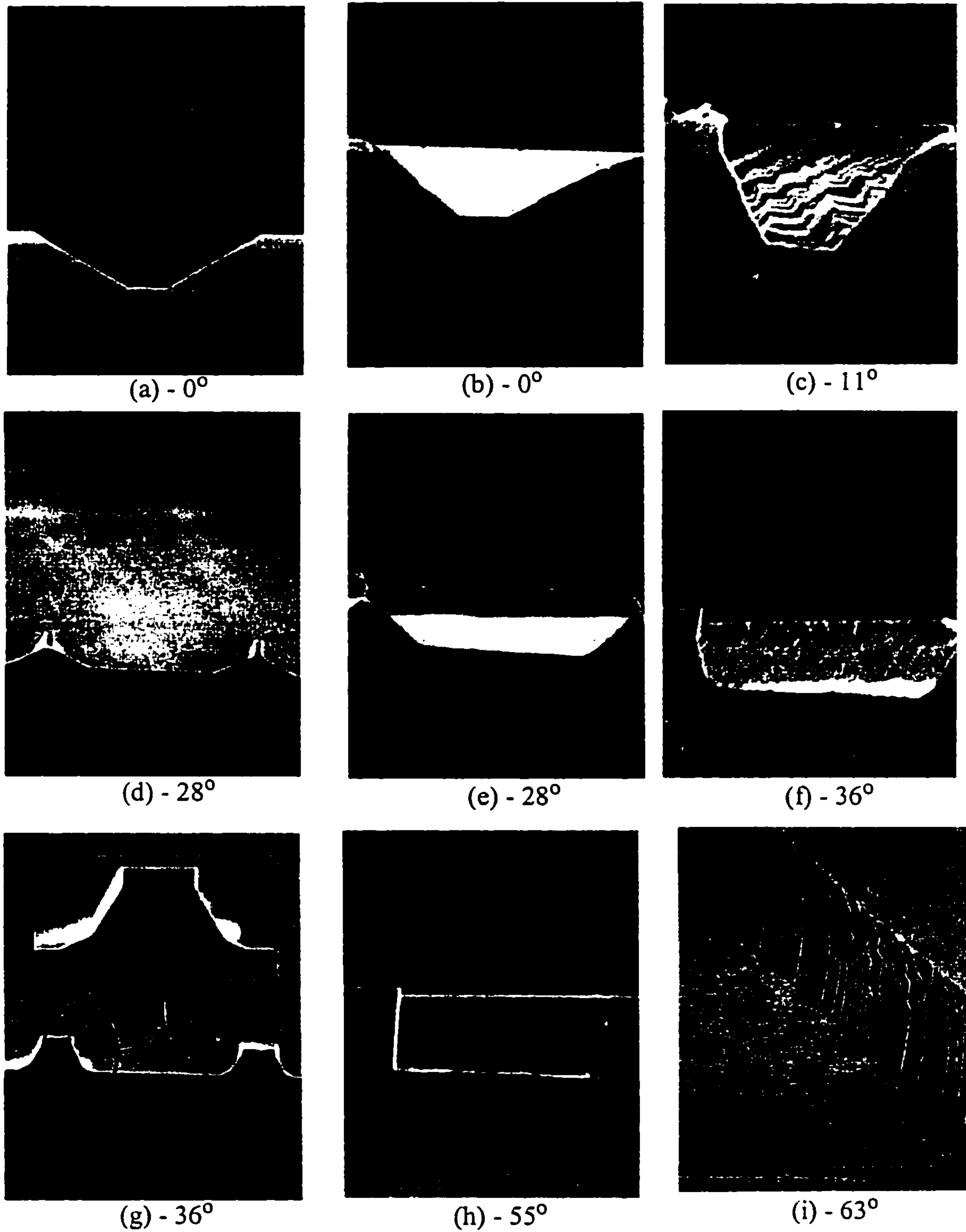

FIGURE 5.2: Scanning electron micrographs taken at various deviation angles for the {110} silicon etched in 25wt% TMAH at 80° C.

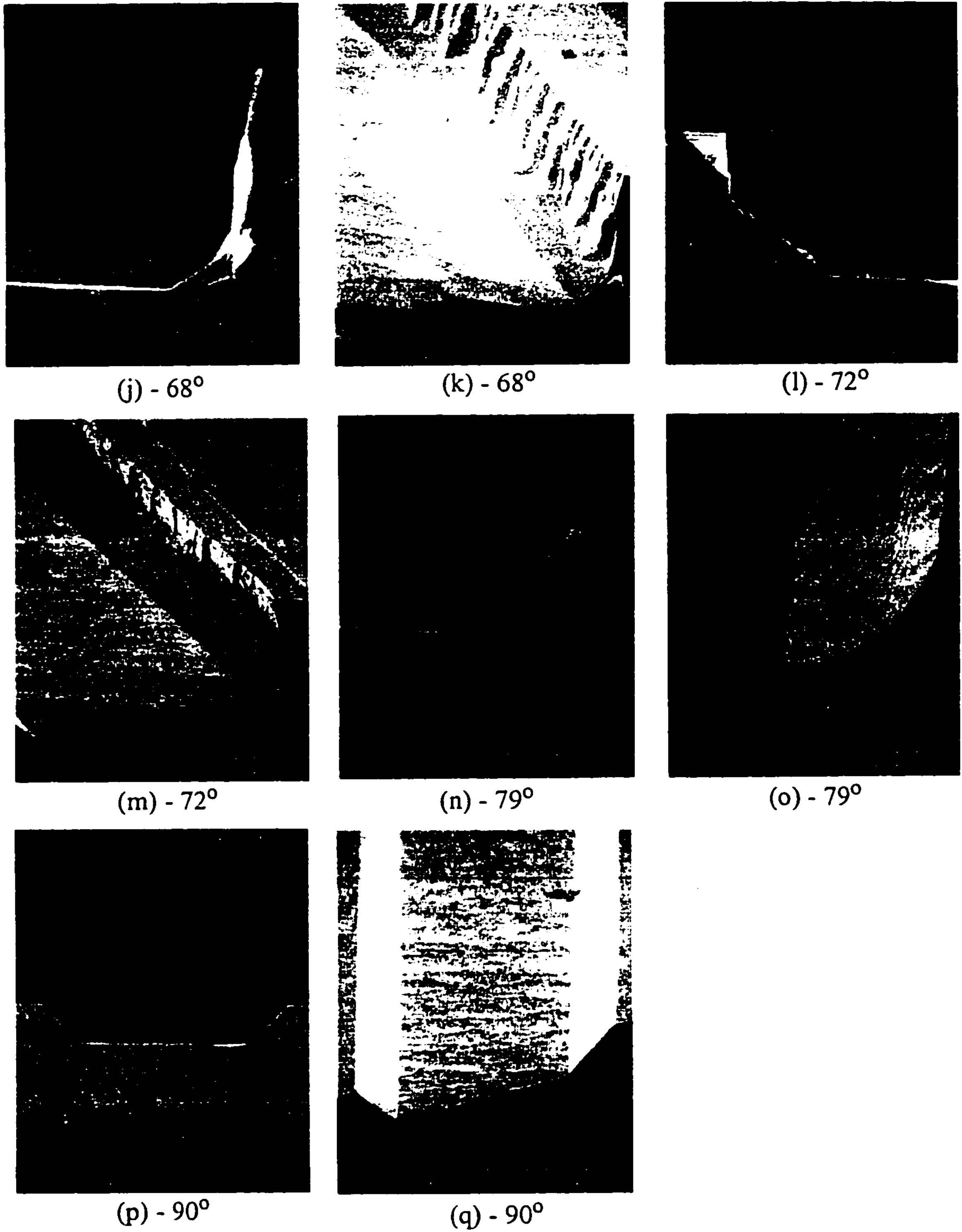

FIGURE 5.2: Scanning electron micrographs taken at various deviation angles for the {110} silicon etched in 25wt% TMAH at 80° C.

The under-etch rate for the 25wt% case is shown in Figure 5.1(a). From the figure we can see that there are two minima at $\delta = 0^o$ and at $\delta = 180^o$, where the emerging plane is 35.3^o inclined {111} plane. There are two more minima at $\delta = 55^o$ and at $\delta = 125^o$, where the emerging plane is vertical {111} plane. There is also a local minimum at $\delta = 90^o$.

Similarly, there are two maxima at $\delta = 25^o$ and at $\delta = 154^o$, and there are two other maxima at $\delta = 74^o$ and at $\delta = 105^o$.

TABLE 5.1. Si {110} etched in 25wt%TMAH

δ Range in degrees	No. of Facets	Facet Descriptions	Under-etched planes (Model Identifiers)	Trenches
0 - 5	1	about 35° inclined, very smooth	K-35-45-(90)	No
6 - 15	1	~30° inclined, rough	K-35-45-(90)	No
16 - 29	2	1st: 90°, very smooth 2nd: ~30°, smooth	1st: K-90-90-(90) 2nd: K-35-45-(90)	No
30 - 37	3	1st: ~90°, rough 2nd: >45°, smooth 3rd: ~30°, rough	1st: K-90-90-(90) 2nd: P-35-60-(90) 3rd: K-35-45-(90)	No
38 - 44	2	1st: 90°, rough 2nd: >45°, smooth	1st: K-90-90-(90) 2nd: P-35-60-(90)	No
45 - 55	1	90°, rough and becomes to very smooth	K-90-90-(90)	No
55 - 65	1	90°, very smooth and becomes rough	P-90-90-(90)	No
66 - 71	2	1st: 90°, rough, larger than the 2nd facet 2nd: 35° - 40°, smooth	1st: P-90-90-(90) 2nd: K-35-45-(90)	No
72 - 76	2	1st: 90°, rough, 2nd: 35° - 40°, smooth	1st: P-90-90-(90) 2nd: K-35-45-(90)	No
77 - 88	2	1st: 55°-45°, smooth 2nd: 40° - 45°, smooth	1st: K-90-45-(35) 2nd: K-35-45-(90)	No
89 -90	1	45°, smooth {100} plane	K-35-45-(90)	No

Region 0° - 5°: In this range of δ, the under-etched surface is a single facet and is very smooth. These planes follow the K-35-45-90 model. SEM at $\delta = 0^o$ is shown in Figure 5.2 (a) and (b), this shows the smooth {111} plane.

Region 6° - 15°: The under-etched surface still follow the K-35-45-90, and are single faceted but the planes get rougher as the deviation angle increases. SEM at $\delta=11^o$ is shown in Figure 5.2(c) and can be seen to be rough, this kind of roughness that is seen on the SEM shows that this is a kink-row based plane.

Region 16° - 29°: In contrast to the first two regions, in this range of deviation angles the emerging face consists of two facets. The first facet is vertical and smooth were as the second facet follows the K-60-35-90 family of planes and is nearly smooth. SEMs at deviation angle $\delta = 28^o$ are shown in Figures 5.2 (d) and (e).

Region 30° - 37°: In this range, the emerging face is three faceted. The first facet is vertical and rough, rough vertical planes are common in (110) etching [24]. The second facet is smooth and greater than 45° inclined P-35-60-90 family of planes and the third facet is smooth K-35-45-90 family of planes. The 2nd and the 3rd facets are not very smooth and at the same time they are not rough either. This is evident from the SEM in Figure 5.2 (g), which shows the spoke at $\delta = 36^o$. As the deviation angle increases, the 3rd facet diminishes. The top facet in this range is also the k-row based K-90-90-90 planes.

Region 38° - 44°: In this range of deviation angles, the K-35-45-90 family of planes no longer exist. The under-etched surface is made of two planes; the first being vertical and rough and the second nearly smooth P-35-60-90 family of planes. As deviation angle increases, the 2nd facet get smaller.

Region 45° - 55°: Here the under-etched surface face is single faceted and vertical. The emerging plane is very rough at 45° but as deviation angle increases the emerging plane becomes smoother and at $\delta = 55^o$, the emerging plane is very smooth. At $\delta = 55^o$, the

emerging plane is the vertical {111} plane. This can be seen in the Figure 5.2 (h).

Region 55° - 65°: In this region as well the emerging facet is vertical and smooth at $\delta = 55^\circ$ and becomes rough as the deviation angle increases. Figure 5.2 (i) shows the rough vertical side wall at deviation angle $\delta = 63^\circ$. This kind of roughness seen on the emerging plane tells that it belongs to the PBC based planes, the P-90-90-90 family of planes.

Region 66° - 71°: In this range of deviation angles the emerging face is double faceted the first being the rough and vertical P-90-90-90 planes where as the second facet is smooth and shallow, they follow the K-35-45-90 planes. Here the first facet is larger than the second facet, and can be seen clearly seen in the Figures 5.2 (j) and (k) at $\delta = 68^\circ$.

Region 72° - 76°: In this range of deviation angles the emerging plane still follow the same pattern as in the previous range except that the first facet is larger than the second facet. SEMs taken at $\delta = 72^\circ$ shown in Figures 5.2 (l) and (m) illustrate this. As the deviation angle increases the first facet get smoother. In this range, the top facet is rough hence can not be determined if it belongs to the P-90-90-90 or the K-90-45-35. But is assumed to be the P-90-90-90 family as they are close to vertical.

Region 77° - 88°: In this region, the emerging surface is two faceted, the first being steep K-90-45-35 family of planes and nearly smooth. And the second facet follows the K-35-45-90 family of planes. As the deviation angle increases both facets becomes smoother and the K-35-45-90 family of planes dominate. SEMs at deviation angle $\delta = 79^\circ$ are shown in Figures 5.2 (n) and (o), these show that both the planes are smooth.

Region 89° - 90°: As described in the previous range of deviation angles, the K-35-45-90 planes start to dominate and finally in these two spokes the under-etched surface was single faceted and belong to the P-60-35-90 family. At the deviation angle $\delta = 90^\circ$, the emerging plane is the 45° inclined {100} plane. The SEMs at $\delta = 90^\circ$ are shown in Figures 5.2 (p) and (q).

5.1.1.2 Si{100} etched at 80°C

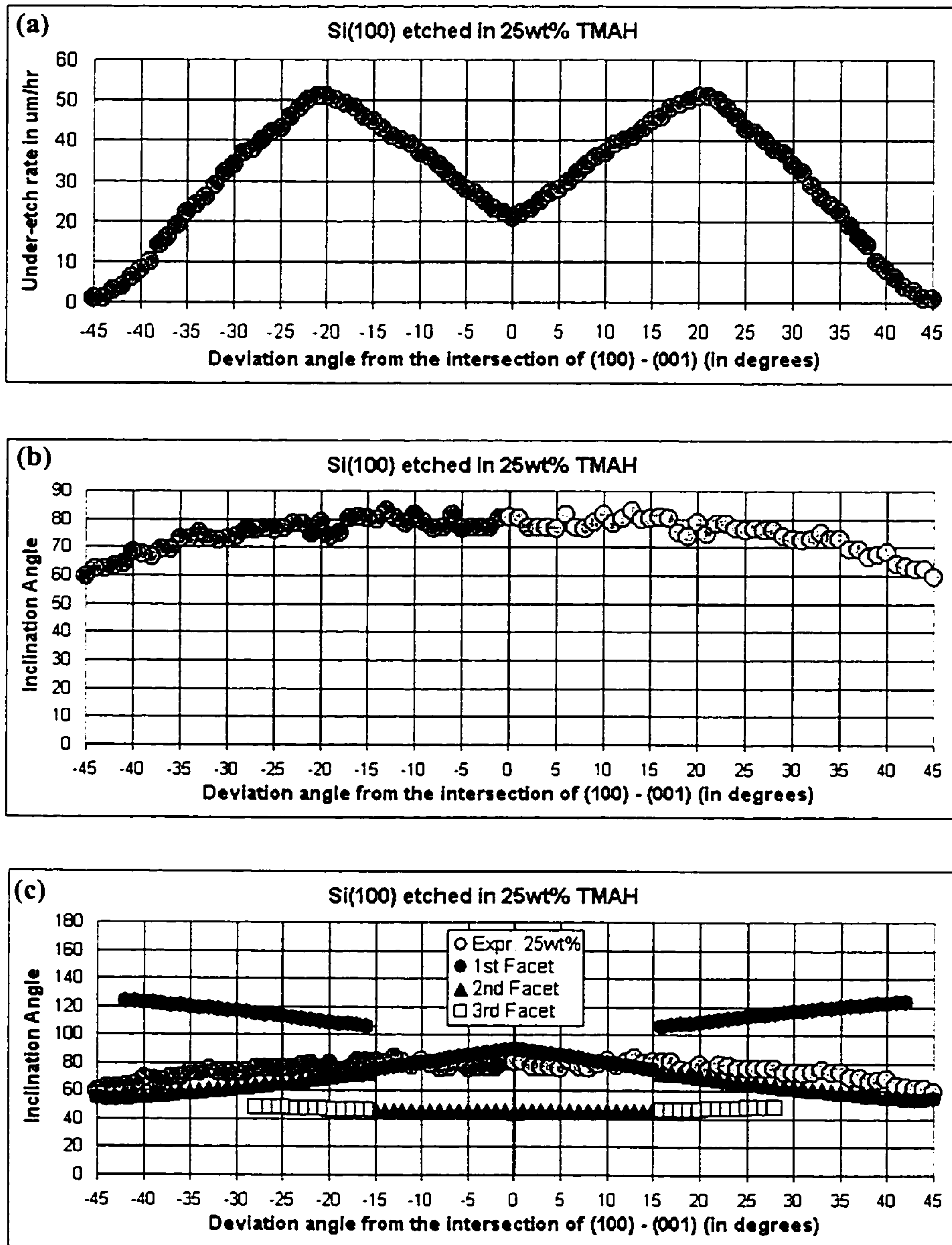

FIGURE 5.3: Si{100} etched in 25wt% TMAH at 80°C; (a) Under-etch rate, (b) Inclination angle, and (c) Facet details.

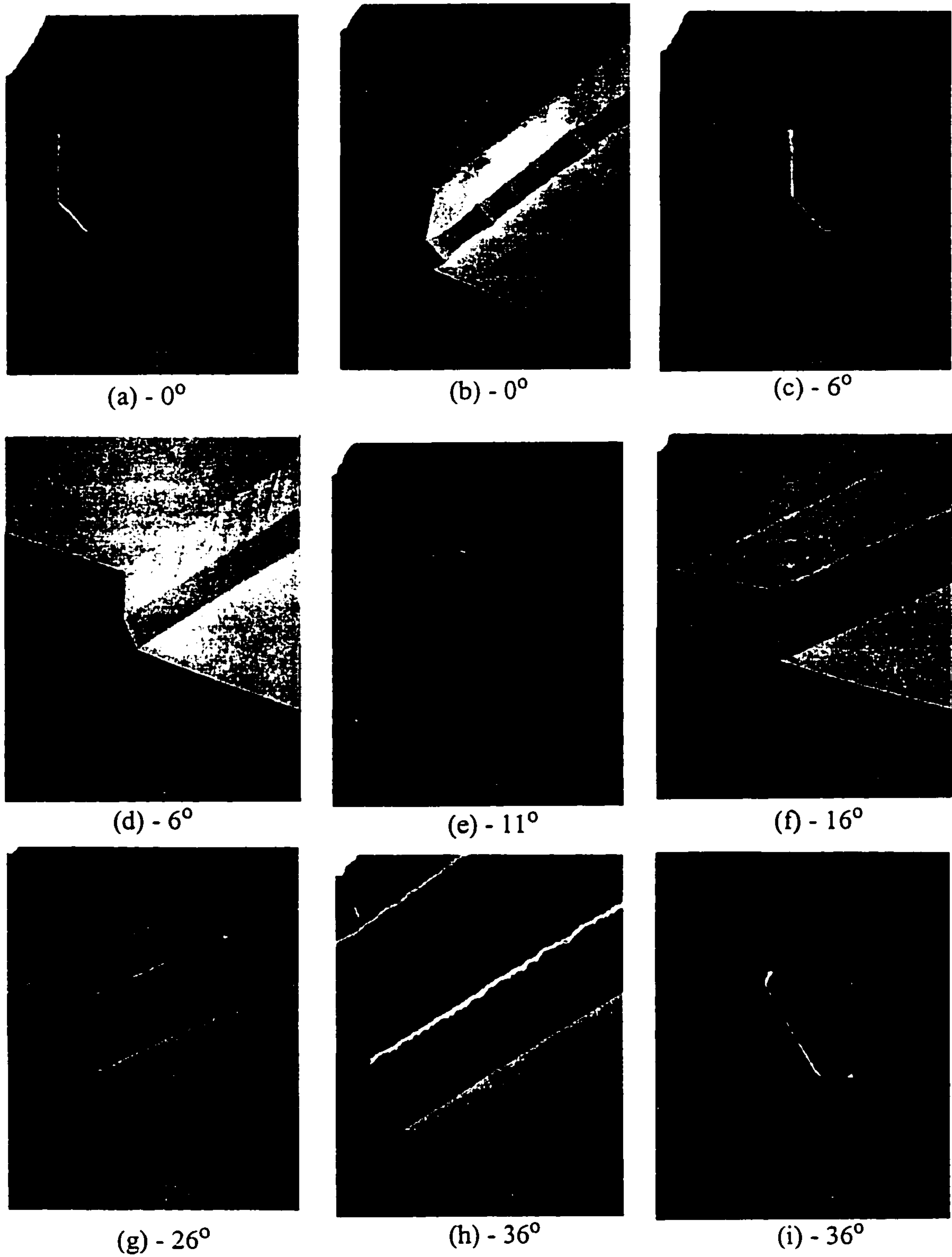

FIGURE 5.4: Scanning electron micrographs taken at various deviation angles for the {100} silicon etched in 25wt% TMAH at 80° C.

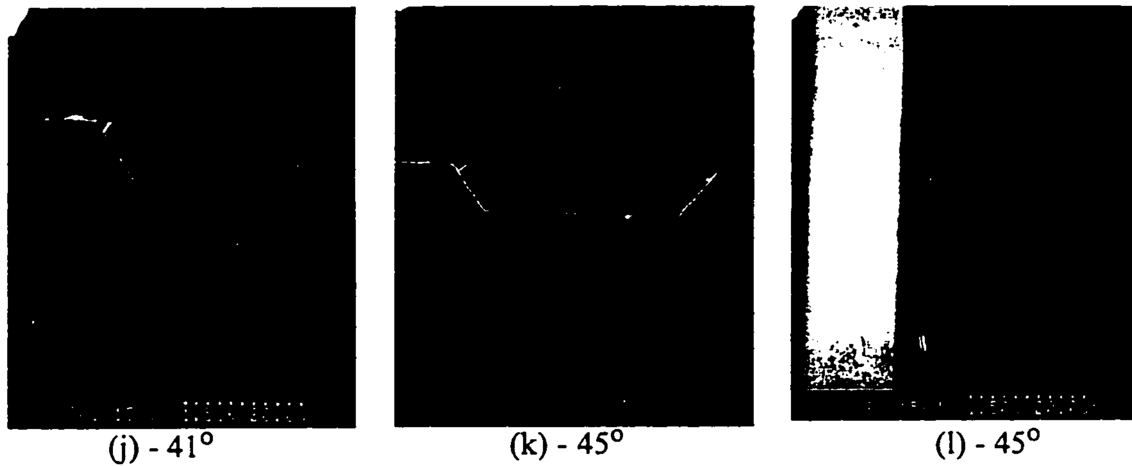

FIGURE 5.4: Scanning electron micrographs taken at various deviation angles for the {100} silicon etched in 25wt% TMAH at 80° C.

Fig. 5.3 (a) plots the under-etch rate for the variation of deviation angles from -45° to 45°. From the graph it is clear that we have a local minimum at δ = 0°.The etch-rate is maximum at δ = 22°. There are two global minima at δ = -45° and δ = 45°, where the emerging plane is the {111} plane.

TABLE 5.2. Si{100} etched in 25wt% TMAH

δ Range in degrees	No. of Facets	Facet Descriptions	Under-etched planes (Model Identifiers)	Trenches
0 -15	2	1st: 90° - 75°, smooth 2nd: ~45°, smooth	K-126-90-54 P-54-45-54	No
16 - 28	3	1st: > 90°, smooth and becomes rough 2nd: 75° - 65°, smooth 3rd: ~45° - 50°, smooth	K-54-90-126 K-126-90-54 P-54-45-54	No
29 - 42	2	1st: > 90°, rough 2nd: 65° - 55°, rough	K-54-90-126 K-126-90-54	No
43 - 45	1	54.7° {111} at δ = 45°	P-54-45-54	No

The inclination angles of the under-etched emerging surface formed while etching {100} silicon is shown in Figure 5.3 (b). The emerging surface is not simply single-faceted but are two-faceted for most deviation angles and three faceted for some deviation

angles. The different regions are summarized in the Table 5.2. and the SEM show the facets at different deviation angles, which are shown in Figure 5.4.

Region 0° - 15°: In this range of δ, the emerging face is two faceted, the top facet belongs to the k-row based planes, belonging to K-126-90-54 family. The second facet consists of PBC-based planes and belongs to P-54-45-54 family. As the deviation angle increases the roughness in the first facet increases, but does not become very rough. The second facet, the PBC-based planes, are very smooth in the entire range. At $\delta = 0^{\circ}$, the first facet is a vertical {100} plane and the second facet is a 45°-inclined {110} plane. These can be seen in the Figures 5.4 (a) and (b). Figures 5.4 (c) and (d) show the cross-sectional and side views of the spoke at $\delta = 6^{\circ}$. Figure 5.4 (e) shows the spoke at $\delta = 11^{\circ}$.

Region 16° - 28°: In this region the emerging surface is composed of three facets, the top first facet is inclined at an angle greater than 90° to the wafer surface and belongs to K-54-90-126; such inverted under-etched planes have been observed by other researchers [62]. The second facet belongs to the K-126-90-54 and is little rough. The third facet belongs to the P-54-45-54 family. Of the three facets, the second facet dominates and the first and third facets are small. Figures 5.4 (f) and (g) show the spokes at $\delta = 16^{\circ}$ and $\delta = 26^{\circ}$ respectively.

Region 29° - 42°: This region is very similar to the Region 16° - 28°, except that there is no third facet. The Figures 5.4 (h) and (i) show the side-view and cross-sectional view of the spokes at $\delta = 36^{\circ}$.

Region 43° - 45°: The emerging surface is single faceted and belongs to the P-54-45-54. At $\delta = 45^{\circ}$, the emerging plane is the smooth 54.7° inclined {111} plane, Figure 5.4 (k) shows the cross-section of the spoke at $\delta = 45^{\circ}$. Figure 5.4 (l) is the top view of the etch cavity $\delta = 45^{\circ}$, this shows the smoothness of the under-etched {111} plane and the etched (100) silicon surface.

5.1.2 Etching in 19wt% TMAH

5.1.2.1 Si{110} etched at 80°C

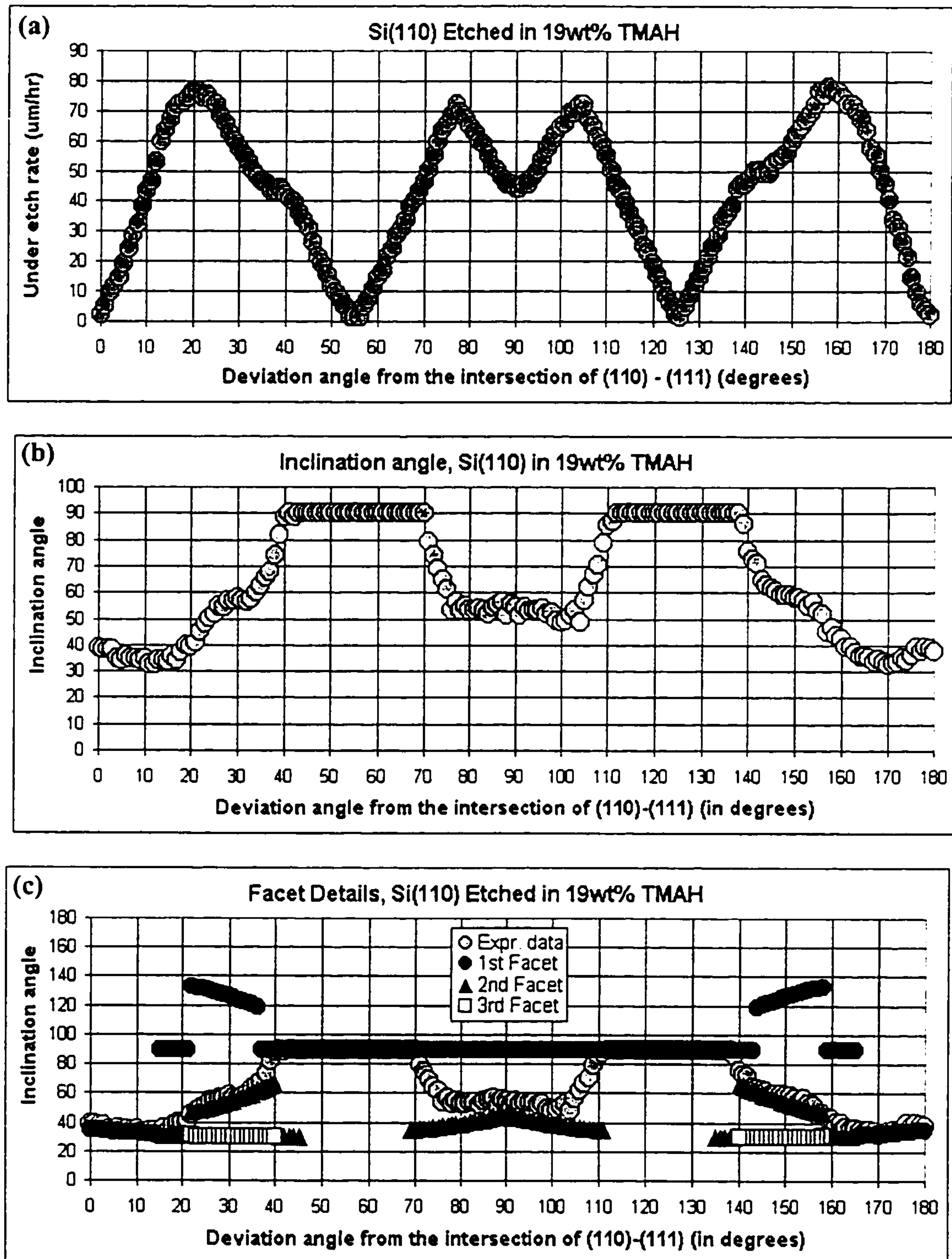

FIGURE 5.5: Si(110) etched in 19wt% TMAH at 80°C; (a) Under-etch rate, (b) Inclination angle, and (c) Facet details.

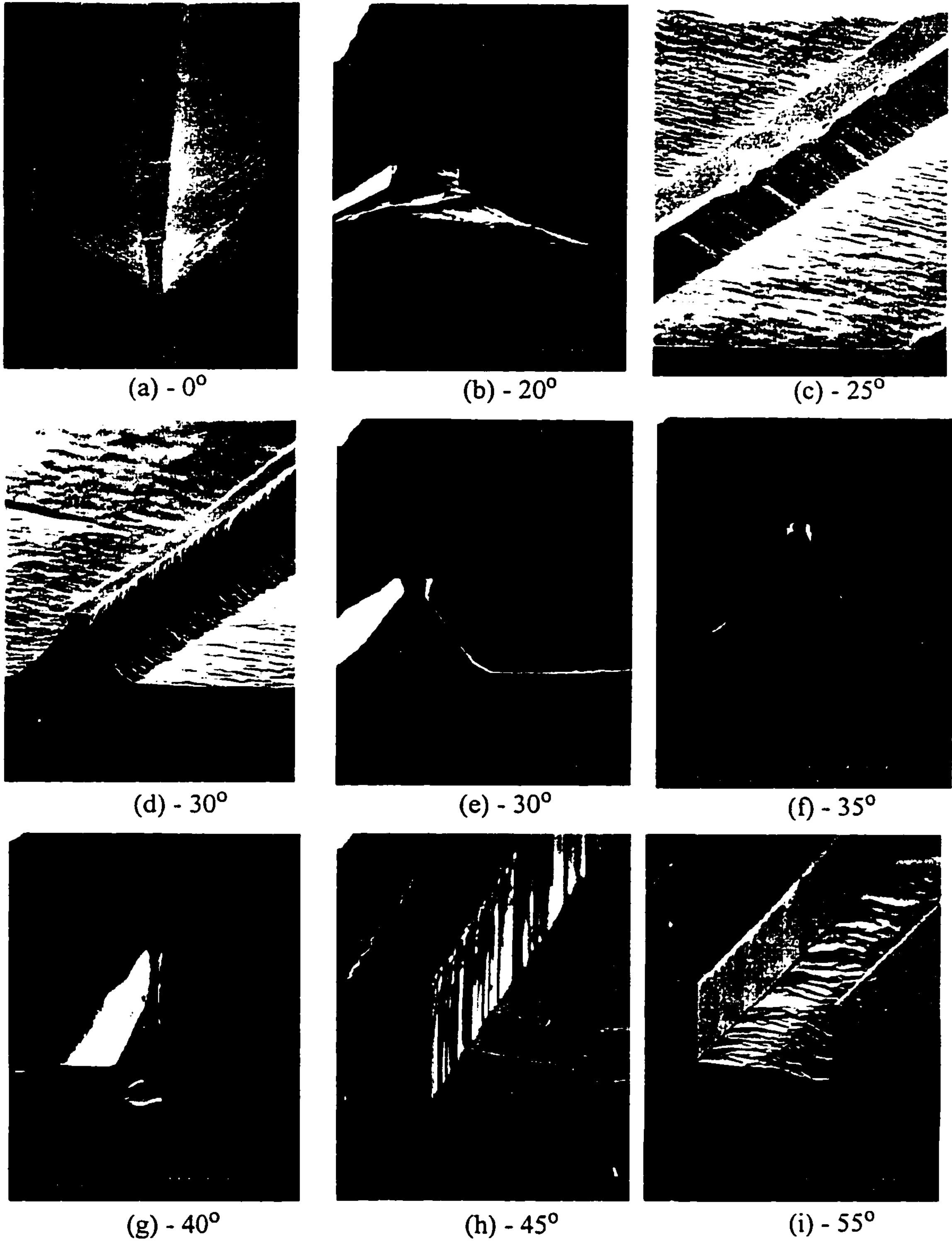

FIGURE 5.6: Scanning electron micrographs taken at various deviation angles for the {110} silicon etched in 19wt% TMAH at 80° C;

(j) - 65°

(k) - 65°

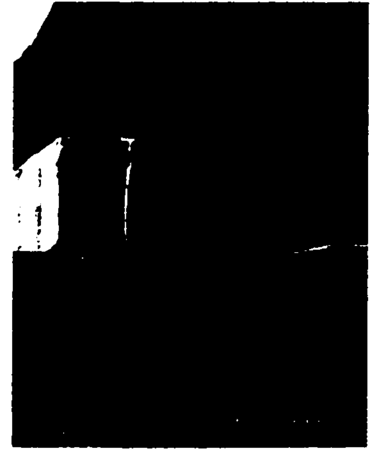
(l) - 70°

(m) - 70°

(n) - 75°

(o) - 75°

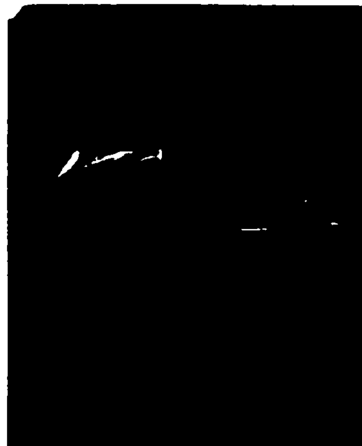
(p) - 90°

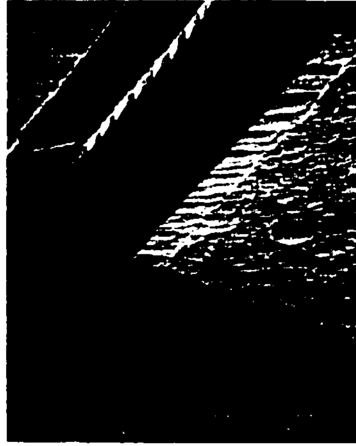
(q) - 90°

FIGURE 5.6: Scanning electron micrographs taken at various deviation angles for the {110} silicon etched in 19wt% TMAH at 80° C.

The under-etch rate for the 19wt% case is shown in Fig. 5.5(a). From the figure we can see that there are two minima at $\delta = 0^o$ and at $\delta = 180^o$, where the emerging plane is the 35.3^o inclined {111} plane. Also there are two more minima at $\delta = 55^o$ and at $\delta = 125^o$, where the emerging plane is vertical {111} plane. There is also a local minimum at $\delta = 90^o$.

Similarly, there are two maxima at $\delta = 21^o$ and at $\delta = 159^o$, and there are two other maxima at $\delta = 77^o$ and at $\delta = 103^o$. Also, we can see a notch at $\delta \approx 38^o$ and at $\delta \approx 142^o$. This change can also be seen in the inclination angle graph in Fig. 5.5(b).

TABLE 5.3. Si{110} etched in 19wt% TMAH

δ Range in degrees	No. of Facets	Facet Descriptions	Under-etched planes (Model Identifiers)	Trenches
0 - 10	1	35° -30°, very smooth	K-35-45-(90)	No
11- 18	1	1st: 90°, smooth 2nd: <45°, smooth	1st: K-90-90-(90) 2nd: K-35-45-(90)	No
19 - 35	3	1st: >90°, rough 2nd: >45°, not smooth 3rd: ~30°, rough	1st: P-145-120-(90) 2nd: P-35-60-(90) 3rd: K-35-45-(90)	Yes, very shallow
36 -40	3	1st: ~90°, rough 2rd: >45°, not smooth 3rd: ~30°, almost smooth	1st: K-90-90-(90) 2nd: P-35-60-(90) 3rd: K-35-45-(90)	Yes, very shallow
41 - 45	2	1st: ~90°, rough 2nd: ~30°, smooth, very small	1st: K-90-90-(90) 2nd: K-35-60-(90)	Yes, very shallow
46 - 55	1	90°, rough and becomes smooth as δ increases	K-90-90-(90)	Yes, very shallow
55 - 68	1	90°, smooth and becomes rough as δ increases	P-90-90-(90)	Yes
69 - 90	2	1st: ~90°, rough 2nd: 30°- 45°, smooth	1st: P-90-90-(90) 2nd: K-35-60-(90)	Yes

Region 0° - 10°: In this range of δ, the emerging face is single faceted and is very smooth. These planes are of the K-35-45-(90) family. SEM at $\delta = 0^o$ is shown in Figure 5.6 (a), this shows the smooth {1 1 1} plane on the under-etched side wall of the cavity.

Region 11° - 18°: In this range of δ, the emerging face is composed of two facets, first facet is a vertical plane belonging to the K-90-90-(90) family and the second facet follows the K-35-45-(90) family. Both the facets are smooth. SEM at $\delta= 20^o$ is shown in Figure 5.6 (b). Here the second facet is longer than the first (top) facet.

Region 19° - 35°: In contrast to the first two regions, in this range of deviation angles the emerging face consists of three facets. The first facet is inclined at an angle greater than 90° and is rough, this belongs to the family P-145-120-(90) (which is the inverse of the P-35-60-(90) family planes). The second facet belongs to the P-35-60-(90), it is very interesting to see that the first and the second facets are made of the same type of planes, except that they are inverted (they are the same planes crystallographically). The third facet follows the K-35-45-(90) family of planes and is not smooth. Figure 5.6 (c) shows the side view of the spoke at deviation angle $\delta = 25^o$, this shows the roughness of the three facets. SEMs at $\delta = 30^o$ are shown in Figures 5.6 (d) and (e). In the side view, one can see the roughness on the top and bottom facets and on the cross-sectional view one can clearly visualize the facet inclination angles. Figure 5.6 (f) shows the cross-sectional view of the spoke at deviation angle $\delta = 35^o$. We can see that as the δ increases the top facet becomes smaller. In this range the second facet is the largest of all the three facets. This can be seen from the effective inclination angle graph, the effective inclination angle is very close to the inclination angle of the second facet. In this range of deviation angles we can see very shallow trenches/trench features on the sides of the spokes.

Region 36° - 40°: Here in this range, the emerging face is again three faceted; the first facet is vertical and rough belonging to K-90-90-(90) family. The second and the third facets still follow the same planes as in the range 19° to 35°. The third facet is almost smooth.

There are very shallow trenches on the sides of the spokes. Figure 5.6 (g) shows the spoke at $\delta = 40^o$, top facet is rough and is nearly a vertical plane, second facet is smooth and the third facet is also smooth and is very small. As the deviation angle increases, the third facet vanishes.

Region 41° - 45°: In this range of deviation angles, the emerging surface is two faceted. The K-90-90-(90) family of planes form the first facet which is vertical and rough. The second facet is nearly smooth and are the K-35-45-90 family of planes. The second facet is very small compared to the first facet, hence the effective inclination angle is almost 90°. Very shallow trenches can be see on the sides of the spokes. Figure 5.6 (h) shows the spoke at $\delta = 45^o$, here the dominant plane is the first facet which is rough and vertical, but you can still see the very small smooth second facet. In this range, as the deviation angle increases, the first facet is more dominant. On the bottom of the etch cavity, we can see the visible difference in surface roughness at the edges which differentiates the trench from the center of the etch cavity.

Region 46° - 55°: Here the emerging face is single faceted and vertical, belonging to the K-90-90-(90) family. The emerging plane is very rough at 45° but as the deviation angle increases the emerging plane becomes smoother and at $\delta = 55^o$, the emerging plane is very smooth. At $\delta = 55^o$, the emerging plane is the vertical {111} plane. This can be seen in the Figure 5.6 (i).

Region 55° - 68°: In this region of deviation angles the emerging facet is vertical. The side wall is smooth at $\delta = 55^o$ and becomes rough as the deviation angle increases. Figures 5.6 (j) and (k) show the rough vertical wall at deviation angle $\delta = 65^o$. These planes belong to the P-90-90-(90) family.

Region 69° - 90°: In this range of deviation angles the emerging face is double faceted the first being the rough and vertical P-90-90-(90) family of planes. Where as the second

facet is smooth, they follow the K-35-45-(90) planes. The Figures 5.6 (l) and (m) show the spokes at $\delta = 70^o$, we can see that the first facet is rough and vertical. The second facet is smoother and is a ~35°-inclined plane. As the deviation angle increases from 69° to 75°, the top facet becomes rough and roughest at 75°. Also, as the deviation angle increases, the top facet becomes smaller and the second facet starts to dominate on the under-etched surface. Figures 5.6 (n) and (o) show the spokes at $\delta = 75^o$, the first facet is very rough about vertical and the second facet is smooth and ~42° inclined. As the deviation angle increases in the range $75^o < \delta < 90^o$, the top facet becomes smoother and smaller. Figures 5.6 (p) and (q) show the spoke at $\delta = 90^o$, here the first facet is very small and vertical. The second facet is smooth and inclined at 45°. The top facet at $\delta = 90^o$ is the vertical {110} plane and the second facet is the 45° inclined smooth {100} plane.

5.1.2.2 Si{100} etched at 80°C

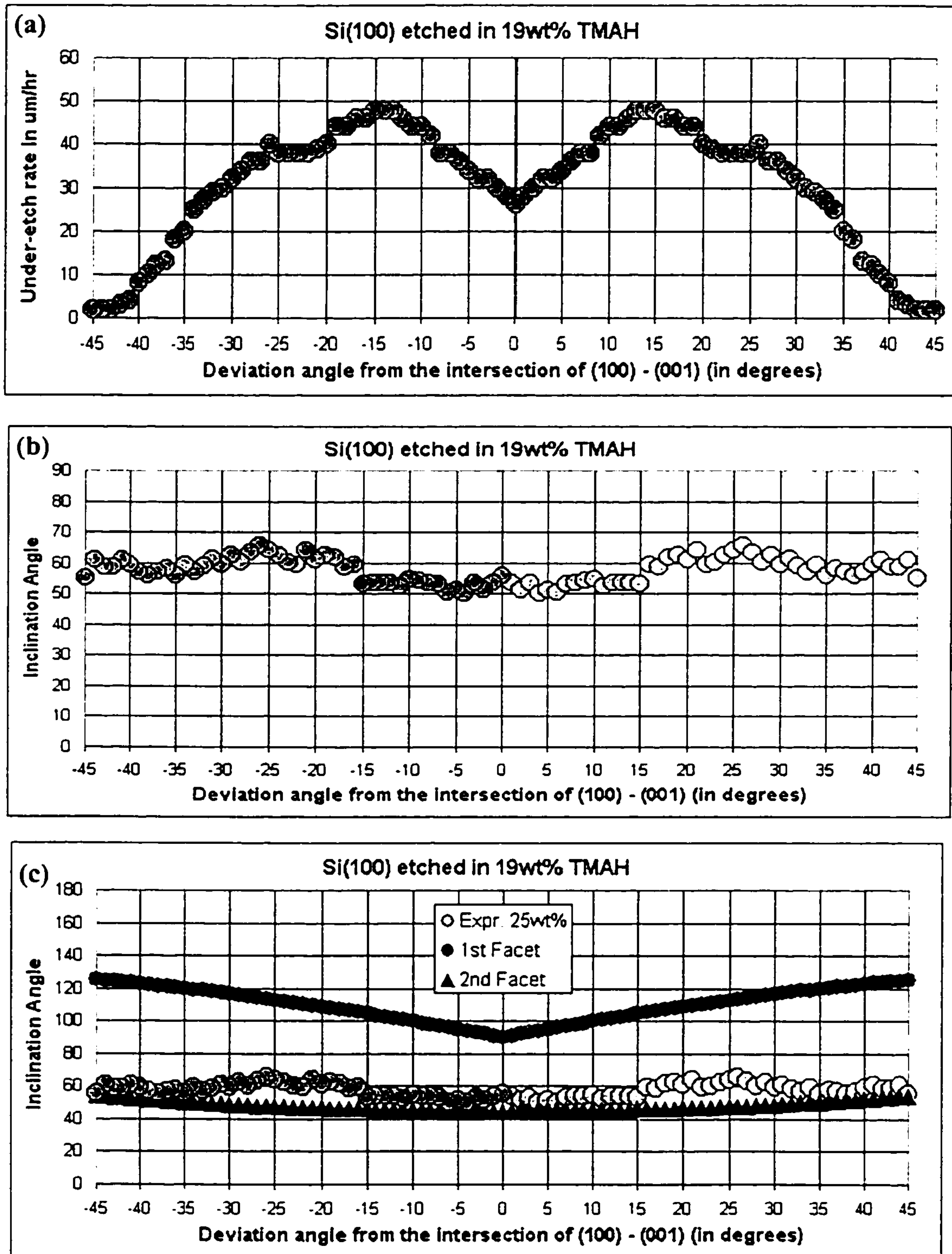

FIGURE 5.7: Si{100} etched in 19wt% TMAH at 80°c; (a) Under-etch rate, (b) Inclination angle, (c) Facet details.

Figure 5.7(a), plots the under-etch rate for the variation of deviation angles from -45° to 45°. From the graph we can see a local minimum at $\delta = 0^o$. The etch-rate is maximum at $\delta = 14^o$. There are two global minima at $\delta = -45^o$ and $\delta = 45^o$. In this 19wt% case we can see a notch at $\delta = 26^o$, which is not seen in the 25wt% case.

Inclination angle of the emerging surface is plotted in Figure 5.7(b), the emerging surface is not single faceted in this case as well. The under-etched surface is two faced in the entire range, but is composed of different family of planes at different deviation angles. This is summarized in Table. 5.4. The {100} etched surface is found to have very small hillocks scattered all over the etched surface, this can be seen on the SEMs in Figure 5.8.

TABLE 5.4. Si{100} etched in 19wt% TMAH

δ Range in degrees	No. of Facets	Facet Descriptions	Under-etched planes (Model Identifiers)	Trenches
0	2	1st: Vertical and smooth {111} plane 2nd: 45°, {110} plane	K-54-90-(126) P-54-45-(54)	No
30 - 45	2	1st: > 90°, smooth-rough - smooth 2nd: >45°, rough - smooth	K-54-90-(126) P-54-45-(54)	No

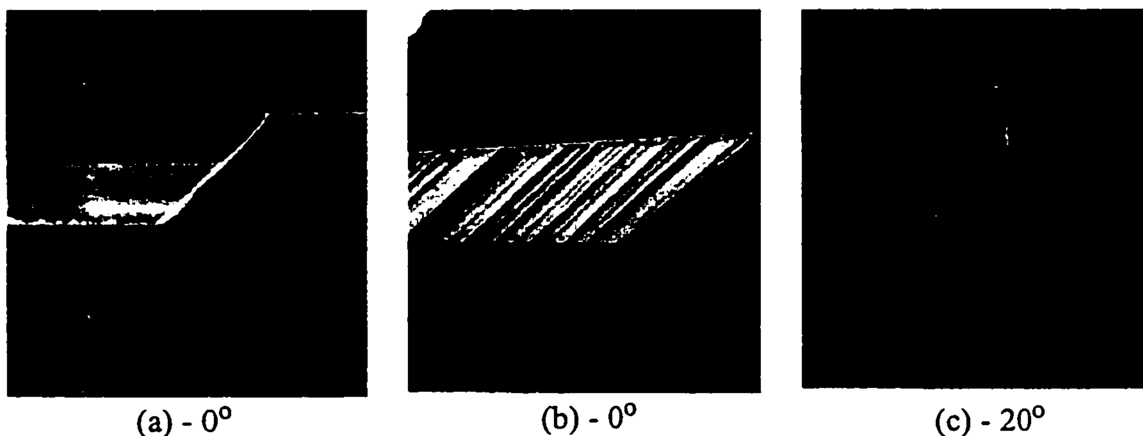

(a) - 0° (b) - 0° (c) - 20°

FIGURE 5.8: Scanning electron micrographs taken at various deviation angles for the {100} silicon etched in 19wt% TMAH at 80° C.

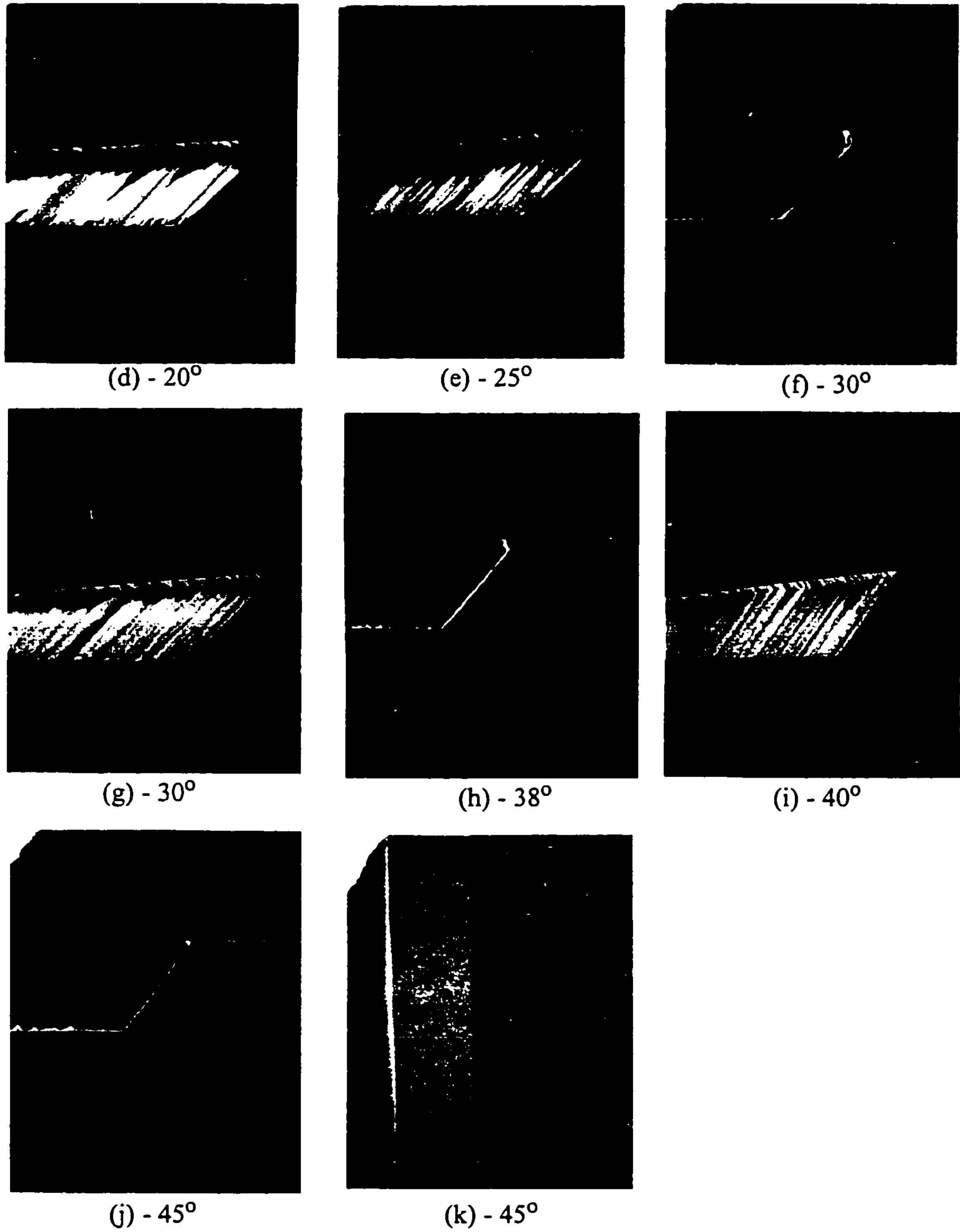

FIGURE 5.8: Scanning electron micrographs taken at various deviation angles for the {100} silicon etched in 19wt% TMAH at 80° C.

Deviation angle 0°: At deviation angle $\delta = 0^{o}$, the under-etched emerging surface is two faceted. The top facet is smooth and vertical {111} plane. The second facet is the 45°-inclined {110} plane. Figures 5.8 (a) and (b) show the cross-sectional view and side-view of spoke at $\delta = 0^{o}$ respectively. As can be seen from the SEMs the top facet is very small, and the under-etched surface is dominated by the second facet, the {110} plane.

Region 1° - 45°: In this range, the under-etched emerging face is two faceted, the top facet is > 90° and belongs to K-54-90-(126) family of planes; the second facet belongs to the P-54-45-(54) family of planes. The top facet is initially smooth but becomes really rough as the deviation angle increases and is the roughest at about $\delta = 25^{o}$; after that the top facet becomes smoother as the deviation angle increases. In the range where $\delta < 25^{o}$, the top facet is very rough that the cross-sectional view seem to show the top facet to be vertical, one can be easily fooled by the cross-sectional view. When observed carefully using the side view of the spoke it was evident that the top facet is in fact inclined at an angle > 90°. This can be seen from the Figures 5.8 (c) and (d) showing the cross-sectional and side view of spoke at $\delta = 20^{o}$.

The second facet is initially rough and becomes smoother as deviation angle increases. It can be seen that in the entire range, the second facet dominates the under-etched surface. Various SEMs of the spokes in this range are shown in Figures 5.8 (c) to (i). At deviation angle $\delta = 45^{o}$ the top facet is very very small and is the 125.3°-inclined {111} plane. The second facet is the 54.7°-inclined {111} plane. The SEMs of the spoke at $\delta = 45^{o}$ are shown in Figures 5.8 (j) and (k).

5.1.3 Etching in 17wt% TMAH

5.1.3.1 Si{110} etched at 80°C

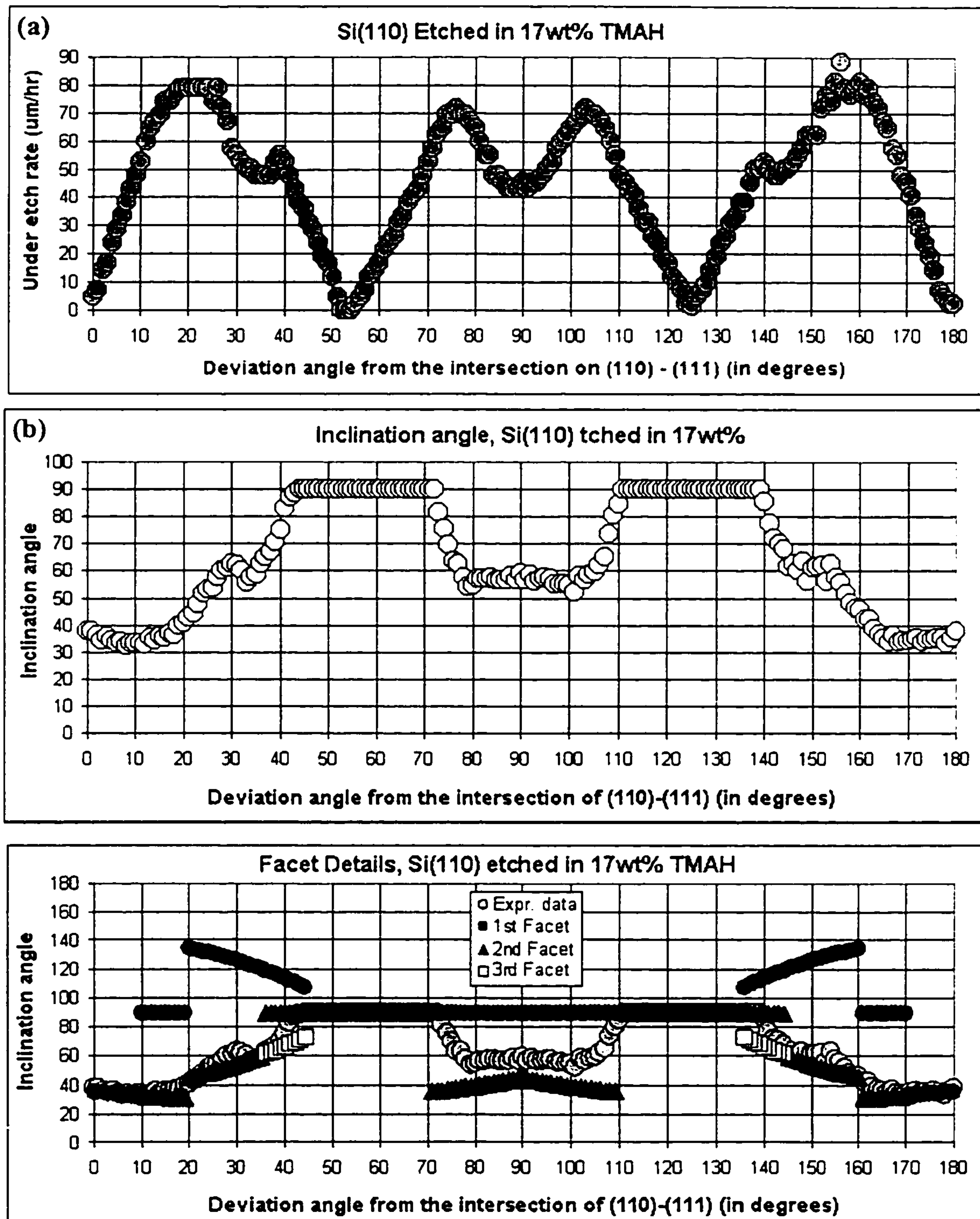

FIGURE 5.9: Si{110} etched in 17wt% TMAH at 80°C; (a) Under-etch rate, (b) Inclination angle, and (c) Facet details.

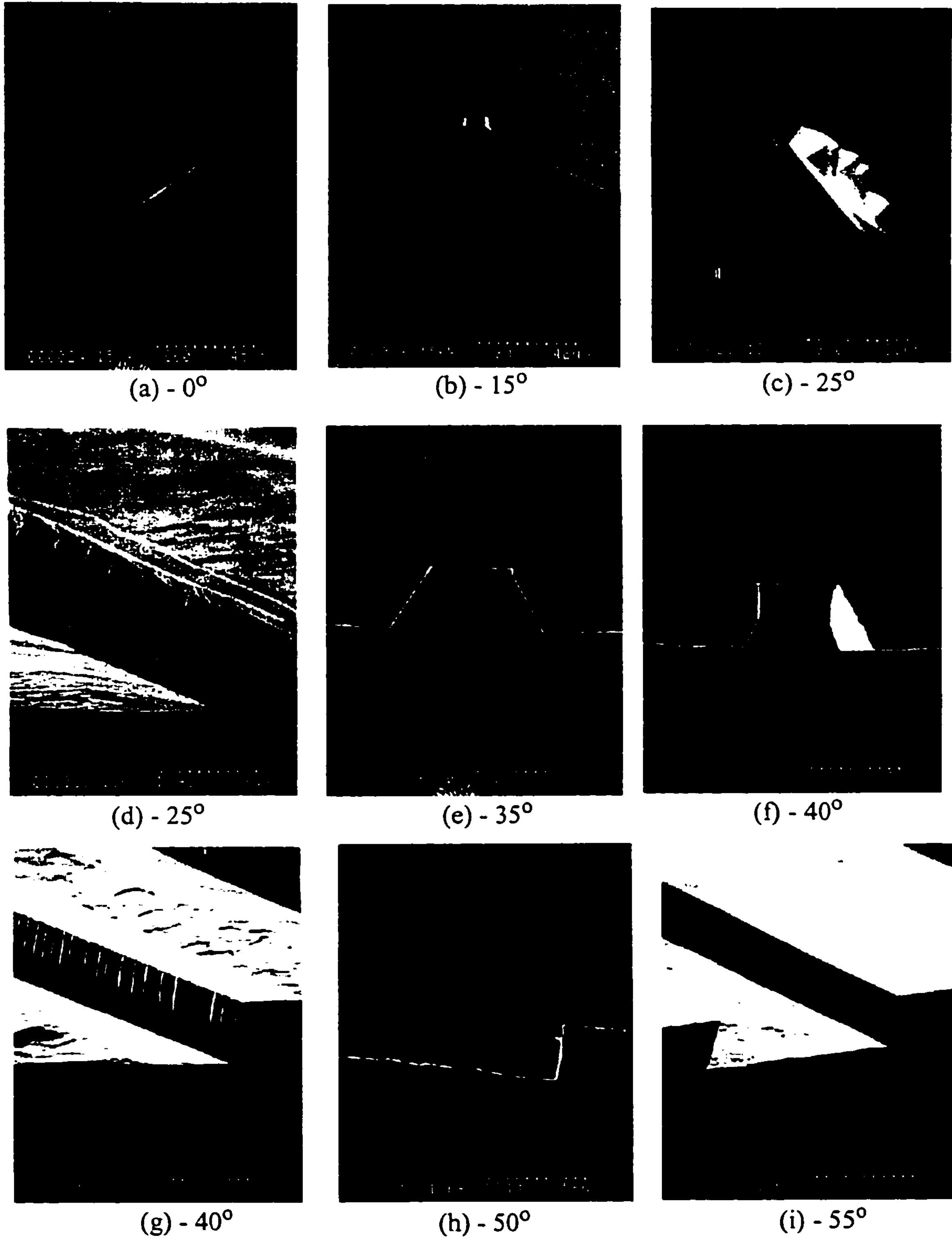

FIGURE 5.10: Scanning electron micrographs taken at various deviation angles for the {110} silicon etched in 17wt% TMAH at 80° C.

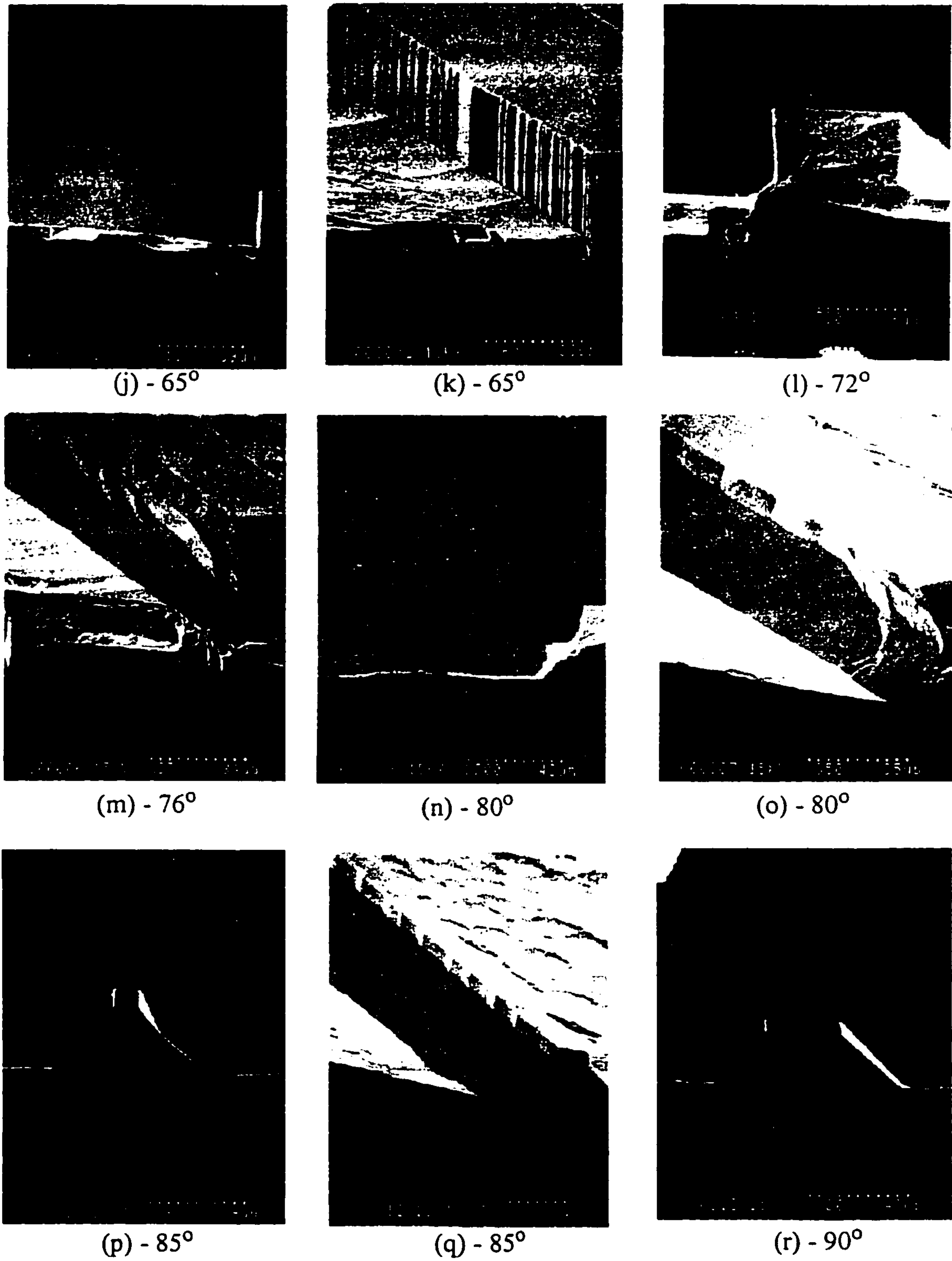

FIGURE 5.10: Scanning electron micrographs taken at various deviation angles for the {110} silicon etched in 17wt% TMAH at 80° C.

Figure 5.9 (a) shows the under-etch rate for the 17wt% case. Form the graph we can see that there are two minima at $\delta = 0^o$ and at $\delta = 180^o$ as expected, where the emerging plane is 35.3^o inclined {111} plane. Also there are two more minima at $\delta = 55^o$ and at $\delta = 125^o$, where the emerging plane is vertical {111} plane. There is also a local minimum at $\delta = 90^o$. Similarly, there are two maxima at $\delta = 76^o$ and at $\delta = 103^o$, and there are two other maxima at δ around 24° and at δ around 156°. Also, we can see a notch at $\delta = 39^o$ and at $\delta = 140^o$. The notch in the 17wt% is more prominent than the 19wt% case. This notch can also be seen in the inclination angle graph in Figure 5.9 (b).

TABLE 5.5. Si{110} etched in 17wt% TMAH

δ Range in degrees	No. of Facets	Facet Descriptions	Under-etched planes (Model Identifiers)	Trenches
0 - 9	1	35° -30°, very smooth	K-35-45-(90)	No
10 - 19	2	1st: 90°, smooth 2nd: < 30°, smooth	1st: K-90-90-(90) 2nd: K-35-45-(90)	No
20 - 30	2	1st: >90°, rough 2nd: >45°, not smooth 3rd: ~30°, not smooth	1st: P-145-120-(90) 2nd: P-35-60-(90) 3rd: K-35-45-(90)	No, But can see features
31 - 35	2	1st: >90°, rough 2nd: >45°, not smooth	1st: P-145-120-(90) 2nd: P-35-60-(90)	No, But can see features
36 - 44	3	1st: >90°, rough 2nd: =90°, not smooth 3rd: >45°, not smooth	1st: P-145-120-(90) 2nd: K-90-90-(90) 3rd: P-35-60-90	No, But can see features
45 - 55	1	1st: Vertical, smooth	1st: K-90-90-(90)	No, But can see features
55 - 70	1	1st: Vertical, smooth, becomes rougher	1st: P-90-90-(90)	No, But can see features
71 - 90	2	1st: ~90°, rough 2nd: 35°- 45°, smooth	1st: P-90-90-(90) 2nd: K-35-45-(90)	No, But can see features

Region 0º - 9º: In this range of δ, the emerging face is single faceted and smooth. These planes are of the K-35-45-(90) family. SEM at δ = 0° is shown in Figure 5.10 (a), this shows the smooth {111} plane.

Region 10º - 19º: Here the under-etched emerging face is composed of 2 facets, first facet is a vertical plane belonging to the K-90-90-(90) family and the second facet follows the K-35-45-(90) family. Both the facets are smooth. SEM at δ = 15° is shown in Figure 5.10 (b).

Region 20º - 35º: In this range, the under-etched emerging face is made of two facets. The first facet is inclined at an angle greater than 90° and is rough, this belongs to the family P-145-120-(90) (which is the inverse of the planes belonging to the family P-35-60-(90)). The second facet belongs to the P-35-60-(90), it's very interesting to see that the first and second facets are made of the same planes, except that they are inverted (they are the same planes crystallographically). SEMs at deviation angle δ = 155° (25°) are shown in Figures 5.10 (c) and (d). The SEM on Figure 5.10(c), the spoke on left show that the under-etched surface is three faceted. But when we look at the side view of the same spoke (Figure 5.10 (d)) we can see that the under-etched surface is composed of only two facets. The interface between the first and the second facet is very rough as can been seen on the SEM. The rough interface between the second facet and the bottom of etch cavity make the interface look like a facet, but this is not true. As the deviation angle increases, the top facet becomes smaller and the second facet dominates the under-etched surface. Figure 5.10 (e) shows the cross-sectional view of the spoke at δ = 35°, where the top facet is very small. In this range we can see trench features on the sides of the spokes, see Figure 5.10 (d).

Region 36º - 44º: Here in this range of deviation angles, the under-etched surface has three facets. The first facet still belongs to the P-145-120-(90) family and is very small compared to the other two facets.The second facet is vertical and belongs to the K-90-90-

(90) family, this facet dominates the under-etched surface. The second facet becomes smoother as the deviation angle increases and also becomes larger as the deviation angle increases. The third facet belongs to the P-35-60-(90) family and is very smooth and becomes smaller as the deviation angle increases. Figures 5.10 (f) and (g) show the cross-sectional and side view of the spoke at $\delta = 40^{o}$, the roughness of these facets can be seen in Figure 5.10 (g).

Region 45° - 55°: In this region, the under-etched surface is single faceted and vertical. They belong to the K-90-90-(90) family of planes. The emerging plane becomes smoother as the deviation angle increases At $\delta=55^{o}$, the emerging plane is the very smooth {110} plane. Figure 5.10 (h) shows the cross-sectional view of the spoke at $\delta = 50^{o}$, it shows the rough vertical emerging plane. And Figure 5.10 (i) shows the side view of the spoke at $\delta = 55^{o}$, it shows the smooth vertical {110} plane.

Region 55° - 70°: In this region of the under-etched surface is single faceted and vertical. They belong to the P-90-90-(90) family of planes. The emerging plane becomes rougher as the deviation angle increases At $\delta = 55^{o}$, the emerging plane is the very smooth {110} plane. Figures 5.10 (j) and (k) show the spoke at $\delta = 65^{o}$, Figure 5.10 (j) shows the cross-sectional view and the Figure 5.10 (k) shows the side view where you can clearly see the roughness in vertical emerging plane. From the Figure 5.10 (k) we can see a difference in roughness of the etched bottom surface, the edges are smoother when compared to the center of the etched cavity bottom. This shows that we can visually see trench features but they are not deep enough to be called as trenches.

Region 71° - 90°: In this region the emerging surface is composed of two facets, first facet is rough and vertical plane belonging to the P-90-90-(90) family and the second facet belongs to the K-35-45-(90) family and is smooth. Initially the first facet is larger than the second facet, but as the deviation angle increases the second facet, K-35-45-(90) dominates. Figure 5.10 (l) shows the cross-sectional view of the spoke at $\delta = 72^{o}$, we can see

that the first facet dominates the under-etched surface. Figure 5.10 (m) shows the side view of the spoke at $\delta = 76^o$, this shows the roughness of the facets, the top facet is rougher than the second facet. The top facet is roughest at $\delta = 76^o$. Figures 5.10 (n) and (o) show the spokes at $\delta = 80^o$ and Figures 5.10 (p) and (q) show the spokes at $\delta = 85^o$, from these SEMs you can clearly see the roughness on both the facets. Also, one can see that as the δ increases, the first facet becomes smaller and the second facet dominates. Figure 5.10 (r) shows the cross-sectional view of the spoke at $\delta = 90^o$, here the second facet dominates the under-etched surface and is the smooth 90° inclined {100} plane.

5.1.3.2 Si{100} etched at 80°C

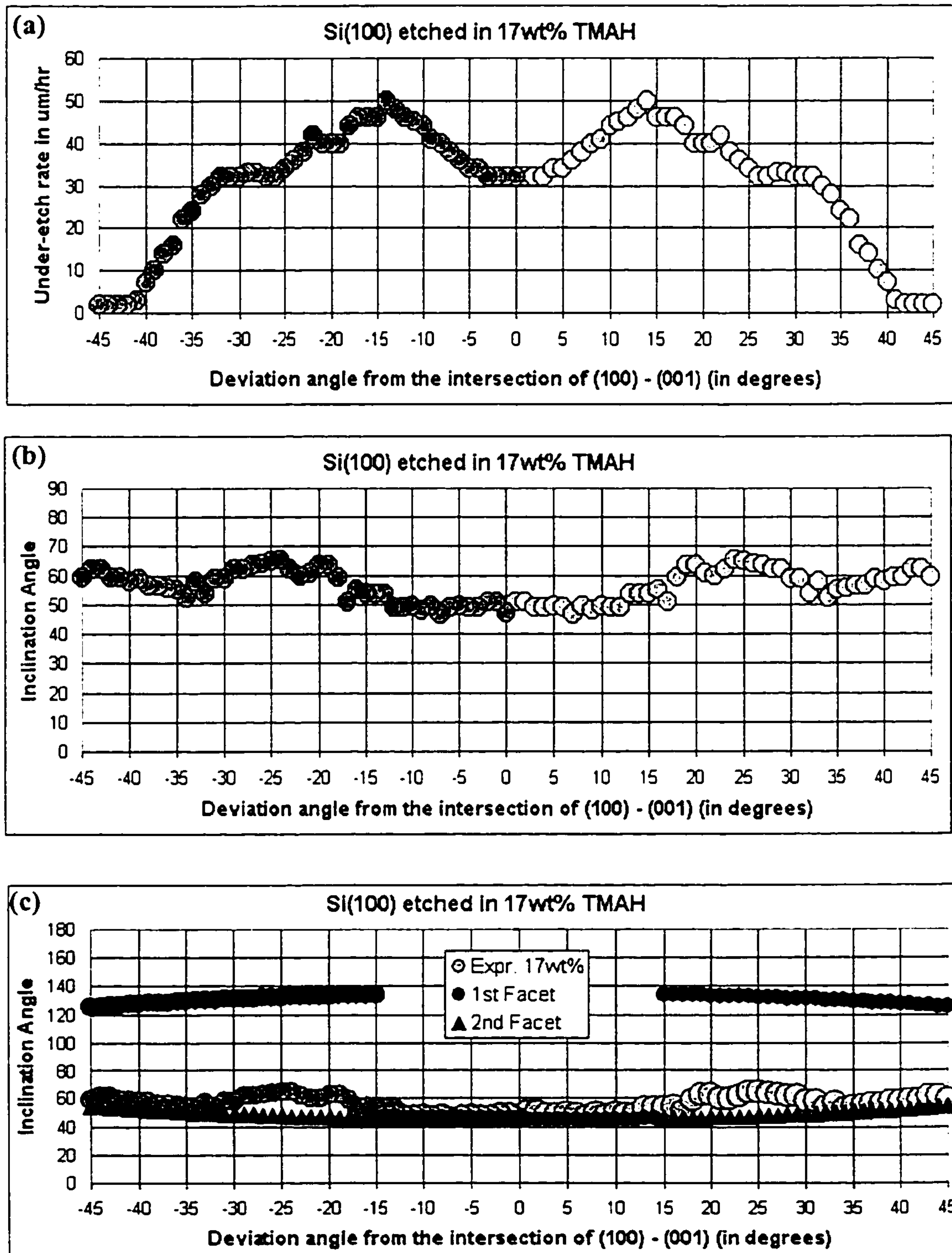

FIGURE 5.11: Si{100} etched in 17wt% TMAH at 80°C; (a) Under-etch rate, (b) Inclination angle, and (c) Facet details.

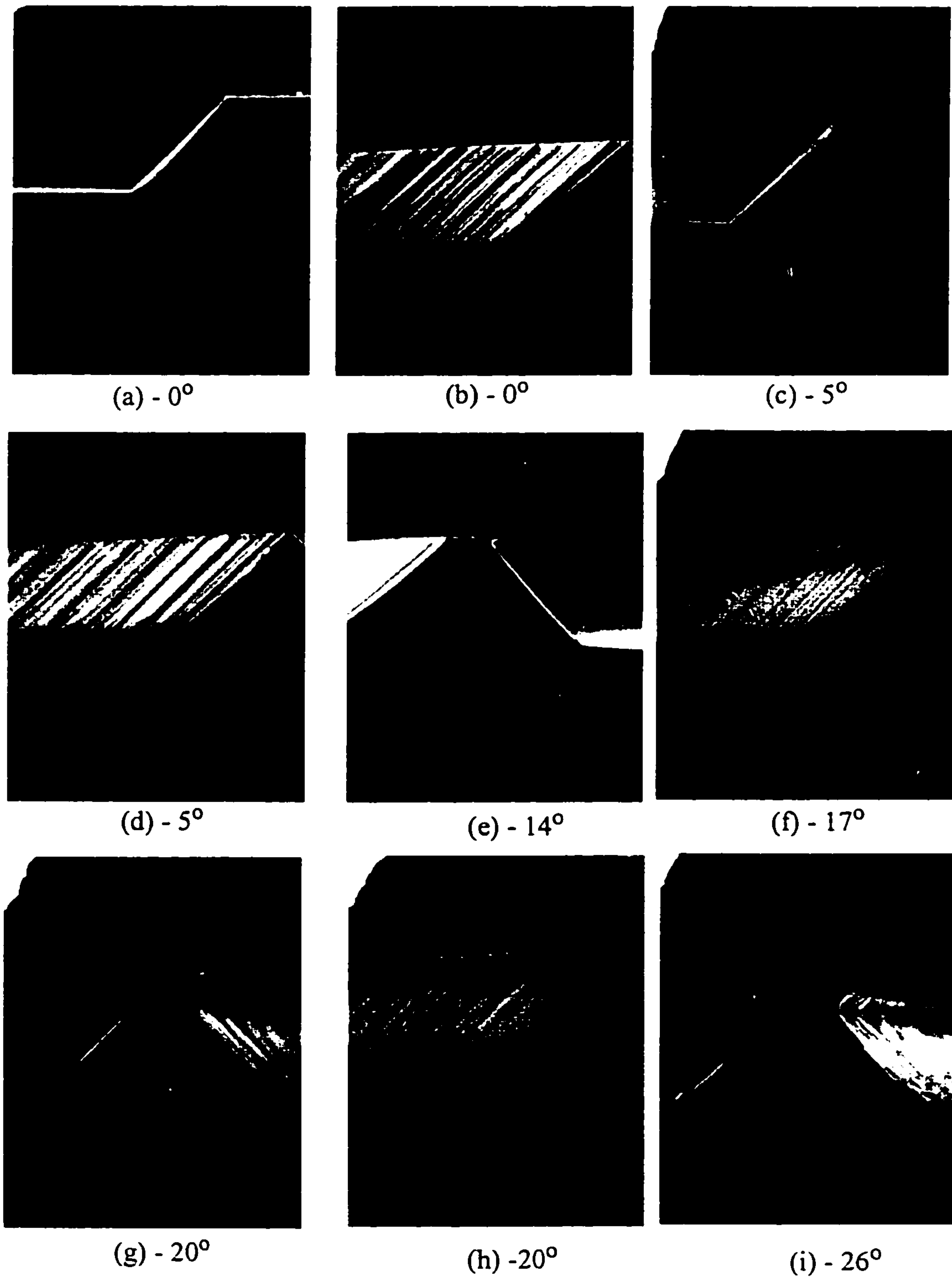

FIGURE 5.12: Scanning electron micrographs taken at various deviation angles for the {100} silicon etched in 17wt% TMAH at 80° C

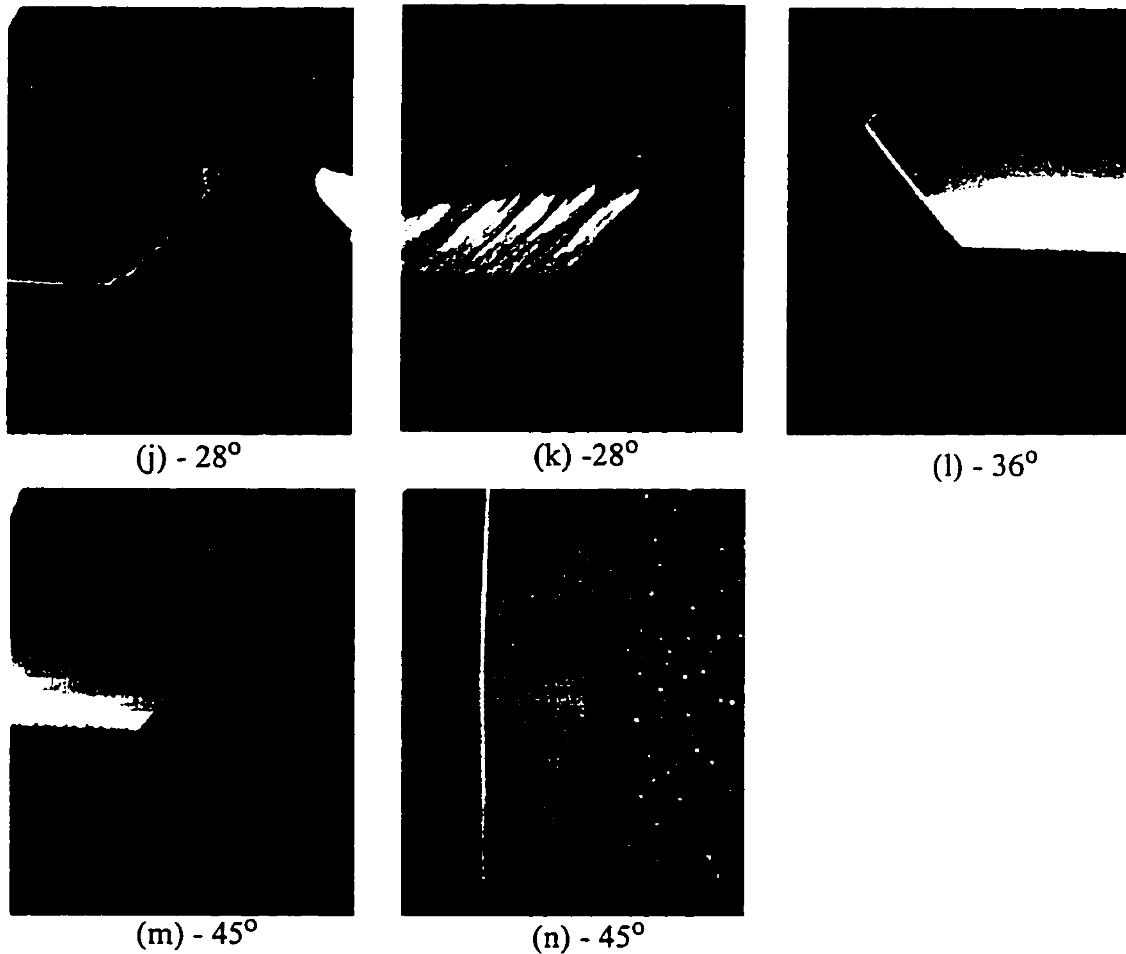

FIGURE 5.12: Scanning electron micrographs taken at various deviation angles for the {100} silicon etched in 17wt% TMAH at 80° C

Figure 5.11 (a), shows the under-etch rate plotted against the deviation angles. From the graph we can see a flat local minimum at $\delta = 0^{\circ}$ to 2°.The etch-rate is maximum at $\delta = 14^{\circ}$. There are global minima at every 45°.

Inclination angle of the emerging surface is plotted in Figure 5.11 (b), in this case also the emerging surface is single or two faceted. The facets are composed of different family of planes at different deviation angles. This is summarized in the Table. 5.6. The {100} etched surface is found to have very small hillocks scattered all over the etched surface, this can be seen on the SEMs taken at $\delta = 45^{\circ}$, in Figure 5.12 (m).

TABLE 5.6. Si{100} etched in 17wt% TMAH

δ Range in degrees	No. of Facets	Facet Descriptions	Under-etched planes (Model Identifiers)	Trenches
0 - 14	1	~ 45°, not smooth	P-54-45-(54)	No
15 - 45	2	1st: > 90°, very rough - becomes smooth 2nd: rough - becomes smooth	P-126-135-(126) P-54-45-(54)	No

Region 0° - 14°: In this rage of deviation angles the emerging surface is single faceted and is not smooth. These planes belong to P-54-45-(54) family of planes. Figures 5.12 (a) and 5.12 (b) show the cross-sectional view and the side view of the spoke at deviation $\delta = 0^\circ$. And Figures 5.12 (c), (d) and (e) show some spokes in this range of deviation angles. We can see that all the under-etched planes in this range have the same roughness features.

Region 15° - 30°: Here in this range of deviation angles, the under-etched emerging surface is double faceted. The first facet is very rough and vertical, the second facet is rough and inclined at a shallower angle. The first facet belongs to the P-126-135-(126) family. The second facet belongs to the P-54-45-(54) family. The first and the second facets are the same crystallographic planes. As the deviation angle increases both the facets becomes smoother. In particular facets at deviation angles > 35°, the facets are very smooth. The top facet is roughest at around $\delta = 20^\circ$ (Figure 5.12 (h)). As the deviation angle increases from 15°, the top facet becomes longer and is the longest at around 20°. After 20°; as the deviation angle increases, the top facet becomes smaller and the second facet starts to dominate the emerging surface. One can barely see the first facet at deviation angle of 45°, see Figure 5.12 (m). Figures 5.12 (f) to (n) show the SEMs of spokes in this range of deviation angles. At deviation angle $\delta = 45^\circ$, the second facet is the 54.7° inclined smooth {111} plane.

In general the etched Si(100) surface has few hillocks, see Figure 5.12 (n). Also, it's very interesting to see that all the under-etched planes belong to the PBC based planes.

5.1.4 Etching in 15wt% TMAH

5.1.4.1 Si{110} etched at 80°C

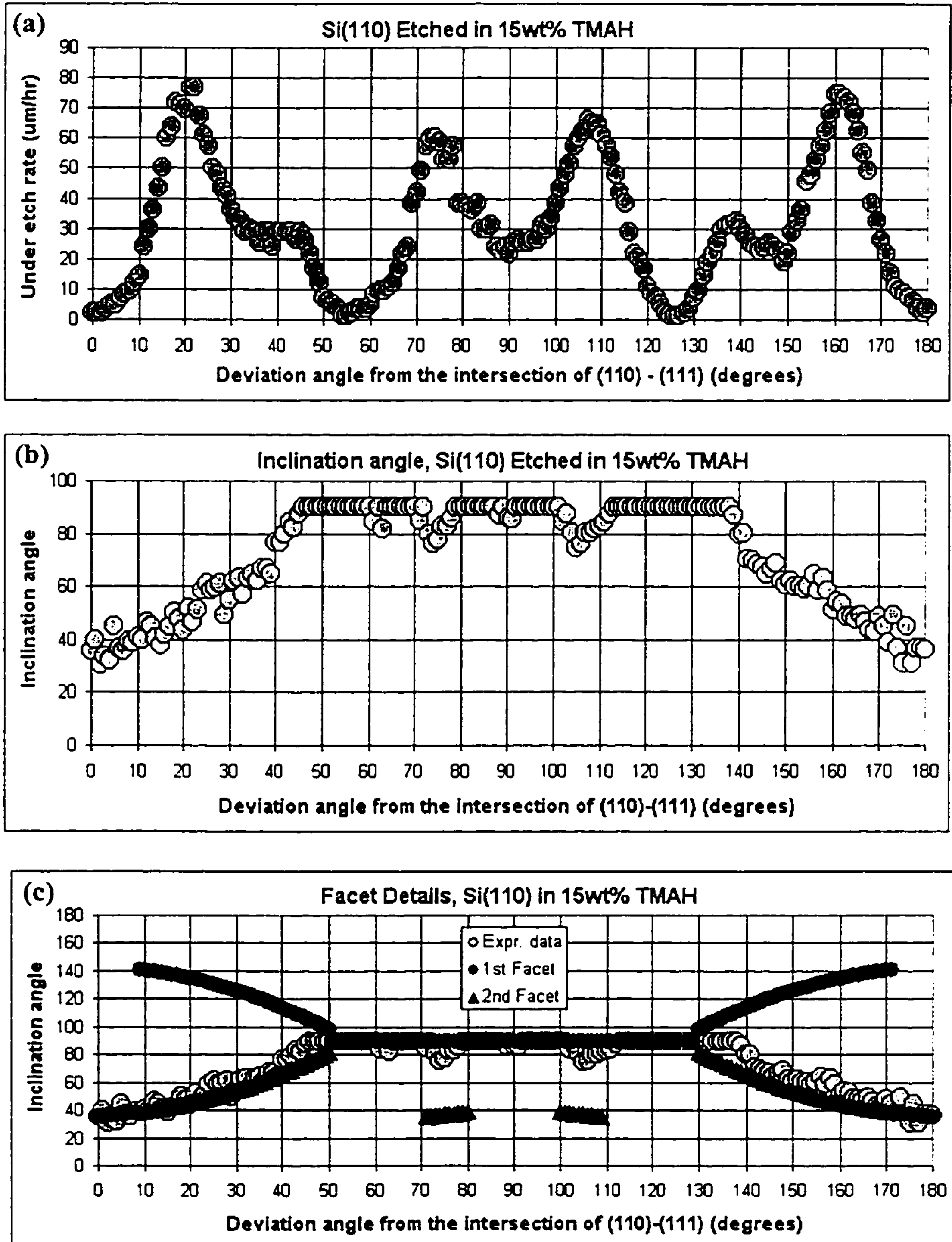

FIGURE 5.13: Si{110} etched in 15wt% TMAH at 80°C; (a) Under-etch rate, Si(110), (b) Inclination angle, and (c) Facet details.

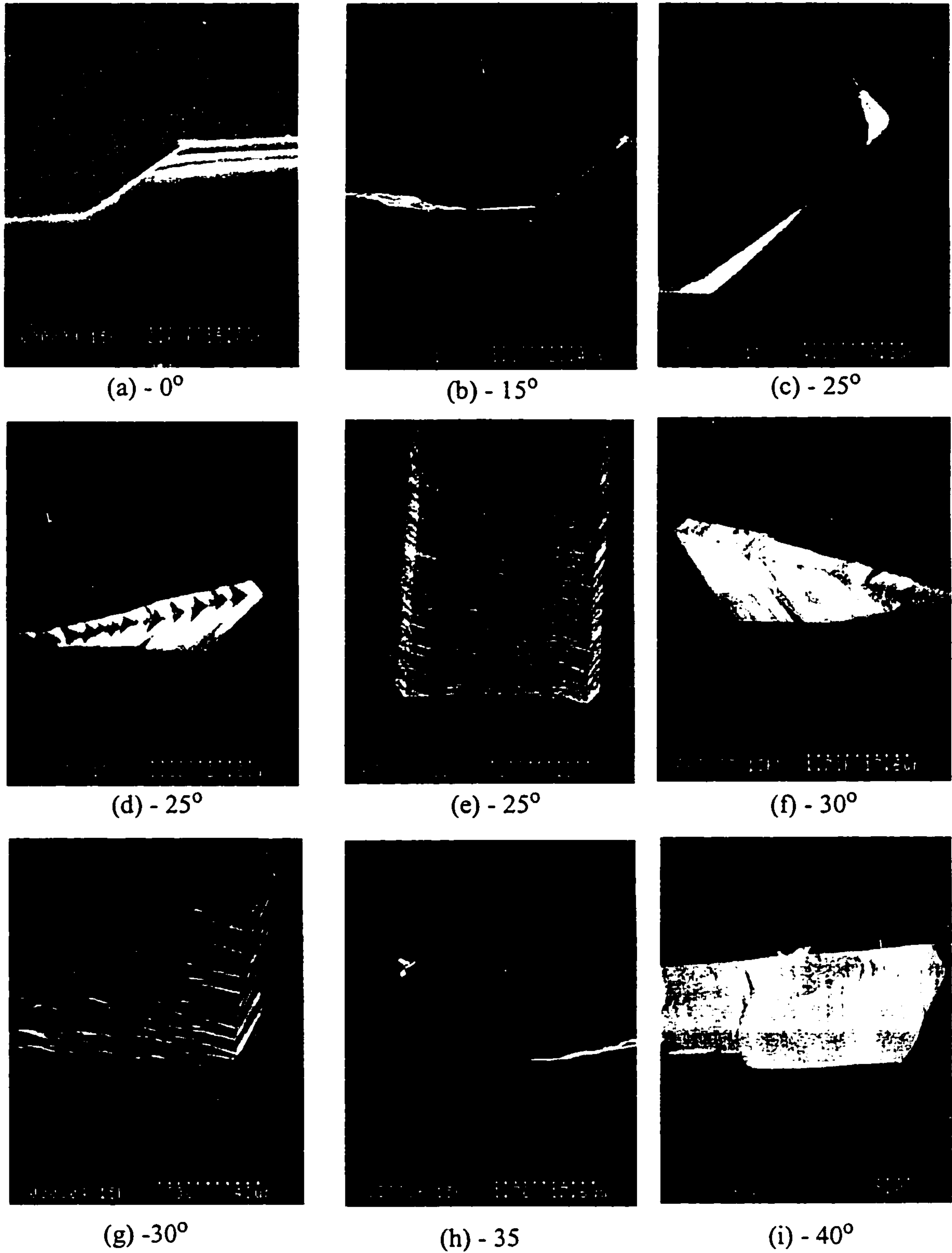

FIGURE 5.14: Scanning electron micrographs taken at various deviation angles for the {110} silicon etched in 15wt% TMAH at 80° C.

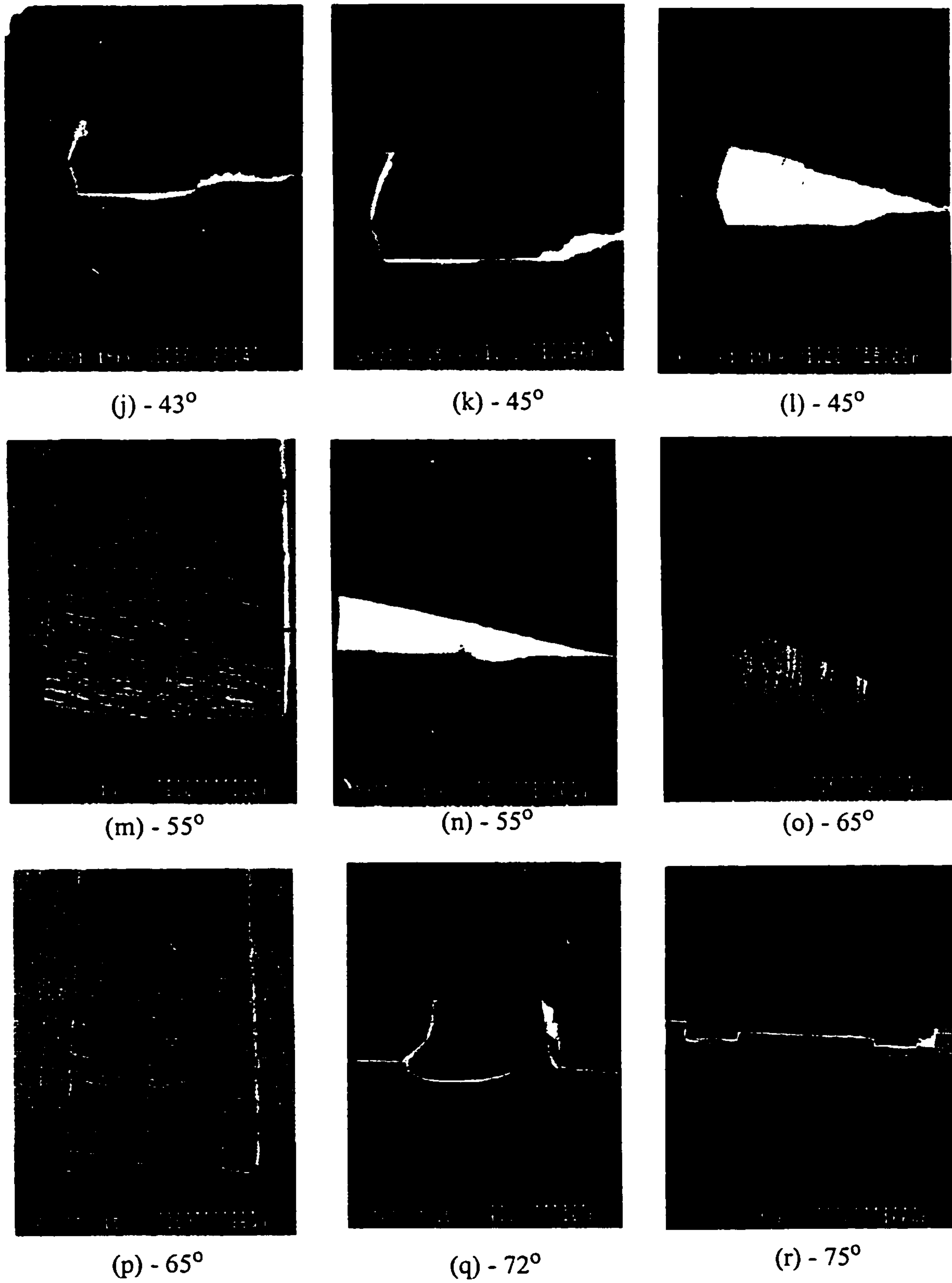

FIGURE 5.14: Scanning electron micrographs taken at various deviation angles for the {110} silicon etched in 15wt% TMAH at 80° C.

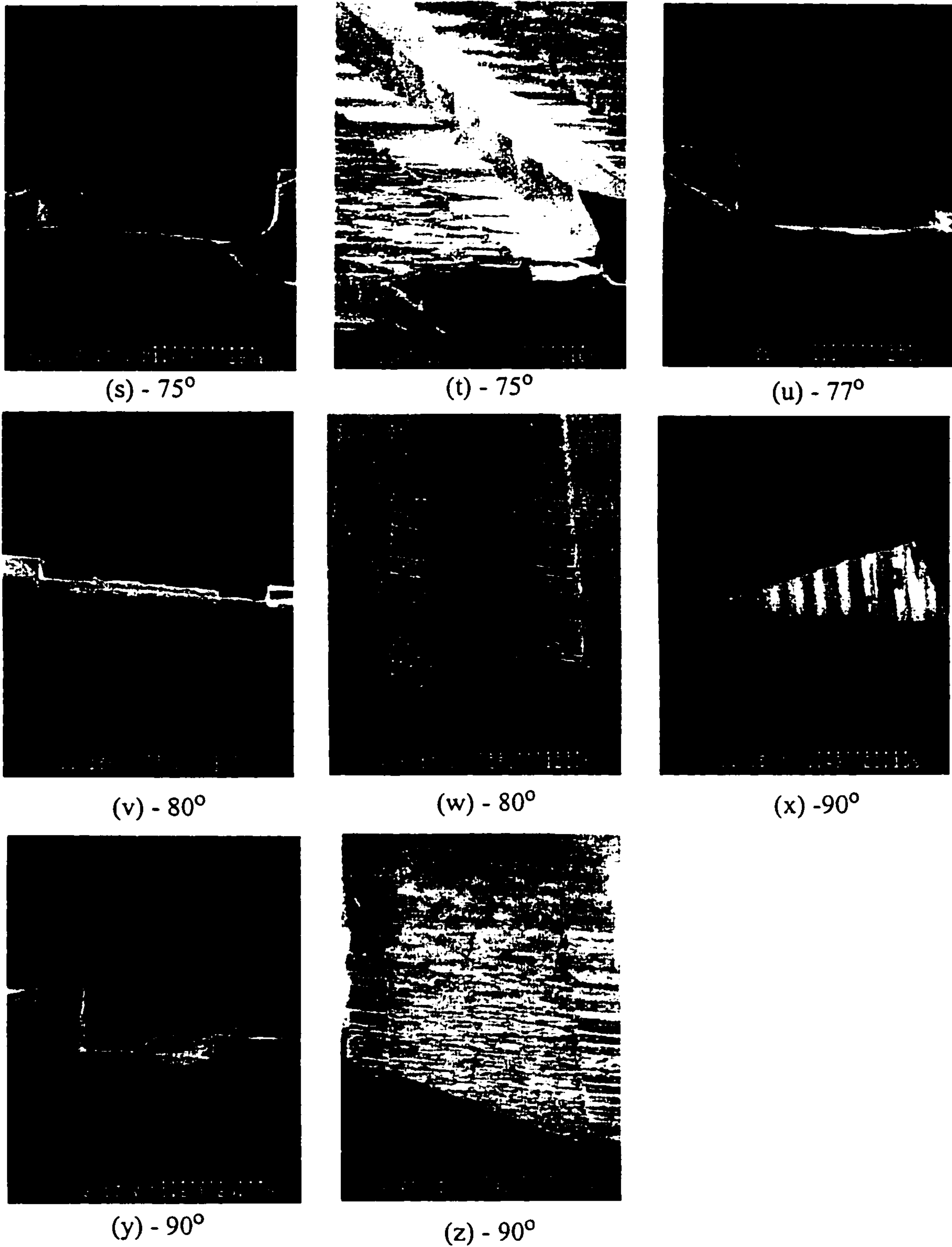

FIGURE 5.14: Scanning electron micrographs taken at various deviation angles for the {110} silicon etched in 15wt% TMAH at 80° C.

TABLE 5.7. Si{110} etched in 15wt% TMAH

δ Range in degrees	No. of Facets	Facet Descriptions	Under-etched planes (Model Identifiers)	Trenches
0 - 9	1	little rough	P-35-60-(90)	No, But can see features
10 - 50	2	1st: > 90°, rough 2nd: > 40°, rough	1st: P-145-120-(90) 2nd: P-35-60-(90)	Yes
51 - 55	1	1st: ~90° rough becomes smoother	1st: K-90-90-(90)	Yes, vanishes as δ increases
55 - 70	1	1st: ~90° smooth becomes rougher	1st: P-90-90-(90)	No, begins as δ increases
71 - 80	2	1st: 90°, rough 2nd: <45°, not smooth	1st: P-90-90-(90) 2nd: K-35-45-(90)	Yes
81 - 90	1	1st: >90°, rough	1st: P-90-00-(90)	Yes

Region 0° - 9°: In this range of δ, the emerging face is single faceted and is a little rough. These planes are of the P-35-60-(90) family. SEM at δ = 0° is shown in Figure 5.14 (a), this shows the near smooth {111} plane. As the deviation angle increases the side wall becomes rougher.

Region 10° - 50°: Here the emerging face is composed of 2 facets, first facet is inclined at an angle greater an 90° and the planes belong to the P-145-120-(90) family. The second facet follow the P-35-60-(90) family. Both the facets are rough in this range. Figures 5.14 (b) to 5.14 (l) shows SEMs and various spokes in this range of deviation angles. In the range δ = 10° to 42°, the bottom facet dominates the under-etched surface. At δ = 43° Figure 5.14(j), both the facets are of the same length. In the range δ = 44° to 50°, the top facet is dominant. Trenches can be seen in the spokes in this range of deviation angles.

Region 51° - 55°: In this range, the emerging face is single faceted and belongs to the K-90-90-(90) family of planes. The planes becomes smoother as the deviation angle increases. The trenches start to disappear as the deviation angle increases. AT $\delta = 55^o$, there is no trench on the spoke. SEM at deviation angle $\delta = 55^o$ is shown in Figures 5.14 (m) and (n).

Region 55° - 70°: In this range, the emerging surface is single faceted and vertical. The emerging planes belong to the K-90-90-(90) family. The planes becomes rougher and the trench start to appear on the spokes as the deviation angle increases. Figures 5.14 (m) to (r) shows the SEMs at the spokes in this range of deviation angles.

Region 71° - 80°: The emerging surface in this range is composed of two facets. The first facet is vertical and belongs to the P-90-90-(90) family.The second facet is shallow and belongs to the K-35-45-(90) family of planes. The second facet disappears as the deviation angle increases. Figures 5.14 (q) to 5.14 (w) show the spokes in this range of deviation angles. The trenches are very deep in this range, Figure 5.14 (s) shows the deep trench on the spoke at deviation angle 80°.

Region 81° - 90°: This region of the under-etched surface is single faceted and vertical. They belong to the P-90-90-(90) family. The plane is rough. Figures 5.14 (x) to 5.14 (z) show the spoke at $\delta = 90^o$, it shows the rough vertical emerging plane. Trenches are seen on the spokes in this range of deviation angles.

<u>Interesting Observation:</u>

Observing the SEMs of the spokes which show the roughness on the etched Si(110) surface, it is seen that the direction of the roughness is unique for each spoke. This can be seen in the SEMs in Figures 5.14 (e), (m), (p), (w) and (z). The direction of roughness is same as the direction of the periodic bond chain as described in chapter 3. The simple example for this is the spoke at $\delta = 90^o$, where direction of roughness is perpendicular to

the mask edge (Figure 5.14 (z) and Figure 5.15), and the direction of PBC at δ =90° is also straight across. Where as at δ =0° the PBC direction is parallel to the mask edge.

FIGURE 5.15: Direction of roughness on the spoke at deviation angle δ = 90°

From the Figure 5.15 it is seen that the roughness on the trench is also in the same direction of roughness on the centre of the spoke. More about the roughness on the etched (110) surface is discussed in Chapter 6.

5.1.4.2 Si{100} etched at 80°C

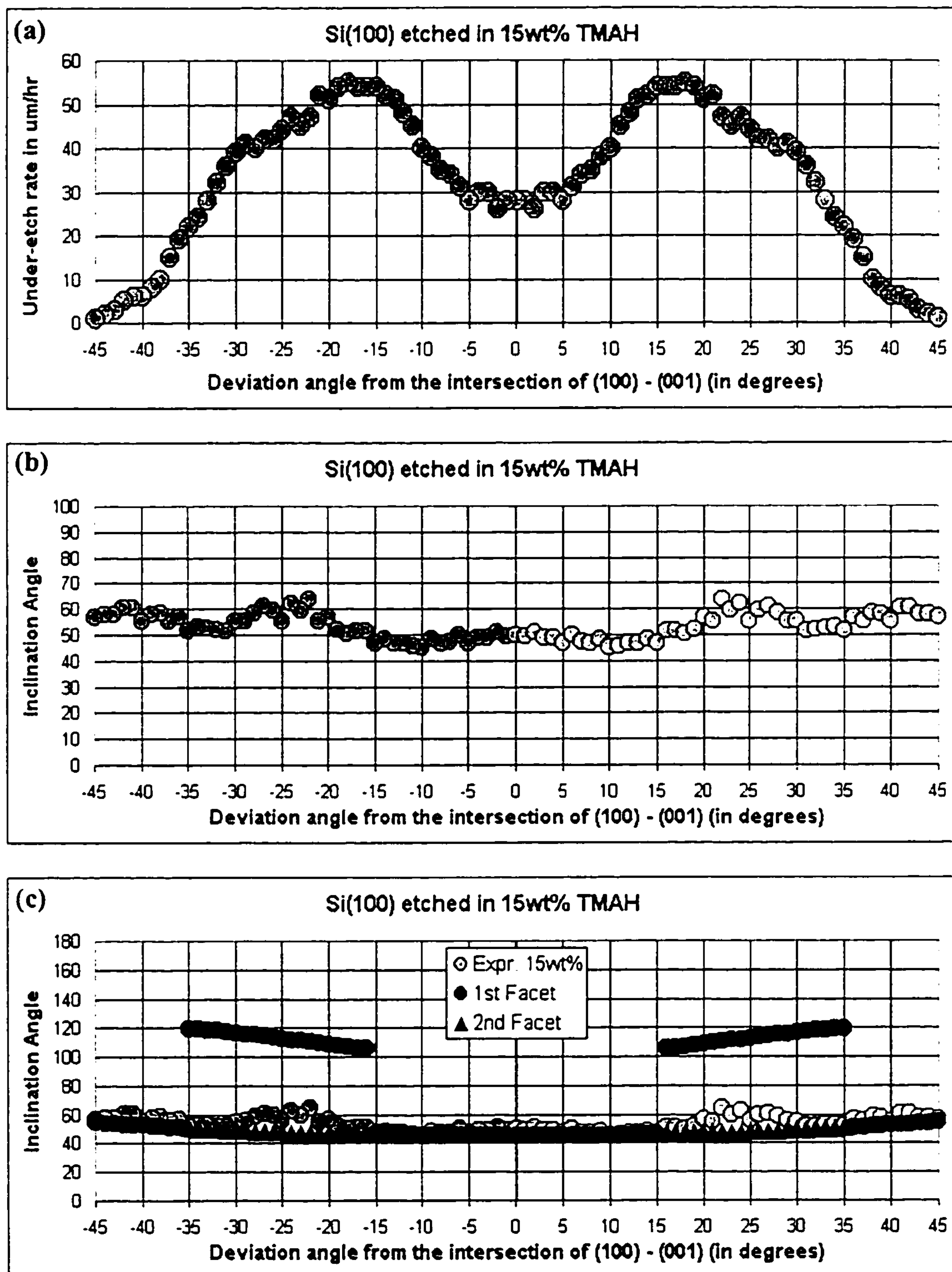

FIGURE 5.16: Si{100} etched in 15wt% TMAH at 80°C; (a) Under-etch rate, (b) Inclination angle, and (c) Facet details.

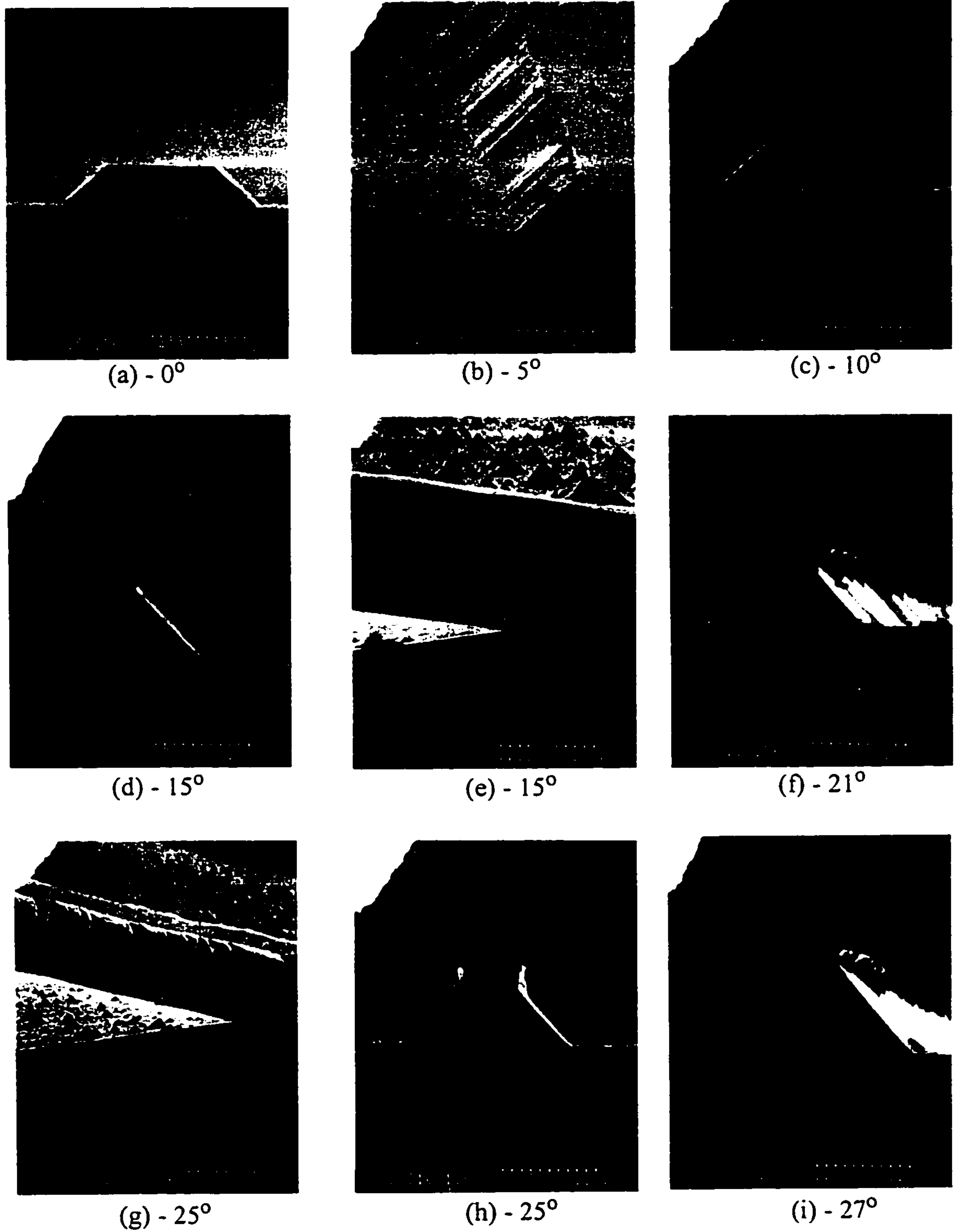

FIGURE 5.17: Scanning electron micrographs taken at various deviation angles for the {100} silicon etched in 15wt% TMAH at 80° C.

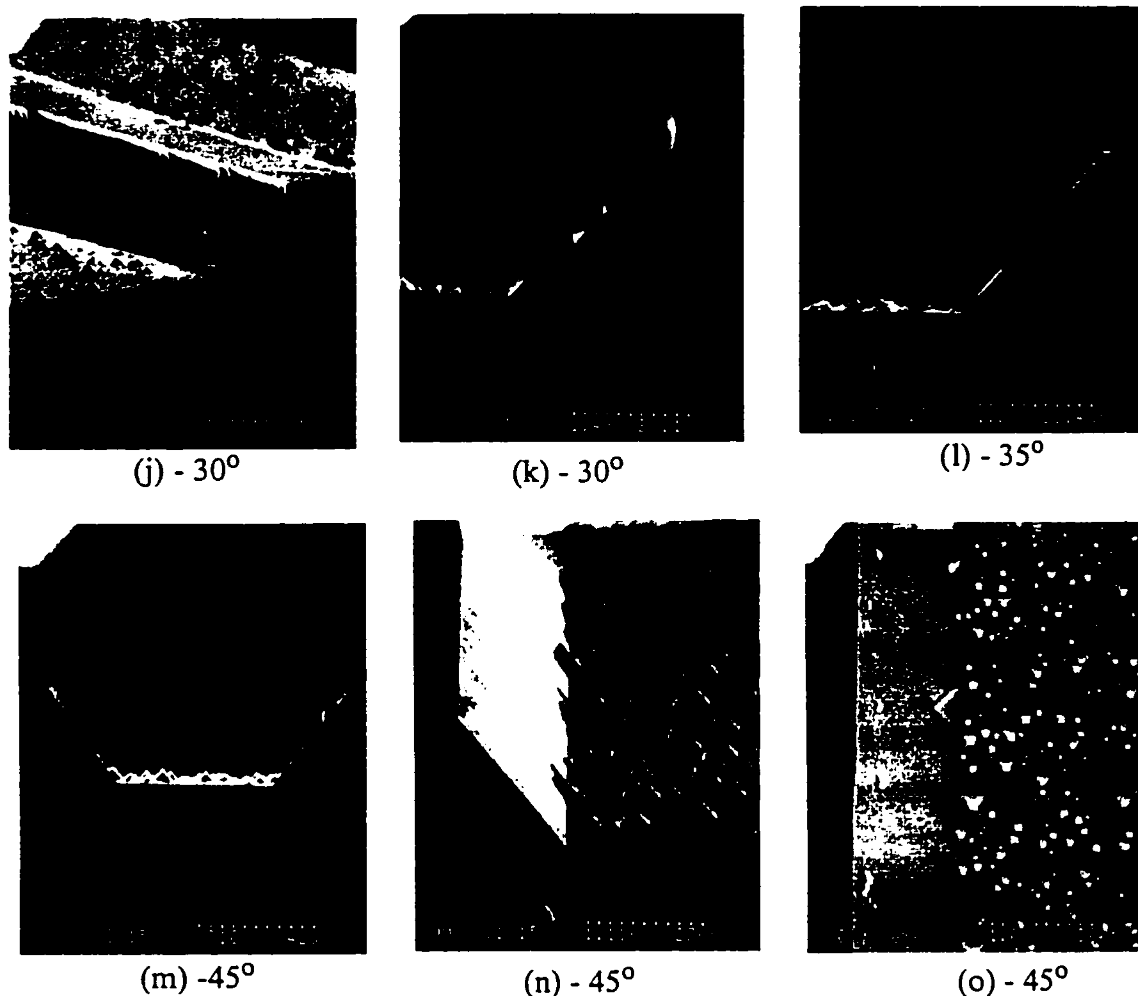

FIGURE 5.17: Scanning electron micrographs taken at various deviation angles for the {100} silicon etched in 15wt% TMAH at 80° C.

TABLE 5.8. Si{100} etched in 15wt% TMAH

δ Range in degrees	No. of Facets	Facet Descriptions	Under-etched planes (Model Identifiers)	Trenches
0 - 15	1	~45°,smooth - rough - smooth	P-54-45-(54)	No
16 - 34	2	1st: >90°, rough 2nd: smooth	K-126-135-(126) P-54-45-(54)	No
35 - 45	1	1st: smooth	P-54-45-(54)	No

Region 0° - 15°: In this range of deviation angles, the under-etched emerging surface is single faceted and the planes belong to the P54-45-(54) family of planes. The plane becomes smoother as the deviation angle increases. The (100) surface of the etch cavity is very rough with lot a of hillocks. SEMs in Figure 5.16 (a) to Figure. 5.16 (e) show the spokes in this range of deviation angles. The hillocks on the bottom of the etched cavity can be seen in Figure 5.16 (b), this shows how dense the hillocks appear on the of the etched cavity.

Region 16° - 34°: In this range, the emerging face is two faceted. The first facet is rough and inclined at an angle greater than 90° to the wafer surface and belongs to the K-126-90-(90) family of planes. The second facet is smooth and follows the P-54-45-(54) family of planes. Initially the first facet is very small and as the deviation angle increases the first facet starts to get larger and can be very clearly seen. The first facet is largest at about $\delta = 25^{\circ}$. But as the deviation angle further increases the first facet becomes smaller and then vanishes. SEMs in Figures 5.16 (f) to 5.16 (k) show the spokes in this range of deviation angles. The roughness in the interface between the first and the second facet sometimes make the first facet look vertical in the cross-sectional view, as seen in Fig. 5.16(h).

Region 35° - 45°: In this range of δ, the emerging face is single faceted. The emerging planes belong to the P-54-45-(54) family of planes and are smooth. SEMs in Figure 5.16 (l) to Figure 5.16 (o) show the spokes in this range of deviation angles. Figures 5.16 (m) to 5.16 (o) show the smooth {111} plane formed at $\delta = 45^{\circ}$.

The bottom of the etch cavity is seen to be full of hillocks. The hillocks are formed by the {111} planes at all the sides, hence the hillocks have smooth faces.

5.1.5 Etching in 12wt% TMAH

5.1.5.1 Si{110} etched at 80°C

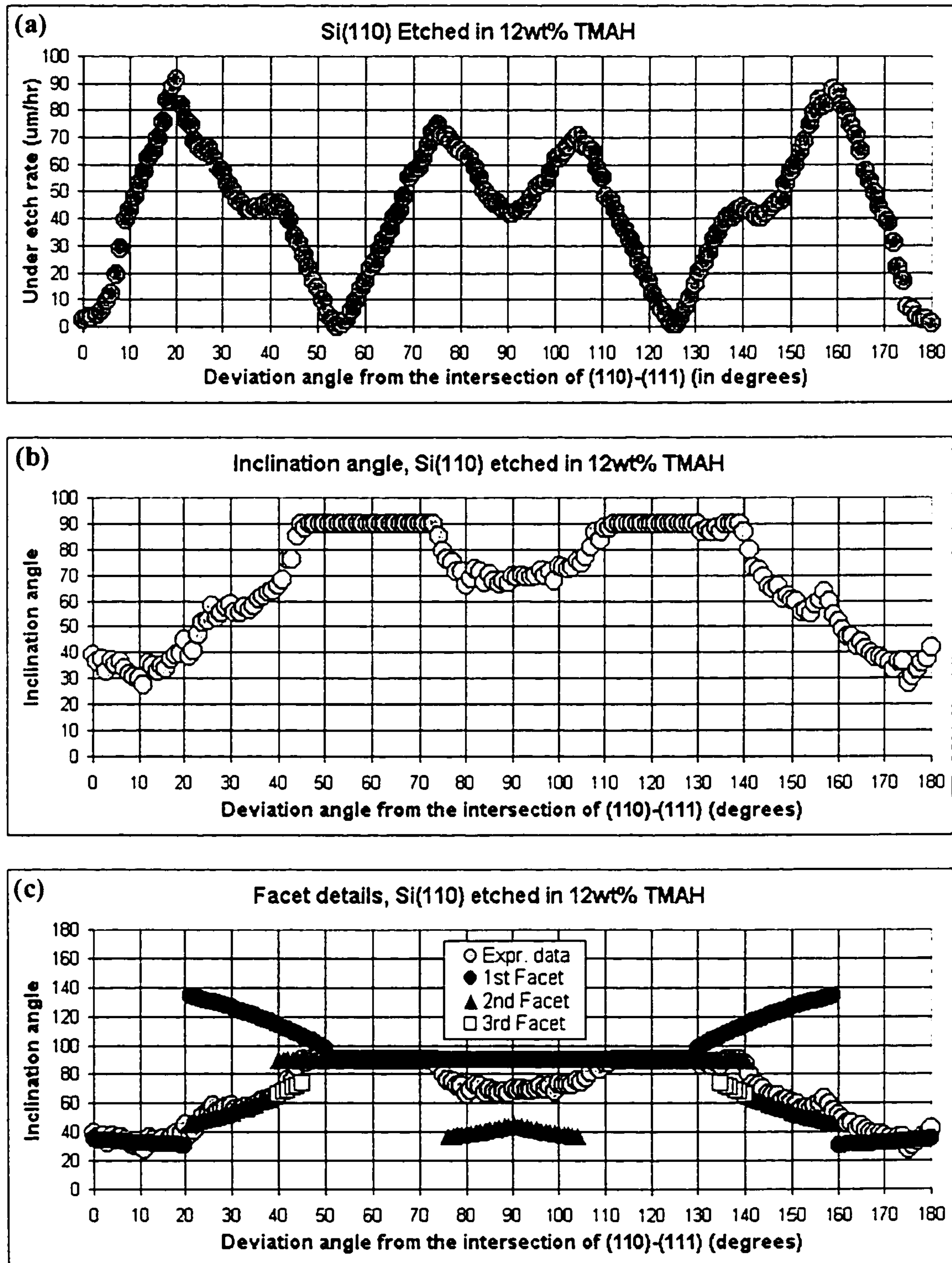

FIGURE 5.18: Si{110} etched in 12wt% TMAH at 80° C; (a) Under-etch rate, (b) Inclination angle, and (c) Facet details.

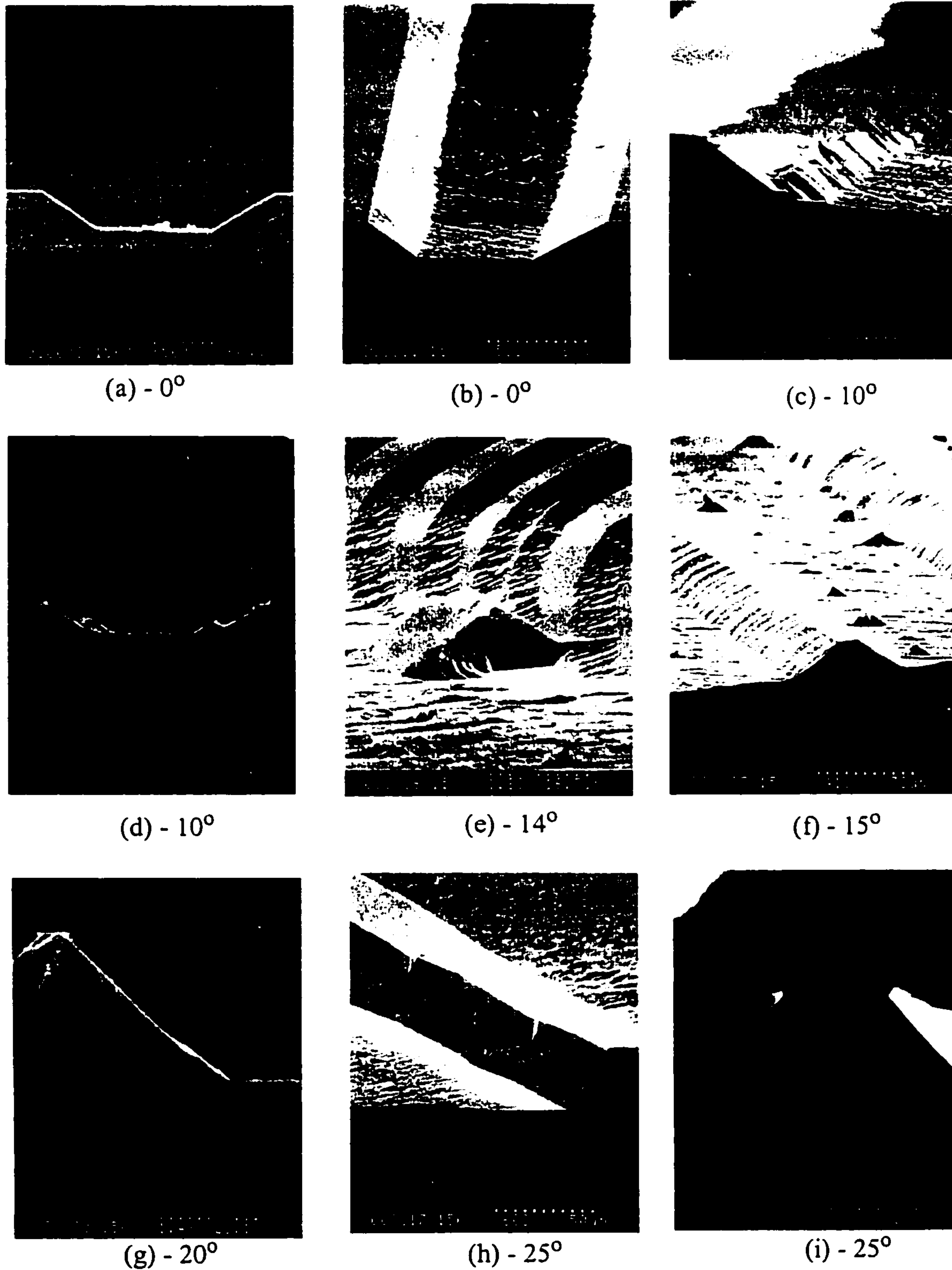

FIGURE 5.19: Scanning electron micrographs taken at various deviation angles for the {110} silicon etched in 12wt% TMAH at 80° C.

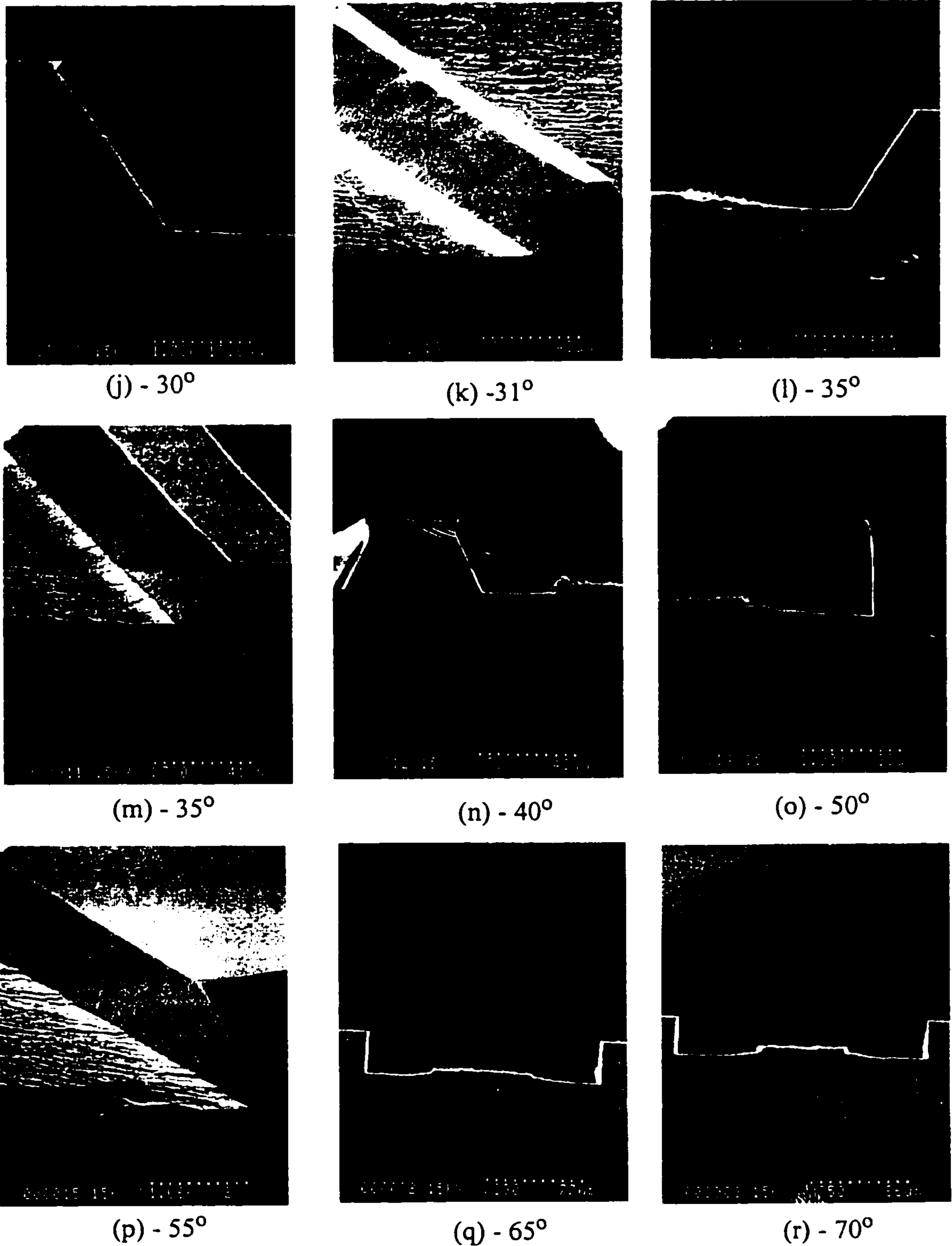

FIGURE 5.18: Scanning electron micrographs taken at various deviation angles for the {110} silicon etched in 12wt% TMAH at 80° C.

(s) - 75°

(t) - 76°

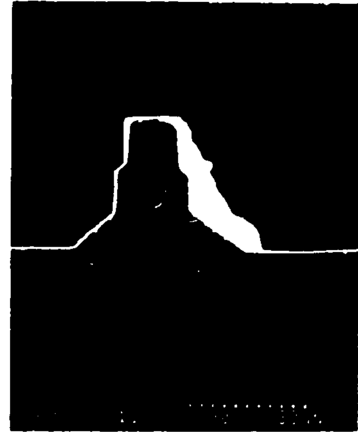

(u) - 78°

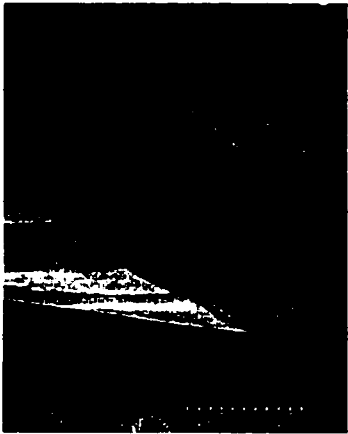

(v) - 79°

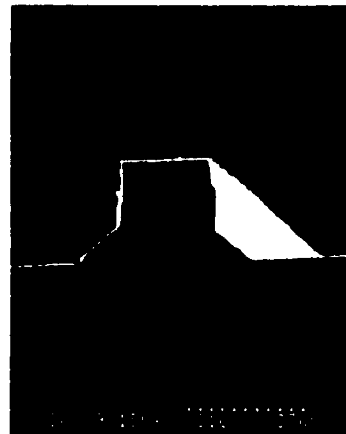

(w) - 80°

(x) - 85°

(y) - 85°

(z) - 90°

(aa) - 90°

FIGURE 5.18: Scanning electron micrographs taken at various deviation angles for the {110} silicon etched in 12wt% TMAH at 80° C.

TABLE 5.9. Si{110} etched in 12wt% TMAH

δ Range in degrees	No. of Facets	Facet Descriptions	Under-etched planes (Model Identifiers)	Trenches
0 - 19	1	smooth, becomes rougher	K-35-45-(90)	No
20 - 39	2	1st: smooth, very small 2nd: rough, becomes smooth	P-145-120-(90) P-35-60-(90)	No, But can see features
40 - 45	3	1st: smooth, very small 2nd: smooth (small) 3rd: smooth	P-145-120-(90) K-90-90-(90) P-35-60-(90)	Yes, Shallow
46 - 50	2	1st: not smooth 2nd: not smooth	P-145-120-(90) K-90-90-(90)	Yes, Shallow
51 - 55	1	1st: smooth	K-90-90-(90)	Yes
55 - 75	1	1st: smooth, becomes rougher	P-90-90-(90)	Yes
76 - 90	2	1st: rough 2nd: rough, becomes smooth	P-90-90-(90) K-35-45-(90)	Yes

***Region 0° - 19°*:** In this range of deviation angles the emerging facet is single faceted. They belong to the K-row K-35-45-(90) family of planes. Figures 5.18 (a) to (f) show the SEMs in this range of deviation angles. The under-etched plane at deviation angle 0° is the 35° inclined, smooth {111} plane. As the deviation angle increases the under-etched emerging plane becomes rougher. There are no trenches on the sides of the wagon-wheel spokes in this range of deviation angles. As can be seen from the SEMs, the etched surface has a few hillocks. In particular they can be seen near to the under-etched side wall.

***Region 20° - 39°*:** Here in this range, the under-etched emerging surface is two faceted and both belong to the PBC-based planes. The top facet belongs to the P-145-120-(90) family, and is very small compared to the second facet. The second facet belongs to the P-35-60-(90) family of planes. The second facet dominates the under-etched emerging sur-

face. The top and bottom facets belong to the same crystallographic planes. Figures 5.18 (g) to (m) show the SEMs in this range of deviation angles. In this range of deviation angles, we can see trench features on the sides of the spokes. The second facet is initially rough but becomes smoother as the deviation angle increases. The roughness pattern is very repetitive, this can be seen on the under-etched plane at deviation angle 25°, shown in Figure 5.18 (h). This means that the trenches are not deep enough to be called trenches, but we can clearly see the difference in the etched bottom surfaces, this can be seen from Figures 5.18 (i), (l) and (n).

Region 40° - 45°: The under-etched emerging surface in this range is three faceted. The first facet belongs to the P-145-120-(90) family and is very small. The second facet belongs to the K-90-90-(90) family. The third facet belongs to the P-35-60-(90) family of planes. Figure 5.18 (n) shows the SEM at deviation angle $\delta = 40^{\circ}$. In this range of deviation angles, as the deviation angle increases, the third facet quickly vanishes and the vertical, second facet dominates. In the entire range, the first facet is very small. Here the trenches can be clearly seen but, they are shallow.

Region 46° - 50°: In this range of deviation angles, the under-etched emerging surface is two faceted. In fact this range is similar to the Region 40° - 45°, where the third facet has completely disappeared. The first facet is very small and belongs to the P-145-120-(90) family. The second facet is smooth and belongs to the K-90-90-(90) family of planes. Here the trenches can be clearly seen but, they are shallow. Figure 5.18 (o) shows the SEM at deviation angle $\delta = 50^{\circ}$.

Region 51° - 55°: In this range the emerging surface is single faceted and is vertical. The vertical emerging plane belongs to the K-90-90-(90) family of planes and is smooth. Figure 5.18 (p) shows the SEM at deviation angle $\delta = 55^{\circ}$, this shows the vertical {111} plane. In this range, the trench disappears as the deviation angle increases and at $\delta = 55^{\circ}$, there is no trench, this can be seen in Figure 5.18 (p).

Region 55° - 75°: Here the under-etched emerging surface is single faceted and is vertical belonging to the P-90-90-(90) family of planes. As the deviation angle increases the emerging plane becomes rougher and the trenches start to appear. Figures 5.18 (p) to (s) show the SEMs in this range of deviation angles.

Region 76° - 90°: In this range of deviation angles the under-etched emerging surface is double faceted. In addition to the vertical PBC based planes, k-row based planes starts to appear as the second facet. The top, first facet is vertical and rough belonging to the P-90-90-(90) family. The second facet is shallow, smooth and belongs to the K-35-45-(90) family of planes. Trenches can be seen on the sides of the spokes in the entire range. Figures 5.18 (t) to (aa) show the SEMs in this range of deviation angles. Figures 5.18 (z) and (aa) show the SEMs at $\delta = 90^{\circ}$, this shows the smooth second facet inclined at 45° to the {110} wafer surface. This smooth, 45° inclined plane is the {100} plane.

5.1.5.2 Si{100} etched at 80°C

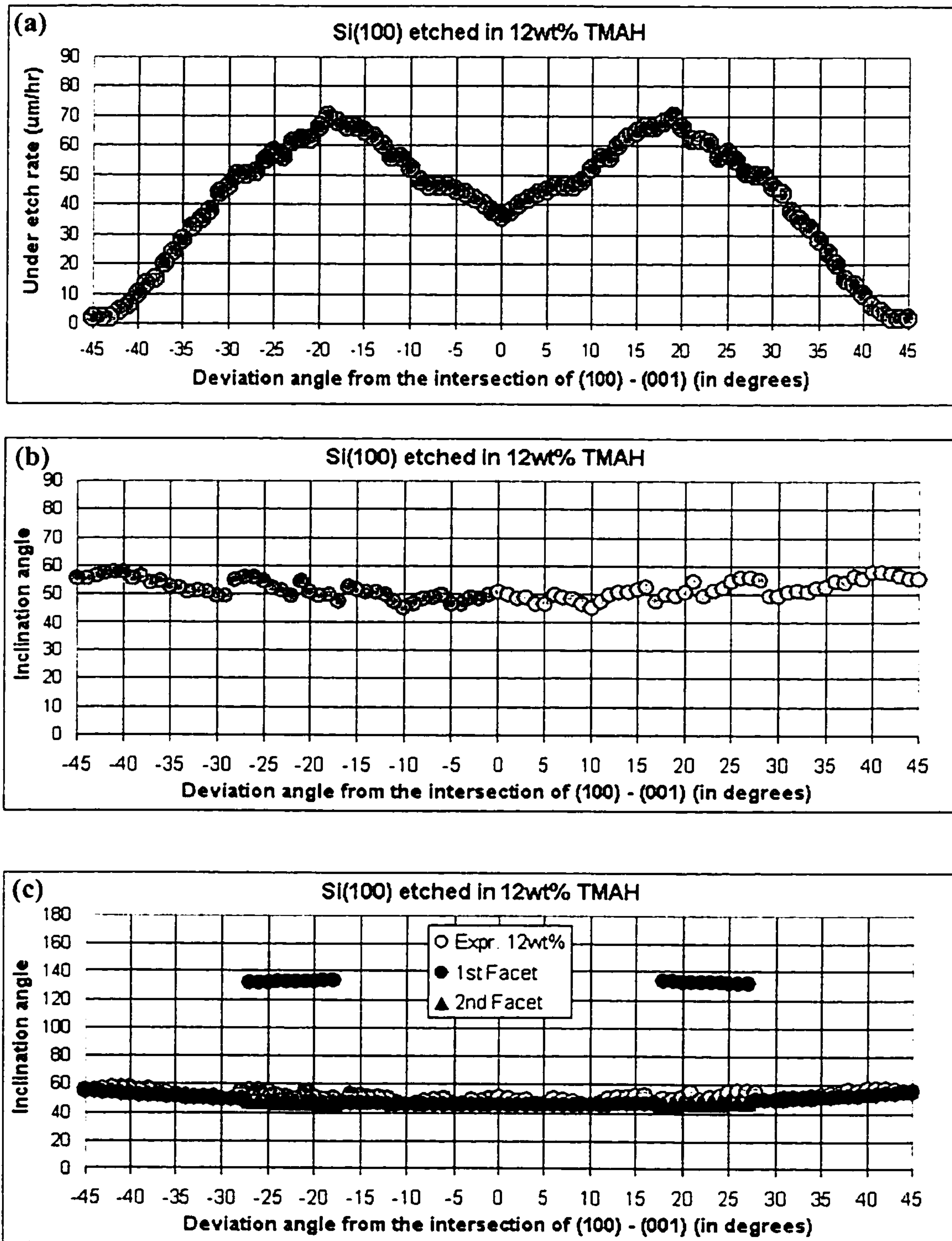

FIGURE 5.20: Si{100} etched in 12wt% TMAH at 80°C; (a) Under-etch rate, (b) Inclination angle, (c) Facet details.

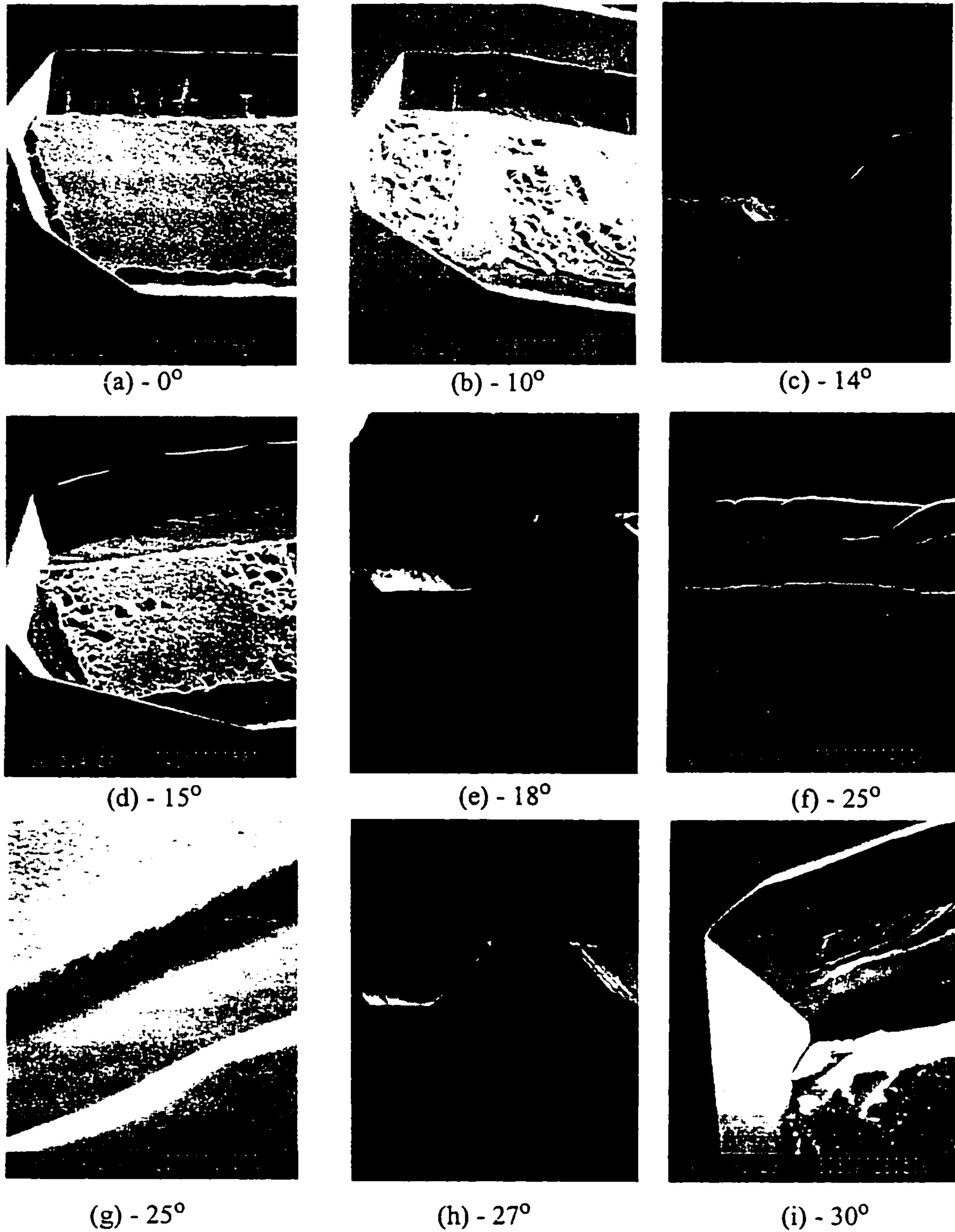

FIGURE 5.21: Scanning electron micrographs taken at various deviation angles for the {100} silicon etched in 12wt% TMAH at 80°C

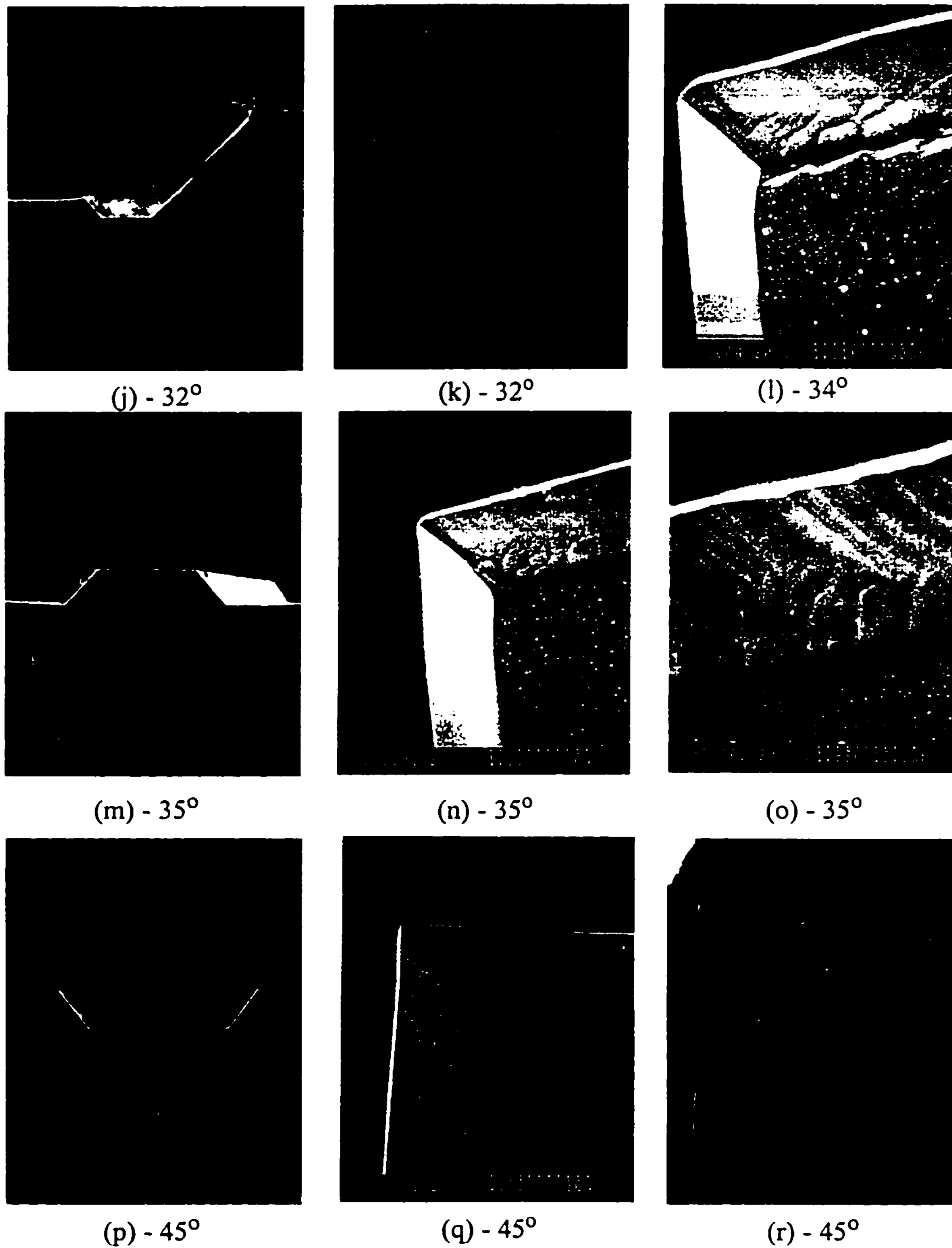

FIGURE 5.21: Scanning electron micrographs taken at various deviation angles for the {100} silicon etched in 12wt% TMAH at 80° C.

TABLE 5.10. Si{100} etched in 12wt% TMAH

δ Range in degrees	No. of Facets	Facet Descriptions	Under-etched planes (Model Identifiers)	Trenches
0 - 17	1	1st: smooth	P-54-45-(54)	Yes
18 - 27	2	1st: >90°, rough 2nd: smooth	P-126-135-(126) P-54-45-(54)	Yes
28 - 34	1	1st: smooth - little rough	P-54-45-(54)	Yes
35 - 45	1	1st: little rough - smooth	P-54-45-(54)	No

Region 0° - 17°: In this range the under-etched emerging surface is single faceted and is almost smooth. These planes belong to the PBC-based planes, the P-54-45-(54) family of planes. Figures 5.21 (a) to (d) show the SEMs in this range of deviation angles. The etched (100) surface is very rough which is evident from the SEMs. This roughness on the (100) surface is common in the lower concentration TMAH etches. There are deep trenches in the sides of the spokes. The inside, small side wall of the trench has the same roughness of the under-etched emerging plane. Therefore they both belong to the same crystallographic planes.

Region 18° - 27°: In this range the emerging surface is double faceted, the first facet is inclined at an angle greater than 90° and belong to the P-126-(135)-126 family of planes. The second facet is shallow, PBC-based planes inclined at an angle lesser than 90° and belongs to the P-54-(45)-54 family of planes. The second facet dominates the under-etched emerging surface. Figures 5.21 (e) to (h) show the SEMs in this range of deviation angles. Deep trenches were observed in the sides of the spokes, Figure 5.21 (g) shows the close-up of the trench at deviation angle of 25°. Both sides of the trenches are composed by the same crystallographic planes.

Region 28° - 34°: Here in this range of deviation angles, the emerging surface is single faceted and they belong to the P-54-45-(54) family of planes. Figures 5.21 (i) to (l) show

the SEMs in this range of deviation angles. Initially the under-etched emerging plane is smooth but as the deviation angle increases, the plane becomes a little rougher. Trenches can be seen in the entire range of deviation angles; but as the deviation angle increases, the trenches get shallower and narrower.

Region 35° - 45°: Again, in this range the emerging surface is single faceted and belongs to the P-54-45-(54) family of planes. Initially the under-etched emerging planes are a little rough but becomes smoother as the deviation angle increases. Figures 5.21 (n) to (r) show the SEMs at $\delta = 45^{\circ}$, here the emerging plane is the smooth 54.7° inclined {111} plane. There are no trenches in the entire range of deviation angles. The roughness on the etch bottom decreases as the deviation angle increases, the roughness trend on the bottom of etched spokes can be seen from the SEMs in Figure 5.21.

5.1.6 Etching in 9wt% TMAH

5.1.6.1 Si{110} etched at 80° C

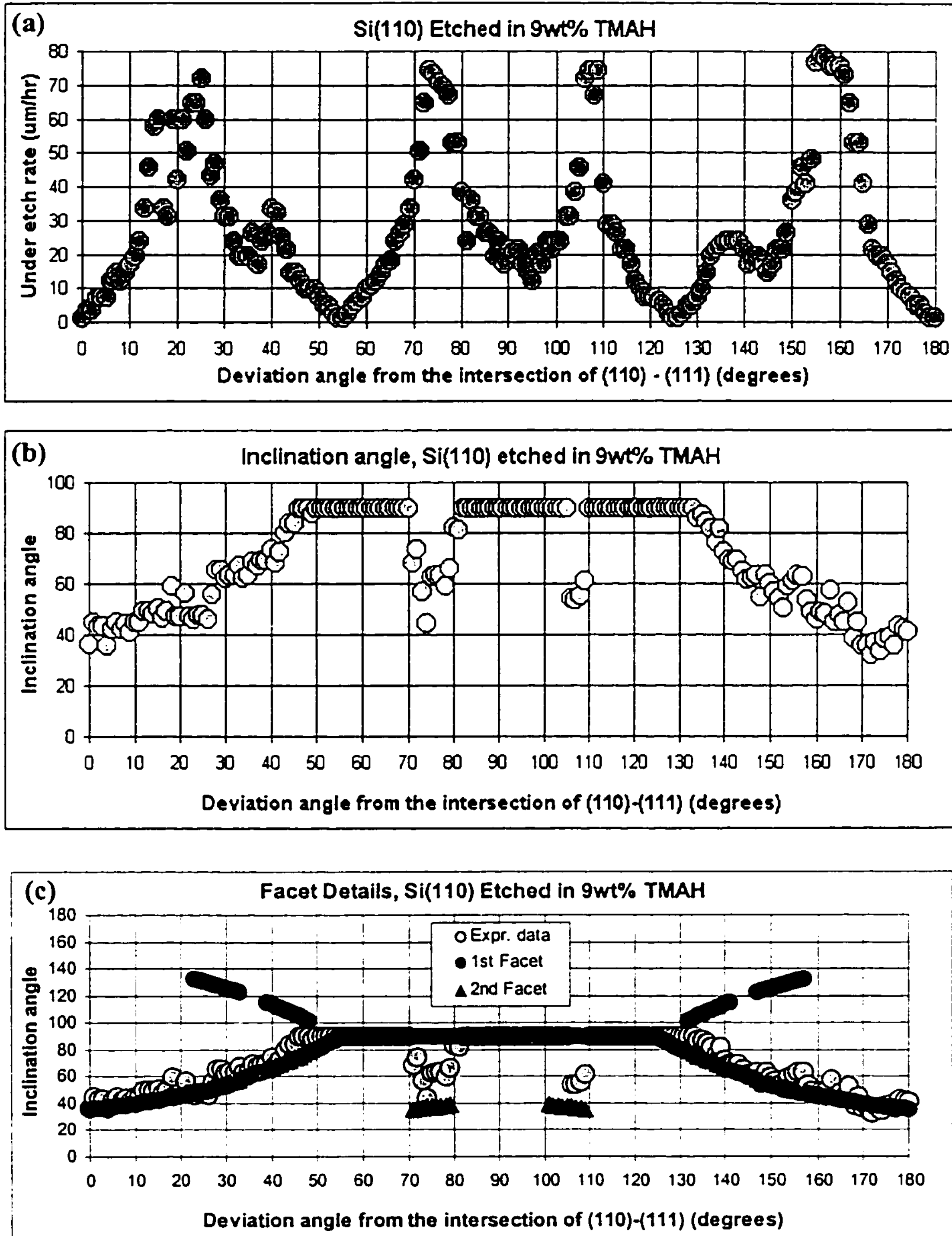

FIGURE 5.22: Si{110} etched in 9wt% TMAH at 80°C; (a) Under-etch rate, (b) Inclination angle and (c) Facet details.

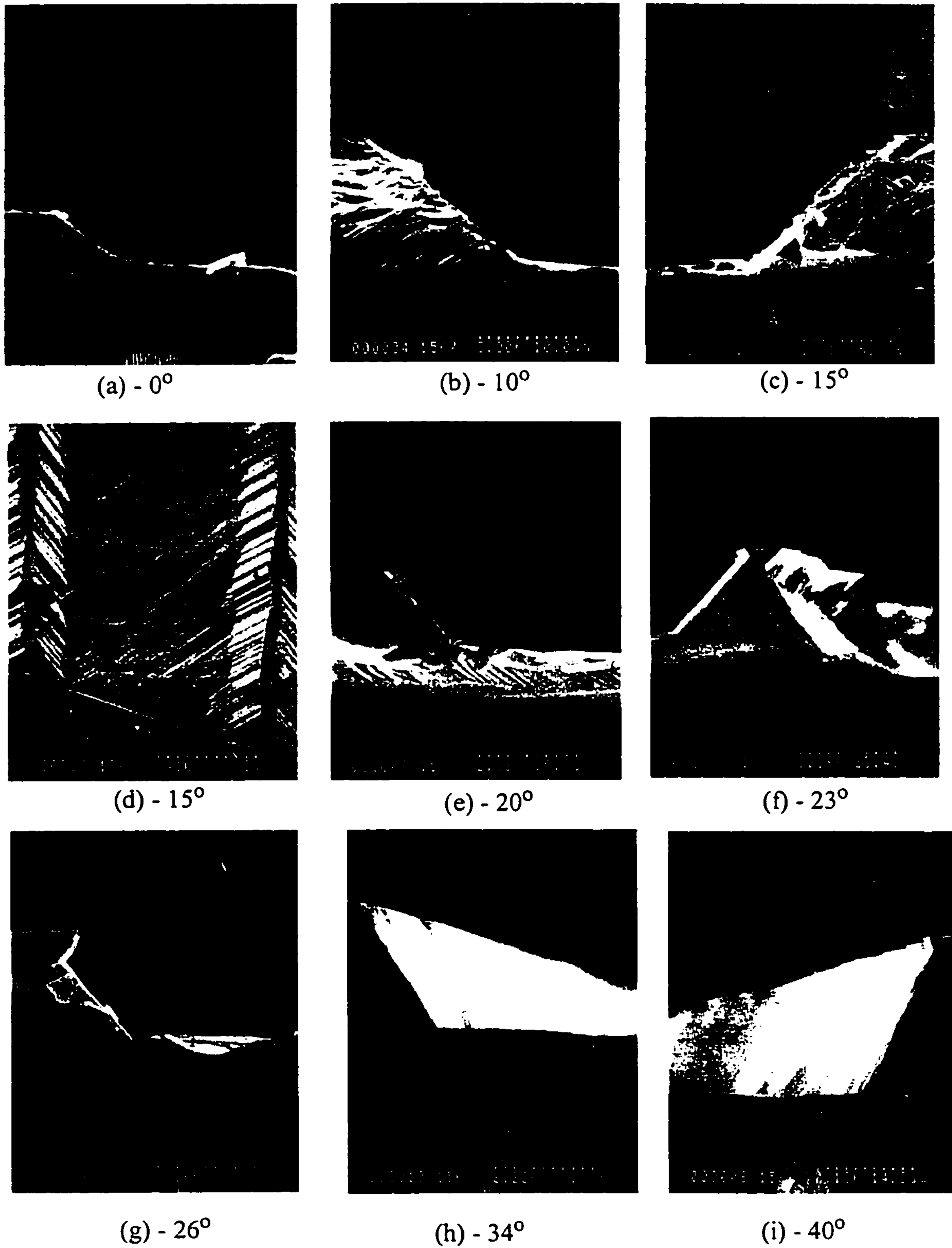

FIGURE 5.23: Scanning electron micrographs taken at various deviation angles for the {110} silicon etched in 9wt% TMAH at 80° C.

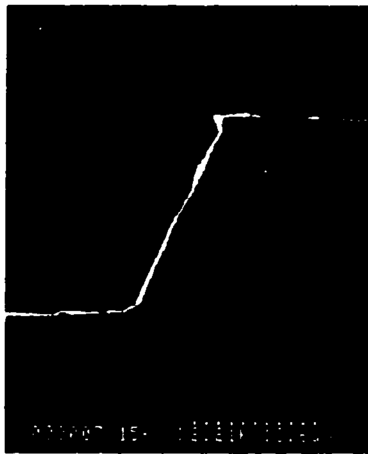

(j) - 40°

(k) - 43°

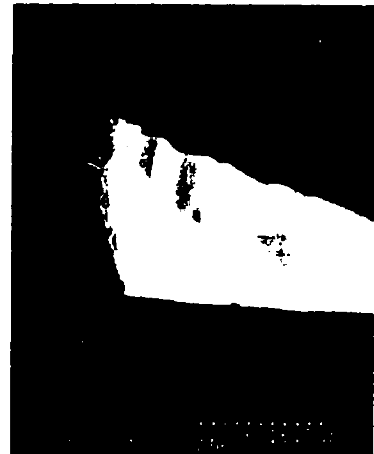

(l) - 45°

(m) - 50°

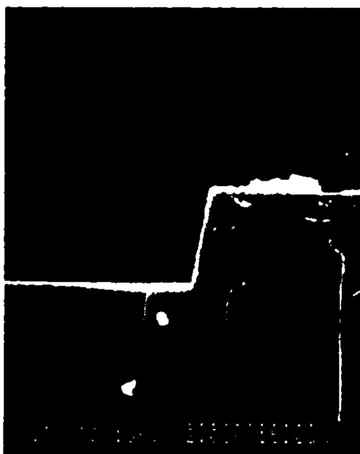

(n) - 50°

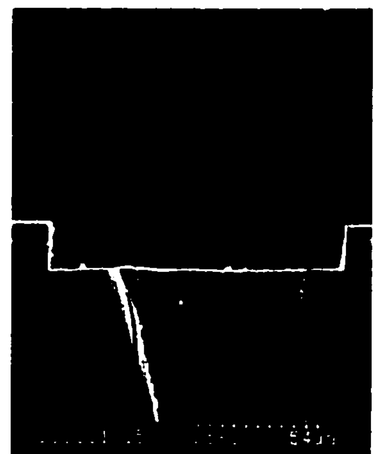

(o) - 55°

(p) - 55°

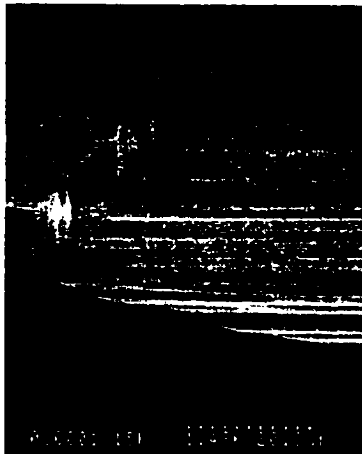

(q) - 65°

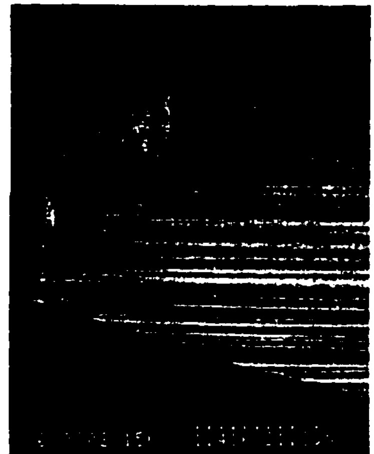

(r) - 70°

FIGURE 5.23: Scanning electron micrographs taken at various deviation angles for the {110} silicon etched in 9wt% TMAH at 80° C.

(s) - 71°

(t) - 71°

(u) - 73° and 74 °

(v) -78 °

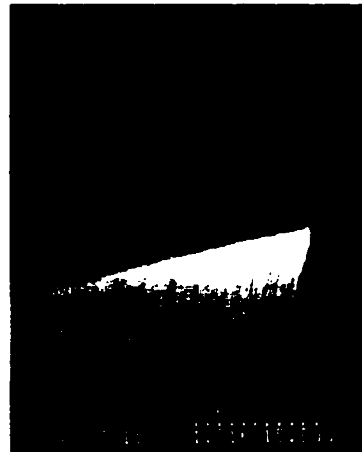

(w) - 80°

(x) - 90°

FIGURE 5.23: Scanning electron micrographs taken at various deviation angles for the {110} silicon etched in 9wt% TMAH at 80° C.

TABLE 5.11. Si{110} etched in 9wt% TMAH

δ Range in degrees	No. of Facets	Facet Descriptions	Under-etched planes (Model Identifiers)	Trenches
0 - 22	1	35° -40°, rough	P-35-60-(90)	No
23 - 33	2	1st: > 90°, rough 2nd: > 45°, rough - smooth	1st: P-145-120-(90) 2nd: P-35-60-(90)	No
34 - 38	1	1st: > 45°, smoother	1st: P-35-60-(90)	No
39 - 48	2	1st: > 90° 2nd: > 45°, Little rough	1st: P-145-120-(90) 2nd: P-35-60-(90)	No
49 - 55	1	1st: > 45°, smooth	1st: P-35-60-(90)	No
55 - 70	1	1st: 90°, becomes rough	1st: P-90-90-(90)	No
71 - 79	2	1st: = 90°, rough 2nd: <45°	1st: P-90-90-(90) 2nd: K-35-45-(90)	No
80 - 90	1	1st: little rough	1st: P-90-90-(90)	No

Region 0° - 22°: In this range the under-etched emerging surface is single faceted and is a little rough. The emerging planes belong to the P-35-60-(90) family of planes. Figures 5.23 (a) to (e) show the SEMs in this range of deviation angles. As can be seen on the SEMs, as the deviation angle increases the under etched emerging surface becomes rougher.

Region 23° - 33°: In this range the emerging surface is two-faceted. First facet is rough and is inclined at an angle greater than 90° to the wafer surface, and these planes belong to the P-145-120-(90) family. And the second facet is rough and follows the P-35-60-(90) family of planes. Figures 5.23 (f) to (g) show the SEMs in this range of deviation angles. In this range, initially the first facet is small but becomes larger as the deviation angle increases. After a few degrees the first facet again becomes smaller and finally vanishes. The first facet is largest at about 26°.

Region 34º - 38º: Here in this range, the under-etched emerging surface is single faceted and the planes belong to P-35-60-(90) family. As the deviation angle increases, the emerging plane becomes smoother. Figure 5.23 (h) shows the SEM at deviation angle of 34°.

Region 39º - 48º: In this range the emerging surface is two-faceted, the first facet is inclined at an angle greater than 90° to the wafer surface, and belongs to the P-145-120-(90) family. And the second facet is little rough and follows the P-35-60-(90) family of planes. Figures 5.23 (i) to (l) show the SEMs in this range of deviation angles. Here again in this range, initially the first facet is small but becomes larger as the deviation angle increases. After a few degrees the first facet again becomes smaller and finally vanishes. The first facet is largest at about 45°. This is very similar to the range 23° - 33° range.

Region 49º - 55º: In this range the under-etched emerging surface is single faceted, smooth and follows the P-35-60-(90) family of planes. Figures 5.23 (m) to (p) show the SEMs in this range of deviation angles. At deviation angle $\delta = 55^\circ$, the emerging plane is the vertical, smooth {111} plane.

Region 55º - 70º: The under-etched emerging surface is again single faceted but is vertical in this entire range of deviation angles. They belong to the P-90-90-(90) family. As the deviation angle increases the emerging plane becomes rougher. This can be seen on the side wall of the spoke at deviation angle $\delta = 70^\circ$, shown in Figure 5.23 (r).

Region 71º - 79º: In this range the emerging surface is two-faceted, the first facet is rough, vertical, and belongs to the P-90-90-(90) family. And the second facet is little rough and is inclined at around 45° to the {110} wafer surface. The second facet belongs to the K-34-45-(90) family of planes. In this range, we see a few hillocks on and near the second facet. Figures 5.23 (s) to (v) show the spokes in this range and also show the hillocks. The hillocks on the second facet is sometimes really large which makes the second

facet really large. This can be seen in Figure 5.23 (u). We can see that the roughness of the hillocks abruptly change the length of the second facet at $\delta = 74^o$, when compared to the spoke at $\delta = 73^o$. In general the second facet becomes smaller as the deviation angle increases.

Region 80° - 90°: In this range the emerging surface is single faceted, rough and vertical. At $\delta = 90^o$, the emerging plane is the vertical {100} plane, this is shown in Figure 5.23 (x). Here again, we can see hillocks at the interface of the under-etched emerging surface and the etch cavity bottom {110} plane.

In the entire range of deviation angles, there are no trenches in the sides of the spokes.

5.1.6.2 Si{100} etched at 80°C

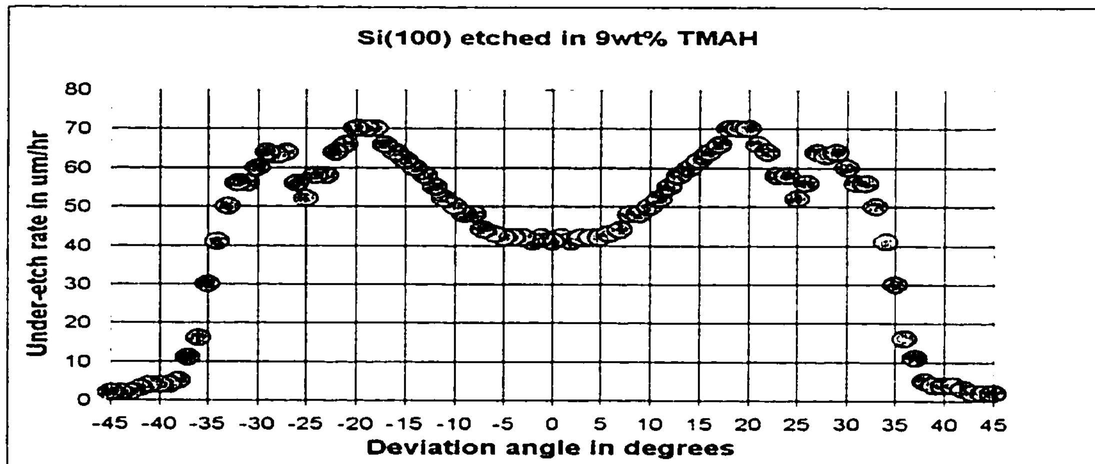

FIGURE 5.24: Si{100} etched in 9wt% TMAH at 80°C; (a) Under-etch rate, (b) Inclination angle, (c) Facet details.

Due to the roughness on the under-etched emerging surface it was very difficult to measure the UESHP accurately and hence the effective inclination of the under-etched emerging surface was not calculated for this case. SEMs were taken on the spokes to study the features on the under-etched surface and the facet inclination angles. From the SEMs its clear that the interface between the under-etched surface and the etched cavity bottom

is very rough to make any UESHP measurements. In some spokes the trench was found only on one side of the spoke sides (at $\delta = 37^{o}$, Figure 5.25(j)).

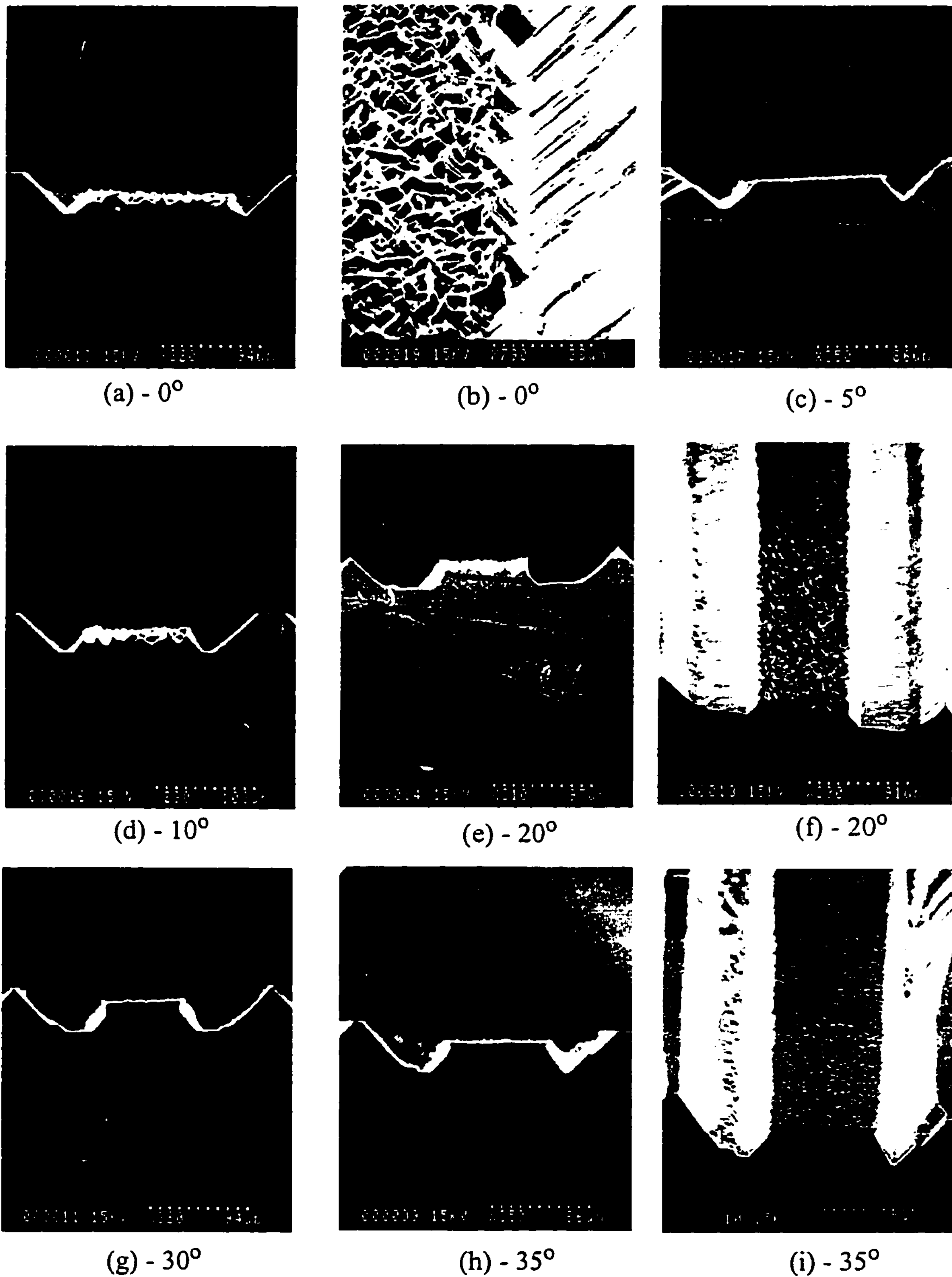

FIGURE 5.25: Scanning electron micrographs taken at various deviation angles for the {100} silicon etched in 9wt% TMAH at 80° C.

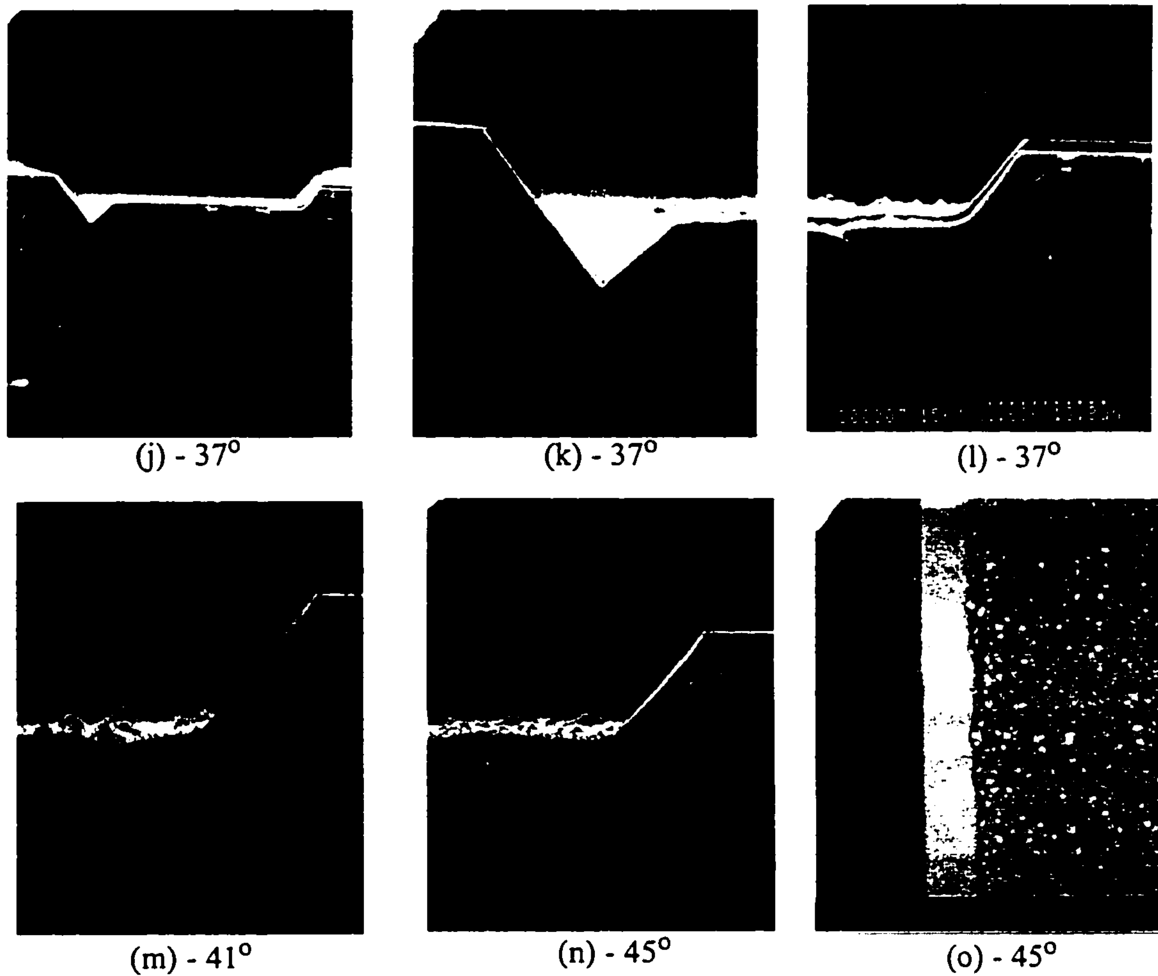

FIGURE 5.25: Scanning electron micrographs taken at various deviation angles for the {100} silicon etched in 9wt% TMAH at 80° C.

TABLE 5.12. Si{100} etched in 9wt% TMAH

δ Range in degrees	**No. of Facets**	**Facet Descriptions**	**Under-etched planes (Model Identifiers)**	**Trenches**
1 - 37	1	Rough, becomes smoother	P-54-45-(54)	Yes
38 - 45	1	Smooth	P-54-45-(54)	No

Region 0° - 37°: In this range of deviation angles the emerging surface is single faceted and rough. They belong to the P-54-45-(54) family of planes. As the deviation angle

increases, the emerging plane becomes smoother. Figures 5.25 (a) to (l) show the SEMs on spokes in this range of deviation angles. There are deep trenches on the spokes in this range of deviation angles. As the deviation angle increases, the trench disappears. At $\delta = 37^o$, the spoke had trench on only one side. The sides of the spokes are 0.5^o apart, so with in a difference of 0.5^o the trench features abruptly vanishes which shows that the etching is very much orientation dependent.

Region 38° - 45°: In this range the emerging surface is smooth, single faceted and has no trenches. The emerging planes belong to the P-54-45-(54) family of planes. At $\delta = 45^o$, the emerging plane is the smooth, 54.7^o inclined {111} plane. Figures 5.25 (n) and (o) show the spoke at t $\delta = 45^o$.

The etched {100} surface is very very rough as can be seen on the SEMs. It is interesting to see that the under-etched emerging planes in the 9wt% case are always the PBC based planes as in the 12wt% TMAH case.

CHAPTER 6

Removal Rates Fitting and Discussion

Important in the analysis of anisotropic etch properties of an etch system (etchant and etch conditions) are the etch properties of the most common crystallographic planes, the {100}, {110} and {111} planes. Also of importance are the etch properties of the masking material, but in this work the main focus is on the etch rates of the common crystallographic planes. Using the facet information and under-etch rates that were presented in Chapter 5 and the simple atomic model described in Chapter 3, the removal rates of PBCs or k-rows (f_p *and* f_k) are calculated for several cases in each etchant concentration.

6.1 Etch Depth, Etch Rates and Removal Frequencies

The etch rates of {100} and {110} silicon planes can be found from the etch depth of the etch cavities on {100} and {110} silicon respectively. The table below shows the etch rates of {100} and {110} planes calculated from the average etch depths of the respective etch cavities at all deviation angles.

TABLE 6.1. Etch rates of {100} and {110} vs. TMAH Concentration

Const wt%	Etch Rate	
	{100}	{110}
25	24.3	36.6
19	29.2	40.5
17	32.7	39.5
15	35.1	17.7
12	36.8	32.9
09	-	20.9

The etch rates of {100} and {110} planes are plotted in Figure 6.1.

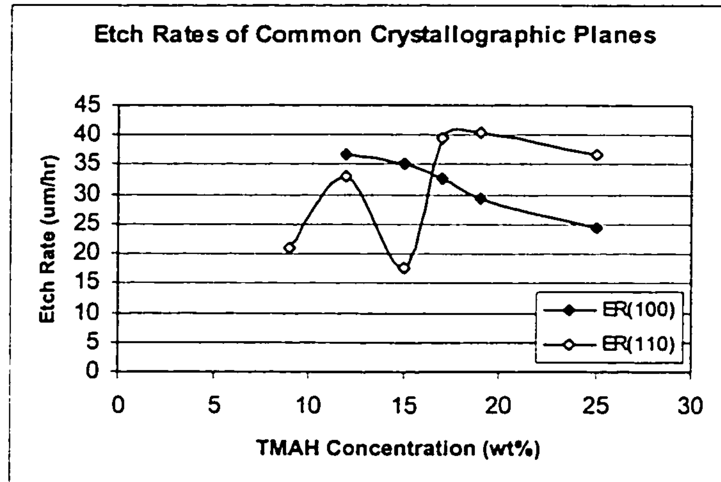

FIGURE 6.1: Etch rates of {100} and {110} vs. TMAH Concentration

6.1.1 Removal Frequencies

As presented earlier, the {100} plane is formed by rows of atoms, each with two dangling bonds (*kinks*). The {100} bulk silicon is made of stacks of these layers with kinks. And similarly the {110} plane is formed by periodic bond chains (*PBCs*). The {110} bulk silicon is made of stacks of these PBC layers. This makes it easy to calculate the *kink-row* and *PBC* removal rates from the etch rates of {100} and {110} planes respectively.

6.1.1.1 Crystal basics

Distances between different atoms of the unit cube are important and are used in most of the calculations in this section. The Figure 6.2 shows the distances between the most common atoms in a unit cell. From this the inter layer distance of the common planes {100}, {110} and {111} can be calculated.

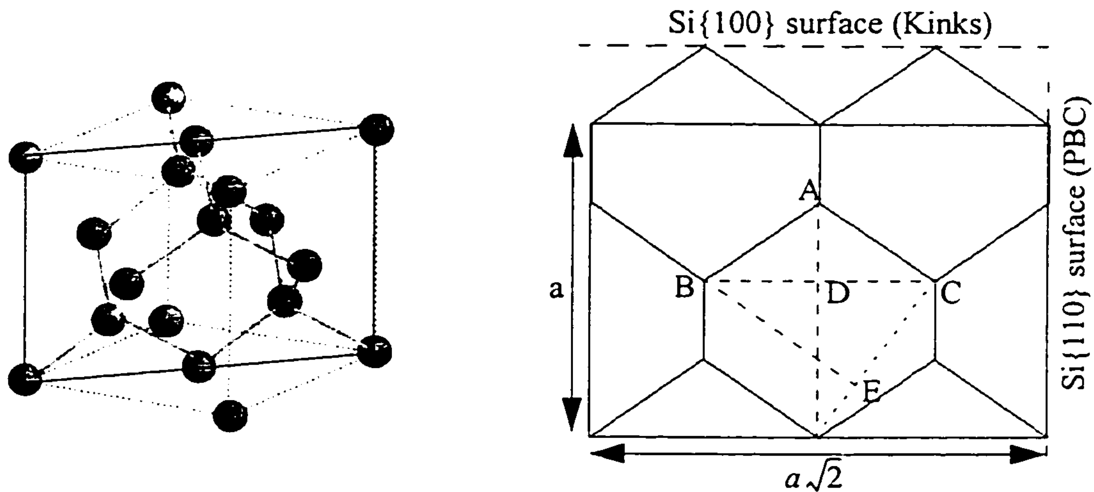

FIGURE 6.2: Silicon unit cube and representation of inter atomic distances.

$$AD = \frac{a}{4} = 0.25a \quad \text{- distance between (100) planes}$$

$$BD = \frac{a\sqrt{2}}{4} = 0.3536a \quad \text{- distance between (110) planes}$$

$$BE = a\frac{\sqrt{3}}{3} = 0.577a \quad \text{- distance between (111) planes}$$

where a is the lattice constant of silicon, $a = 5.43 \times 10^{-10}$m.

6.1.1.2 Kink-row removal frequency {100}

When a {100} layer is exposed to the etchant, all the atoms or kinks are exposed to the etchant at the same time. All the atoms on the {100} surface that are exposed to the etchant have the same crystallographic features (two dandling bonds). This model approximates that (nominally, on average) all will be etched simultaneously, exposing the next layer of atoms. According to this approximation, the first layer of atoms or kinks should be completely be etched before the atoms on the next layer can be etched. So the etch progresses in steps. The kink-row removal frequency f_k (rate at which a row of *kink* atoms is etched) can be calculated from the step length, the distance between two adjacent {100} planes and the experimental etch rate of {100} plane.

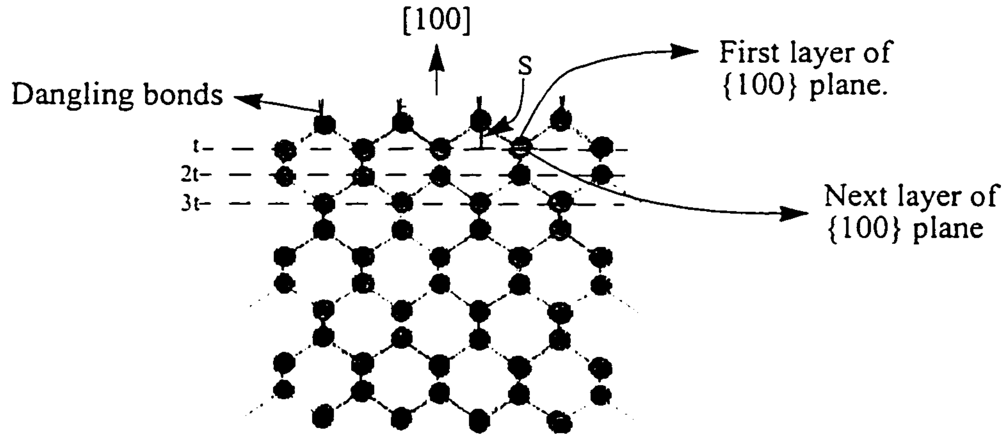

FIGURE 6.3: Layers of {100} planes to illustrate the step length

As can be seen on the Fig. 6.3, the step length s = 0.25 x a. And the kink-row removal frequency f_k is given by

$$f_k = \frac{ER(100)}{0.25 \times a} = 7.33 \times 10^9 \times ER(100) \quad \#/\text{hr}$$

6.1.1.3 PBC removal frequency {110}

By a similar argument, and approximation the first layer of exposed PBCs should be completely removed before the next layer of PBCs can be attacked. When the {110} plane, composed of PBC structures is exposed to the etchant, and when one of the atoms on the periodic bond chain is attacked, the next atom on the PBC is weakened and is very quickly etched. This process continues and very quickly removes the complete chain, this process may be called "zipping". The PBCs are initially stable until one of the atoms on the PBC link is attacked, but once one of the atoms is etched the complete chain is etched quickly.

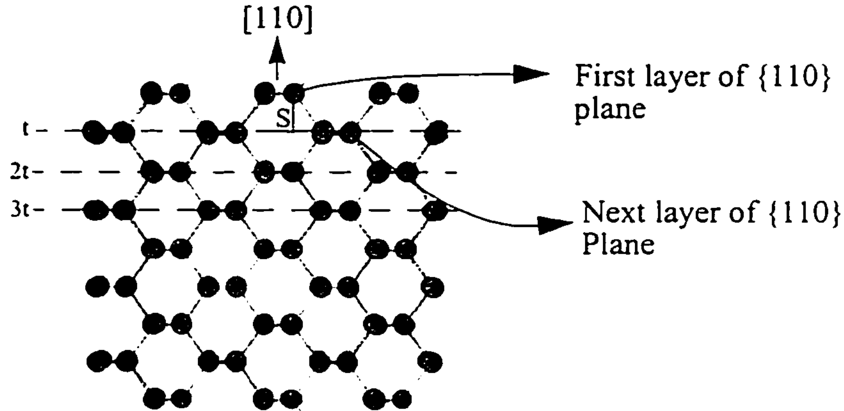

FIGURE 6.4: Layers of {110} planes to illustrate the step length

Similarly the f_p, PBC removal frequency can be calculated from the step length S = $\frac{1}{2\sqrt{2}}a$ = $0.3536a$ between two adjacent {110} planes, and the experimental etch rate of {110}. The PBC removal frequency, f_p is given by

$$f_p = \frac{ER(110)}{0.3536a} = 5.21 \times 10^9 \times ER(110)\ \#/\text{hr}$$

TABLE 6.2. Removal Rates vs. TMAH Concentration

Const. wt%	f_k (x 10^5) (#/hr)	f_p (x 10^5) (#/hr)
25	1.78	1.91
19	2.14	2.11
17	2.40	2.06
15	2.57	0.92
12	2.70	1.71
9	-	1.09

The removal rate of PBCs tend to be lower than the kink-row removal rates except at 25wt% case. At lower concentrations the $f_p << f_k$. It is interesting to note that the PBC removal rate at 15wt% is very low. The removal rates (f_k and f_p) vs. TMAH concentration are plotted in Figure 6.5.

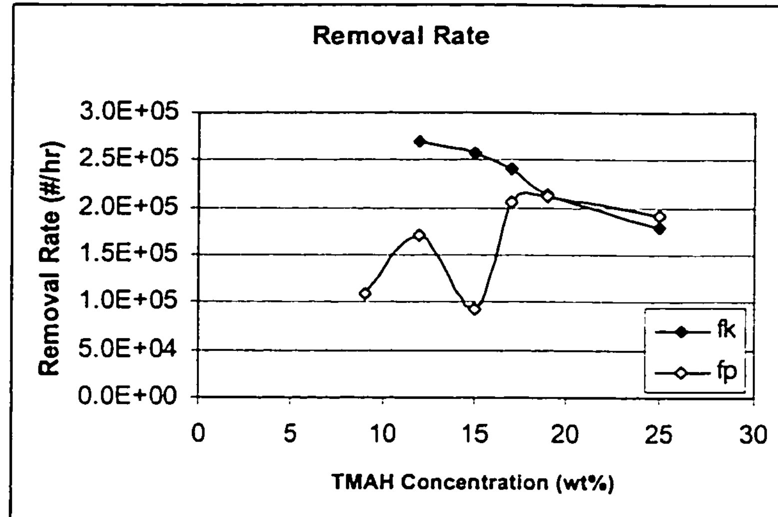

FIGURE 6.5: Removal Rates vs. TMAH Concentration

The above mentioned method of calculating f_k and f_p is valid only for {100} and {110} planes. Another method can also be used to calculate the removal rates, based on the angle between plane and the closest {111} plane. This method is described in Chapter 3 and is discussed in more detail with the calculations based on the experimental data in the later section of this chapter.

6.2 Under Etch, Etch Rates and Removal Frequencies

The common {100}, {110} and the {111} planes can also often be found as one of the emerging under-etched planes at certain deviation angles, in both cases of the (100) silicon and {100} and {110} wafer surfaces. Hence the etch rates of these planes can be calculated from the observed data. The mask-edge deviation angles at which these common planes appear as emerging planes are tabulated in the Tables 6.3 and 6.4 below.

TABLE 6.3. Emerging Planes on (110) Silicon

Deviation Angle (δ)	Emerging Plane	Inclination Angle
0°	(111)	35.26°
35.26°	(110)	60°
55°	(111)	90°
90°	(100)	45°
	(110)	90°

TABLE 6.4. Emerging Planes on (100) Silicon

Deviation Angle (δ)	Emerging Plane	Inclination Angle
0°	(100)	90°
	(110)	45°
45°	(111)	54.7°

Based on the emerging plane angles and the experimental data, the etch-rates of the {100}, {100} and {111} can be calculated. In the case where the emerging face is composed of two facets the etch-rates of the planes are calculated as illustrated in Figure 6.6. In many two-facet cases, the first facet is always vertical and hence makes the calculations easy.

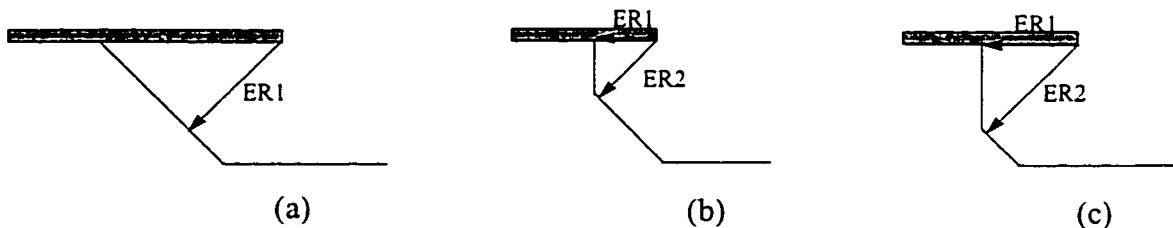

FIGURE 6.6: Illustration of emerging planes and etch rate calculation

Figure 6.6 above shows these different forms of the emerging planes. Fig 6.6 (a) shows the simple single-facet case, where the etch rate of the emerging plane can be calculated from $ER = UER \times \sin\theta$, where θ is the inclination angle of the emerging plane. There are also cases where the under-etched surface is two faceted. As an example consider the

Si(110) at $\delta = 90^o$, where the under-etched surface can have two facets. The first facet is the vertical {110} and the bottom facet is the 45° inclined {100} plane. Figure 6.6 (b) and (c) illustrates such case. The difference between the Figures 6.6 (b) and (c) is that the UESHP (under-etched surface horizontal projection) is smaller than the MUC (mask under cut) in (b) and UESHP is larger than MUC in (c). In such two facet cases (1st: 90° and the 2nd: 45°), the etch-rates of the planes can be calculated from

$$ER_1 = UER \text{ and}$$

$$ER_2 = \frac{(UER - UESHP + Depth)}{\sqrt{2}}$$

The etch-rate of the (100) planes and (110) planes at various concentrations of TMAH are calculated from the above equations. The calculated etch rates of these planes vs. TMAH concentration are tabulated in Table 6.5. In addition to the calculated etch rates, the etch rates from cavity etch depths (from Table 6.1) are included in in Table 6.5.

TABLE 6.5. Etch Rates of {100} and {110} planes vs. TMAH Concentration

Const. wt%	Si (100), $\delta = 0^o$		Si(110), $\delta = 90^o$		Cavity Etch Depth	
	ER(100) (μm/hr)	ER(110) (μm/hr)	ER(100) (μm/hr)	ER(110) (μm/hr)	ER(100) (μm/hr)	ER(110) (μm/hr)
25	21	29.7	22.6	-	24.3	36.6
19	26	25.5	40.7	44.4	29.2	40.5
17	-	32	45.8	45.6	32.7	39.5
15	-	28	-	21.6	35.1	17.7
12	-	36	48.4	42	36.8	32.9
9	-	41	-	21.6	-	20.9

As we can see from the Table 6.5 above, the etch rates of the same types of planes etched at same concentration are not the same. Note that the etch rate of (110) planes at 15wt% TMAH have a very sharp decrease when compared to the etch rates at 12wt% and 17wt% cases. The etch rates of {100} and {110} on both (100) and (110) wafers vs. TMAH concentration are plotted and presented in Figure 6.7.

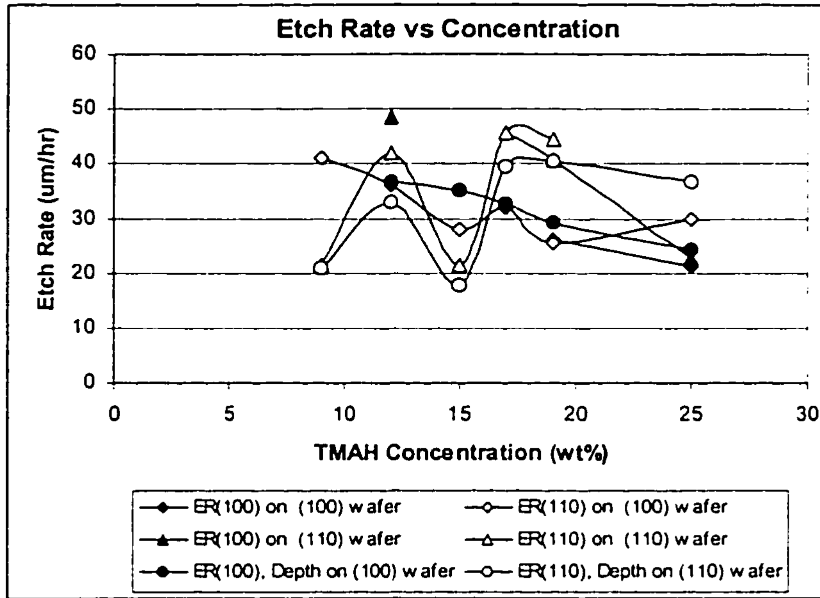

FIGURE 6.7: Etch rates of {100} and {110} planes vs TMAH concentration

Due to this very unexpected behavior observed at 15wt% TMAH etch, the experiment was repeated and the same results were observed.

6.3 Under-Etched Planes: PBC's and Kink-Rows

Chapter 5 presented the detailed underetch data, including facet inclination angles as a function of mask-edge deviation angle. In most cases, the facet inclination angles matched the theoretical inclination angles predicted by the model in Chapter 3. Since the model assumed that ALL facets would be pbc-based, or kink-row-based, this broad observation supports the assumptions outlined in Chapter 3:

(1) Each PBC on the etch-front plane must be removed mostly as a unit, before the next one is removed.

(2) Assumption (1) implies that the rate of removal of a kink on a PBC must be much greater than the rate of formation of new kinks on a previously intact PBC.

(3) In order for ER(θ_K) to hold, entire rows of kinks must be mostly removed before the next row of kinks is attacked.

Of course, certain isolated facets exhibited substantial roughness, indicating that, on an atomic scale, for those particular facets, the step based model was too simplistic. However, overall, the assumptions are confirmed, and this is a very important result: For most underetched facets, over a wide range of TMAH concentrations, the facets are composed of pbc-based or kink-row-based planes, and entire pbc's and kink-rows are removed largely as a unit. In other words, the probability of removing an atom on an already-broken pbc or kink-row is much greater than the probability of nucleating a new break in an intact pbc or kink-row.

These assumptions will be used to further extract pbc and kink-row removal frequencies in the upcoming sections.

6.4 Under-Etch Rate Model Fit to Calculate Removal Frequencies

Expanding the concept of calculating the etch rate in Chapter 3, Section 3.5, the etch mechanism in silicon is modeled by a small number of basic atomic structures: flat Si{111} planes, periodic bond chains (Si{110} planes are fields of such features), and kink-rows (Si{100} planes are fields of such features), with row and bond orientations alternating from one atomic layer to the next. Surface reconstruction is not considered, and the Si{111} plane is assumed to be the only inherently flat plane serving as a reference for the propagation of steps. The model assumes that any etched surface can be interpreted as having indices of the form $\{hhk\}$ or $\{hkk\}$, where $h \geq k$. Any surface having indices $\{hhk\}$ is composed of steps defined by pbc's, while any surface having indices $\{hkk\}$ is composed of steps defined by regular kink-rows. While these assumptions may not be true for all cases, they cover a wide enough set of data to make them useful.

In accord with basic crystal growth and etch models, etching is simply modeled as the

movement of steps. The model is developed from the Figure 3.3, assuming that, in a unit of time (*1/f*), the etch propagates by one step-advancement width *s* (assumed to occur on each step simultaneously), the etch rate can be calculated from Eq 3.1. So for the two generic cases, the pbc-defined {hhk} surface, and for "k-based" {hkk} surface, from Eq 3.4 and Eq 3.5 the etch rates will be as follows:

$$ER_p(\theta_p) = 3.31\mathring{A}\ f_p \sin(\theta_p) \quad \text{(Eq 6.1)}$$

$$ER_k(\theta_p) = 3.31\mathring{A}\ f_k \sin(\theta_k) \quad \text{(Eq 6.2)}$$

where f_p and f_k are the removal frequencies (in #/hr) of pbc's and kink-rows, respectively, and θ_p and θ_k are the angles between the {111} flat plane in question and the pbc-based, or k-based plane being considered. The numerical values of the step width and height are taken to be the same for both pbc-defined and k-defined cases. These types of equations can only be expected to hold within certain angle intervals close to the flat reference plane. For large enough θ, interactions with other flat planes may dominate. For a given silicon wafer surface, such as {110} or {100}, there are several distinguishable {111}-family planes (discussed in Chapter 3), each of which can potentially serve as a flat plane, to which θ can be referenced.

The orientation of these {111} planes with respect to the wafer surface is of critical importance in interpreting etch behavior. The {100} surface presents four symmetric {111} planes, each inclined by 54.7° to the horizontal, and the {110} surface presents vertical {111} planes in a parallelogram arrangement, and two 35.3° inclined {111} planes.

Etching Si{100}, there is only one type of variation of (θ_p) and (θ_k). The inclination angles of pbc-based planes vary between 54.7° and 45°, while kink-row based planes vary between 54.7° and 90°. The step widths for both the type of planes are shown in Table 6.6 below.

TABLE 6.6. Step width of Various Planes on (100) Silicon

Pair-Variation Identifier	Dev-Angle (δ) Range	Step width (s) on {100} surface
P-54-45-54	–45 - 0 - +45	3.83 Å
K-54-90-126	–45 - 0 - +45	3.83 Å

On the other hand, for the etching of Si{110}, the relevant possibilities are summarized in abbreviated form in the Table 6.7 below. Also presented are their step widths which will be used in model fits.

TABLE 6.7. Step width of Various Planes on (110) Silicon

Pair-Variation Identifier	Dev-Angle (δ) Range	Step width (s) on {110} surface
K-35-45-90	0-90-125	3.83 Å
K-145-135-90	0-90-125	3.83 Å
P-35-60-90	0-35-55	3.83 Å
P-145-120-90	0-35-55	3.83 Å
K-90-90-90	125-0-55	3.31 Å
P-90-90-90	55-90-125	3.31 Å

Based on these step widths and the type of emerging plane, we can fit etch rate equations Eq 3.4 and Eq 3.5 on the experimental etch rate graphs to get the removal frequencies (f_k or f_p depending on the emerging plane). Due to the way the step widths are calculated, using these step widths in the equations will result directly in under-etch rate. In these fits, the UER data is matched only to the first facet planes which are inclined at an angle less than 90°. Even though the inverse planes (e.g. K-35-60-90 and K-145-120-90) are of the same family, the UER is not the same because of the plane orientation with respect to wafer surface. So in all these f_k/f_p fits, top facets inclined at an angle less than 90° are fitted to the UER. In special cases where the first facet is inclined at an angle greater than 90° and is very small, this simple rule is ignored and the UER is fitted based on the second facet.

6.4.1 (100) Silicon Etching

6.4.1.1 TMAH 25wt% Case

From the experimental results (Figure 5.3) and from SEM observations (Figure 5.4), the first facet of the under-etched surface, type of plane vs. deviation angle are found and are tabulated in Table 6.8 below.

TABLE 6.8. First facet of the Under-etched surface on Si(100) etched in 25wt% TMAH

δ Range	First Facet
0 -15	K-126-90-54
16 - 42	K-54-90-126
43 - 45	P-54-45-54

By knowing the type of plane forms that forms the first facet and the step width, the under-etch rates can be calculated. By varying the values of f_p or f_k, the calculated UER are fitted to the experimental data on the corresponding range of deviation angles. Though in the range of deviation angles 16° to 42° the first facet is K-54-90-126, which is inclined at an angle greater than 90°, we still can fit the UER based on the second facet K-126-90-54 because the first facet (K-54-90-126) is very small. The fitted UER curves are over laid on the experimental UER data, shown in Figure 6.8 with the corresponding removal frequencies f_p or f_k, in this case only the f_k.

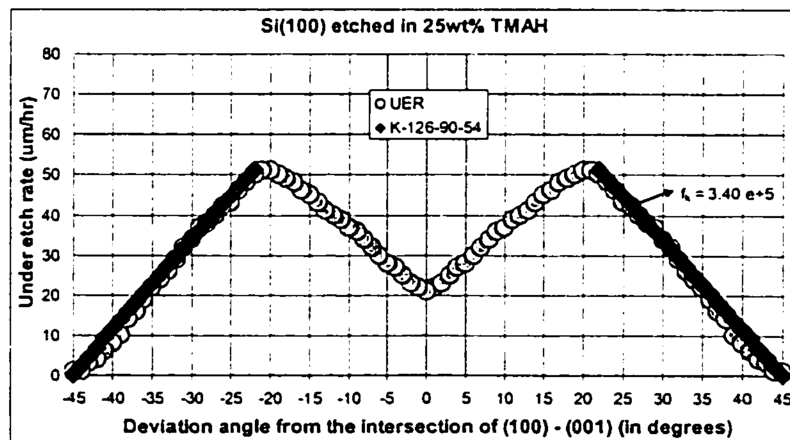

FIGURE 6.8: Experimental (100) UER data for 25wt% TMAH and fitted theoretical UER curves with corresponding kink-row removal frequency (#/hr).

Similarly, from the facet information presented in Chapter 5, fits were done where possible for all other concentrations. Again, the fits were only made where the first facet of the under-etched surface was inclined at an angle less than 90°. Si(100) etched in 19wt%, and 17wt% had the first facets inclined at an angle greater than 90° in the entire range of deviation angles and hence were not fitted to the theoretical UER fits. And for the 9wt% etch, the data is not fitted because the experimental data looks very noisy. The UER graphs with fitted theoretical UER curves and the calculated removal frequencies for other concentrations are shown in graphs in Figure 6.9 and Figure 6.10.

6.4.1.2 TMAH 15wt% Case

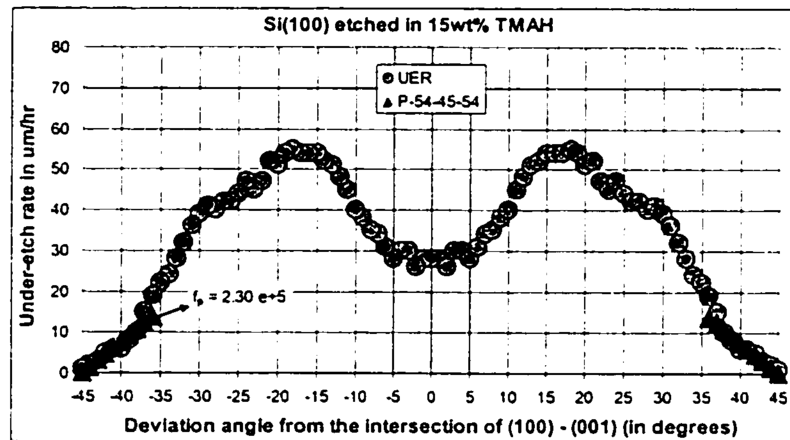

FIGURE 6.9: Experimental (100) UER data for 15wt% TMAH and fitted theoretical UER curves with corresponding PBC removal frequency (#/hr).

6.4.1.3 TMAH 12wt% Case

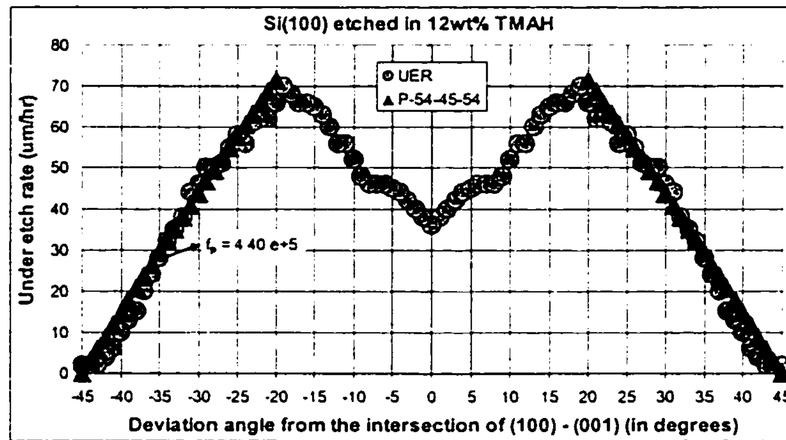

FIGURE 6.10: Experimental (100) UER data for 12wt% TMAH and fitted theoretical UER curves with corresponding PBC removal frequency (#/hr).

6.4.2 (110) Silicon Etching

6.4.2.1 TMAH 25wt% Case

From the experimental results (Figure 5.1) and from SEM observations (Figure 5.2), the first facet of the under-etched surface, type of plane vs. deviation angle is tabulated in Table 6.9 below. From these information, the type of plane that forms the first facet and step width; the under-etch rates are calculated from the equations. By varying the f_p or f_k, the calculated UER is fitted on to the experimental data to find the exact values of f_p and f_k.

TABLE 6.9. First facet of the Under-etched surface on Si(110) etched in 25wt% TMAH

δ Range	First Facet
0 - 15	K-35-45-(90)
16 - 55	K-90-90-(90)
55 - 76	P-90-90-(90)
77 - 88	K-90-45-(35)
89 -90	K-35-45-(90)

From this information on the first facet, the UER curves for Si{110} etched in 25wt%

TMAH is fitted to the appropriate UER(δ_p) or UER(δ_k) in certain ranges and the corresponding f_p and f_k values are calculated. The fitted UER curves are over laid on the experimental UER data, shown in Figure 6.11 with the corresponding removal frequencies f_p and f_k.

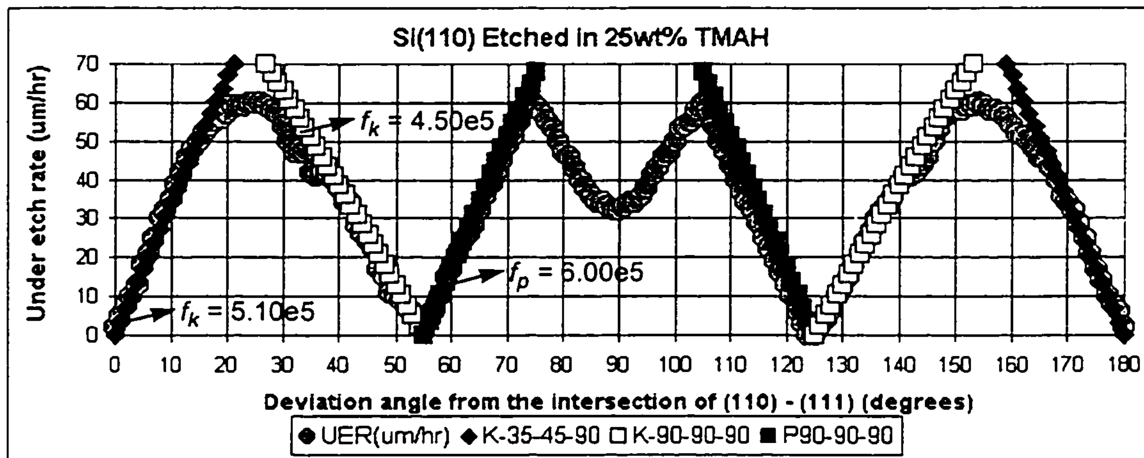

FIGURE 6.11: Experimental (110) UER data for 25wt% TMAH and fitted theoretical UER curves with corresponding PBC and kink-row removal frequencies (#/hr).

Similarly, this fitting was done for all other concentration etches. The UER graphs with fitted theoretical UER curves and the removal frequencies for other concentrations are shown in graphs in Figure 6.9 to Figure 6.13.

6.4.2.2 Other Concentrations

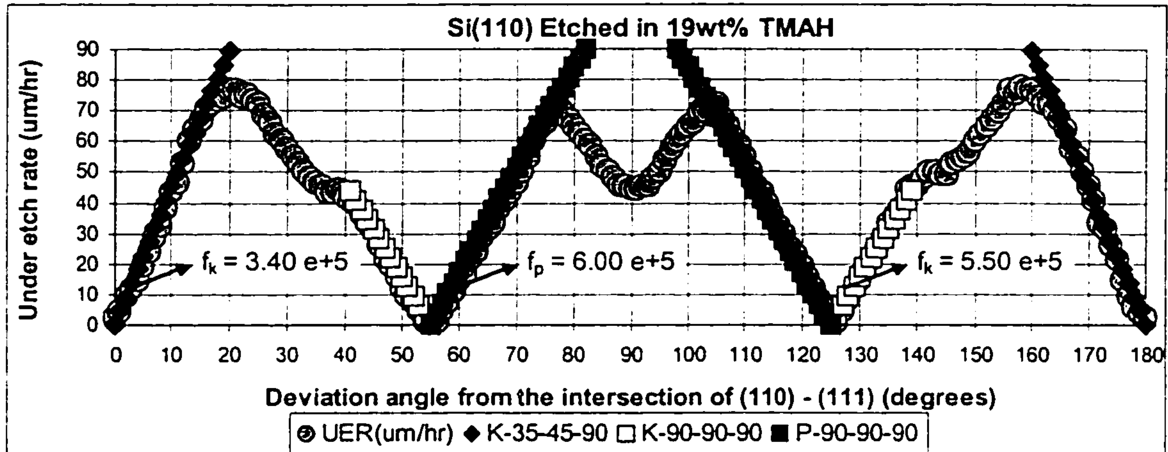

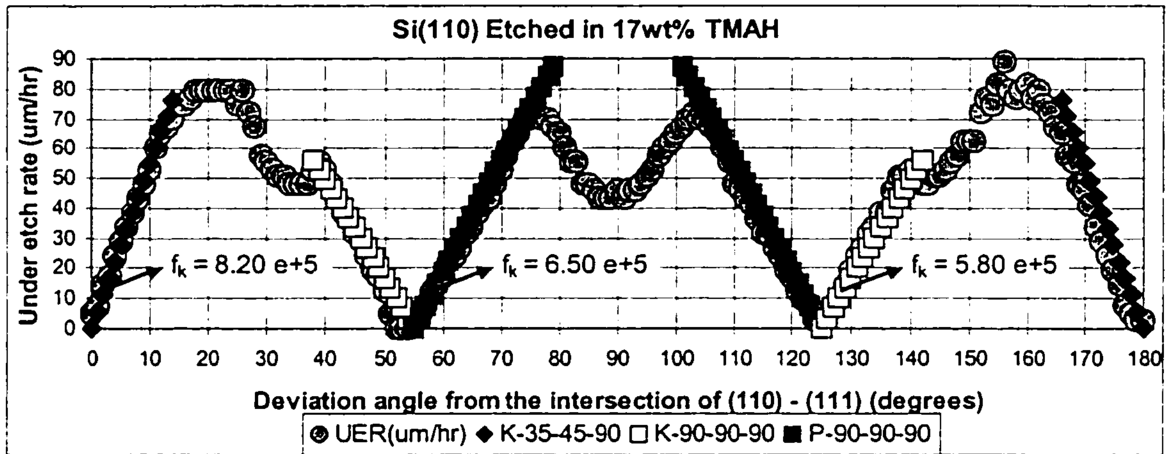

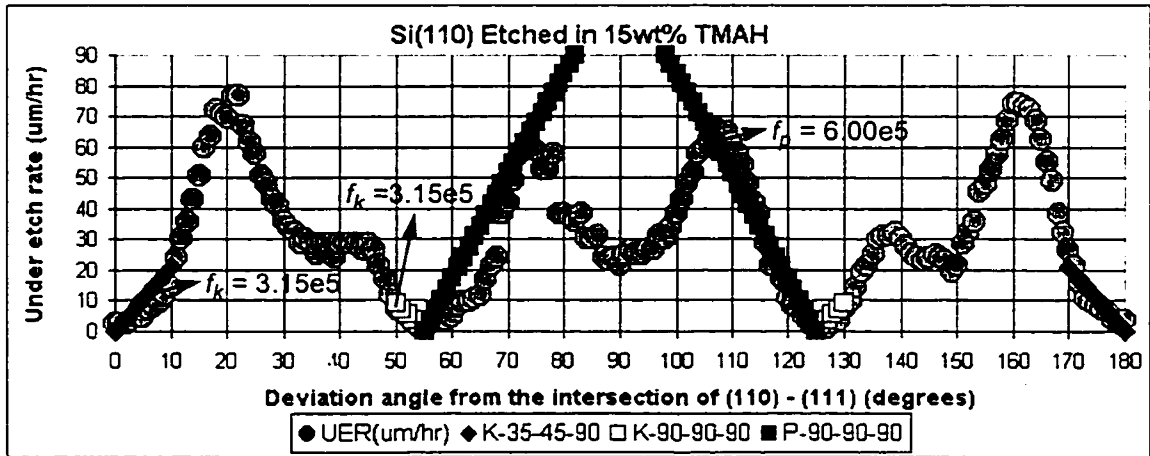

FIGURE 6.12: Experimental UER data for 19wt%, 17wt% and 15wt% TMAH and fitted theoretical UER curves with corresponding PBC and kink-row removal frequencies (#/hr).

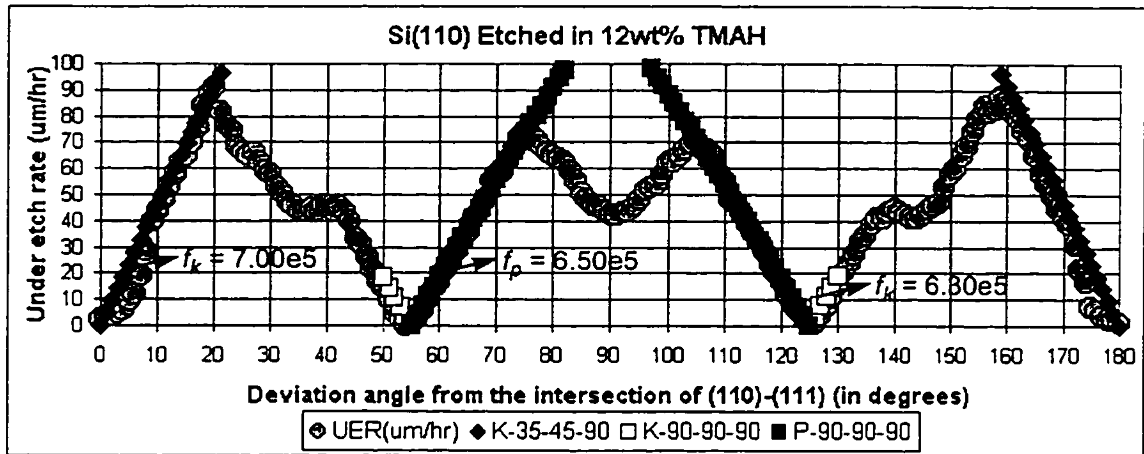

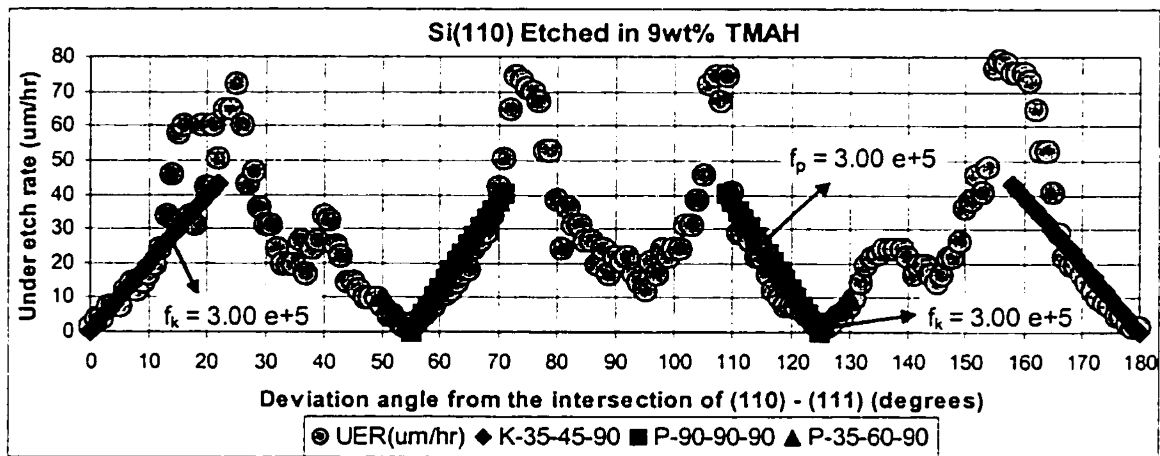

FIGURE 6.13: Experimental UER data for 12wt% and 9wt% TMAH and fitted theoretical UER curves with corresponding PBC and kink-row removal frequencies (#/hr).

6.4.3 Removal rate vs. TMAH Concentration

The fitted removal frequencies for the Si(100) and Si(110) etches are summarized in this section.

6.4.3.1 Removal Frequencies in Si(100)

The removal frequencies that were used to fit the (100) experimental under-etch rate data are summarized in this section. Both the kink-row removal frequency and PBC removal frequency calculated for different concentration etches are summarized in Table 6.10.

TABLE 6.10. PBC/Kink-row Removal Frequency on Si(100)

Pair-Variation Identifier	PBC/Kink-row Removal Frequency f_p or f_k (x 10^5) /hr					
	25wt%	19wt%	17wt%	15wt%	12wt%	9wt%
K-54-45-126	3.40	-	-	-	-	-
P-54-45-54	-	-	-	2.30	4.40	-

As we can see from the table, in most etch cases the first facet was the inverted planes which were inclined at an angle greater than 90° with respect to the (100) wafer surface and hence the removal frequencies were not calculated. With this discrete data it is very difficult to compare the removal frequencies. Hence the removal frequencies calculated on Si(110) are considered, this is discussed in the next section.

6.4.3.2 Removal Frequencies in Si(110)

The removal frequencies that were used to fit the (110) experimental under-etch rate data are summarized in Table 6.11 below.

TABLE 6.11. PBC/Kink Removal Frequency on Si(100)

Pair-Variation Identifier	PBC/Kink Removal Frequency f_p or f_k (x 10^5) /hr					
	25wt%	19wt%	17wt%	15wt%	12wt%	9wt%
K-35-45-90	5.10	6.80	8.20	3.15	7.00	3.00
K-90-90-90	4.50	5.50	5.80	3.15	6.30	-
P-35-60-90	-	-	-	-	-	3.00
P90-90-90	6.00	6.00	6.50	6.00	6.50	3.00

From the above table, it is clear that etching (110) silicon provides rich variations of data. When comparing the removal frequencies in (100) and (110) cases, it is clear that the removal rates, both PBC and kink removal rates are lower in (100) case.

For easier analysis these removal frequencies are plotted on a graph. The graph in Fig. 6.14 below shows the relation between the removal frequencies and TMAH concentrations. The removal rate of each *Pair-Identifier variation* with respect to etchant concentration will help to understand the etch mechanism.

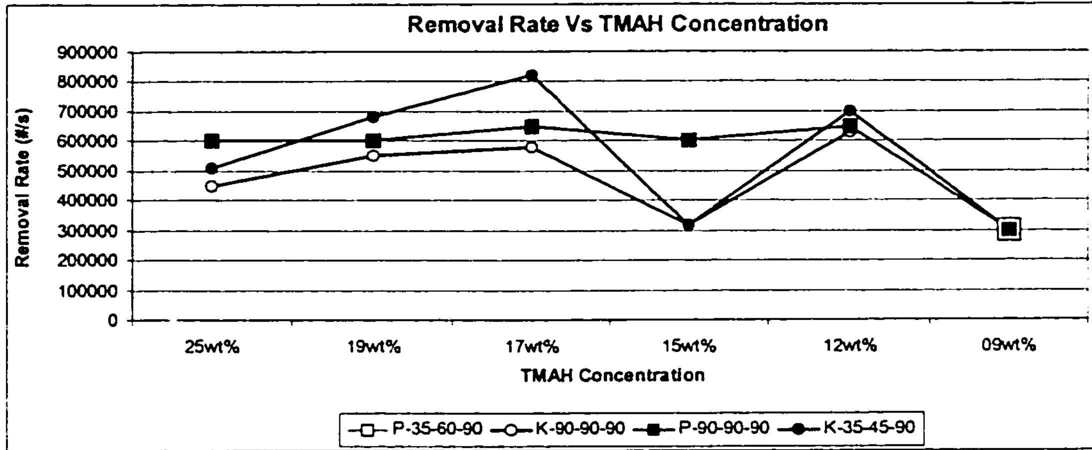

FIGURE 6.14: Removal rate vs. TMAH concentration. The P-35-60-90 type is seen only at 9wt% TMAH etch.

K-35-45-90

This kink-row removal frequency increases as the TMAH concentration reduces. But 15wt% and lower concentrations do not behave intuitively, 15wt% and 9wt cases have very low removal rates and both are ~3.0 x 10^5/hr.

K-90-90-90

This kink-row removal frequency increases as the TMAH concentration reduces. But the 15wt% is the odd case where the kink-row removal frequency sharply decreases, and is equal to the K-35-45-90 kink-row removal frequency.

P-90-90-90

From the graph, we see that this PBC removal rates are almost constant for all concentration etches (~6.0 x 10^5/hr) but for the 9wt% etch where it sharply decreases.

P-35-60-90

This type is found only on the 9wt% case.

At lower concentrations, 9wt% and 12wt%, the removal frequencies are all roughly equal. At the medium concentrations, 17wt% and 15wt%, the removal rates vary substantially. At 15wt%, both of the kink-row removal frequencies are the same and the PBC removal frequency is double the kink-row removal frequency.

The higher the removal rate, the more the etch is dependent on that particular *Pair-Identifier*, either kink-row oriented or PBC oriented etch.

A potential cause for different removal frequencies under same etch conditions may be related to effects acting at the boundaries between different facets on the under-etched surfaces (see Chapter 7 on Recommendations for Future Work).

6.5 Comparison to {110} and {100} Etch Rates Studied by Other Researchers

This section compares the results of other researchers working with TMAH. The etch rates of the common low index planes, (100) and (110) planes compared, since most researchers have mainly studied the etch rates of these common low index planes[1]. Studying and recording the etch rates of other crystallographic planes are very useful, in particular the etch rates of fast etch planes are of critical importance when designing a mask or a corner compensation structure. Hence the wide range of experimental data from this work can be used in a variety of applications. As a correlation to other researchers work, the etch rates of (100) and (110) from this work and others are summarized in this section. In addition to the etch rates of various planes, their surface roughness is studied and are reported in this work (Chapter 5).

6.5.1 (100) Silicon

The table below shows the etch rates of (100) planes at different concentrations at 80°C

1. Note that this work studies etch rates of a wider range of planes.

measured in this work, by S. Naseh [28], O. Tabata [10], and A. Merlos [16].

TABLE 6.12. Etch Rate of Si (100), Comparison

TMAH Const.	This Work	S. Naseh [28]	O. Tabata [10] (approx. from Graph)	A. Merlos [16]
25wt.%	24.3	23.2	29.4	23
19wt.%	29.2	-	35.4	-
17wt.%	32.7	-	36	-
15wt.%	35.1	35	37.5	32
12wt.%	36.8	-	42	-
9wt.%	-	-	45	-

The results from this work very closely match with the results from S. Naseh and A. Merlos. The etch rates from this work follow the same trend of results from O. Tabata, that is the etch rates decrease with increasing concentration, but the etch rates measured by O. Tabata are relatively larger than that is measured in this work. The dependencies of the etch rate of (100) silicon vs. TMAH concentration are shown in Figure 6.15 below.

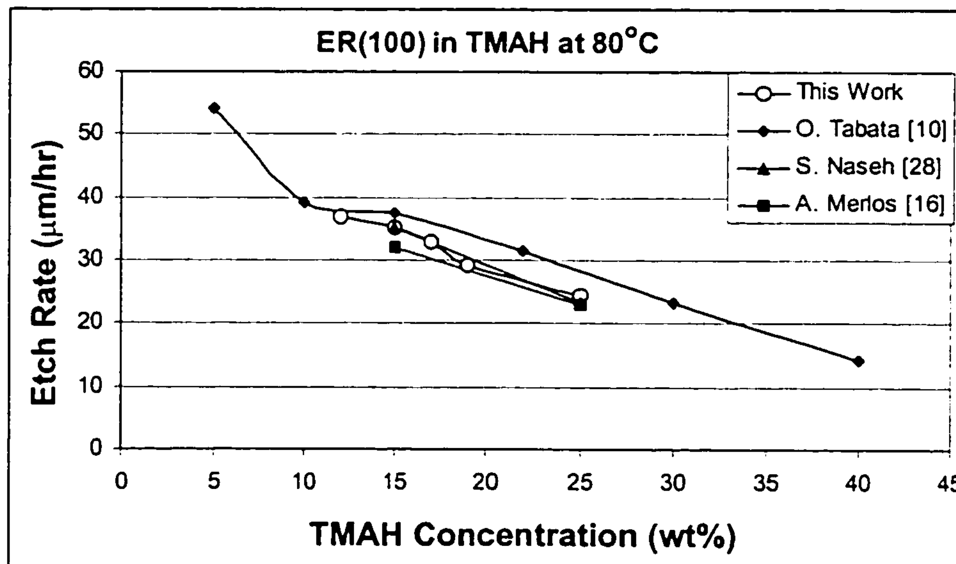

FIGURE 6.15: Etch rates of (100) Vs. TMAH concentration, from various work.

In general, we observe that the (100) etch rate decreases as the TMAH concentration increases.

6.5.2 (110) Silicon

The (110) etch rate variation vs. TMAH concentration was studied. Results from this work were compared to measurements made by O. Tabata [10], the comparison is shown in Figure 6.16.

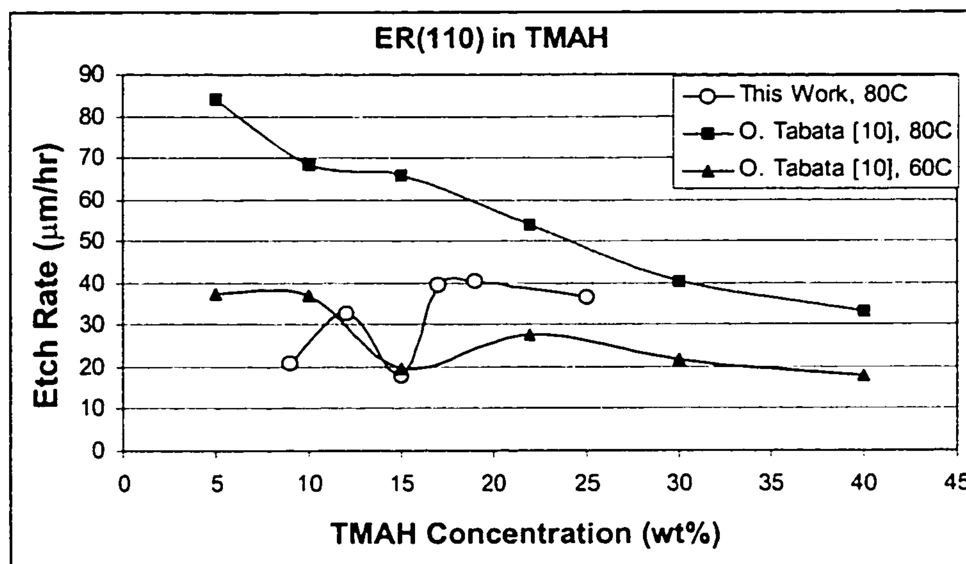

FIGURE 6.16: Etch rates of (110) Vs. TMAH concentration, from Tabata [10] and this work.

From the graph in Figure 6.16 we see that the etch rates measured from this work are lower than what is measured by O. Tabata under the same conditions (80°C). Also, we can see from the graph in Figure 6.16, on data from this work there is a sharp drop in etch rate at 15wt%. A similar drop at 15wt% can be seen in O. Tabata's work. However, the etch rate drop at 15wt% in O. Tabata's work occurs only in the 60°C etch case and not on the 80°C etch case. Due to this strange observation at 15wt% TMAH, the experiment was repeated and similar results were observed. No explanation for this discrepancy is available at present. However, it should be noted that Tabata's results were different from Merlos' and Naseh's on {100} silicon. Thus slightly different etch conditions may be an explanation. This discrepancy could be the subject for a more detailed future study.

6.6 Etched Surface Roughness

Most of the research in the field of anisotropic etching is focussed on the final shape of the etch cavity, the way the side walls are formed as a result of etching [2 - 8, 40 - 42, 49, 55]. The quality of the surface or surface roughness of the etched silicon substrate is also an important for the following two reasons. The first, the surface roughness of the interior cavity is a crucial factor that determines device performance on fluidic micro-devices. And secondly, studying the surface roughness helps better understand the mechanisms of anisotropic etching [53]. The surface roughness defines the boundary between the etch cavity bottom and the emerging under-etched surface, this boundary effect finally impacts the shape of the etch cavity. In some cases there are trench like features that are formed at the side wall and bottom surface boundary; the Si(110) etched in 15wt% TMAH is a very good example for this.

6.6.1 Roughness on (100) Surface

The roughness on the etched (100) surface was studied by SEMs, the SEMs of the Si(100) surface etched at various TMAH concentrations at 80°C are shown in Figure 6.16. All the SEMs shown in Figure 6.16 are the spokes at deviation angle $\delta = 45^{o}$. But the roughness on the etched (100) in the entire range of deviation angles are found to be very similar to what is shown in Figure 6.16. All the SEMs show the {111} side wall of the spoke, and it can be seen that the {111} plane is relatively smooth at all concentration etches. On the 15wt% case we can see that the hillocks formed at the edge of the spoke gets merged with the emerging {111} side wall, this has been observed by other researchers [18, 61].

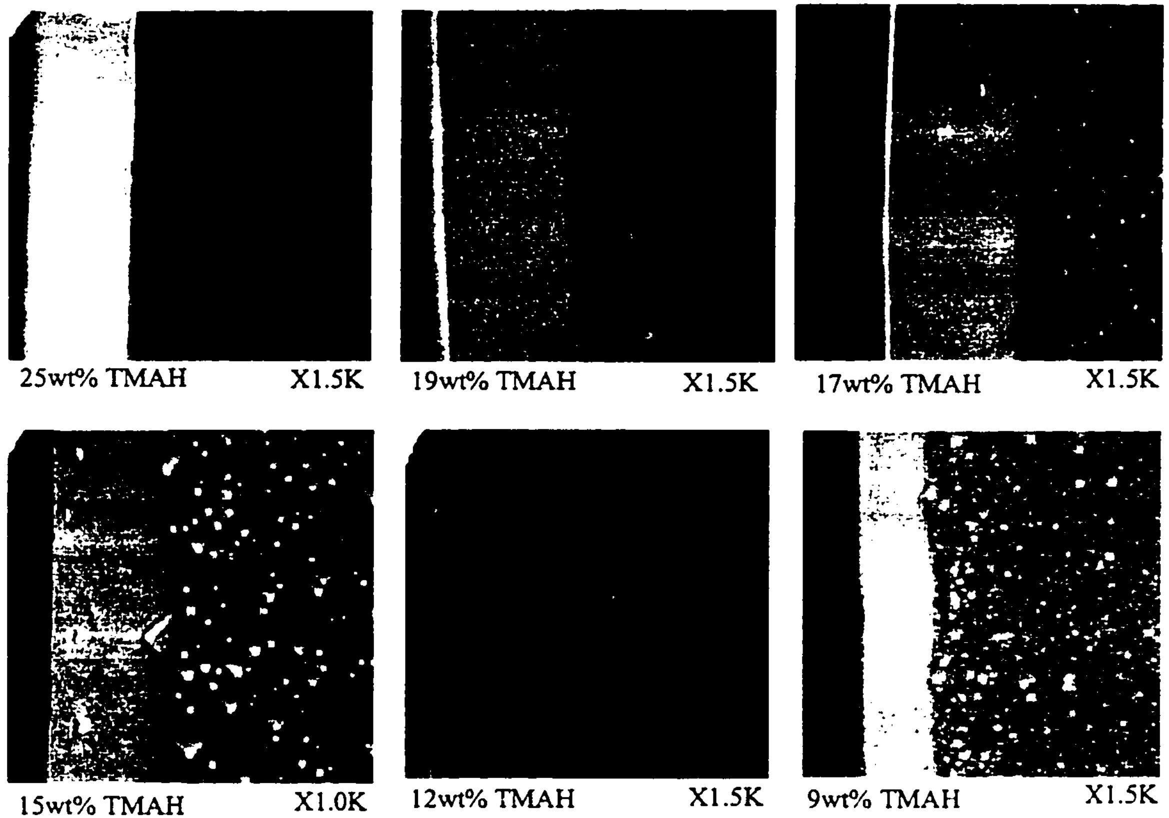

FIGURE 6.17: Surface roughness of Si(100) etched in various concentrations of TMAH.

It can be seen from the SEMs that the quality of the etched surface or surface roughness is mainly depends on the TMAH concentration. For higher concentrations of TMAH, the etched (100) surface is smooth. At 25wt% TMAH, the etched Si(100) surface is found to be free of hillocks. As the TMAH concentration decreases, the etched (100) surface becomes rough and has hillocks. The density and the size of the hillocks increases as the TMAH concentration decreases. The very interesting case is the 12wt% case where the etched (100) plane is relatively smooth, but still has very small hillocks.

6.6.2 Roughness on (110) Surface

The roughness on etched {110} surfaces was studied at different concentrations. The SEMs in Figure 6.20 show the roughness patterns on etched {110} surfaces. All of the SEMs in the figure are taken on wagon wheel spokes at deviation angles around 90°. Unlike the {100} surfaces, the {110} surfaces are rough for all concentrations. The roughness on {110} surfaces appear to be related to the direction of the PBCs on the etched surfaces. Etches in KOH resulted in similar roughness [53]. At higher concentrations of TMAH (25wt% to 17wt%), the surface is more irregular, and the relation of the roughness to the direction of the underlying PBCs is not clear. However, at lower concentrations (15wt% to 9wt%), the roughness has a particular orientation aligned parallel to the direction of the PBCs on the {110} surface.

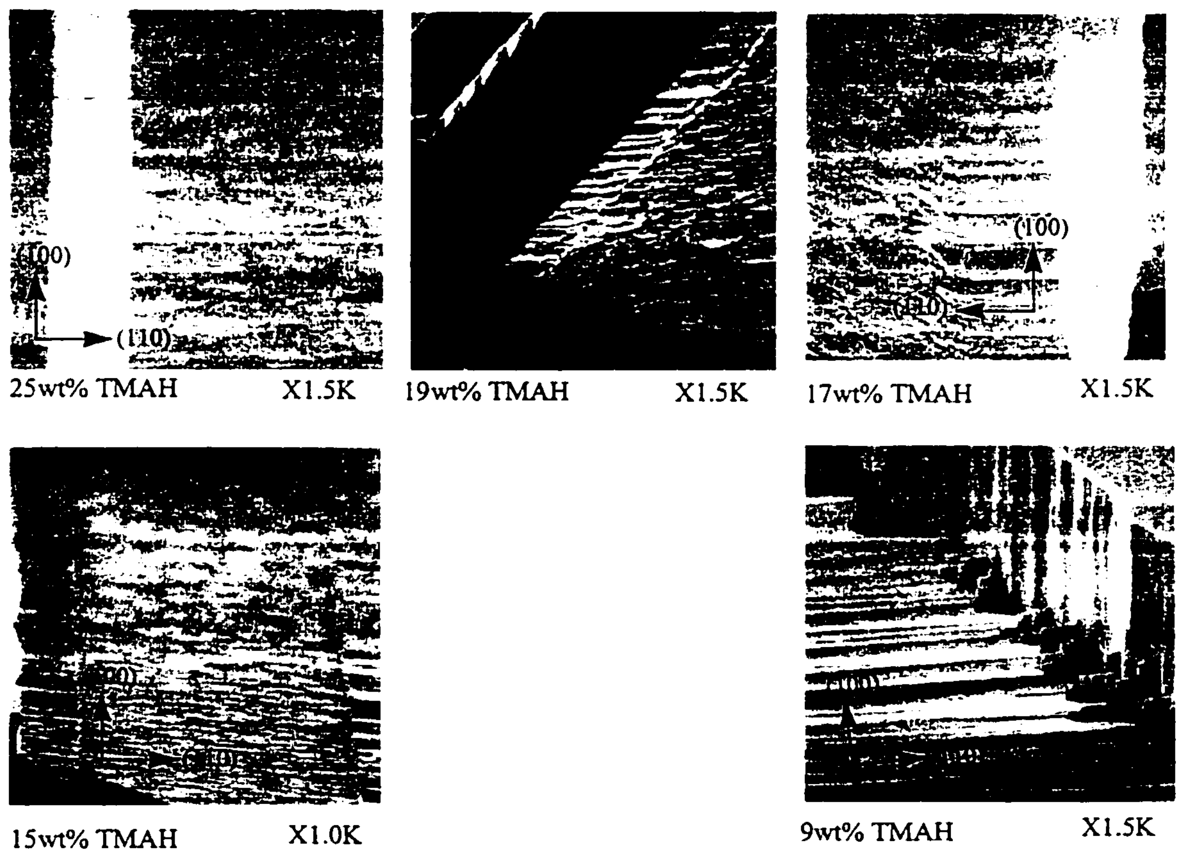

FIGURE 6.18: Surface roughness of Si(110) etched in various concentrations of TMAH.

As can be seen on the SEMs in Figure 6.20, unlike the {100} case, hillocks do not appear on the etched {110} surfaces. However, hillock-like structures do appear on certain UNDER-etched (non-{110}) surfaces. In 9wt% TMAH, at $\delta = 71^{o}$, the under-etched surface is two-faceted. The top facet is vertical, and the second facet is inclined at approximately 45°. The second facet is a near-{100} plane, and this *facet* is found to have hillocks on it. The SEM in Fig. 6.21 shows the hillocks on this 45-degree-inclined surface.

FIGURE 6.19: Hillocks on the ~(100) surface, the 2nd facet of the under-etched surface.

Other researches, K. Sato [53] have observed that the roughness on the etched (110) surface not only depend on the etchant concentration (KOH) but also depends on the etch time.

CHAPTER 7

Conclusions, Contributions and Suggestions for Future Work

7.1 Conclusions:

The main conclusions of this thesis are summarized below:

- The technique of using wagon-wheel-based under-etch experiments [13, 20] is confirmed again [20] to be useful in obtaining useful data for atomic modeling of anisotropic etching of silicon.
- Under-etch experiments on Si{110} wafers are shown to provide a rich and complex array of data for study of atomic modeling of anisotropic etching of silicon. These are especially useful since the same crystallographic features are presented to the etchant in different geometrical configurations (such as inclination angles and relationship to other planes and mask material).
- The combination of using both Si{100} and Si{110} for under-etch experiments in the same etchant conditions provides a very useful framework for analysis of etch rates of common crystallographic features.
- Especially on Si{110}, under-etch experiments reveal multi-faceted under-etched surfaces, with rich, complex variations of roughness, crystal features exposed, and inclination angles.
- The fact that the under-etched facets match the geometrically predicted inclination angles within a narrow tolerance indicates that the vast majority of under-etched surfaces in this work are defined by periodic bond chains or kink-rows. In ranges where

the under-etched facets do not exactly match to the predicted inclination algles, the facets are observed to be rough (perhaps due to inter-facet interactions), these rough surfaces (not planes) do not belong to PBC or Kink-row defined planes.

- The behavior of under-etched surfaces is shown to depend dramatically on the concentration of TMAH in the range 25wt% to 9wt%. The emerging facets, crystal features (pbc-based vs. k-row-based), and roughness all vary in a complex manner as one varies the TMAH concentration.

- A simple step-based model was used to extract removal frequencies of pbc's and kink-rows from certain sections of the under-etch data. Removal frequencies are in certain cases well-defined, for certain ranges of mask-edge deviation angle. These tend to be in the vicinity of {111} planes, where the etch rate is low and the spacing between steps is large. However, in many cases, different ranges on the same wafer yield different removal frequencies for the same PBC-based or kink-row-based atomic structure.

- There are also clear ranges of the mask-edge deviation angles where this simple model (based on steps on {111} planes) cannot properly fit the data. These tended to be in the vicinity of {110} or {100} planes appearing as under-etched facets.

- Overall, in many cases, the same crystallographic features etching in the same or equivalent etchant solutions, resulted in significantly different etch rates.

7.2 Contributions:

The Approach of Relating Under-etched Surface to Crystal Features:

While wagon-wheel experiments are not new, and while the silicon crystal structure has been well known for many decades, the study of atomic modeling of anisotropic etching of silicon had not used the combined approach presented in this thesis. By studying in detail the variations of etch rates of faster etching planes, and relating them to a small set of relevant crystal features, important insights can be found which would not otherwise be obvious.

Systematic Identification of the Step orientations and Pair Variation Identifiers, and their use in forming a complete summary of available inclination angles:

Again, while the silicon crystal structure has been known and well-understood for many decades, the direct relation of under-etched facets to step-based variations between pairs of {111} planes had not been highlighted before this.

Most Under-etched Surfaces are Pbc-based or Kink-row Based:

The detailed data on facet inclination angles of multi-faceted under-etched surfaces correlates very well with the predicted theoretical inclination angles. Therefore, it is geometrically proven that most under-etched surfaces (facets) are defined by pbc's (with indices {hhk}, where $h > k$), or kink-rows (with indices {hkk}).

A Body of Experimental Under-etch Data for a Single Etchant (TMAH) over a Range of Concentrations:

Under-etch experiments at 80°C were performed, and the results were recorded in detail, for six different concentrations: 25wt%, 19wt%, 17wt%, 15wt%, 12wt%, and 9wt%. This body of data can serve as a foundation for much future analysis, toward

atomic modeling of anisotropic etching of silicon.

Do the Same Crystal Features Always Etch at the Same Rate in the Same Etchant?

Crystal-based modeling of etch anisotropy begins with the hypothesis that the same crystal features exposed to the etchant should always etch at the same rate in a given etchant composition and conditions. While this is a good starting point for modeling and analysis, this work proves that in many cases the hypothesis is false. There are significant variations in etch rate.

Does a Simple Step-Based Model Apply to Anisotropic Etching of Silicon?

A simple step-based model (based on steps on flat {111} planes), can fit substantial portions of the under-etch data, using a single removal frequency applicable within a certain range of the mask-edge deviation angles. However, these removal frequencies can vary from one sub-section to another on the same wafer. Also there are clear ranges of the mask-edge deviation angles (near {110} or {100} facets) where this simple model cannot properly fit the data. This resolves some confusion about this question in the research field.

List of Publications Stemming from this Work:

A. Pandy, L. M. Landsberger, and M. Kahrizi, "Mask-Under-Etch Experiments of Si{110} in TMAH", Proceedings of IEEE Canadian Conference on Electrical and Computer Engineering, Edmonton, Canada, May 9-12, 1999, pp. 1621 - 1626.

A. Pandy, L. M. Landsberger, and M. Kahrizi, "Mask-under-etch characterization of Si{110} in TMAH", Canadian Journal of Electrical and Computer Engineering, 25, No. 1, 2000, p. 19.

L. M. Landsberger, A. Pandy, and M. Kahrizi, "Silicon Etch Anisotropy in Tetra-

Methyl Ammonium Hydroxide: Experimental and Modeling Observations", Sensors and Materials, Vol. 13, No. 5, 2001, pp. 293 - 301.

A. Pandy, L. M. Landsberger, B. Nikpour, M. Paranjape, M. Kahrizi, "Experimental Investigation of High Si/Al Selectivity During Anisotropic Etching in TMAH", Journal of Vacuum Science and Technology, Mar/Apr 1998, pp. 868 - 872.

M. Paranjape, A. Pandy, S. Brida, L. M. Landsberger, M. Kahrizi, M. Zen, "A Dual-Doped TMAH Etchant for MEMS Applications", Journal of Vac. Sci., Vol. 18, Issue 2, Mar. 2000, pp. 738 - 742.

7.3 Suggestions for Future Work

This thesis provides a body of data which can be subject to much further analysis and theoretical modeling, to find the reasons for deviations from the ideal crystal-based etching model.

- Effects due to the interactions between facets on an under-etched surface may be in effect. This may lead to more experiments to observe the evolution of the facets as the etched cavities become deeper.
- Careful study of the nature of facets where substantial roughness occurs is in order, especially where those facets appear in conjunction with very smooth adjacent facets.
- Careful study of the anomaly around 15wt%, perhaps by more experiments such as at 16wt%, 15.5wt%, 14.5wt%, 14wt%.

- Since there are distinct ranges of deviation angles where the step-based model fits, with apparently distinct transitions to regions where the step based model does not fit, careful study of the crystallography of these transitions is in order: what crystallographic features occur at these transitions?
- What types of experimental factors can subtly affect {110} etch rate data to cause a large discrepancy between this work and Tabata's?

References

[1] Kurt Petersen, "The Silicon Micromechanics Foundry",Micro Robots and Teleoperators Workshop, Proceedings of IEEE, Hyannis, Massachusetts, Nov. 9-11, 1987.

[2] Heikki Kuisma, Tapani Ryhanen, Juha Lahdenpera, Eero Punkka, Sami Ruotsalainen, Teuvo Sillanpaa, Heikki Seppa, "A Bulk Micromachined Silicon Angular Rate Sensor", Transducers 1997, pp. 875 - 878

[3] Behrouz Thesis, "A micromachined silicon vibrating-beam angular rate sensor : a design and implementation study", Ph. D Thesis, 1998, Concordia University.

[4] M. Kahrizi, M. Paranjape, L. M. Landsberger, "CMOS-Compatible Micromachined Two-dimensional Vertical Hall Magnetic-field Sensor", Journal of Vacuum Science Technology A, Mar/Apr 1998. pp. 873 - 875.

[5] Ralf Voss, Karin Bauer, Wilhelm Ficker, Tanjo Gleissner, Winfried Kupke, Matthias Rose, Stefan Sassen, Josef Schalk, Helmut Seidel, Erwin Stenzel, "Silicon Angular Rate Sensor for Automotive Applications with Piezoelectric Drive and Piezoresistive Read-out", Transducers 1997, pp. 879 - 882.

[6] Nim H. Tea, V Milanovie, Christian A. Zincke, John S. Suehle, M. Gaitan, Mona E Zaghloul, "Hybrid Postprocessing Etching for CMOS-Compatible MEMS", Journal of MicroElectroMechanical Systems1997, pp. 363 - 372.

[7] E. Hoffman, B. Warneke, E. Kruglick, J. Weigold, K.S.J. Pister, "3D Structures with Piezeresistive Sensors in Standard CMOS", IEEE 1995, pp. 288 - 293.

[8] K. E. Peterson, "Silicon as a Mechanical Material", Proc. of IEEE Electron Devices, 1982, p. 420.

[9] Kenneth E. Bean, "Anisotropic Etching of Silicon," IEEE Transactions on Electron Devices, Vol. ED-25, No. 10, Oct. 1978, pp. 1185 - 1192.

[10] O. Tabata, R. Asahi, H. Funabashi, K. Shimaoka, S. Sugiyama, "Anisotropic Etching of Silicom in TMAH Solutions", Sensors and Actuators A 34, 1992, pp. 51 - 57.

[11] A. Pandy, L. M. Landsberger, and M. Kahrizi, "Mask-under-etch characterization of Si{110} in TMAH", Canadian Journal of Electrical and Computer Engineering, 25, No. 1, 2000, p. 19.

[12] L. M. Landsberger, S. Naseh, M. Kahrizi, and M. Paranjape, "On Hillocks Generated During Etching of Si in TMAH", Journal of Microelectromechanical Systems, Vol. 5, 1996, pp. 106 - 116.

[13] O. Tabata, Proceedings of IEEE-MEMS, "Anisotropy and Selectivity Control of TMAH", 1998, Heidelberg, Germany, pp. 229 - 233.

[14] K. Sato, M. Shikida, T. Yamasiro, M. Tsunekawa, and S. Ito, "Charecterization of Anisotropic Etching Properties of Single-Crystal Silicon: Surface Roughening as a Function of Crystallographic Orientation", Proceedings of IEEE-MEMS, 1998, Heidelberg, Germany, p. 201.

[15] M. Sekimura, "Anisotropic Etching of Surfactant-Added TMAH Solution", Proceedings of IEEE MEMS, Orlando, USA, 1999, p. 650 - 655.

[16] A. Merlos, M. Acero, M. H. Bao, J. Bausells, and J. Esteve, "TMAH/IPA Anisotropic Etching Charecteristics", Sensors and Actuators A 37-38, 1993, p. 737 - 743.

[17] M. Elwenspoke, U. Lindberg, H. Kok, and L. Smith, "Wet Chemical Etching

Mechanism of Silicon", Proceedings of IEEE workshop MEMS, Oiso, Japan, 1994, pp. 223 - 228.

[18] S. S. Tan, M. L. Read, H. Han, and R. Boudreau, "Mechanisms of Etch Hillock Formation", Journal of Microelectromechanical Systems, Vol. 5, 1996, pp. 66 - 72.

[19] Don L. Kendall, "A new theory for the anisotropic etching of silicon and some underdeveloped chemical micromachining concepts," Journal of Vac. Sci. Tech, A8 (4), Jul/Aug 1990, pp.3588 - 3605.

[20] H. Seidel, L. Csepregi, A. Heuberger, H. Baumgartel, "Anisotropic Etching of Crystalline Silicon in Alkaline Solutions", Journal of Electrochemical society, 137, 1990, p. 3612.

[21] L. M. Landsberger, A. Pandy, and M. Kahrizi, "Silicon Etch Anisotropy in Tetra-Methyl Ammonium Hydroxide: Experimental and Modelling Observations", Sensors and Materials, Vol. 13, No. 5, 2001, pp. 293 - 301.

[22] A. Pandy,L. M. Landsberger, and M. Kahrizi, "Mask-Under-Etch Experiments of Si{110} in TMAH", Proceedings of IEEE Canadian Conference on Electrical and Computer Engineering, Edmonton, Canada, May 9-12, 1999, pp. 1621 - 1626.

[23] J. Van Schtelen, K. Sato, E. Van Veenendaal, A. J. Nijdam, J. G. E. Gardeniers, W. J. P. Van Enckevort, M. Elwenspoek, "Simulation of Anisotropic Wet-Chemical Etching Using a Physical Model", Proceedings of IEEE MEMS, Orlando, USA, 1999, p. 332.

[24] R. A. Wind, M. A. Hines, "Macroscopic Etch Anisotropies and Microscopic Reaction Mechanisms: A Micromachined Structure for the Rapid Assay of Etchant Anisotropy", Surface Science 460, 2000, pp. 21 - 38.

[25] A. J. Nijdam, J. W. Berenschot, J. van Suchtelen, J. G. E. Gardeniers and M. Elwenspoek, "Velocity Sources as an Explanation for Experimentally Observed Variations in Si{111} Etch Rates", Journal of Micromech. Microeng, 9, 1999, pp 135 - 138.

[26] B. Hannemann and J. Fruhauf, "New and Extended Possibilities of Orientation Dependent Etching in Microtechnics", IEEE, 1998, pp. 234- 239.

[27] Ben G. Streetman, "Solid state electronic devices", Chap 2, Englewood Cliffs, N.J. : Prentice Hall, c1995, p. 29.

[28] S. Naseh, "Experimental Investigation of Anisotropic Etching of Silicon in Tetra-Methyl Ammonium Hydroxide", Thesis: Master of Applied Science, Concordia University, September 1995.

[29] U. Schnakenberg, W. Benecke and P. Lange, Technical Digest, Transducers 1991, Sanfransisco, CA, USA, June 24 - 28, 1991, pp. 815 - 818.

[30] E. Steinsland, M. Nese, A. Hanneborg, R. W. Bernstein, H. Sandmo, and G. Kittilsland, "Boron Etch-Stop in TMAH Solutions", The 8th International Conference on Solid-State Sensors and Actuators, and Eurosensors IX, Stockholm, Sweden, June 25 - 29, 1995, pp. 190 - 193.

[31] S. Naseh, L. M. Landsberger, M. Paranjape, and M. Kahrizi, "Experimental Investigations of Anisotropic Etching of Si in TMAH", Canadian Journal of Physics, (Suppl.) 74, 1996, pp. 579 - 584.

[32] A. Pandy, L. M. Landsberger, B. Nikpour, M. Paranjape, M. Kahrizi, "Experimental Investigation of High Si/Al Selectivity During Anisotropic Etching in TMAH", Journal of Vacuum Science and Technology, Mar/Apr 1998, pp. 868 - 872.

[33] M. Paranjape, A. Pandy, S. Brida, L. M. Landsberger, M. Kahrizi, M. Zen, "A Dual-Doped TMAH Etchant for MEMS Applications", Journal of Vac. Sci., Vol. 18, Issue 2, Mar. 2000, pp. 738 - 742.

[34] E. H. Klaassen, R. J. Reay, C. Storment, J. Aundy, P. Henry, A. P. Brokaw, and G. T. A. Kovacs, "Micromachined Thermally Isolated Circuits", Solid-State Sensor and Actuator Workshop, Hilton Head, South Carolina. June 2-6, 1996, pp. 127 - 131.

[35] Y. Uenishi, M. Tsugai, M. Mehregany, "Micro-Opto-Mechanical devices fabricated by anisotropic etching of (110) silicon," pp. 319 - 324.

[36] Don L. Kendall, "On etching very narrow groves in silicon," Applied Physics Letters, Vol. 26, No. 4, 15 Feb. 1975, pp. 195 - 198.

[37] Handbook of Microlithography, Micromachining and Microfabrication. Vol. 2: Micromachining and Microfabrication. pp. 43 - 44.

[38] J. G. E Gardeniers, W. E. J. R. Maas, R. Z. C. Van Meerten and L. J. Giling, "Influence of temperature on the crystal habit of silicon in the Si-H-Cl CVD system," Journal of Crystal Growth 96 (1989) pp. 832 - 842.

[39] O. Than and S. Buttgenbach, "Simulation of Anisotropic Chemical Etching of Crystalline Silicon Using a Cellular Automata Model", Sensors and Actuators A, Vol. 45, 1994, pp. 85 - 89.

[40] Ernest Bassous, "Fabrication of Novel Three-Dimentional Microstructures by the Anisotropic Etching of (100) and (110) Silicon," IEEE Transactions on Electron Devices, Vol. ED-25, No. 10, Oct. 1978, pp. 178 - 185.

[41] Les. M. Landsberger, M. Kahrizi, M. Paranjape, and S. Naseh, "Variation of

Under-Etched Planes Appearing in Bulk-Micromachined Silicon Using TMAH Etchant", Sensors and Materials, Vol. 9, No. 7, 1997, pp. 417 - 426.

[42] H. L. Offerins, K. Kuhl, and H. Sandmaier, "Methods for the Fabrication of Convex Corner in Anisotropic Etching of (100) Silicon in Aqueaous KOH", Sensors and Actuators A, Vol. 25-27, 1991, pp. 9 - 13.

[43] K. P. Wu, W. H. Ko, "Compensating Corner Undercutting in Anisotropic Etching of (100) Silicon", Sensors and Actuators, Vol. 18, 1989, pp. 207 - 215.

[44] D. B. Lee, "Anisotropic Etching of Silicon," Journal of Applied Physics, Vol. 40, No. 11, Oct. 1969, pp. 4569 - 4574.

[45] S. Naseh, L. M. Landsberger, M. Paranjape, B. Nikpour, and M. Kahrizi, R.Antaki, J.F. Currie, "Release-Control Structure for Post-Process Release of A Micromachined Cantilever", Sensors and Materials, Vol 10, No.5, Oct. 1998, pp.287-296.

[46] E. S. Ammar, T. J. Rodgers, "UMOS Transistors on (110) Silicon," IEEE Transactions on Electron Devices, Vol. ED-27, No. 5, May. 1980, pp. 907 - 914.

[47] D. M. Allen, I. A. Routledge, "Anisotropic etching of silicon: a model diffusion controlled reaction," IEEE Proceedings, Vol. 130, Pt. I, No. 2, April 1983, pp. 49 - 56.

[48] Lloyd D. Clark, Jr. and David J. Edell, "KOH:H_2O Etching of (110) Si, (111) Si, SiO_2, and Ta," Micro Robots and Teleoperators Workshop, Proceedings of IEEE, Hyannis, Massachusetts, Nov. 9-11, 1987.

[49] B. Kim, and D. D. Cho, "Aqueous KOH Etching of Silicon (110), Journal of Electrochemical Society, Vol. 145, No. 7, July 1998, pp. 2499 - 2508.

[50] Handbook of Microlithography, Micromachining and Microfabrication. Vol. 2: Micromachining and Microfabrication. pp. 57 - 71.

[51] O. Tabata, "Anisotropy and Selectivity Control of TMAH", pp. 229 - 233.

[52] J. G. Hooley, "The Kinetics of the Reaction of Silica with Group I Hydroxides", Canadian Journal of Chemistry, Vol. 39, 1961, pp 1221 - 1230.

[53] K. Sato, M. Shikida, T. Yamashiro, M. Tsunekawa, and S. Ito, "Charecterization of Anisotropic Etching Properties of Single-Crystal Silicon: Surface Roughening as a Function of Crystallographic Orientation", IEEE, 1998, pp. 201 - 206.

[54] K. Ohwada, Y. Negoro, Y. Konaka, and T. Oguchi, "Groove Depth Uniformation in (110) Si Anisotropic Etching by Ultrasonic Wave and Application to Accelerometer Fabrication", IEEE, 1995, pp. 100 - 105.

[55] H. K. Triew and W. Mokwa, "A Generalized Model Describing Corner Undercutting by the Experimental Analysis of TMAH/IPA", Journal of Micromech. Microeng. B, 1998, pp. 80 - 83.

[56] D. L. Kendall, "Vertical Etching of Silicon at Very High Aspect Ratios", Annual review of Mater. Sci., 9, 1979, pp. 373 - 403.

[57] P. Glembocki, G. R. de Guel, and D. L. Kendall, "Hydration Model for Anisotropic Etching of Si in Aqueous Alkali Hydroxides", Journal of Electrochemical Society, 138, 1991, p. 1055.

[58] D. L . Kendall, G. R. de Guel, and S. M. Park, Journal of Electrochemical Society, 132, 1985, p. 221C.

[59] H. Seidel, L. Csepregi, A. Heuberger, and H. Baumgartel, "Anisotropic Etching of Crystalline Silicon in Alkaline Solutions, I", Journal of Electrochemical Society,

137, 1990, p. 3612.

[60] D. R. Ciario, "Corner Compensation Structures for (110) Oriented Silicon," Micro Robots and Teleoperators Workshop, Proceedings of IEEE, Hyannis, Massachusetts, Nov. 9-11, 1987.

[61] M. Elwenspoek, "The Form of Etch Rate Minima in Wet Chemical Anisotropic Etching of Silicon", Journal of Micromech. Microeng., 6, 1996, pp. 405 - 409.

[62] C. Strandman, L. Rosengren and Y. Backlund, "Fabrication of 45° Optical Mirrors on (100) Si Using Wet Anisotropic Etching", IEEE, 1995, pp. 244 - 249.

Appendix A

Derivation of the Deviation angle δ vs. θ and Inclination angle α vs. δ in the (100) and (110) System

A.1 The (100) System

A.1.1 Derivation of Deviation Angle δ vs. θ in the (100) System

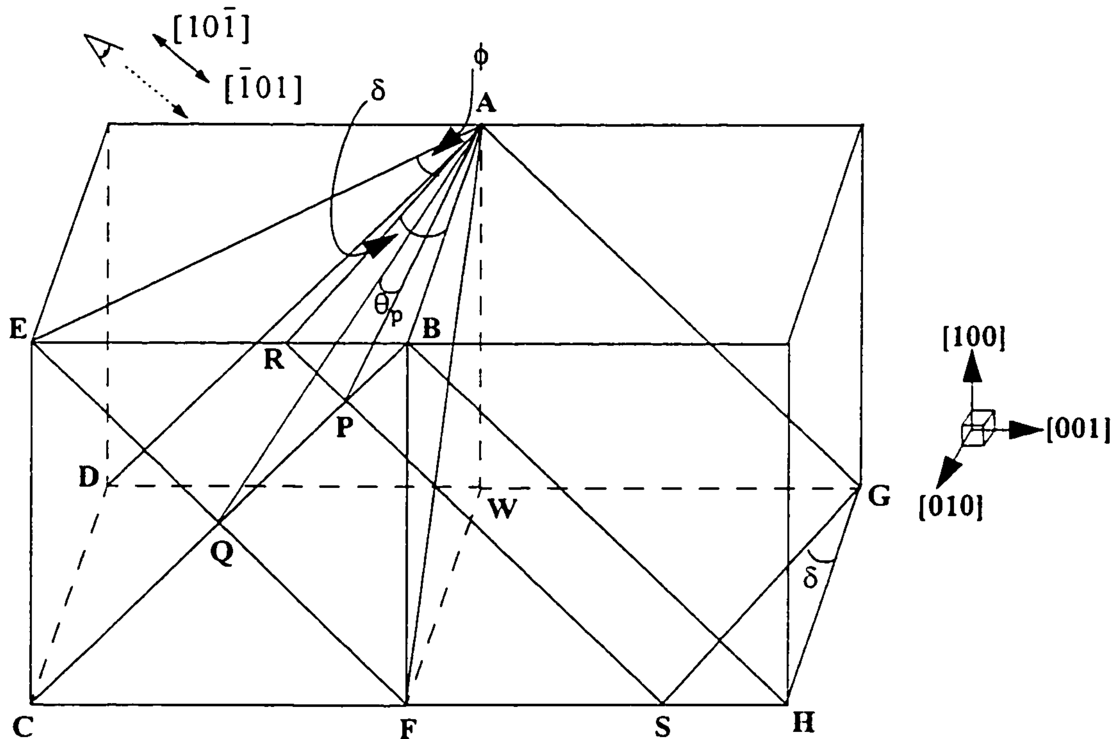

Figure A.1: The geometry in this diagram corresponds to the lattice view in Figure. 3.9, if the reader views from the upper left.

In the Figure A.1, the plane AGHB represents the (101) plane (the model plane) and EAFQ represents the (1 1 1) plane. Plane ABCD is the (1 0 $\bar{1}$) plane, and is equivalent to the plane of the page in Figures 3.4 - 3.15. Angle θ_P is measured in the ABCD plane, and θ_P is the angle PAQ. The angle θ_P is measured between the line of intersection of EAF

plane (111) with ABCD plane $(10\bar{1})$ and the line of intersection of EAF plane (111) with the model plane. In the Figure A.1, the rotated model plane is the AGSR plane which is rotated from the AGHB (101) plane to the EAF (111) plane.

$$\theta_P = \angle PAQ = \angle BAQ - \angle BAP$$

The model plane is rotated from the AGHB (101) plane to AEF (111) plane, where θ_P varies from 35.26° to 0°. This range represents half of the P-54-45-(54) as described in section 3.6.3.

The deviation angle, δ, is measured in the EAB the (100) plane, from the intersection of (001)-(100) (line AB) and the rotated model plane (AGSR plane in the Figure A.1). δ is the $\angle BAR$, in the same plane as the angle $\angle RAE$, which is denoted by ϕ. Therefore, the deviation angle can be given as $\delta = \angle BAR = 45^o - \phi$

A.1.1.1 For PBC-defined Planes:

$$\theta_p = \angle PAQ = 35.3^o - \mathrm{atan}\left(\frac{PB}{AB}\right) \Rightarrow \frac{PB}{AB} = \tan(35.3^o - \theta_P)$$

$$\delta = \mathrm{atan}\left(\frac{RB}{AB}\right) \text{ but } RB = \sqrt{2}PB \text{ therefore } \delta = \mathrm{atan}\left(\frac{\sqrt{2}PB}{AB}\right)$$

From the above equations, the deviation angle can be calculated from

$$\delta = \mathrm{atan}[\sqrt{2}\tan(35.3^o - \theta_p)] \text{ for } 0 \le \theta_p \le 35.3^o \quad \text{(Eq 3.1)}$$

Boundary conditions

δ	θ_p	**Plane**	**Plane**
0°	35.26°	AGHB	(101)
-45°/45	0°	AEF	$(111)/(1\bar{1}1)$

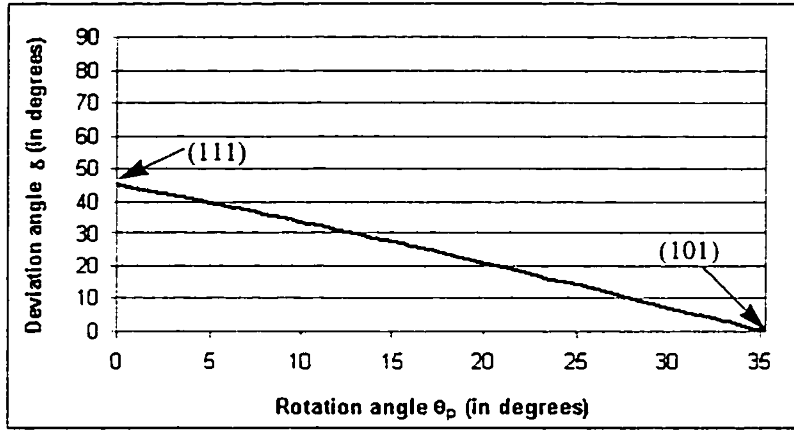

Figure A.2: Relation between rotation angle θ_p and deviation angle δ for the PBC defined planes in (100) silicon.

A.1.1.2 For Kink-defined Planes:

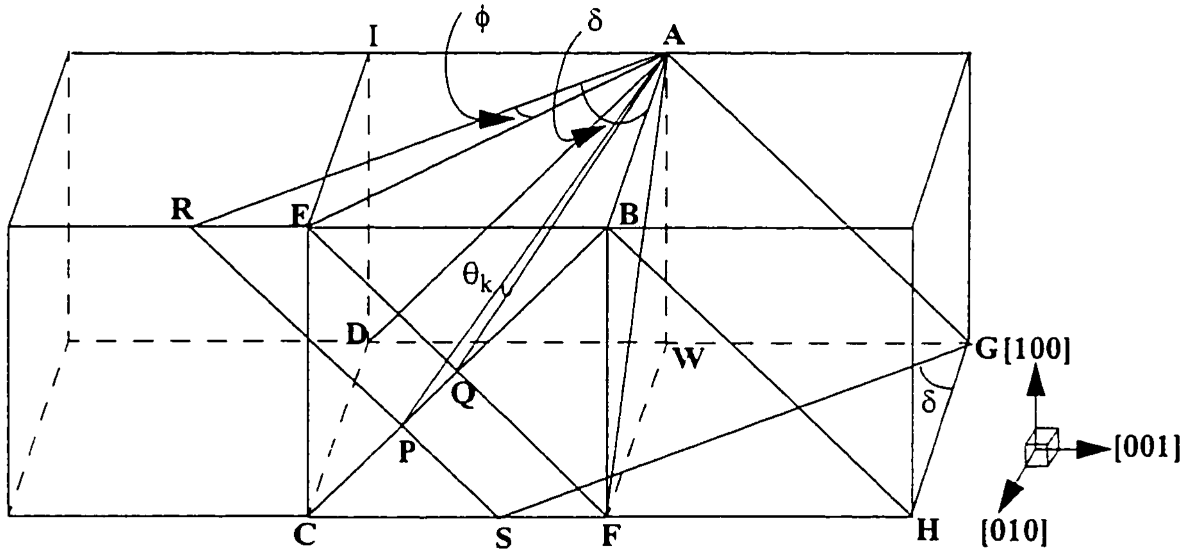

Figure A.3: Illustration of Kink based planes on (100) silicon.

For the kink based planes consider the same Figure A.1 with an added unit cell on the left, this is shown in Figure A.3 above. The angle θ_k is measured between the line of intersection of EAF plane (111) with ABCD plane $(10\bar{1})$ and the line of intersection of EAF plane (111) with the model plane, AGSR. In the Figure A.3 the model plane AGSR is rotated from the EAF (111) plane to the AIDW $(0\bar{1}0)$ plane.

$$\theta_k = \angle PAQ = \operatorname{atan}\left(\frac{PB}{AB}\right) - 35.3^o \Rightarrow \frac{PB}{AB} = \tan(35.3^o + \theta_K)$$

$$\delta = \operatorname{atan}\left(\frac{RB}{AB}\right) \text{ , but } RB = \sqrt{2}PB \text{ therefore } \delta = \operatorname{atan}\left(\frac{\sqrt{2}PB}{AB}\right)$$

Therefore the deviation angle $\delta = \operatorname{atan}[\sqrt{2}\tan(35.3^o + \theta_k)]$ for $0 \le \theta_k \le 54.7^o$

Boundary conditions

δ	θ_p	**Plane**	**Plane**
-45°	0°	AEF	(111)
-90°	54.7°	ADW	$(0\bar{1}0)/(010)$

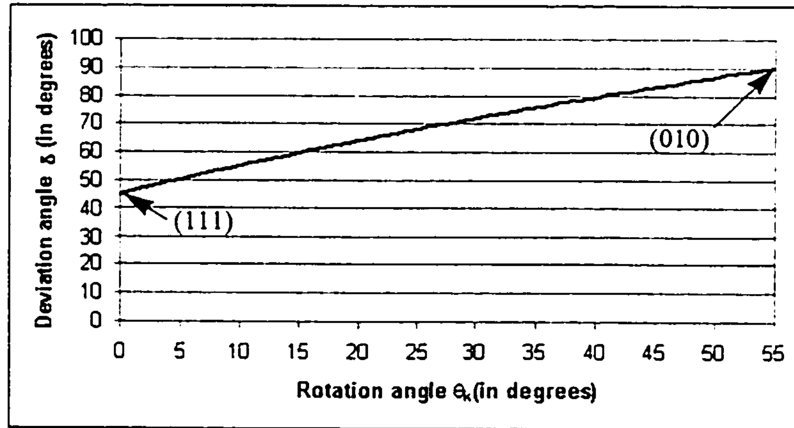

Figure A.4: Relation between rotation angle θ_k and deviation angle δ for the PBC defined planes in (100) silicon.

A.1.2 Derivation of Inclination angle α vs. δ in the (100) system

Using the same geometrical construct, one can derive the inclination angles of PBC-defined and Kink-defined planes in the (100) coordinate system. Note that in the $(10\bar{1})$ system used in Figures 3.4-3.12, these planes are perpendicular to the page.

A.1.2.1 PBC Defined Planes

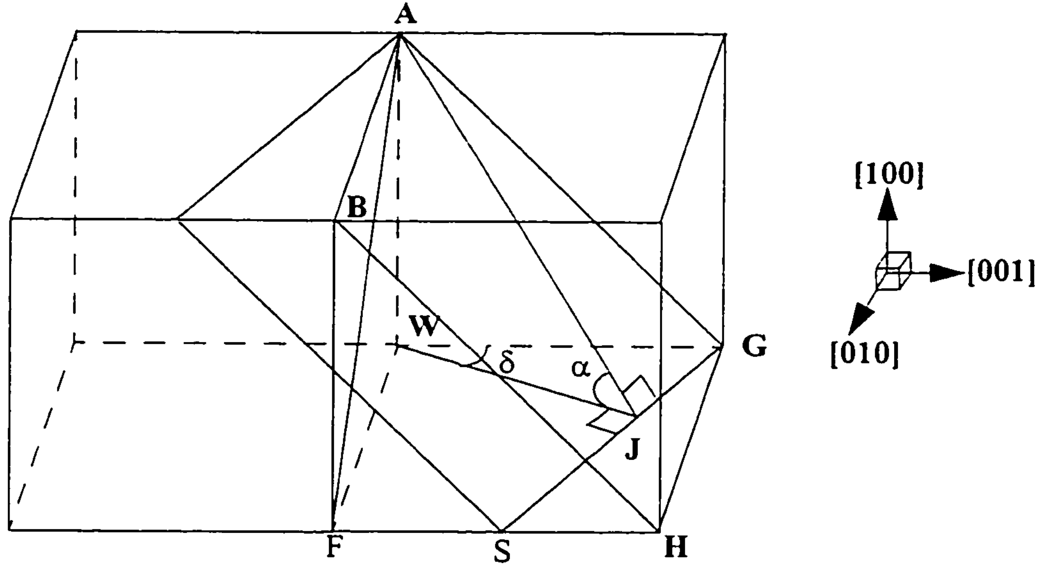

Figure A.5: Illustration of the inclination angle α.

PBC-defined planes, the inclination angle $\alpha_p = \text{atan}\left(\frac{WA}{WJ}\right)$.

then, $\frac{WJ}{WG} = \cos\delta = \frac{WJ}{WA}$, hence the inclination angle can be given as

$\alpha_p = \text{atan}\left(\frac{1}{\cos\delta}\right)$ for $0^o \le \delta \le 45^o$.

Boundary conditions

δ	α	**Plane**	**Plane**
0°	45°	AGHB	(101)
-45°	54.7°	AGF	(111)

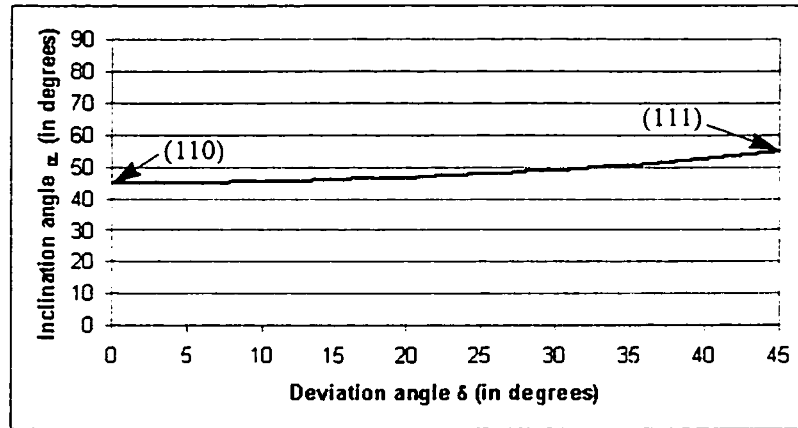

Figure A.6: Relation between deviation angle δ and inclination angle α for the PBC defined planes in (100) silicon.

A.1.2.2 Kink Defined Planes

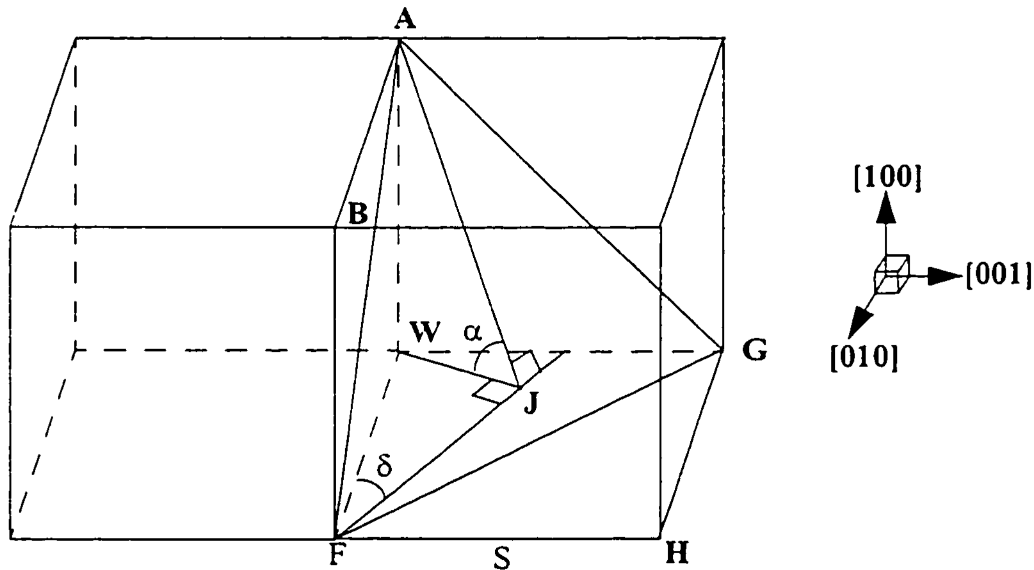

Figure A.7: Illustration of the inclination angle α in kink defined planes.

Similarly, for the Kink-defined planes, the inclination angle is given by $\alpha_k = \operatorname{atan}\left(\frac{WA}{WJ}\right)$. The kink defined planes are between the 90° inclined ABFW (100) plane and the 54.7° inclined AFG (111) plane. For the simplicity of graphical representation, the Figure A.7 shows the kink based planes with deviation angles δ between 270°

and 315°, this is the same as 0° to 45° (as one can see the inclination angles are symmetrical for every 90° and is a mirror image for every 45°).

From Figure A.7, $\sin\delta = \frac{WF}{WF} = \frac{WJ}{WA}$, hence the inclination angle can be given as

$\alpha_k = \operatorname{atan}\left(\frac{1}{\sin\delta}\right)$ for $270^o \le \delta \le 315^o$ or $0^o \le \delta \le 45^o$.

Boundary conditions

δ	α	**Plane**	**Plane**
45°	54.7°	AGF	(111)
0°	90°	ABNF	$(00\bar{1})/(001)$

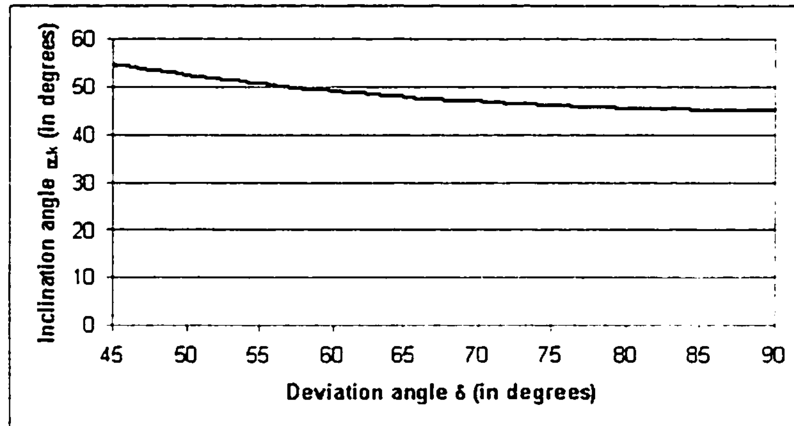

Figure A.8: Relation between deviation angle δ and inclination angle α for the Kink defined planes in (100) silicon.

In addition to these PBC-based and kink-based planes there are other PBC-based and kink-based which are the inverse of these planes at the same deviation angles. Figure A.9 illustrates the inclination angles of these planes vs. deviation angle δ in addition to the standard planes. Due to the symmetric nature of emerging planes over the range of deviation angles, only a 90° range is shown in the figure.

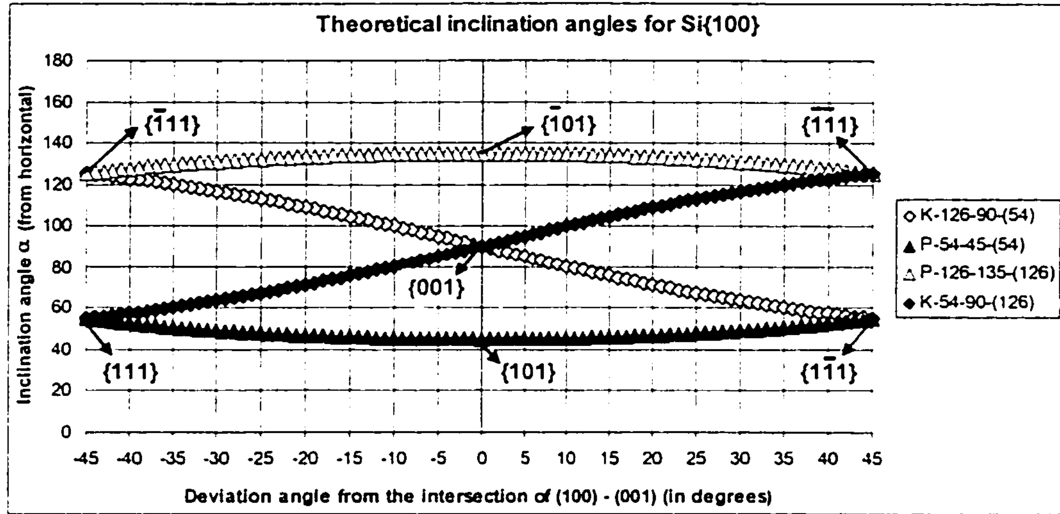

Figure A.9: Theoretical inclination angle of emerging planes vs. deviation angles in Si(100).

A.2 The (110) System

A.2.1 Derivation of the Deviation angle δ vs. θ and Inclination angle α vs. δ in the (110) System

Similar to the derivation in the (100) coordinate system, geometrical constructs are considered in representative unit cells. Figure A.10 shows the conventional unit cell and coordinate system, with the (110) plane highlighted, to represent the (110) wafer surface.

As in the (100) system, the mask-edge deviation angle in the plane of the wafer surface is denoted by δ, the rotation of the under-etched plane is denoted by θ, and the inclination angle of the under-etched plane with respect to the wafer surface is denoted by α. The under-etch plane is the plane which forms the side wall of the etch cavity at deviation angle δ. In Figure A.10 the plane DBFH represents the [110] wafer surface and the plane ABGH represents the under-etch plane. In the figure, the model plane or the under-etch ABGH is at deviation angle δ = 35.26°. The inclination angle of the model plane a = 60°,

a {110} plane.

The plane rotation, θ, is measured with respect to the intersection of the wafer surface with the 35.26° inclined (111) plane. The deviation angle in the wafer surface, δ, is measured with respect to the intersection of this (111) plane with the wafer surface.

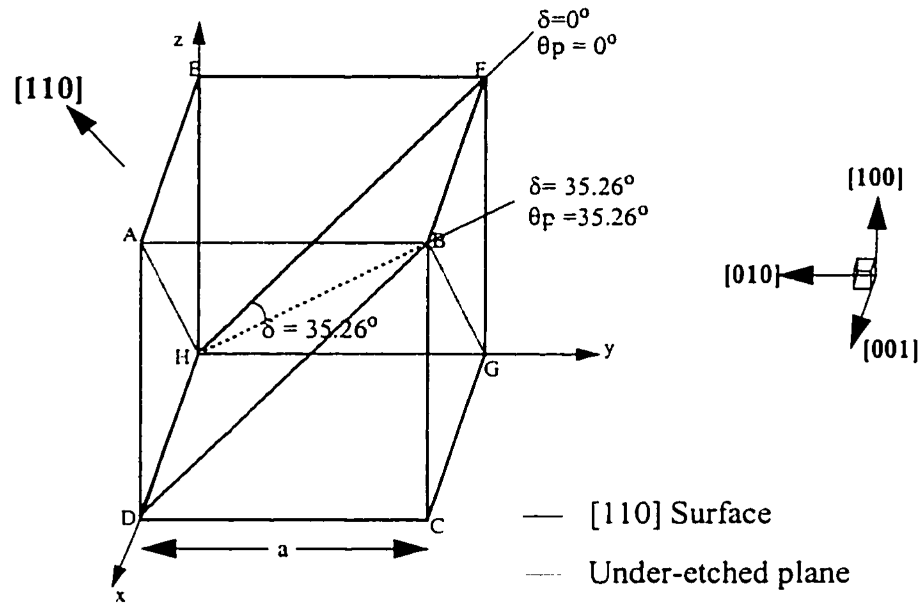

Figure A.10: Illustration of deviation angle δ in the (110) system.

Again, two modes are considered, PBC-defined planes and kink-defined planes. These are represented by θ_P and θ_K. Both these types of planes are discussed in the following sections.

A.2.1.1 PBC-Defined Planes

Due to the complexity of the plane variations in this (110) geometrical construct, the PBC-defined planes are split into two ranges of rotation angles.

A.2.1.1.1 PBC-defined Planes, Angle Range: $0^o \le \theta_p \le 35.26^o$ *(P-35-60):*

In Fig. A.11, the same coordinate system and point indicators are used as in Fig. A.10. The (110) wafer surface is again indicated by HFBD. The PBC-planes are the planes HCBE, HCF and the planes between them. The plane HCRS is on intermediate model plane between the HCF (111) plane, and the HCBE (011) plane. The variations of δ and α can be found by rotating the HCRS plane around the HC line. The angle θ_p represents this rotation angle away from the HCF (111) plane.

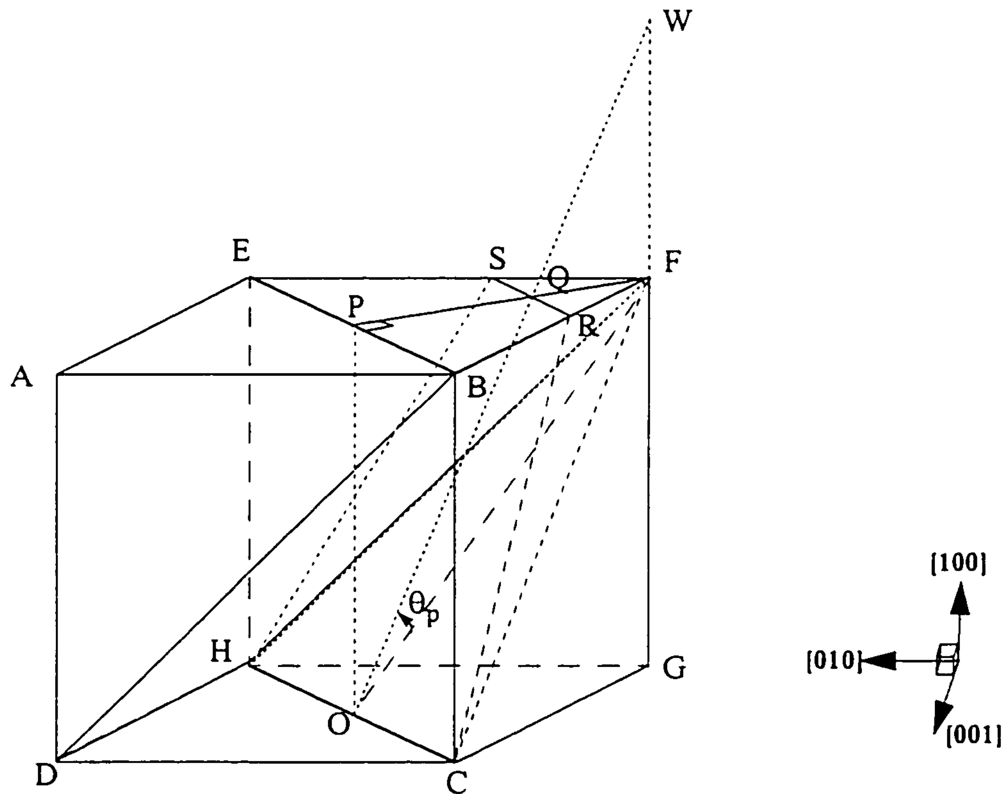

Figure A.11: Illustration of PBC-based planes on (110) silicon, in the range $0^o \le \theta_p \le 35.26^o$.

In the Fig. A.11, the angle $\angle POF = 35.26^o$, and $\theta_P = \angle FOQ$.

$$\frac{PQ}{PO} = PQ = \tan(35.26^o - \theta_P)$$

$$PF = \frac{\sqrt{2}}{2} \Rightarrow FQ = \frac{\sqrt{2}}{2} - PQ = \frac{1}{\sqrt{2}} - PQ = \frac{1 - \sqrt{2}PQ}{\sqrt{2}}$$

Consider the plane HFBD, the (110) plane shown in Figure A.12, this figure helps to visualize how and where the model plane HCRS intersects with the (110) plane.

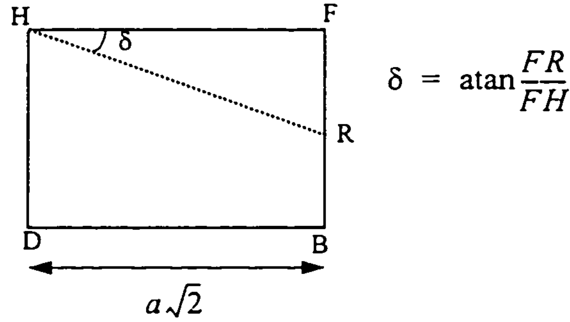

$$\delta = \operatorname{atan}\frac{FR}{FH}$$

Figure A.12: PBC based model plane intersecting the (110) plane.

$FR = \sqrt{2}FQ$ and $BR = \sqrt{2}PQ$, hence the deviation angle δ is given by,

$$\delta = \operatorname{atan}\frac{FR}{FH} = \operatorname{atan}\left(\frac{1}{\sqrt{2}} - \tan(35.26^o - \theta_P)\right), \text{ for } 0^o \le \theta_p \le 35.26^o.$$

The inclination angle, α of the model plane with respect to the (110) wafer surface can also be calculated, using the Miller indices of the model plane as it varies. Below given are the intercepts of the model plane. The Miller indices are given by the reciprocals of the intercepts. Note that the side of the conventional unit cell is normalized to = 1.

x-intercept: $GW = GF + FW = 1 + FW$, $\frac{FP}{PQ} = \frac{FG + FW}{FG} \Rightarrow 1 + FW = \frac{1}{PQ\sqrt{2}}$

x-intercept: $\frac{1}{PQ\sqrt{2}} = \frac{1}{\sqrt{2}\left(\frac{1}{\sqrt{2}} - \tan\delta\right)} = \frac{1}{1 - \sqrt{2}\tan\delta}$

y-intercept: 1 and *z-intercept:* 1

hence the *Miller Indices of the model plane:* $((1 - \sqrt{2}\tan\delta)\ 1\ 1)$.

The inclination angle α of the model plane with respect to the (110) silicon can hence be calculated from the dot product of the model plane with the (110) wafer surface, to find:

$$\alpha = \operatorname{acos}\left(\frac{1 \times (1-\sqrt{2}\tan\delta) + 1 \times 1 + 1 \times 0}{\sqrt{(1-\sqrt{2}\tan\delta)^2 + 1^2 + 1^2} \times \sqrt{1^2 + 1^2 + 0}}\right)$$

$$\alpha = \operatorname{acos}\left(\frac{\sqrt{2} - \tan\delta}{\sqrt{3 + 2\tan\delta(\tan\delta - \sqrt{2})}}\right), \text{for } 0^o \le \theta_p \le 35.26^0 .$$

A.2.1.1.2 Angle Range $35.26^o \le \theta_p \le 70.5^o$ ***(P-60-90):***

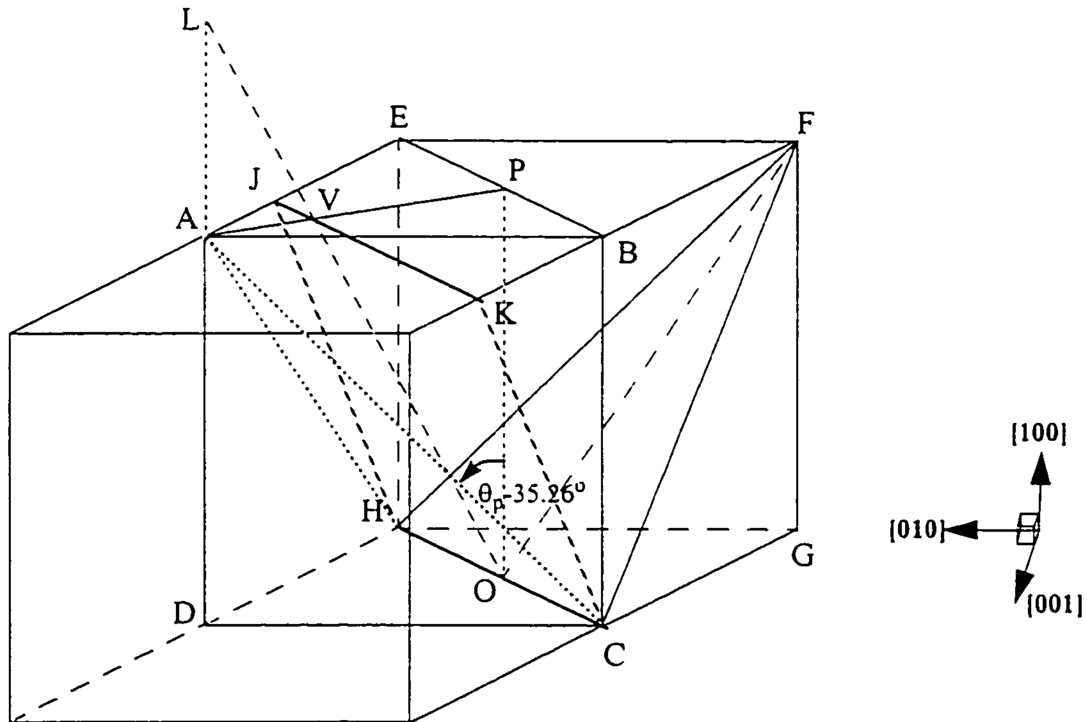

Figure A.13: Illustration of PBC-based planes on (110) silicon, in the range $35.26^o \le \theta_p \le 70.5^o$**.**

In Fig. A.13, the plane HCKJ is the intermediate model plane between the HCBE (011) plane, and the HCA $(1\bar{1}\bar{1})$ plane. The variations of δ and α can again be found by rotating the HCKJ plane around the HC line. The angle θ_P, represents this rotation angle away from the HCF (111) (reference) plane, $\theta_P = \angle FOV$.

Here, $\angle VOP = \angle FOV - \angle FOP = \theta_P - 35.26^o$

Consider the plane HFBD, the (110) plane shown in Figure A.14, this figure helps to visualize how and where the model plane HCKJ intersects with the (110) plane.

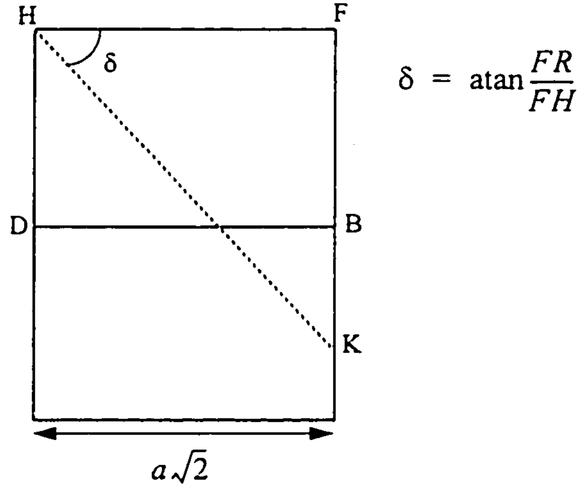

Figure A.14: PBC based model plane intersecting the (110) plane.

$$\tan\delta = \frac{FB + BK}{FH} = \frac{1 + BK}{\sqrt{2}}$$

$$BK = VP\sqrt{2} \Rightarrow \tan\delta = \frac{1 + \sqrt{2}VP}{\sqrt{2}} = \frac{1}{\sqrt{2}} + VP \Rightarrow VP = \tan\delta - \frac{1}{\sqrt{2}}$$

$\frac{VP}{PO} = \tan(\theta_P - 35.26^o) \Rightarrow VP = \tan(\theta_P - 35.26^o)$, hence the deviation angle,

$$\delta = \operatorname{atan}\left(\frac{1}{\sqrt{2}} + \tan(\theta_P - 35.26^o)\right) \text{ , for } 35.26^o \le \theta_p \le 70.5^o$$

The inclination angle, α, of the model plane with respect to the (110) wafer surface can again be calculated, using the Miller Indices of the model plane as it varies. Below given are the intercepts of the model plane. The Miller indices are given by the reciprocals of the intercepts. Note that the side of the conventional unit cell is normalized to = 1.

$$x - intercept = -(1 + LA)$$

$$\frac{AP}{VP} = \frac{AD + LA}{AD} = 1 + LA \text{ but } \frac{AP}{VP} = \frac{\sqrt{2}}{2VP} = \frac{1}{\sqrt{2}VP} \text{ therefore } 1 + LA = \frac{1}{\sqrt{2}VP}.$$

hence the $x-intercept = \frac{-1}{\sqrt{2}VP} = \frac{1}{1-\sqrt{2}\tan\delta}$

y-intercept: 1, *z-intercept:* 1

Miller Indices of the model plane: $((1-\sqrt{2}\tan\delta)\ 1\ 1)$.

The inclination angle can then be calculated from the dot product of the model plane with the (110) wafer surface, to find:

$$\alpha = \operatorname{acos}\left(\frac{\sqrt{2}-\tan\delta}{\sqrt{3+2\tan\delta(\tan\delta-\sqrt{2})}}\right) \text{ for } 35.26^o \le \theta_p \le 70.5^o.$$

A.2.1.2 Kink-based Planes

A.2.1.2.1 Angle range $0^o \le \theta_p \le 54.7^o$ *(K-35-45):*

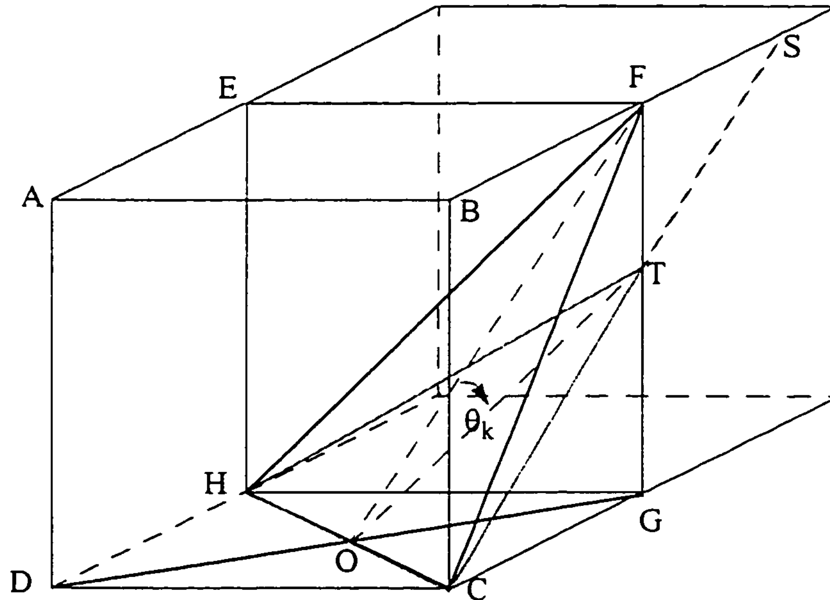

Figure A.15: Illustration of Kink-based planes on (110) silicon, in the range $0^o \le \theta_p \le 54.7^o$.

In Fig. A.15, the plane HCT represents the Kink-based model plane. The model plane is rotated along the line HC and from the point F to G. The angle θ_K, represents this rotation angle away from the HCF (111) (reference) plane. The deviation angle δ and the inclination angle α of the model planes can be calculated as follows.

$$\angle FOG = \operatorname{atan}\left(\frac{FG}{OG}\right) = \operatorname{atan}\left(\frac{1}{\sqrt{2}/2}\right) = 54.7^o$$

$$\frac{TG}{OG} = \tan(54.7 - \theta_K), \text{ also } \frac{TG}{OG} = TG\sqrt{2} \Rightarrow TG = \frac{\tan(54.7 - \theta_K)}{\sqrt{2}}$$

$$\tan\delta = \frac{FS}{FH} = \frac{1}{\sqrt{2}}$$

$$\frac{BF + FS)}{BF} = \frac{FG}{TG} = \frac{1}{TG} \Rightarrow 1 + FS = \frac{1}{TG} \Rightarrow FS = \frac{1}{TG} - 1$$

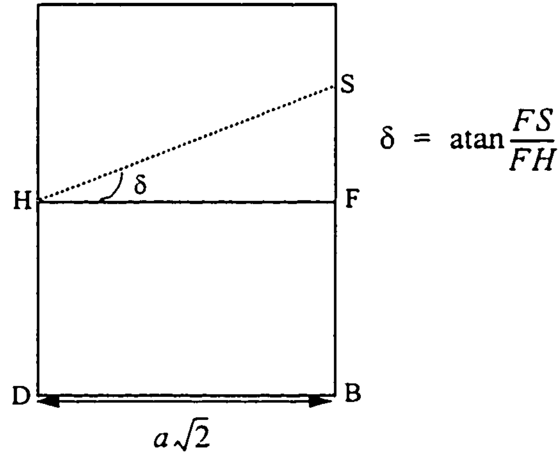

Figure A.16: Kink based model plane intersecting the (110) plane.

$$\delta = \operatorname{atan}\left(\frac{FS}{FH}\right) = \frac{FS}{\sqrt{2}}$$

$$\text{but } \frac{(BF + FS)}{BF} = \frac{FG}{TG} = \frac{1}{TG} \Rightarrow 1 + FS = \frac{1}{TG} \Rightarrow FS = \frac{1}{TG} - 1$$

$$\text{Therefore } \tan\delta = \frac{FS}{\sqrt{2}} = \frac{1 - TG}{TG\sqrt{2}} = \frac{\sqrt{2} - \tan(54.7 - \theta_K)}{\sqrt{2}\tan(54.7 - \theta_K)}$$

Hence the deviation angle is given by

$$\delta = \operatorname{atan}\left(\frac{\sqrt{2} - \tan(54.7 - \theta_K)}{\sqrt{2}\tan(54.7 - \theta_K)}\right), \text{ for } 0^o \le \theta_p \le 54.7^o$$

Below given are the intercepts of the model plane. The Miller indices are given by the reciprocals of the intercepts. Note that the side of the conventional unit cell is normalized to = 1.

x-intercept: TG, *y-intercept:* 1, *z-intercept:* 1

$$FS = \frac{1}{TG} - 1 \Rightarrow TG = \frac{1}{1 + FS}, \text{ but } \tan\delta = \frac{FS}{\sqrt{2}} \Rightarrow FS = \sqrt{2}\tan\delta$$

$$TG = \frac{1}{1 + \sqrt{2}\tan\delta}$$

Miller Indices of the plane: $(1 + \sqrt{2}\tan\delta\ \ 1\ \ 1)$.

The inclination angle α of the model plane with respect to the (110) silicon can hence be calculated from the dot product of the model plane with the (110) wafer surface, which is

$$\alpha = \operatorname{acos}\left(\frac{1 \times (1 + \sqrt{2}\tan\delta) + 1 \times 1 + 1 \times 0}{\sqrt{(1 + \sqrt{2}\tan\delta)^2 + 1^2 + 1^2} \times \sqrt{1^2 + 1^2 + 0^2}}\right)$$

$$\alpha = \operatorname{acos}\left(\frac{\sqrt{2} + \tan\delta}{\sqrt{3 + 2\tan\delta(\tan\delta + \sqrt{2})}}\right), \text{ for } 0^o \le \theta_k \le 54.7^o.$$

A.2.1.2.2 Angle Range** $54.7^o \le \theta_p \le 109.5^o$ **(K-45-90):

In Fig. A.17, the plane HCN represents this Kink-based model plane. The model plane is rotated along the line HC and from the point G to F'.The angle (θ_K- 54.7°), represents this rotation angle away from the HCF (100) (reference) plane.

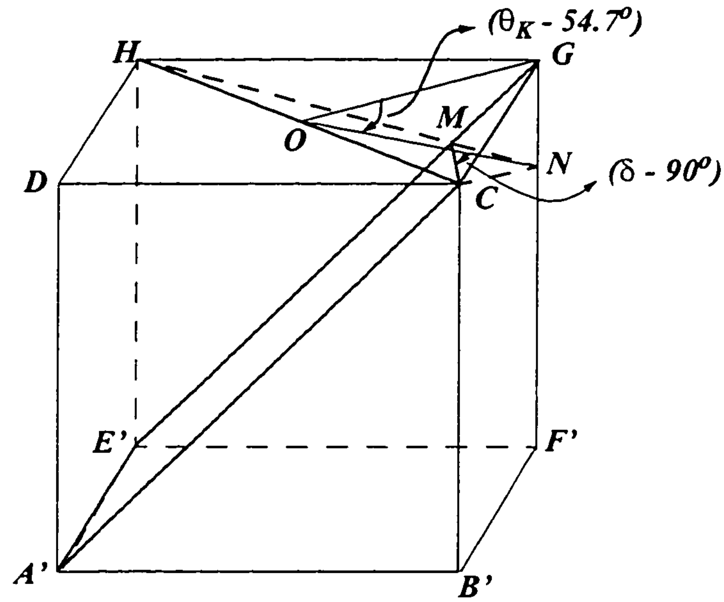

Figure A.17: Illustration of Kink-based planes on (110) silicon, in the range $54.7^o \le \theta_p \le 109.5^o$.

The deviation angle δ and the inclination angle α of the model planes can be calculated as follows.

$$\frac{GN}{GO} = \tan(\theta_K - 54.7^o) \Rightarrow GN\sqrt{2} = \tan(\theta_K - 54.7^o)$$

$$\frac{MG}{CG} = \tan(\delta - 90^o) \Rightarrow MG = \tan(\delta - 90^o)$$

$$\delta = \mathrm{atan}(MG) + 90^o$$

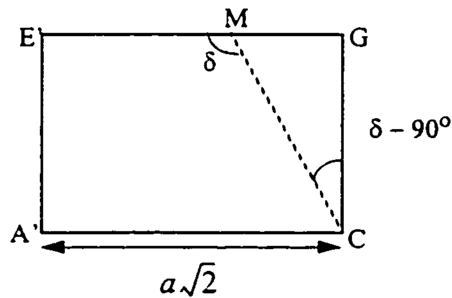

Figure A.18: Kink based model plane intersecting the (110) plane.

To find MG, consider the figure below, showing the plane HGF'E'

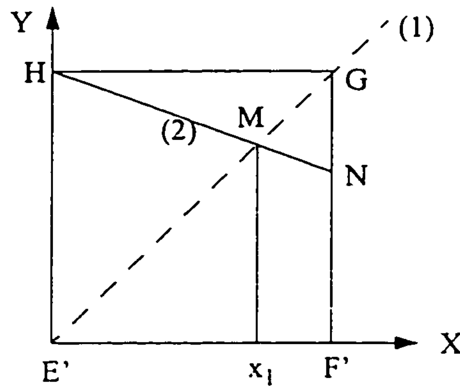

Equation of line (1): $y = x$

Equation of line (2): $y = 1 - (GN)x$

At point M the intersection of two lines, both lines have the same coordinates, hence

$x = 1 - (GN)x$, which gives $x_1 = \frac{1}{1 + GN}$

$$MG = (1 - x_1)\sqrt{2} = \left(1 - \frac{1}{1 + GN}\right)\sqrt{2} = \sqrt{2}\left(\frac{GN}{1 + GN}\right)$$

$$\delta = \operatorname{atan}\left(\frac{\tan(\theta_K - 54.7^o)\sqrt{2}}{\sqrt{2} + \tan(\theta_K - 54.7^o)}\right) + 90^o \text{, for } 54.7^o \le \theta_p \le 109.5^o$$

Similar to the previous cases, the inclination angle of the model plane can be calculated from the Miller Indices

x-intercept: $-GN$, *y-intercept:* 1 and *z-intercept:* 1

Miller Indices of the plane: $(-\frac{1}{GN}\ 1\ 1)$.

The inclination angle α of the model plane with respect to the (110) silicon can hence

be calculated from the dot product of the model plane with the (110) wafer surface, which is

$$\alpha = \operatorname{acos}\left(\frac{-\frac{1}{GN}+1}{\sqrt{\frac{1}{GN^2}+2} \times \sqrt{2}}\right) = \operatorname{acos}\left(\frac{GN-1}{\sqrt{2} \times \sqrt{1+2GN^2}}\right)$$

but $MG = \frac{\sqrt{2}GN}{(1+GN)} \Rightarrow GN = \frac{MG}{\sqrt{2}-MG}$, also $MG = \tan(\delta - 90^o) = \frac{-1}{\tan\delta}$

therefore $\alpha = \operatorname{acos}\left(\frac{-(\tan\delta + \sqrt{2})}{\sqrt{2+(1+\sqrt{2}\tan\delta)^2}}\right)$

The deviation angles, δ and the inclination angles α, calculated from the above equations are valid for the range, $54.7^o \le \theta_p \le 109.5^o$.

The deviation angle vs. inclination angle of the emerging plane in the entire range is plotted in the Figure A.19.

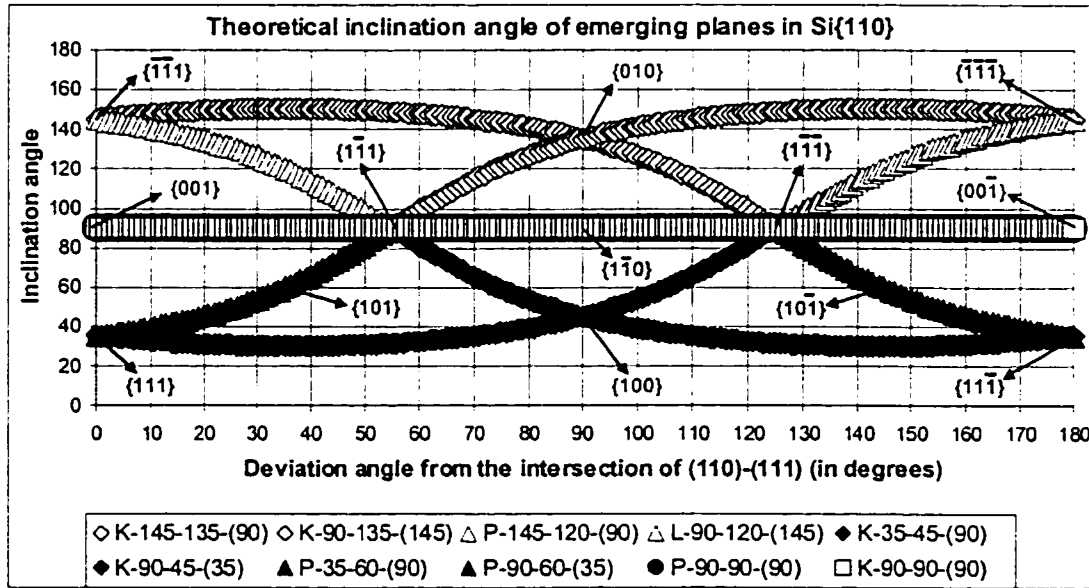

Figure A.19: Theoretical inclination angle of emerging planes vs. deviation angles in Si(110)

Appendix B

RCA Cleaning Process

Step 1: The samples are boiled in a solution of H_2SO_4:H_2O_2, 1:1 for 5 minutes. This step removes any organic contamination on the surface of the sample. This mixture of solution is also called piranha solution. The samples are thoroughly washed in DI water after this step.

Step 2: The samples are boiled in a solution of NH_4OH:H_2O_2:H_2O, 1:1:5 for 5 minutes. This step removes the organic contaminations on the surface of samples and also removes some kinds of metal like group IB, IIB metals and some other metals like gold, silver, copper, nickel, cadmium, zinc cobalt and chromium are dissolved and removed. The samples are thoroughly washed in DI water after this step.

Step 3: The samples are dipped in dilute HF, HF:H_2O, 1:50 for 15 seconds. This step removes any thin layer of native oxide. The samples are thoroughly washed in DI water after this step.

Step 4: The samples are dipped in a solution of HCl: H_2O_2: H_2O, 1:1:5 for 5 minutes at a temperature of 80°C. This step removes the alkali ions from the surface of the samples. After this step the samples should be thoroughly rinsed in DI water and then blow dried with nitrogen.